Development of a Low-Power Molecular Microwave Plasma

and

Its Applications as an Atom Source for Atomic Spectroscopy

by

Richard S. Lysakowski Jr.

Dissertation submitted to the Faculty of the

Virginia Polytechnic Institute and State University

in partial fulfillment of the requirements for the degree of

Doctor of Philosophy

in

Chemistry

APPROVED:

Raymond E. Dessy, Chairman

Paul E. Field

Gary L. Long

John G. Mason

James P. Wightman

March 5, 1987

Blacksburg, Virginia

Development of a Low-Power Molecular Microwave Plasma

and

Its Applications as an Atom Source for Atomic Spectroscopy

by

Richard S. Lysakowski Jr.

Raymond E. Dessy, Chairman

Chemistry

(ABSTRACT)

The major thrusts of this work have been: 1) To develop a high-efficiency low-power TM-010 microwave cavity for nitrogen support gas at atmospheric pressure, 2) To discover and physically characterize potential laser and emission spectroscopic applications of this atom source, with a particular emphasis on laser-induced fluorescence.

The result is the most efficient microwave-induced plasma cavity for nitrogen at one atmosphere that exists to date, giving stable and analytically useful molecular plasmas with only 50 Watts applied power. It is called the "High-Efficiency Molecular Microwave Plasma" (HEMMP) cavity. The HEMMP possesses excellent vaporization and atomization properties. It can handle aqueous sample flows of around 1 mL/min, introduced as an aerosol from a nebulizer. A detection system and sampling system were designed and an analytical instrument was built around the HEMMP cavity. Details of construction, operating conditions and operation of the instrument are described.

Applications investigated include laser-induced fluorescence (LIF), atomic emission spectroscopy (AES), and laser-enhanced ionization (LEI) [also known as the opto-galvanic effect (OGE)]. The major emphasis of the application work has been physical characterization of the low-power nitrogen plasma as an atom source for LIF.

This is the first time that either laser-induced fluorescence or laser-enhanced ionization have been observed and extensively characterized in any microwave-induced plasma (MIP). This is also the first time that atomic emission has been studied in a low-power N_2-MIP. LIF, AES, and LEI signal intensities were studied as a function of applied microwave power, support gas flow rate, signal observation height, and support gas composition using nitrogen and argon mixtures. Results for LIF yielded detection limits in the very low parts per billion range, and for AES in the low parts per billion range. Limit of detection (LOD) and background noise studies were done for all 3 techniques. Signal intensities were measured as a function of laser light intensity for LIF and LEI. Laser saturation was not observed with 300 mW power from the CW dye laser. The effects of electrode geometry and applied electrode voltage on LEI signals were also studied. Extensive background spectral studies were done for the nitrogen plasma.

Analytical feasibility has been demonstrated for AES, LIF, and LEI in the low-power nitrogen MIP. The results presented provide the background physical investigations required for a full-scale development of these techniques for chemical analysis.

Acknowledgements

There are so many people whose presence in my life has contributed to and supported the completion of this work that is would require many pages to acknowledge them all. So for those of you whom are not mentioned explicitly, know that your presence is deeply appreciated.

First, to my Parents, my sisters and and my brother without whose support I would never have made to where I am now, I give my deepest thanks.

To all of my friends who have been there for support, Thank You: including , , ..., and the many members of Dr. Dessy's Research Group.

For their technical assistance on numerous occasions:
To for his creative ways of doing science, he is a tribute to all creative thinkers and hard workers.
To for his assistance with computer programming; he is one of the greatest FORTH programmers ever born.
I would like to thank for his insight on many occasions, and particularly for his expertise in realigning the lasers.
To , , in the Chemistry Dept. Glass Shop - your patience and assistance was invaluable.
To , , and your machine shop knowledge helped make this work possible, and your humor made it that much more fun.

Special thanks go to at N.C. State for many helpful hints, shared design information and results before publication, and frank discussions on microwave cavities.

deserves special recognition for his much needed research advice which allowed this project to flow more smoothly and quickly to completion. I am deeply grateful for his contributions and the opportunities to participate with his research group.

Thanks go to the the Chemistry Dept. of Virginia Tech, particularly Drs. Wolfe and Graybeal, for doing as much as they did to ensure that I had financial support during my entire time in graduate school.

Professor Raymond Dessy, and his wife deserve special recognition for creating a unique research environment which allows students to grow and expand personally and professionally to the point where they are able to work independently at the Ph.D. level. Their encouragement and support is forever appreciated.

Table of Contents

List of Illustrations

List of Tables

I) INTRODUCTION

Modern technological problems have placed ever-increasing demands upon scientists to probe more deeply into the nature of matter. The field of analytical chemistry is no exception. It is the analyst's job to quantitatively and qualitatively identify the components of various industrial, medical and environmental samples. All manner of samples are the analyst's purview - organic, inorganic, organometallic and biological samples, comprising atomic and molecular gases, liquids, solids, and their mixtures. To have a single method of analysis for all types of samples is an analyst's dream. While it is unrealistic to think that one tool can be developed that is useful for all situations, tools which are more universal, selective, and sensitive can simplify the analyst's job and are always welcome.

It is the quest for more universal detectors which motivates much of the current research and development of new analytical methods. Analytical plasmas offer the potential of such universality for atomic analysis. Many types of plasmas have been investigated for use as analytical tools, from very low-current glow discharges and hollow cathode discharges, to spark and high-current arc discharges (1 , 2 , 3 , 4 , 5 , 6) Both direct-current and alternating-current power sources have been used.

Of the many alternating current plasmas, the radio-frequency inductively-coupled plasma (ICP) has been the most successful, if measured by the number of papers published. Many thousands more papers have appeared on ICP theory and applications than on any

other type of analytical plasma. ICP's are so well-developed for routine analysis because of huge fiscal and man-power investments by commercial interests.

By contrast, another type of analytical plasma, the microwave-induced plasma (MIP) has only evolved within the last decade to the point where its usefulness as a universal, selective and sensitive detector is beginning to be recognized. Commercial development of the MIP will greatly elevate its analytical utility, possibly making it rival that of the ICP.

Microwave resonant cavities, like many other plasma sources, can be quite troublesome until all of the design problems have been successfully solved using knowledge gained through experimentation. The critical electrical and mechanical design details of these cavities are still being identified and explored. Design parameters are almost well enough understood to allow commercial development. Microwave plasma research has developed from a not-very-well-understood art to more like a science.

The biggest problems which slowed the acceptance of MIP's into everyday usage by the analyst have traditionally been:

1) The need to operate MIPs at reduced pressure, which adds expense, complication, and labor to their implementation.
2) The inability of the MIP to tolerate solvents, particularly aqueous aerosol solutions, without being extinguished.
3) Inefficient power transfer to the MIP plasma resulted in over-heating of the microwave instrumentation.
   This has necessitated water or air cooling of instrumentation; including cavities, connectors, cables, and components.
   Such requirements complicate the operation of these plasmas.

As a general-purpose analytical atom reservoir, traditional MIPs had no chance of competing with the ICP, which operates at 1 atmosphere and handles aqueous sample solutions very well. MIPs were restricted to usage as gas chromatographic (GC) detectors (7) and electrodeless discharge lamps (EDL), which are sources of intense monochromatic light often used for photoionization and fluorescence studies (8). Low-pressure MIPs are well-suited as GC detectors since they require low gas flow rates, and can be vacuum-interfaced fairly easily. Electrodeless discharge lamps offer the advantages of low input-power requirements, freedom from electrode-material contamination, and the ablity to get different emission lines by changing discharge support materials.

The principal advantages of the MIP, its low power requirements, and low flow rates, have continually inspired investigators to develop its potential as an atom source for spectrochemical analysis. These advantages are significant for the MIP, since some of the major criticisms of the ICP have been its large power and gas consumption. Gas costs are particularly high since purified inert gases must be used. Such operating costs can easily equal the purchase price of the instrument over its lifetime.

Significant breakthroughs in overcoming the major MIP drawbacks were made by the new MIP cavity designed in 1976 by Beenakker (9 , 10 , 11). Using his original design for an MIP resonant cavity, it is possible to sustain helium and argon MIPs at atmospheric pressure **WITH** aqueous aerosol flowing into the plasma. Aqueous aerosol operation requires either slightly higher power operation or aerosol desolvation to remove most of the solvent. However, problems with plasma extinction are greatly diminished, and the plasmas operate at 1 atmosphere.

This breakthrough spawned further development, to the point where the Beenakker cavity is the most successful MIP plasma source thus far. Yet problems still remain due to inefficient power transfer (hence overheating) and aqueous sample introduction (12). And, it is not possible to generate low-power molecular plasmas using Beenakker's original design.

The research presented in this dissertation solved the problem of efficient power transfer to molecular microwave plasmas, which in turn facilitated aqueous aerosol introduction.

A Short History of This Research

In this work the development of a plasma resonator cavity for nitrogen was originally motivated by the search for a very efficient source of active nitrogen. A high concentration of metastable nitrogen molecules was desired as the energy-transfer medium in a laser-assisted ionization scheme designed to eliminate one or more of the laser photons needed to excite an analyte to the ionization continuum. The energy of the metastable nitrogen molecule (6.1 eV) would replace a high-energy UV laser photon. Normally 2 or 3 laser photons are required to reach the ionization continuum for most elements. This requires rather heroic instrumentation and involves considerable cost.

The scheme for metastable-energy-transfer-assisted resonance ionization spectroscopy is called METARIS. A diagram of the METARIS process is given in Appendix C, Figure 115 on page 306. Experiments done by Jim Bergquist in our laboratory using a nitrogen laser and a hollow-cathode discharge as a source of active nitrogen gave results that indicated that a higher concentration of active nitrogen was required if these species were to substitute for a laser photon (13). Higher operating pressures and an alternate energy pump were suggested as a solution in the literature (14).

Microwave plasmas were chosen because microwave generators are readily available. They are low cost, easy to use, and the circuitry requires few components. This required the development of a resonator cavity capable of sustaining microwave discharges in nitrogen at atmospheric pressure using a low-power generator. Subsequent spectroscopic investigations of this excitation source showed that it does not produce a great deal of active nitrogen because of the quenching which occurs at atmospheric pressure. Later experiments by the

author using a CW-laser, the microwave cavity developed, and a microarc sampler gave signal-to-noise ratios which probably preclude the use of the METARIS technique for routine analytical work. However, the cavity development did open several exciting areas of research. Early experiments clearly demonstrated easily visible, very intense fluorescence signals. The METARIS experiments were therefore abandoned in favor of examination of laser-induced fluorescence (LIF).

It became obvious that the first stage in developing this technique into an analytical method, was a complete physical characterization of the plasma to elucidate how the plasma spectrometer system's major variables (flow rate, applied power, observation height, gas composition, and laser power) affected the observed fluorescence. The spectral features of the analyte atomic emission also needed characterization since atomic emission represents a major source of background noise in many fluorescence methods. These studies are also interesting in their own right since emission spectroscopy is also a very powerful tool used for analysis.

Early in the characterization of the plasma as an atom source for fluorescence it was found that erratic operation of the microarc sampler was a major source of noise. The microarc sampler is a low-current, high-voltage, half-wave rectified glow discharge formed between two electrodes. It operates near the glow-to-arc plasma transition region (15). It is a discrete sampler which efficiently sputters and atomizes samples from a low-temperature filament. It is very small in size, and handles low-microliter quantities of sample. The microarc sampler was particularly irreproducible as it aged or became contaminated by analytical debris. Consistent operation is highly dependent on the surface conditions of the two electrodes. This is not a variable that is easy to control in routine practice. Electrode replacement proved to be the only way to reinstate optimum functioning of the sampler. This was too time-consuming and labor-intensive to be used in an extensive characterization of the MIP which could extend over a few hundred hours.

Recognizing that a continuous sampler would make plasma characterization easier, a continuous, glass frit nebulizer was adopted and optimized for the MIP flow characteristics (16). It is described in Chapter III, Section B. It worked very well and was used to physically characterize the MIP as an atom source for fluorescence and emission. This work forms the major portion of the dissertation. The instrument's performance was then optimized to produce maximum signal intensities and analytical feasibility studies were performed.

During the course of the LIF experiments, an interesting and potentially useful observation was made. There was a noticeable delay between the time the laser beam was turned out of the plasma and the time that the analyte emission signal returned back to the ambient level. This suggested that significant plasma heating was occurring because of the absorption of the laser radiation. And that there was probably a measureable laser-enhanced ionization (LEI) effect. Since the apparatus for the LIF and LEI experiments do not differ much, the LEI experiments were tried again before the entire system was dismantled. Strong LEI signals for sodium were detected!! This is the first time that this effect has been observed in any MIP. Enough data was gathered to characterize the LEI effect for analytes in the MIP, and to prove the feasibility of this technique for atomic analysis.

Statement of Purposes and A Synopsis of Experimental Results

The purpose of this work is to further explore and develop the potential of the MIP as a tool for analytical atomic spectroscopy. Specifically, this dissertation focuses on two things.

1. Development of a low-power molecular MIP at 1 atmosphere.

2. Characterization of the MIP, particularly the nitrogen MIP, as an atom source for atomic emission and laser-induced fluorescence spectroscopy.

First, a low-power, microwave-induced plasma resonator cavity was developed for use at atmospheric pressure with molecular support gases, particularly nitrogen gas. The resonator cavity is a modified Beenakker-type, internally-tuned, TM-010 cavity, called the "High-Efficiency TM-010 MIP Cavity" , (17). The cavity developed for molecular plasmas is different from the that for monatomic plasmas. Thus, the name "High-Efficiency Molecular Microwave Plasma" (HEMMP) cavity is used to differentiate it from ones used for monatomic support gases. Chapter II, Section B. discusses the cavity design considerations and constructional details.

The cavity is the most power-efficient resonator developed to this date for nitrogen microwave plasmas at one atmosphere. As little as 38 watts of applied microwave power is required to sustain a dry nitrogen plasma at 1 atmosphere. **With** an aqueous aerosol flowing thru the plasma, stable plasmas of nitrogen with good atomization and excitation properties can be generated with as little as 50 watts of power. Experiments to characterize how power transfer efficiency is affected by microwave antenna probe geometry were performed. For nitrogen-containing plasmas a straight-wire probe provides the best power transfer. With this type of probe, the nitrogen MIP cavity tuning is relatively insensitive to flow rate and power changes as compared to argon MIPs.

Spectral characterizations of the nitrogen emissions indicate that much quenching of the metastable ("active") nitrogen is occuring. The nitrogen MIP has visible yellow and blue bands. These are called, respectively, the First Positive and Second Positive emission bands of the nitrogen molecule. The metastable state believed to be most responsible for metastable energy transfer from active nitrogen to analytes is the N_2 (A) state. Large quantities (0.1%) of this species are indicated by the presence of detectable UV bands (called the Vegard Kaplan bands). The absence of such measureable bands in these studies indicate that metastable energy transfer due to the N_2(A) state of active nitrogen is not the predominant mechanism of excitation in the nitrogen MIP.

Spectroscopic temperatures were studied as a function of 3 variables: observation height above the cavity, support gas composition (% argon in nitrogen), and microwave power applied to the cavity. Spectroscopic temperatures are greatest near the cavity wall and inside the cavity. They do not vary appreciably for different mixtures of argon in nitrogen. Spectrocopic temperatures range from 4250 to 5350 degrees K as power is varied from 90 to 180 watts.

The problem of water quenching the plasma has been eliminated with the cavity described herein. Sample introduction is traditionally the Achilles' heel of analytical spectroscopy; for MIP's, solvent loading of the plasma often causes the plasma to extinguish. Putting water vapor, in particular, into MIPs was a problem because of the very large microwave power absorption band of the water molecule around 2450 MHz. The same absorption band normally used to cook food in microwave ovens, is so strong that previous low-power MIP's did not possess the necessary energy density to handle more than miniscule amounts of water. The nitrogen plasma is very tolerant of water vapor aerosols, being able to handle over 1 mL/min.

The final result is a plasma source which is robust, and low-cost to build and operate; and it provides good vaporization, atomization, and excitation properties. Experimental details and results of the MIP cavity experiments are discussed in Chapter II, Section C.

Second, applications that use the Highly-Efficient Molecular MIP source were explored. A spectroscopic instrument was constructed which incorporates the MIP source. Measurements were done using the nitrogen MIP as an atom and ion source for continuous-wave (CW) laser-induced fluorescence (LIF), and as an atomization, ionization, and excitation source for conventional atomic emission spectroscopy (AES). *This is the first time that laser-induced fluorescence has been observed and extensively characterized in any microwave plasma.*

The operating parameters that most affect performance of plasma systems for spectrochemical analysis, such as the MIP, ICP, and other electrical discharges are: power applied to the discharge, flow rate of the discharge support gas, and viewing geometry. In the MIP and ICP the discharge pressure is normally 1 atmosphere; for other types of discharges, pressure is often varied and critically affects spectrochemical performance. The spectrochemical experiments performed for this work critically evaluate how applied microwave power, support gas flow rate, support gas composition (mixtures of N_2 and Ar), and observation height affect the signal and the noise background, hence analytical performance of the instrument constructed.

In addition to nitrogen MIPs, characterization of argon and mixed argon/nitrogen MIPs as atom sources for LIF and AES was also done to allow direct comparisons of all three types of plasmas to be made. This is important since different types of MIP's are most often compared using different instrumental setups.

LIF and AES signals are greatly affected by changes in microwave power, flow rate, and gas composition. The lowest flow rates provide the most intense LIF and AES signals in nitrogen-containing plasmas. Pure argon plasmas require low to medium flow rates to give the most intense LIF and AES signals. Large changes in microwave power greatly affect the extent of analyte atomization and ionization in the plasma. Hence, the intensities of atomic and ionic fluorescence and emission are significantly affected by large variations in microwave power. Gas composition greatly affects intensities measured for LIF and AES, wherever plasma excitation energy is needed beyond atomization alone. Low concentrations of nitrogen in argon favor the production of excited atomic and ionic analyte states from which LIF and AES can proceed.

Results for LIF indicate the optimum instrumental settings are fairly element-specific, particularly observation height and applied microwave power. This is to be expected when one considers the differences in the ionization and excitation potentials of the analytes

introduced, and the excitation temperatures in the plasma. Another variable studied which significantly affects LIF intensities is the laser light intensity. Laser saturation of the optical atomic transitions did not occur at the maximum CW laser powers of 300 milliwatts. Results from the LIF and AES characterization studies are presented in Chapter III, Section C.

Finally, analytical feasibility studies were done which provide estimations of the utility of these methods in comparison with others. Analytical working curves were constructed using aqueous solutions of Na and Ba spanning six to seven orders of concentrative magnitude. Linear dynamic ranges (LDR) were extracted from these calibration curves and limits of detection (LOD) were calculated.

The analytical feasibility studies give limits of detection in the very low parts-per-billion (ppb) range for LIF and sub-parts-per-million range for AES. Linear dynamic ranges ranged from 3 to 5.5 orders of magnitude for both LIF and AES. All of these studies were done using sodium and barium as test analytes. Experiments were also done to see how LDR's and LOD's vary with MIP power and gas composition. All of the experimental details and results are discussed in Section C of Chapter III.

And the work provided its own lagniappe. Curiosity prompted one last experiment exploring the laser-enhanced ionization concept that initially nucleated this work and that of Bergquist (13). ***A laser-enhanced ionization (LEI) effect was detected for Na, Ba and Li analytes introduced into the MIP.*** The effects of electrode voltage, electrode geometry, microwave power, laser power, and analyte concentration on the observed LEI signal were measured. These experiments are the most crucial for characterizing these phenomena. Sodium was used as a representative element for these studies. Signals are seen to be linear over 3 orders of magnitude, with a sodium limit-of-detection of 10 parts per billion. Feasibility has been clearly demonstrated for this new analytical method. The apparatus, experiments, and results on laser-enhanced ionization are described in Appendix C.

Next to the development of the Highly-Efficient low-power N2-MIP at 1 atmosphere, the major thrust and most significant contribution of this work is the physical characterization of this new plasma as an atom source for fluorescence and emission spectroscopy. This work provides the fundamental physical chemical research needed for development of the low-power nitrogen MIP as a routine analytical tool.

II) DEVELOPMENT OF A HIGH-EFFICIENCY MOLECULAR MICROWAVE PLASMA

A) HISTORICAL SECTION

After a brief introduction to microwave induced plasmas (MIP's), the history of the TM-010 MIP cavity will be discussed. Since the first TM-010 cavity for spectrochemical analysis was designed by Beenakker in 1976 (9), empirical and theoretical knowledge about TM-010 cavities have been inseparably intertwined, and have advanced together at every step. Virtually all advances have been made with experimenters leading the way. The High-Efficiency Molecular Microwave Plasma (abbreviated "HEMMP") cavity developed by the author is the result of incorporating many previous design improvements into one device. Singular improvements to different cavities were made by various investigators, but the improvements were not all incorporated into one device until the author's work.

The history, theory, and evolution of the TM-010 MIP cavity for spectrochemical analysis can best be understood by integrating pertinent theoretical details at the appropriate points in the historical development. Separating theory from history artificially divides the story into pieces which evolved simultaneously. This chapter focusses on the historical and theoretical

development of TM-010 cavities by other investigators. The next chapter focusses on the TM-010 nitrogen MIP cavity developed by the author.

What is a Microwave Plasma ?:

Plasmas are the fourth state of matter. Plasmas are an electrically-neutral mixture of neutral and ionized matter made of atomic, molecular, or nuclear constituents, in the solid, liquid, or gaseous state. The plasmas under study in this dissertation are gaseous atomic and molecular plasmas. Gaseous plasmas are electrified gases with atoms and molecules dissociated into electrons and positive ions. The electrons in these highly-energetic gases possess enough energy to collide with neutral atoms and ionize them. In electrical discharge plasmas, electrons acquire their energy from the applied electric field. A plasma is self-sustaining if, on the average, each electron has enough energy to create one new electron in the time required for an electron to recombine with an ion or diffuse to the walls of the container.

Microwave-induced plasmas (MIP's) use high-frequency potentials to accelerate electrons to very high speeds. MIP's use some kind of structure to concentrate the electrical energy; the most common containers are rectangular waveguides and resonant cavities. Neutral gases are passed through the structure at the point of greatest electric field intensity. Dielectric breakdown (ionization) of the gas occurs if the electric field is intense enough. The two factors which most influence the dielectric properties of the support gas, hence dielectric breakdown and plasma ignition, are the support gas composition, and its pressure. Once ignited, there is enough energy to atomize and excite species introduced into the plasma. Spectrochemical analysis can then be performed on the excited and ground states of the atoms and ions in the plasma.

Microwave Plasmas - Characteristic Properties:

Microwave plasmas are promising sources for spectrochemical analysis. They possess

numerous advantages over the currently dominant competitor, the inductively-coupled plasma (ICP). Major advantages offered by MIP's are a low initial investment and low operating costs. These cost advantages accrue from the low power and gas consumption, and low cost instrumentation. Power consumption is typically 200 watts or less. Low-power MIP's offer further cost advantages because of the reduced cost of the generator, associated microwave instrumentation, and power used over the lifetime of the generator. Most MIP's in use today operate at 2.45 GHz. This is the frequency generated by most microwave ovens, and their magnetrons are a good, low-cost source of microwave radiation. Low-power MIP's require no air or water cooling of the discharge torch, as is needed by an ICP. Gas consumption is of the order of 1-2 L/min. ICP's require typically 15 L/min of support gases, plus an additional 1-2 L/min for nebulizer gases. Operating costs for the ICP can easily equal the cost of the instrument within its lifetime. An MIP system costs typically $5000 to $10,000 to implement, an ICP can range from $25,000 to $50,000. These savings give the MIP a significant advantage.

Spectroscopic advantages offered by MIP's are a low spectral background, a high degree of atomization and ionization, and very high electron and excitation temperatures. Elements with very high excitation potentials can be effectively excited when helium is employed as the support gas. In particular, the nonmetals are effectively excited, elements which the ICP handles poorly.

There are several practical advantages inherent in MIP's. There are no dangerous high voltages to shock the operator, or RF coils to pose hazards to the operator. There are no electrodes to corrode or cause chemical interferences and the reaction vessels are simpler. Microwave operating frequencies of 2.45 MHz require no bulky shielding to protect electronic recording equipment, such as photomultiplier tubes, computers, and x-y recorders. Only when reflected power is high is power radiated into the atmosphere. All radiation is well-contained under normal operating conditions. These advantages make the MIP a worthwhile candidate for further research and development.

The primary disadvantages of MIP's are, for the most part, problems that may be solved through further investigation. The MIP plasma is farther from thermodynamic equilibrium than the ICP, excitation temperatures are in the range 4000-6000 degrees Kelvin, and gas temperatures about 2000 degrees Kelvin. Operation at atmospheric pressure is difficult, particularly with aerosols at low-power. This usually limits its operation to low pressures. There are difficulties with sample desolvation and vaporization, and a sensitivity to the introduction of molecular species. This has limited sample introduction methods to gaseous samples, microsamples, vapors from gas chromatography systems, and solution nebulization. These problems can be solved with more efficient power transfer and molecular support gases.

Applications of MIP Detectors:

Traditionally the most common application of an MIP has been as a detector for gas chromatography, although some early research focused on the MIP as a spectroscopic source in its own right. Two excellent reviews have recently been written that discuss GC applications of MIP's in depth. A quick summary will be presented here for completeness (12, 7).

A helium MIP is customarily used as a GC detector for several reasons. Helium is a good GC column carrier gas because it is inert. Its low molecular weight allows quick analyses since it rapidly partitions analytes between the carrier stream and the porous stationary phase. Its low MW also gives a high linear velocity without sacrificing the quality of sample separations, and without causing the excessive band broadening of higher MW carrier gases. Helium MIPs also possess large excitation energies because of the high-energy atomic metastable states at 19.82 and 20.61 electron volts. Argon MIPs have been used, but excitation energies of the argon atom metastables are considerably less, 11.55 and 11.72 electron volts. Organic compounds eluting from a GC are more completely atomized in

a helium plasma, and therefore atomic line spectral intensities of the GC eluents are increased relative to those in an argon plasma.

A helium MIP shows less sensitivity to quenching and plasma instability than argon when water is introduced into the plasma as an aerosol. However, using low-power (< 200W) microwave generators it is difficult to generate stable discharges at 1 atmosphere using helium or "wet" argon as the support gas. One typically has to work at reduced pressures or higher powers. Reduced-pressure helium MIPs work well but have the distinct disadvantage of requiring vacuum technology.

Other advantages offered by MIP's as GC detectors are its great sensitivity and selectivity (12). Only mass spectrometers and electron capture detectors offer better sensitivities. GC-MIP detector sensitivities do not vary widely with the type of sample. They can operate in a single-element mode, which greatly simplifies the resulting chromatograms. GC-MIP detectors also give rapid response and have a wide dynamic range (22.). GC samples are small in size and require no desolvation or vaporization. These detectors also facilitate metal speciation of inorganic, environmental, and toxicological samples when operated in the single-element mode. The MIP has established a strong application base as a GC detector. As a spectroscopic atom source it has lagged behind because of the problems mentioned above, primarily solvent loading and the requirement of low-pressure.

TM-010 MIP Cavities - Historical and Theoretical Developments:

In 1976 Beenakker designed a TM-010 resonant cavity capable of sustaining a low-power helium plasma at 1 atmosphere (9 , 10 , 11). The Beenakker cavity was the first cavity to work well at atmospheric pressure using helium or "wet argon" as the support gas. A TM-010 cavity performs well at atmospheric pressure because of the high energy density inside the rather small (typically 22 cc) volume resonator. The electric field intensity, greatest at the center of the cavity, is sufficient to cause and maintain dielectric breakdown in the gas flowing through the center of the cavity. See Figure 1 on page 17.

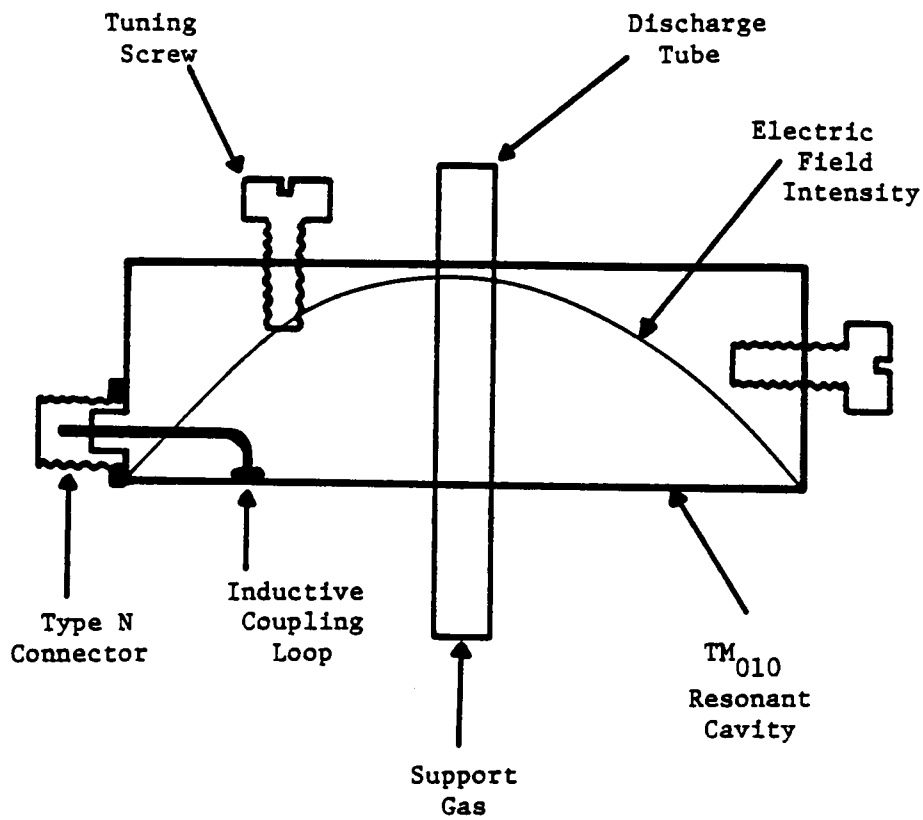

Figure 1. Typical Beenakker Cavity

Beenakker's original cavity worked well as a GC detector, requiring from 20-150 watts of microwave power while using from 30-500 mL/min of support gas. These low flow rates were possible because a very small diameter (1.45 mm i.d.) silica tube was used. When an aqueous solution nebulizer was coupled directly to the cavity the helium plasma was stable down to 50W, and argon down to 20W. This configuration required 1.2 L/min of support gas.

No mention was made of the reflected powers present in Beenakker's original system. However, above 75W applied power, air cooling was necessary to prevent the discharge tube from melting. This indicates that substantial power was being wasted as heat. Besides the overheating problems, there were other functional problems with the original design.

Many problems were encountered by later investigators who copied the original Beenakker design, including Beenakker himself (18 , 19). Particular problems plagued these early users of the TM-010 cavities. At times the plasma discharge could not be initiated at all. Once the discharge was initiated not all of the reflected power could be eliminated. This problem still exists in very many cases today, and is due to improper impedance matching. Reflected power should be minimized so that the system runs cool without the need for air or water cooling. Using the original design, so much power was being wasted as heat that the cavity and the connectors became too hot to touch. This greatly shortens the life of the microwave connectors and the discharge tubes used with the cavity.

TM-010 Cavity Tuning, Impedance Matching, and Power Transfer

A discussion of frequency tuning and impedance matching, and how they are related to power transfer will help to further clarify some key theoretical concepts used later in the historical discussion of the TM-010 cavity.

TM-010 Cavity Tuning:

Tuning means matching the dimensions of the cavity to be an integral multiple of one-half wavelengths of the radiation being introduced into the resonant structure. This defines a cavity that is in resonance with the generator. The Beenakker cavity uses the fundamental mode, which establishes a one-half wavelength standing wave pattern of the electric field, (see Figure 1). All higher electromagnetic modes are undesirable and should be eliminated.

The original Beenakker design has 2 adjustable tuning screws placed radially and axially in the cavity to allow one to effectively narrow the diameter of the cavity and shorten the height of the cavity, respectively. Once a plasma is ignited, the TM-010 cavity requires retuning since the dielectric properties of the ionized plasma differ greatly from those of the neutral support gas. With these tuning screws the cavity volume could be retuned to accommodate the frequency of the generator operating at 2450 MHz. A problem which became evident to later investigators was that the metal tuning screws used to minimize reflected power provided some range of tunability but were unpredictably erratic, rather than smooth and continuous. They also did not eliminate all reflected power and were not used much (18 , 20).

The erratic tuning characteristics of the metal tuning screws arose because higher resonant modes would sometimes unpredictably become stable within the cavity. Constructive interference between these higher modes and the fundamental mode further complicated the situation. The end result was that the reflected power would appear to jump erratically.

Electromagnetic theory states the mathematical design constraint for the TM-010 resonant cavity as

$$f = \frac{c(k_{01})}{\pi \times d}$$

where f = resonant frequency

c = speed of light

k_{01} = 2.405 and is the 0th root of the 1st order Bessel Function

d = cavity diameter

It is useful to notice that the tuning condition depends only upon the diameter of the cavity and not upon the height of the cavity. One can take advantage of this fact when designing for longer residence times (taller cavity height) or higher electric field intensity at a given microwave power level (shorter cavity height).

The equation shown above is for a cavity with no dielectrics within the resonant structure. The discharge tube, the support gas, and the plasma (once it is ignited), all possess dielectric properties which must be considered when designing the cavity. Dielectrics within the resonant cavity shift the resonant frequency to lower values, effectively making the cavity appear as though it were larger. For this reason the cavity is always designed to have a somewhat smaller diameter than will accomodate the typical MIP power generator operating at 2450 MHz. The dimensions are not as easily varied in this type of cavity as they are in an Evenson or slab-line cavity. Normally, the diameter and the height are essentially fixed when the cavity is machined, although Bollo-Kamara et. al. (20) and Rait et. al. (21) have used used extender rings to study emission intensity as a function of cavity height.

The stability point for efficient ignition of an MIP is different than that for stable operation. Two different cavity diameters are required, one for plasma initiation, and another for plasma operation. A high electric field density is required for reliable ignition. Igniting a plasma in the cavity results in "detuning". Power increases cause plasma density increases, which result in further detuning, since plasma dielectric properties change. Such detuning problems

limit the amount of energy which can be absorbed by the plasma without retuning 12.. Retuning usually requires changing cavity dimensions or generator frequency.

An easy way to "vary" the cavity diameter is to radially introduce more or less dielectric into the cavity, tuning it into resonance. The cavity's resonant frequency shift is dependent upon at least two factors: the volume of solid dielectrics introduced into the cavity (as the discharge tube and the tuning elements), and the change in dielectric constant of the support gas as it goes from a neutral to an ionized gas.

Beenakker took advantage of such frequency shifts by cutting a slot in the cavity from the center over to the wall of the cavity and then moving the discharge tube toward or away from the center of the cavity. The tube has the greatest interaction with electric field at the center, and in fact has a nonlinear cosine-type dependence as one inserts the dielectric closer to the cavity center. This type of dependence is to be expected from the sinusoidal nature of the standing wave in the cavity. However, moving the discharge tube away from the center decreases the maximum possible interaction of the electromagnetic radiation with the plasma and so is not an optimal method for tuning.

Another approach, used by Bollo-Kamara and Codding, is to vary the wall thickness of the discharge tube until the required shift is obtained (20). This approach does not allow dynamic retuning as dielectric properties change due to an alteration of flow rate and power conditions. An alternate approach used by previous workers is to leave the discharge fixed at the center of the cavity and to introduce extra dielectric into the cavity through the radial cavity wall. This allows one to have the best configuration for plasma/electric field interaction, and to have maximum tuning capability.

Experiments were conducted by van Dalen and de Galan to measure the magnitudes of the frequency shift as a function of the volume of dielectric introduced, and the shift due to the ignition of a helium plasma (18). Their work was the first to dynamically tune a

Beenakker-type TM-010 cavity using ancillary quartz tuning elements. This provided a significant improvement in tuning capability.

Power Transfer and Impedance Matching:

The ideal situation is to transfer ALL of the applied power through the cavity into the plasma, and to do this for all power levels. The maximum power transfer theorem in electrical theory states that maximum power is transfered when the impedance of the power source and its load are exactly matched, i.e., they possess the same impedance. Impedance is composed of a real part (purely resistive) and an imaginary part (a sum of inductive and capacitive components, also called "the reactive components").

A device such as an MIP cavity possesses resistance, inductance and capacitance, which are felt by the generator. Capacitance and inductance are frequency dependent. Devices such as quartz dielectric tuning rods affect both the resonant frequency, and the impedance matching characteristics of the cavity. This is how frequency tuning and impedance matching interact. The cavity is "tuned" so that the reactive components of the impedance exactly cancel each other out. Then the resistive load of the resonator cavity is "matched" to that of the generator. When the load impedance of the cavity equals the characteristic impedance of the transmission line, there are no reflected waves. Hence, standing waves that cause heating losses do not form on the transmission line. When the impedances are matched, this condition is known as "critical coupling", which gives maximum power transfer, or "unit power transfer".

All practical microwave systems, generators, transmission lines, and components currently used have characteristic impedances of either 50 ohms pure resistance, although 75 ohm components are sometimes used in microwave communications. This characteristic impedance should be explicitly specified when purchasing new components.

Characteristic impedances at high frequencies originate from geometric and dielectric factors. The characteristic impedance refers to the ratio of the electric field to the magnetic field, E/H. The point of introduction of radiation into the cavity should be where the E/H ratio equals 50 ohms. Since these field intensities change when a plasma is ignited, there should be a way to vary the point of power introduction into the cavity. Moving the coupling probe to the point where the E/H ratio is 50 ohms establishes critical coupling once again (see Figure 2 on page 24 for further clarification.)

The original Beenakker-type cavity, and virtually all modified Beenakker-type TM-010 cavities in use today, employ inductive (magnetic field) coupling to introduce microwave power. This is done using an inductive coupling loop entering through the side wall of the cavity and short-circuiting onto the bottom wall, (see Figure 1 on page 17). Coupling efficiency cannot be easily changed with an inductive coupling loop, although a variable-length loop has been used with limited success by Rait et. al. (21).

Van Dalen and de Galan were the first to use capacitive coupling into a TM-010 cavity (18). This mode of power introduction couples power through the electric component of the electromagnetic field. Van Dalen and De Galan were able to vary the penetration depth of the coupling probe by using a modified 1/4-wave Evenson cavity for mounting the probe.

Matus and Boss were the first to design an impedance mechanism which allows radial translation of the probe in a capacitively coupled cavity. This new design greatly improves power transfer into TM-010 cavities (22) The approach of Matus and Boss consists of an antenna probe which penetrates the lid of the cavity through a slot cut along its radius. The probe is mounted on a slider which allows probe translation from near the cavity center to the inside radial wall. Varying the radial position of the antenna probe allows the entire coupling device to move to the point where it feels a potential to current ratio (E/H) of 50 ohms (see Figure 2 on page 24).

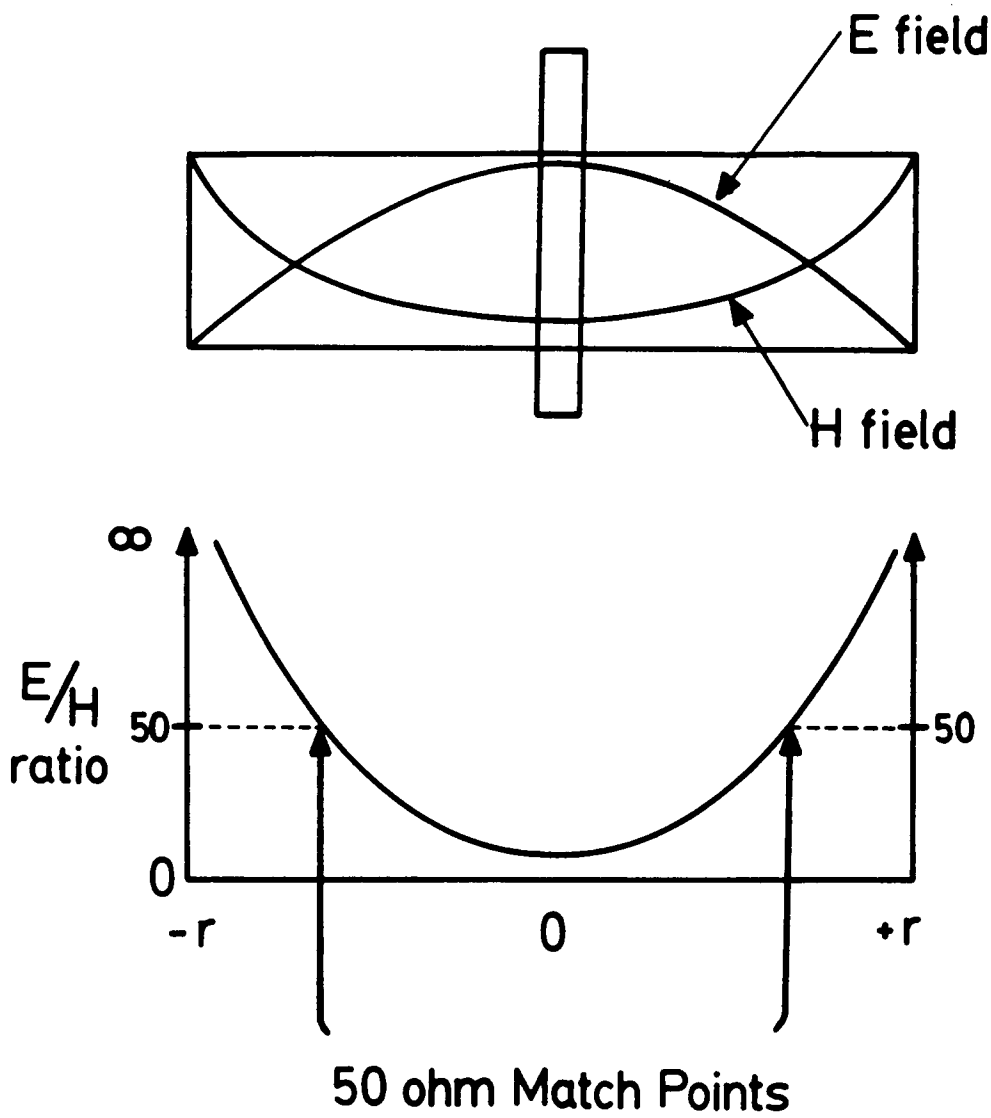

Figure 2. Electric and Magnetic Field Patterns in a TM-010 Cavity

Boss has also found that varying the size and shape of the probe tip greatly varies the extent of inductive and capacitive coupling (23). The best power transfer in an argon MIP is achieved with a circular disc on the end of the antenna probe. Increasing the disc area increases power transfer efficiency. The largest probe area employed was 635 square millimeters (a 19 mm diameter disc). This probe allows 99.999% power transfer efficiency of over 100 watts of microwave power into argon plasmas in a TM-010 cavity.

This power transfer efficiency is a significant improvement over all previous TM-010 cavities. This type of cavity is called the "High-Efficiency" TM-010 cavity to separate it from all previous cavity designs. This cavity has only been used for argon and helium plasmas. It has not been employed for molecular plasmas, which offer distinct advantages that are discussed at the end of this chapter.

Microwave Plasma Theory - Mechanisms of Analyte Excitation:

In MIP's neutral, excited, and ionized gas atoms and molecules exist, as do metastable atoms and molecules. Metastables are excited state species with excited state lifetimes of 1E-3 seconds to greater than 1E+3 seconds. There are also two groups of free electrons, a high-energy group and a low-energy group. There is line emission from atoms, ions, and molecules. No single proposed mechanism accounts for all observed phenomenon. State populations, atom, ion, electron and metastable concentrations, and line intensities cannot be easily predicted using any known plasma model. However, a brief overview of the current views of the excitation processes will be presented to orient the reader for future discussions. First the dominant plasma processes will be discussed, followed by models which incorporate these various processes.

Electron Collision Processes:

Low energy electrons participate in ion-electron recombination reactions (eq. 1). B is a third body required to carry away the energy resulting from recombination. Species B can

carry away the energy as translational energy, or be excited to a higher energy state, from which it can later emit radiation. The photon emitted is continuum radiation since the third body can move away with any magnitude of translational energy. Species B or the ion can be an analyte atom or a plasma gas molecule.

electron + ion + B -----> atom + B + photon (1)

High energy electrons participate in the reverse process of analyte ionization (eq. 2), which is responsible for sustaining the electron concentration, hence the plasma. The resulting ion can emit radiation if the electron transferred more energy than that required for ionization.

electron + atom -----> ion + 2 electrons (2)

High energy electrons can also excite analyte atoms or ions directly, which will subsequently emit photons of discrete wavelengths. This is shown in equation 3.

electron + analyte -----> excited analyte (3)

Metastable Energy Transfer Processes:

Metastables are usually formed "from the top down" through an ionization-recombination mechanism, or through a highly-excited state which is collisionally de-excited down to the metastable state by ground-state support gas molecules. They can also be formed through excited-state energy-pooling processes that involve two or more excited species which combine their energies to produce a metastable with the energy of both excited state species (43).

Metastable atoms and molecules of the support gas can transfer energy over to analyte atoms and ions through the following process:

metastable + analyte -----> excited analyte (4)

The excited analyte can lose its energy through collision with plasma gas or through photon emission.

Penning Ionization:

If the excited analyte in eq. 4 subsequently ionizes, the process is called Penning ionization.

excited analyte -----> ionized analyte + electron (5)

Penning ionization is more probable than metastable energy transfer followed by emission, since an exact match of metastable to analyte energy is not required.

Current Models for Analyte Excitation:

Collisions with free electrons do not account for the observed emission line intensities. A continuous range of energies is available to electrons since they undergo frequent collisions which randomize their motions, particularly at high pressures. Thus one would expect to observe line intensities distributed according to a Boltzmann distribution, which is not the case. Also, emission line intensities do not exhibit the expected decreases with increases in pressure; electron energies decrease as pressure increases because electron collisions become more frequent (25).

Metastables are seen to be crucial for analyte excitation, both directly and through Penning ionization. Helium atoms possess metastables at 19.7 eV and 20.5 eV; helium excimers have energies in the range of 13.3-15.9 eV and 18.3-20.5 eV. Argon has atomic metastables at 11.7 eV and 11.5 eV; argon excimers have energies at 14.0 eV and 10.2 eV. The large excitation energies of these metastables indicate that most elements in the periodic table can be excited using argon or helium metastables.

Non-metals exhibit particularly intense emission lines that originate in ionic energy states 12-16 eV above their ground state. Excitation of elements with intermediate excitation potentials does not always occur. This has been attributed to a "suprathermal" population of upper-level metastable gas molecules. It is most probable that metastables, not electrons, are responsible for non-metal excitation (10).

The radiative-ionization-recombination (RIR) mechanism is the most successful model for explaining the observed analyte emission line intensities. In this model, metastable support gas molecules cause Penning ionization of analytes, then analyte ion recombination occurs with slow-moving electrons. As the analyte recombines, it emits radiation.

This model predicts an increase in analyte emission with increases in microwave power. Power increases cause ionization to increase. The metastable concentration will also increase because of increased recombination. This occurs up to the point where electron density increases cause collisional deactivation of metastables. The RIR model also predicts increasing analyte emission as pressure increases, since at increased pressures there will be more electron-ion recombinations of support gas ions, due to the increase in slow-moving electrons (26 , 14). This results in more metastables. However, the RIR model does not accurately predict measured concentrations of metastable inert gas molecules (25).

A qualitative model of the ICP as a decaying plasma has recently been proposed (27 , 28). It is a "top-down" decay model of the plasma, where it is "decaying from a spatially

heterogeneous zone of primary energy input towards an equilibrium state." This classifies it as a high-energy afterglow. This is obvious since the primary discharge region is not directly viewed in an ICP; the analytical observation zone is 1-3 cm above the load coil. A decaying plasma model needs to take into account many factors. Lifetimes of metastable and radiative excited states of atoms, ions, and molecules need to be included. Electronic, vibrational, rotational, and translational energy transfer cross sections for transitions between the numerous states of these species are also needed. With a fixed energy input and support gas flow rate, the "equilibrium" concentrations of the various species may be calculated. Clearly, such a model will be more accurate since it does not assume any one dominant microscopic process. Dominant pathways would become evident from the calculations, not assumed at the start. This model is also applicable to the MIP since it has a region of primary energy input which decays to an afterglow after exiting the primary discharge. It is easier to apply to the MIP, which is a spatially-homogenous plasma.

The question of excitation mechanisms in MIP's is far from settled. Most likely a combination of the mechanisms outlined above are involved and can be used used to explain the observed spectra, and the measured electron, ion, and gas temperatures. Excitation by electron collision is most likely important for elements with low excitation potentials. Undoubtedly, metastable excitation of high-lying energy states is important for non-metals. The radiative ionization recombination model is important for the production of support gas metastables and excited analytes. The decaying plasma model of the MIP will bring together these individual processes into a unified mechanism.

Local Thermodynamic Equilibrium:

A discussion of plasma "equilibrium" will give the reader an understanding of the similarities and differences between argon and helium MIP's, molecular MIP's, ICP's, and flames.

Very few plasmas are truly in perfect thermal equilibrium, i.e., all species in the plasma, electrons, ions, and neutral species have the same characteristic temperature. The spectroscopic or excitation temperature, the ionization temperature, the electron temperature, and the rotational temperature (also called the "thermal" temperature) must all be equal. Certain small regions of a plasma may reach "local thermodynamic equilibrium" (LTE). However, most laboratory flames and plasmas deviate from LTE, and do so at all pressures. The one instance where the existence of LTE has been demonstrated is in an analytical flame. The secondary combustion zone, above the primary reaction zone, is in LTE. All other regions of the flame depart from LTE (29).

The situation is more severe for high-frequency electrical discharges. MIP's and ICP's are generally not in LTE (30 , 31 , 32). An argon ICP operating at 1000 watts has been demonstrated to be far away from LTE (33). Helium ICP's and MIP's are no closer to LTE (34., 28.). The only high-frequency discharges whose characteristics closely approach LTE are ICP's and MIP's with nitrogen-containing support gases. Molecular gases added to the support gas appear to have a thermalizing effect (35), i.e., rotational, vibrational, translational, and excitation temperatures are almost equal.

Nitrogen Plasma Characteristics

Nitrogen as the support gas in ICP's and MIP's offers certain advantages over the rare gases. It has a higher decomposition efficiency for refractory compounds (29). Also, the resulting plasma is thermally hotter, and it can be operated at lower flow rates than a pure Ar ICP. Analytical results with nitrogen ICP's yield detection limits for many analytes that are comparable to rare-gas ICP's (21 , 36 , 37 , 38 , 39 , 40).

The higher analyte decomposition efficiency results because analyte particles have rotational and vibrational degrees of freedom that can absorb energy from the plasma almost

continuously. And, this energy transfer occurs more efficiently from plasma species which have rotational and vibrational degrees of freedom, i.e. molecular plasma species. Thus the atomization process can occur easily just from the thermal energy of the plasma.

A thermally hotter plasma is attributed to the extra degrees of freedom which nitrogen possesses over the rare gases. Molecular electronic, vibrational and rotational energy storage modes give the nitrogen molecule a considerably higher heat capacity. These modes can store energy from the microwave field which can later be transferred to analytes (41).

The high thermal energy that nitrogen plasmas possess is also attributed to the energy of the nitrogen bond itself. Much of the heat in a microwave plasma is produced by re-association of nitrogen atoms dissociated by the discharge (42). This higher thermal energy produces smaller temperature gradients. Because the energy is more thermal, with fewer high-energy metastable states, a smaller fraction of the analyte is ionized (31).

Association of nitrogen atoms also generates "active nitrogen", metastable atoms and molecules with long lifetimes. The first excited triplet state of the nitrogen molecule, the "A state", is particularly effective at exciting metal atoms. In fact, this is the basis for a very sensitive detection technique, called "Metastable Energy Transfer for Atomic Luminescence" (METAL). In this method, a dielectric discharge (an "ozonizer-type" discharge) produces a high concentration of metastable nitrogen (1E+12 to 1E+16 molecules/cc, depending upon conditions), and vapor-phase metal atoms introduced downstream of the discharge are effectively excited (24). It is particularly effective for trace quantities of metal atoms. Concentrations as low as 1E+4 atoms/cc bismuth have been detected using a similar technique with active nitrogen, called "analytical photon catalysis" (44). Active nitrogen has been investigated for over 100 years, and possesses a vast literature (45). As yet, however, it has not found application as the basis of a major routine analytical technique.

Nitrogen also offers the advantages that it is more available, easier to produce in a pure state, and hence has a lower cost than argon or helium. This is a significant advantage in countries where argon is expensive or not produced locally (39). Nitrogen and other molecular plasmas require greater amounts of power to sustain. However, the cost of the increased power required is offset several times by the decreased cost of molecular gases compared with argon. (31).

Molecular MIP's - Previous Devices and Results

A direct comparison of all of the various devices used to generate molecular MIP's is difficult because the devices are so different. Radial resonant cavities, coaxial resonant cavities, and modified rectangular waveguides have all been used. Some involve capacitive coupling, while others use inductive coupling. And they been constructed for very different purposes, often with very little attention focussed on attaining maximum power transfer into the cavity. Each plasma source will be discussed in turn, describing the various design parameters and operating conditions.

With a 28" long, capacitively-coupled, high-frequency RF torch operating at 1000 MHz, Cobine & Wilbur generated Ar, He, air, carbon dioxide, oxygen, and nitrogen plasmas at 1 atmosphere. The torch could operate with up to 700 watts using the polyatomic gases, but would operate up to only 100 watts using the monatomic gases. The monatomic gases, Ar & He, gave cool flames. The tail flames would not even burn through a piece of paper. The polyatomic gases, oxygen, carbon dioxide, air, and nitrogen, gave very hot flames. Tungsten rods (M.P. = 3370 K) were melted when held in the tail flame. It is not clear if these torches required cooling; however, there were problems with the torch tips burning up. No mention was made of using this plasma source for analytical purposes. The work was done over 35 years ago, primarily for fundamental research in the lighting industry (42).

An air-cooled, quarter-wave coaxial cavity, frequency tuned by a variable piston was designed by Dupret, Vidal and Goudmand. It was used for both monatomic and polyatomic gases (46). Locqueneux-Lefebvre and Ricard generated nitrogen and air plasmas from 10 torr to 1 atmosphere using 130 to 420 watts of power coming from a 2450 MHz generator (47). Again no analytical studies were done. Vibrational excitation ratios were studied and the plasma was found to approach LTE conditions. Vibrational excitation temperatures were found to be in the range of 6000 to 10,000 degrees Kelvin. N_2 ion emissions were found to be predominant at high pressures and high powers. The full power (420 watts) was needed to sustain a nitrogen plasma at 1 atmosphere.

Using a capacitively-coupled single-electrode torch in a rectangular waveguide, Zhang et al sustained an air MIP at 1 atmosphere (32). The discharge tube penetrated the waveguide along the same axis as the antenna probe, and in this way bore some resemblance to a Beenakker cavity. It was used for analytical purposes and was found to be "more resilient to the introduction of water and other molecular species" ,and "could vaporize large amounts of solid samples quickly, (about 0.25 grams)", (48). Limits of detection were typically in the range of 0.1 to 10 ppm. The single-electrode atmospheric pressure MIP does have some problems with electrode contamination since the metal electrode is in the center of the 5000 degree plasma (49.). It was typically operated at 560 watts for an air plasma at 1 atmosphere.

A modified, inductively-coupled TM-010 cavity using nitrogen or air as the support gas was used for analytical purposes by Urh & Carnahan (31). The plasmas show good tolerance to aerosol introduction and gave detection limits in the range of 0.03 to 170 ppm. The flow torch required air-cooling in order that it not melt, even though the plasma support gas used was typically 2.2 L/min. The cavity required water-cooling and operated in the power range of 300 to 500 watts.

The MIP perhaps most similar to the one used in the author's research is that of R.D. Deutsch. He used an inductively-coupled Beenakker-type TM-010 cavity with an axial quartz

tuning rod. He shared his initial designs for the ICP-type tangential flow torch with this researcher. The minimum operating power required for Deutsch's cavity was typically 120 watts; the lower stability limit was 90 watts. However, 220 Watts was required for startup and water cooling was required for operation (50). For emission spectroscopic studies he found that the best S/N results were obtained at the highest power possible. The system was usually operated at 250 watts applied power, which was the limit of the microwave instrumentation.

B) EXPERIMENTAL APPARATUS

Design of the Nitrogen Microwave Plasma System - Overview

The low-power microwave resonator for nitrogen plasmas at 1 atmosphere and the attendant circuitry was designed with three constraints firmly in mind:

a) Lowest Possible Power Consumption

b) Lowest Possible Overall Cost

c) Simplicity

A low-power generator capable of outputting up to 120 Watts was already available in the laboratory. It was desireable to design a resonant cavity for nitrogen at one atmosphere that would use such a low-power generator. Low-power generators are becoming more available, and, as microwave ovens are being mass-produced, the prices of magnetrons are dropping to under $100. The magnetrons in modern microwave ovens are suitable as microwave sources for plasma spectroscopy. Chilukuri & Lichten have described the conversion of circuitry necessary to do this (51).

The most successful and popular cavity designs for atmospheric pressure MIP's are modified versions of the original Beenakker cavity design (9 , 10 , 11). While the MIP has been used successfully with helium and argon as the support gas, nitrogen and other molecular gas plasmas had not been maintained at 1 atmosphere using low-power microwave equipment. The existing Beenakker-type cavity designs for argon and helium plasmas all had problems with excessive power being lost as heat.

Early workers recognized that these heat losses were unnecessary and were due to impedance mismatches between the generator, cables, and microwave cavity. But due to such poor power transfer, it was not recognized that molecular plasmas could be sustained at 1 atmosphere with low power generators (< 200 Watts).

Impedance mismatches result in reflected waves, which cause standing waves to be established along the cables and connectors. This will cause local heating in the cables and connectors. At increased forward powers, reflected power will cause serious heating problems which greatly accelerate oxidation and shorten the life of all the microwave components - including cables, connectors, magnetrons and any other ancillary equipment.

After consulting with all of the current leading researchers using Beenakker cavities, all of the state-of-the-art (ca. 1983) improvements on the original Beenakker design were included in the design of a resonator for use with nitrogen. Singular improvements to different cavities had been made by various investigators, but the improvements remained separate. The author replicated these separate improvements by other workers, and incorporated them all into one cavity simultaneously. The resulting device gives heretofore unequaled performance for nitrogen MIPs at 1 atmosphere. Results of all of the improvements combined will be discussed after each one is explained.

TM010 Cavity - Design Improvements

Internal Impedance Matching Network:

The first major improvement used by the author was the internal impedance matching network designed by L. Matus and C. Boss (17). This accounts for the greatest reduction in power consumption. The internal impedance matching network eliminates the need for all

external matching and tuning elements. Prior to the internal impedance matching network, external double-stub and triple-stub tuners were used to impedance match the generator to the cavity. These external elements are often ineffective at eliminating all reflected power and also dissipate a great deal of heat (18 , 20 , 52). Air cooling of the tuning and matching elements, and air-cooling and water cooling of the cavities have been used to minimize overheating and oxidation problems. None of these solutions focus on the inherent problem - inefficient power transfer thru the cavity into the plasma.

The internal impedance matching and tuning system designed by Matus and Boss is the most efficient approach to date for solving this power transfer problem. Its great efficiency caused Boss et al to give it the name the "Highly-Efficient" or "High-Efficiency" TM-010 cavity to clearly separate it from all other types of TM-010 cavities, particularly ones called "internally-tuned". There have been other types of cavities with internal-tuning mechanisms, but they do not provide the efficiency of power transfer that Boss' approach does. Matus & Boss used this new cavity for argon and helium plasmas only. The author is the first investigator to use it for molecular support gases. See Figure 3 on page 40.

Quartz Tuning Rods:

The second major improvement used by the author is a quartz tuning rod introduced directly into the cavity for tuning purposes. This tuning method was first used for TM-010 cavities by van Dalen and de Galan (18). The cavity is both an inductor and capacitor at the microwave frequencies used, and forms part of a resonant circuit. Introducing dielectric materials into the cavity changes the capacitance of the circuit. It also changes the permittivity of the electric field within the cavity and modifies the apparent volume that the electric field experiences within the cavity. By introducing more dielectric into the cavity, the cavity volume is effectively increased (53). Quartz is the dielectric of choice for this purpose since it has a very high dielectric constant, yet it does not appreciably absorb microwave energy, and it is inexpensive compared with ceramics. Tuning the cavity resonant frequency

to the generator frequency using the quartz tuning rods works much better than the brass tuning stubs used in Beenakker's original design. The brass tuning stubs were experimentally found to be very ineffective, almost useless, in tuning the cavity.

Cavity Dimensions:

The third improvement to the original Beenakker design was modifying the dimensions of the cavity itself. Problems with the original design prompted the author to choose other cavity dimensions. The original cavity was 92.5 mm inside diameter, and 10mm in depth. In the literature it was noted that this size cavity could sometimes be difficult to ignite (18).

The first cavity constructed in this laboratory had a 92.1 mm inside diameter and 10 mm cavity depth, and used the internal impedance matcher with a quartz tuning rod. While it was possible to ignite a nitrogen plasma in the cavity, it was necessary to do so at reduced pressure (about 10 torr) and then slowly bring the pressure up to one atmosphere. While the pressure was being brought up to one atmosphere the quartz rod and impedance matcher positions had to be iteratively adjusted to minimize reflected power. If at any time the reflected power became greater than 50% of the forward power the plasma would extinguish. The cavity behaved as though it were as stable, yet near the edge of an instability region. At higher pressures and flow rates the insertion of the quartz rod into the cavity (which effectively makes the cavity larger) extinguished the plasma. The radial brass tuning stub needed to be inserted over 3/4 of its length into the cavity (which effectively makes the cavity smaller) to help minimize reflected power. All of these factors indicated a smaller cavity was needed.

Nitrogen gas presents a couple of special characteristics which need to be taken into account. It possesses a greater dielectric strength than argon or helium.

Gas	Dielectric Constant
Nitrogen	1.000580
Helium	1.0000684
Argon	1.000517

A larger dielectric constant means a greater shift in resonant frequency. A slightly smaller inside-diameter cavity is needed for nitrogen than for argon or helium.

Also, nitrogen possesses a heat of molecular dissociation which argon and helium do not. This means a higher energy density (hence electric field intensity) will be needed inside the cavity. Thus nitrogen plasmas will generally need more microwave power to be operated at a stable steady-state.

Using the design data and criteria discussed by van Dalen et al (18) a cavity diameter of 88.3 mm was chosen with a cavity depth of 6.0 mm. A shorter depth increases the electric field intensity, particularly in the center of the cavity where the plasma discharge tube is located. After construction of the new cavity, it was found that the plasma would not ignite at all no matter what power, pressure or gas (Ar, N_2 or He) was used. After hollowing out the cavity to 89.1 mm I.D. and 8.9 mm depth, the cavity performed very well, giving an N_2 plasma which ignited easily with 90 watts forward power, 15 watts reflected power. After reflected power was minimized by adjusting the impedance matcher and quartz tuning rod, the power was then reduced to 53 W forward power, 0 Watts reflected power. This cavity works well with nitrogen support gas, is easy to ignite, and relatively stable. It is quite sensitive to changes in quartz rod position, and small changes (1/8 inch) cause significant alterations in reflected power.

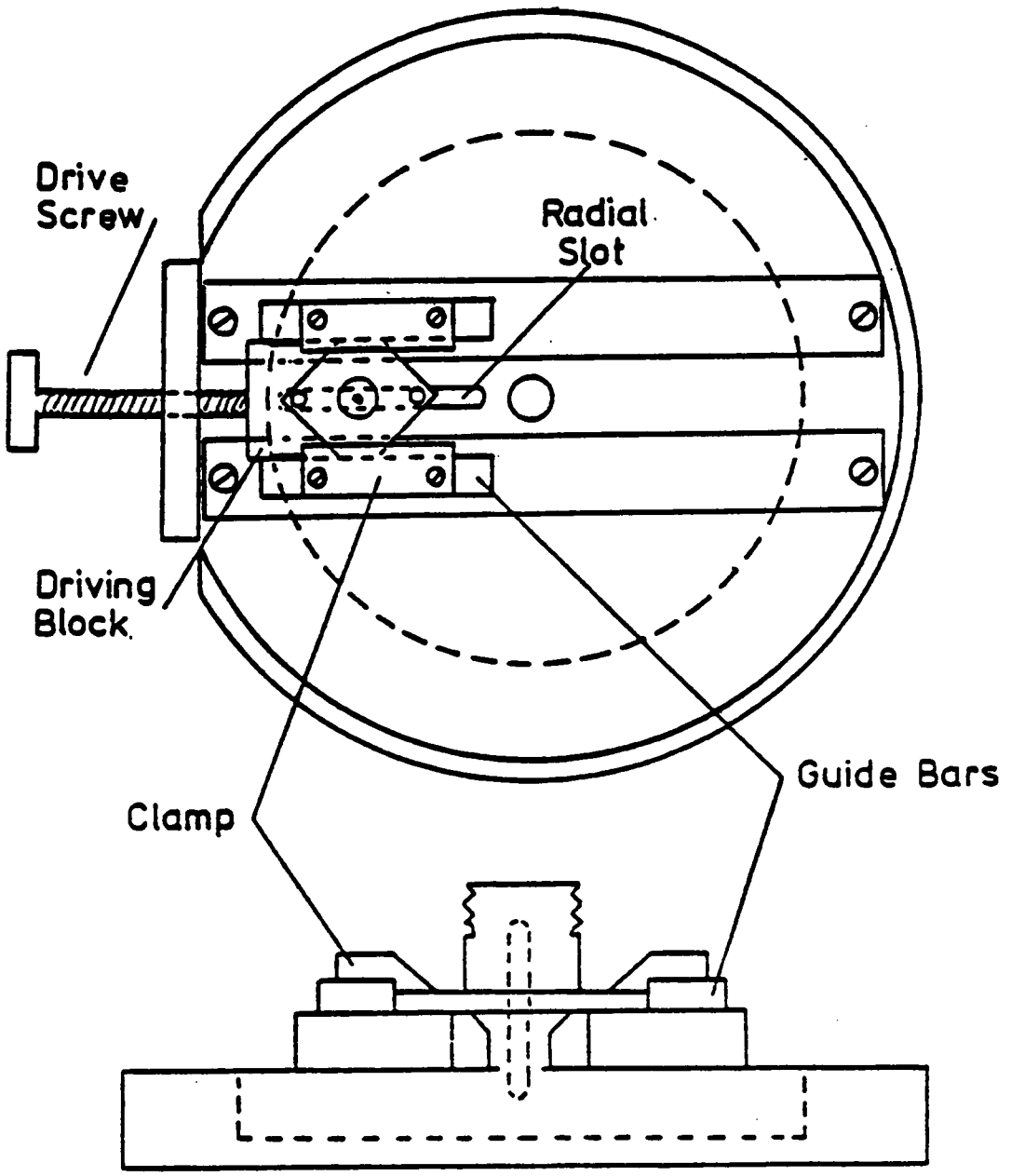

Figure 3. **Impedance Matching Slide Mechanism:** The drive screw translates the antenna probe radially along the slot cut in the cavity lid until the optimal impedance matching conditions are found. This figure was taken from Reference 17.

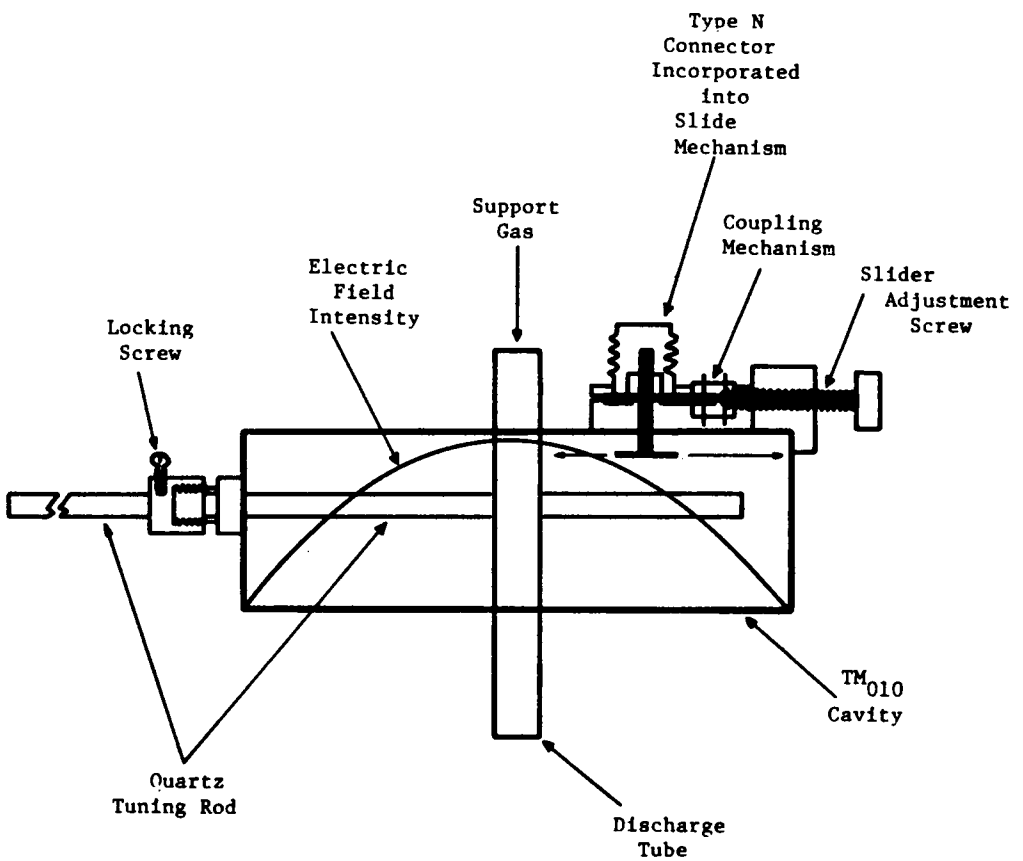

Figure 4. Revised Highly-Efficient TM010 Cavity: Placement of the quartz tuning rod next to the central discharge tube is shown.

Microwave Circuitry

The fourth major improvement to Beenakker's original design was the use of a microwave circulator/isolator circuit for stabilizing the microwave power generator. The use of a circulator/isolator is an standard technique used to protect high-frequency power-generators (54.). A circuitry innovation by the author reduced the number of microwave components required. Hence, circuit cost, complexity, and power loss is greatly reduced.

A circulator/isolator is a microwave component that takes all reflected power coming from the cavity and "circulates" it around to a dissipative load. It does not allow any reflected power to go back to the magnetron. Reflected power going back to the magnetron causes instabilities in the magnetron's oscillations. This generates spurious modes of oscillation in the magnetron, causing spurious frequencies to be generated and increases generator frequency drift. Spurious modes are essentially wasted power since they are not used efficiently by the resonant cavity circuit, which is tuned to one particular frequency. Prohibiting all reflected power from returning to the generator is important. This stabilizes the magnetron by being allowing it to oscillate more freely at only one frequency, giving more power at that frequency. In fact, even if the magnetron power supply has been stabilized through appropriate internal feedback, the magnetron power output will depend very much on the magnitude and phase of the reflected wave (55).

Using a circulator prevents virtually all reflected power from getting to the generator, and the generator is allowed to output its maximum power. However, this does not guarantee that it will go into the plasma. The problem of power transfer will be dealt with more fully later in the results section dealing with the microwave antenna probe.

The original generator did not have a reflected power meter. A way to measure reflected power was needed. A circuit similar to the one shown in Figure 5 on page 43 was

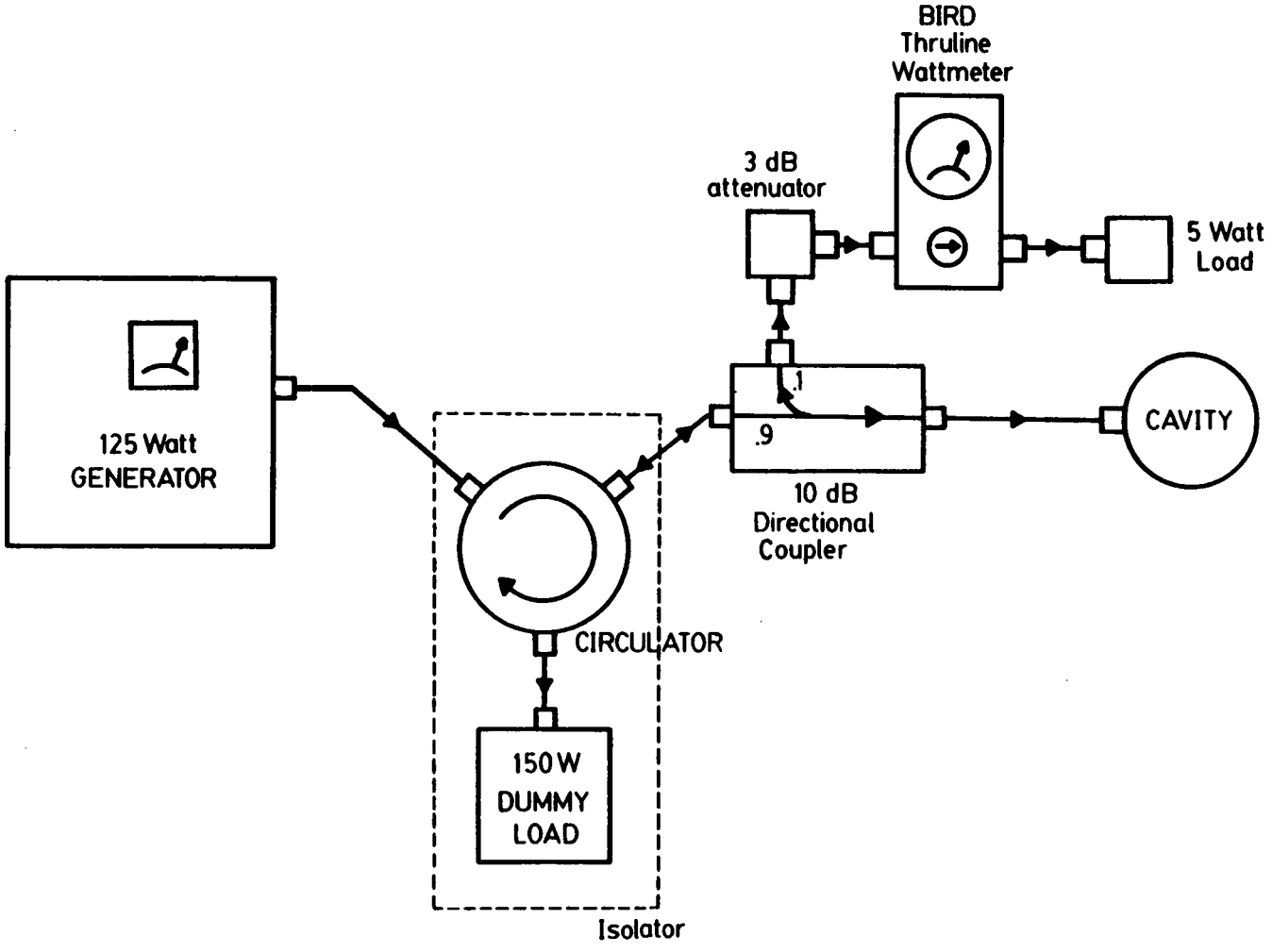

Figure 5. Typical Microwave Power Measurement Circuit

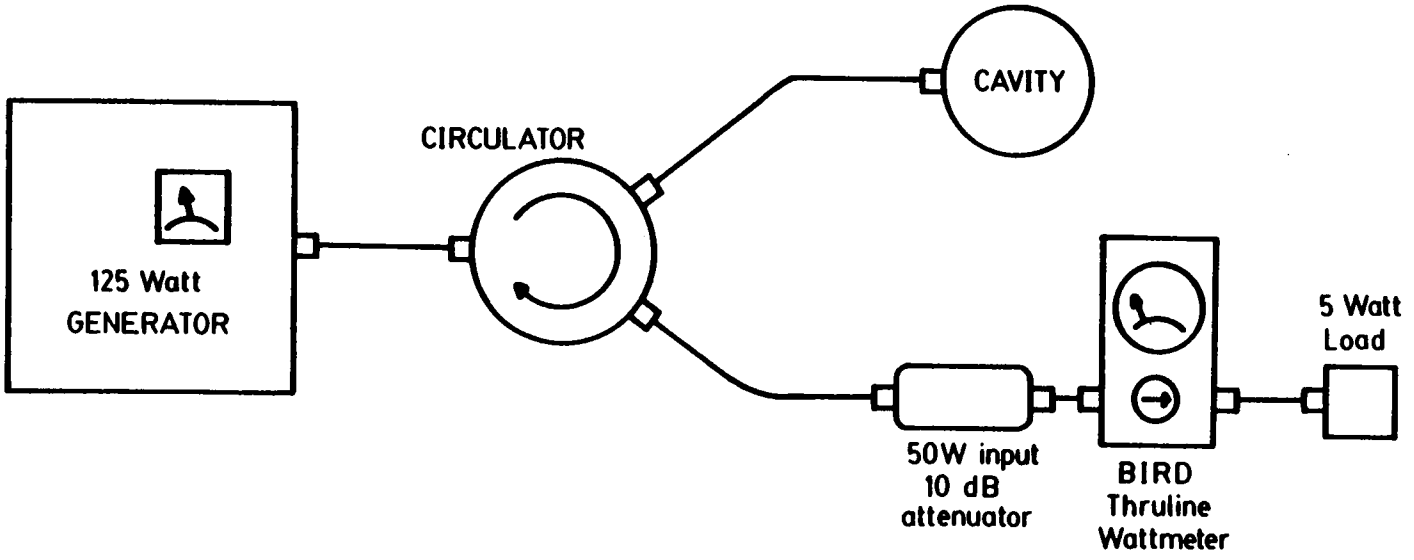

Figure 6. Improved Microwave Power Measurement Circuit

used by van Dalen et al (18). The design is rather complex and it was felt that for a low-power plasma it would never be necessary to dissipate the full power of the generator (150 W) into the dummy load as reflected power. A simpler circuit was designed to eliminate the directional coupler and the 150 W dummy load. Greater than $500 was saved with this approach. The simpler and less expensive circuit is shown in Figure 6 on page 44. This novel circuit performs well for reflected powers less than 50 watts. The original circuit which contains two directional couplers wasted power as heat dissipation in the extra cables, connectors and directional couplers.

Radiation Safety:

The question of a potential safety hazard always exists when using microwave radiation. To test the first cavity (designed and built by this author) a general-purpose, wand-type microwave power meter of the type used to measure leakage from rectangular waveguides, and radiated power from antennas, was borrowed from the University's Electrical Engineering Department. Generally, radiated power increases most when there is a lot of reflected power. Even at greater than 50 watts reflected power, with no plasma lighted, there was less than 1 mW/square centimeter leakage when the wand was held about 0.5 mm from the long slotted hole cut in the lid of the cavity. At a distance of 1 inch from the slot the radiation fell to less than 1 microwatt/square centimeter.

For the second cavity designed by the author, the Radiation & Safety Health Officer on campus used a detector for measuring radiation leakage from microwave ovens. Again with full reflected power the circuit was designed to handle, there was less than 0.1 mW/square centimeter maximum leakage anywhere contiguous to the cavity. The quartz tuning rod had as much leakage as the slot in the cavity lid because it acted like an antenna. The radiation levels the operator receives are low enough for safe operation without worry of blindness or sterility. When the cavity was fully wrapped with aluminum foil there was no detectable

radiation anywhere in the vicinity of the cavity. This safety level is another advantage that the low-power microwave cavity has over other MIP designs and the ICP.

Tangential Flow Torch

The fifth major improvement to Beenakker's original design was to achieve a stable and centered flow pattern within the plasma discharge tube. Initially, 6 mm O.D., 4 mm I.D. pyrex tubes were used. These quickly (within 10 minutes) softened and perforated under the vacuum conditions used in the early experiments. After replacing the pyrex tube with a quartz tube of the same dimensions there were no more problems with immediate softening and perforation. However, at the flow rates used (typically > 0.5 L/min) the plasma bolus is invariably displaced to the wall of the discharge tube. This led to considerable plasma cooling because the plasma bolus was in intimate contact with the inside wall. This also caused the plasma to etch the inside wall, which greatly shortened the lifetime of the tubes and formed microscopic pockets where occluded salt particles could cause memory effects.

To obtain a stable and centered plasma, a centering device called a flow swirler was made. A similar approach had been used by Bollo-Kamara & Codding (20). There, a threaded quartz tube was machined to fit inside of a discharge tube. This is discussed in the MIP Historical Section in Chapter II. The difficulty of machining quartz tubes accurately and easily on a metal lathe precluded the use of quartz as a design material in this laboratory. Instead, a threaded hard-nylon insert, 30 mm long, 4 mm O.D., was turned on a lathe. A pitch of 6 threads per inch was used; the threads had to be cut as deeply as possible, without making the flow swirler too flimsy. This maximized the gas flow through the device. The O.D. of the flow swirler allowed the device to be press-fitted very snugly within the discharge tube, making it immoveable by gas flowing through the tube. It gave a stable, centered plasma because gases were forced to assume a helical or "tangential" flow pattern. See Figure 7 on page 47.

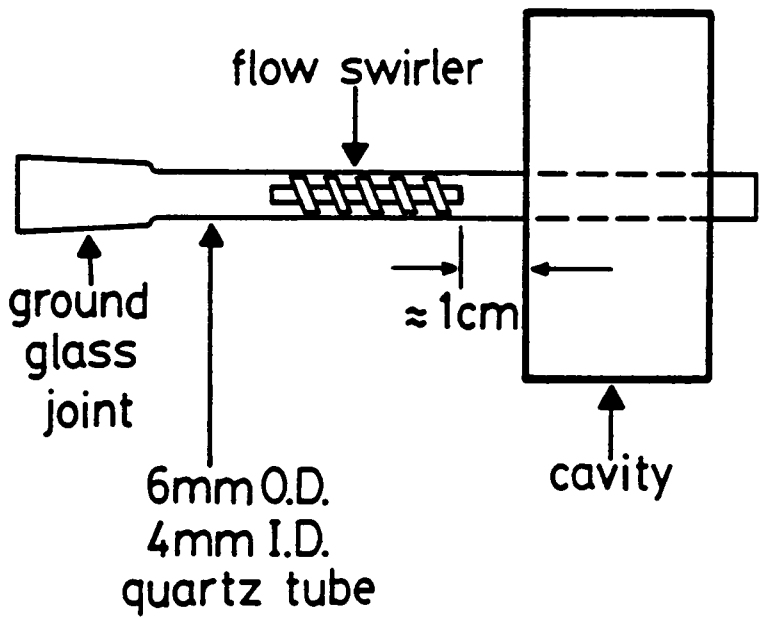

Figure 7. Flow Swirler for Centering and Stabilizing Plasma Flow.

The flow swirler worked very well with nitrogen and nitrogen/argon mixed plasmas. However, with a pure argon plasma the discharge extended so far outside of the cavity, particularly at higher applied powers, that the plasma eventually degraded the nylon, causing impurities to be introduced into the system. This was also a problem when a microarc sampler, of a glow discharge variety, was used upstream of the flow swirler. The plasma from the glow discharge seriously degraded the nylon within a few hours of microarc sampler operation. Alternative materials which have been used by later investigators were Teflon (56) and a high speed steel twist drill (57). These approaches all work very well as long as corrosive substances such as an electrical plasma or highly acidic or basic solutions are not introduced upstream of the flow swirler. A rather typical MIP application using an aqueous solution nebulizer for nearly-neutral pH solutions could use a flow swirler insert. This is a viable alternative to a quartz flow swirler or specialty pieces of glassware which require an experienced glassblower and shop personal.

An alternative to the threaded insert approach was suggested by R. Deutsch (35). This all-quartz design similar in concept to a tangential-flow ICP torch proved to work quite well. The torch dimensions are: 8 mm O.D., 6 mm I.D. outer tube; 1.5 mm O.D., 0.5 mm I.D. center tube. Design details of this torch, which works well with the low-power N_2 -MIP cavity, are given in Figure 8 on page 51. The torches were made by the Glass Shop at Virginia Tech. When experienced glass-blowers are available, making the one-piece torch is easier than machining quartz tubes. This torch design gave plasmas which were easy to ignite, and stable & centered.

The final torch O.D. was chosen to be 8 mm because this size gave easily centerable, stable plasmas that allowed the cavity to remain cool. A 6 mm O.D. torch was tested but did not work well with the low-power N_2 -MIP cavity because of overheating due to power transfer problems. Optimization experiments were conducted with the 6 mm O.D. torch to find a probe depth which would give better power transfer, but none of the depths tried gave good power

transfer, therefore the 6 mm torch was abandoned. Results for all probe optimization experiments are presented in the section on the microwave antenna probe experiments.

Flow rates are not very critical in the torch. A flow rate is desired that provides a stable hydrodynamic flow pattern, i.e., a plasma bolus that is stable and centered. Flow rates of 1.5 L/min through the outer tube (introduced through the the "side-arm"), and 10-20 mL/min through the inner tube were satisfactory.

The 8 mm O.D. torch gave long analyte residence times within the discharge region. Calculations based on fluorescence lifetimes and analyte residence times show that it is possible for an analyte atom to undergo multiple absorption and emission or fluorescence cycles while it exists as the free atom in the hot plasma tail. For both LIF & AES this can offer a sensitivity advantage.

R. Deutsch reported in his development of the moderate-power nitrogen plasma that the center tube could be used for tuning the cavity (35). However, it was found in this work that the center-tube of the torch did not provide much, if any, tuning capability. For practical reasons this method is not desireable because adjustments in the other tuning and matching elements must be made should a torch replacement be necessary, and it is difficult to exactly reproduce the center-tube lengths when new torches are being made in the glass shop. There were also problems with the center-tube closing and/or melting if the center-tube gas flow rate was too low or stopped because of operator error. The range of tuning capability is very small using the center-tube compared with using the quartz tuning rods. Using a tuning rod is far superior technique.

In fact, it was found by accident that the center tube is not really needed at all. While cleaning a torch the center-tube was accidently broken off. The "broken" torch performed just as well when a small flow of gas was resumed through the remaining hole.. It appears that

the side-arm or tangential flow is most responsible for the hydrodynamically stable and centered laminar flow pattern.

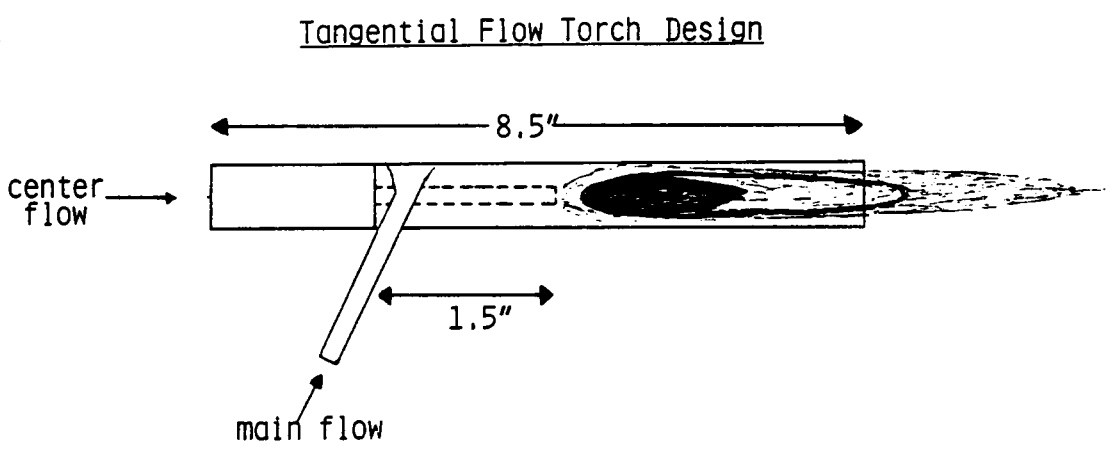

Figure 8. Torch Design

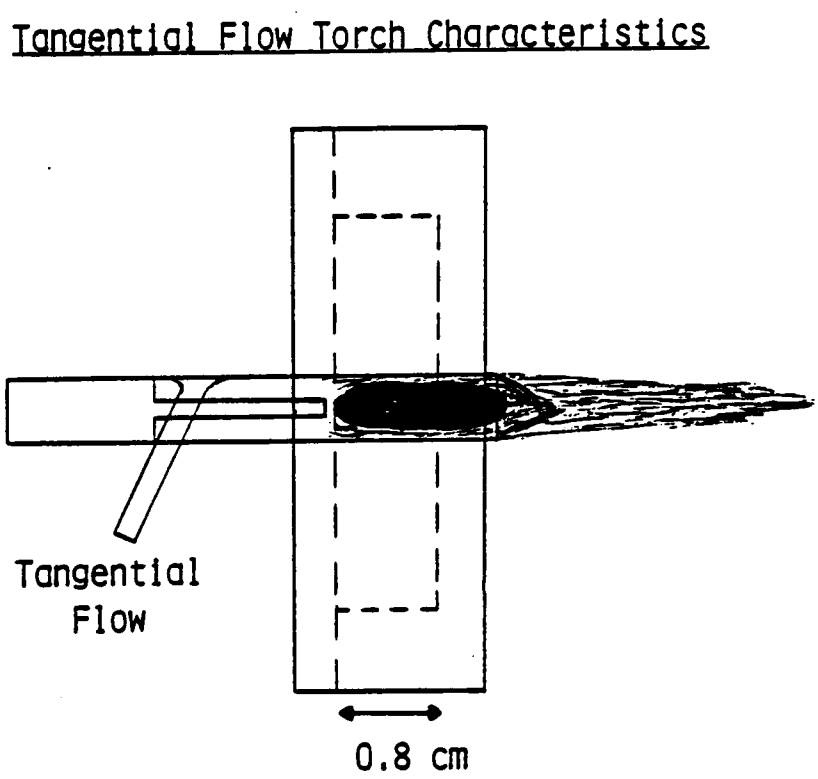

Figure 9. Torch Characteristics: Torch Placement Relative to the MIP Cavity is Shown.

Microwave Cavity Antenna Probe Design

It must be remembered that the microwave cavity and all of its parts form part of a resonant circuit. At high frequencies the sizes and shapes of all components become critical because all elements, even short segments of straight wire, possess inherent inductances and capacitances. These inherent effects can be rather large in some cases. Changing geometry of one part of the circuit even a small amount can alter the resonant frequency of the whole circuit. In a complex system such as a resonant cavity through which a dielectric gas is flowing, it is often easiest to determine optimal geometrical factors experimentally.

This was the case for the microwave coupling probe used to introduce power into the cavity. Its geometrical constraints are very critical. After the low-power atmospheric-pressure nitrogen MIP was successfully developed by this author, it was suggested by C. Boss that power transfer efficiency could be improved by changing the geometry of the microwave antenna probe. Initially a straight wire probe was used by the author. Experiments in Dr. Boss' laboratory had shown that, for argon and helium plasmas, increasing the size of the end of the probe increased the power transfer considerably (57). The rationale is that since the mode of introducing power into the cavity is through capacitive coupling, one could optimize microwave energy transfer into the cavity by optimizing the capacitive factor of the probe inside the resonant cavity.

It is necessary to exactly match the inductance and capacitance of the probe with the cavity structure so that the whole structure, including the lighted plasma, presents a purely resistive 50-ohm impedance to the rest of the circuit. For the nitrogen MIP the probe geometry which gave this 50-ohm match point had to be found experimentally. And as detailed in the Antenna Probe Results Section, the optimal probe geometry for nitrogen plasmas differs considerably from that for argon and helium plasmas.

C) EXPERIMENTAL RESULTS

Plasma Ignition, Stabilization, and Operation

The full initial startup procedure for a new cavity is as follows:

1) Begin with impedance matcher near center of cavity.
2) Start gases flowing (about 1.5 L/min.) through the tangential flow inlet (side-arm).
3) Apply microwave power, up to about 70W minimum.
4) Adjust quartz tuning rod(s) to give minimum reflected power.
   This step is VERY critical for nitrogen.
   Reflected power will go through a rather sharp minimum.
5) Ignite the plasma. If the plasma won't ignite, adjust the impedance matcher until ignition is achieved.
   Increasing the applied microwave power may be required.
6) Once the plasma ignites, minimize the reflected power thru iterative adjustments of the tuning rod(s) and impedance matcher.

Once the quartz tuning rod(s) and impedance matcher are set they can be left alone unless doing fine tuning. On a daily basis, the plasma can be extinguished and reignited without retuning being required.

Either a Tesla coil or a piece of tungsten wire mounted in an insulator can be used to ignite the plasma. A piece of tungsten wire mounted in an insulator (a rubber policeman works well) is the preferred method. It requires no electrical power, and it does not radiate high frequency electrical noise throughout the laboratory. The Tesla coil often resulted in intermittent resetting of the computer ! No such problems were encountered with the tungsten wire. The tungsten wire operates by rapid inductive heating that liberates enough electrons to allow the plasma processes to be initiated.

Once the plasma has been ignited, and is stable and centered, the forward power is reduced to the point where the reflected power is zero. A warmup period of 10-15 minutes allows the plasma and cavity to come to a very stable steady-state.

Occasionally, upon ignition, the N_2 plasma may not be immediately stable and centered. It may appear as a diffuse filament-like plasma circulating around the center of the plasma torch. If it happens, it does so in N_2/Ar mixtures and pure Ar plasmas. It can arise from the use of imperfect tuning and impedance matching conditions. This occurs most often during the ignition and warmup periods of plasma operation, although it sometimes appears even when, after warmup, the perfect tuning and matching have been set on a previously operating plasma. This is because the tuning and matching conditions are different for a lit and an unlit plasma. Once the plasma has been lit and stabilized for 10-20 minutes this problem usually goes away. Occasionally problems arise if the cavity has been operated with high levels of reflected power for a long period of time. High levels of reflected power cause cavity overheating and can change the tuning and impedance matching characteristics so much that the plasma becomes unstable, uncentered, and begins to circulate slowly around the center-tube. The cavity needs to be cooled down if such overheating occurs.

One can usually get around these initial startup problems easily. After the plasma has been ignited but not yet stable and centered, move the plasma torch forward in the cavity, far enough to where the center tube begins to enter the inside of the cavity slightly. Then, retract it out of the cavity. The plasma then collapses from a circulating annulus into a stable and centered plasma bolus.

Several other techniques were discovered which circumvent startup problems with molecular microwave plasmas. At the beginning of the MIP experimental work, pure nitrogen plasmas could not be initiated at 1 atmosphere because the power generator was not supplying enough useful power to the cavity. The pure nitrogen plasma was therefore ignited at low pressure (only 6 Watts applied power are needed to sustain a nitrogen MIP at 10 torr).

Then, while slowly increasing the pressure to 1 atmosphere, the reflected power was minimized by iteratively tuning and matching the cavity. This procedure is time-consuming so a faster method was found. A plasma is initiated using pure argon as a startup gas, and then a gradual switch is made to nitrogen at higher pressure. This procedure works well but also requires operator intervention during startup.

After the generator problem was corrected the plasma could be initiated easily with 1 atmosphere of pure nitrogen using 70 watts minimum microwave power without aerosol flowing into the plasma, or 73 watts with aerosol flowing. Once ignited, the pure nitrogen plasma at 1 atmosphere requires less power to be sustained, 50 watts with aerosol flowing, and 38 watts without aerosol flowing.

If one cannot ignite and center the plasma using the techniques given above, or by adjusting the MIP flow rates or applied microwave power, then there is a serious tuning or matching problem. Most likely a problem has developed with the antenna probe. Ideally the cavity must be tuned and matched to each particular gas composition, microwave power level, and gas flow rate because all of these parameters affect the dielectric properties of the cavity.

Plasma Appearances and Characteristics

The appearances of the nitrogen, argon, and nitrogen/argon mixed plasmas differ considerably, both spatially and in the colors exhibited. The different plasmas are best described pictorially, and are shown in Figure 10 on page 58 and Figure 11 on page 59.

The nitrogen plasma appears as a purple-pinkish-blue plume extending about 2 inches beyond the outside cavity wall. The quartz discharge tube is seen to fluoresce strongly because of ultraviolet light originating inside the primary discharge region.

The argon plasma appears as a bluish-white or purplish-white plume extending about 3/4 to 1 inch outside of the cavity. The discharge tube does not fluorescence as strongly as with the N_2 plasma.

The nitrogen/argon mixed plasmas appear basically the same as the nitrogen plasma. When as little as 5% nitrogen is added to an argon plasma, the plasma properties, including the appearance, shift over to that of a nitrogen plasma. Further confirmation of this shift to basically-nitrogen properties is given in the Results Section on LIF and AES in Chapter III.

Power Transfer Characteristics

The power transfer characteristics of the High-Efficiency Molecular Microwave Plasma (abbreviated "HEMMP") developed by the author are considerably better than that of all previous and current moderate-power molecular MIPs. The plasma required 53 watts to be sustained with aerosol flowing. Sixty watts of power provided analytically useful results for sodium (4 ppb LOD for LIF) under these conditions.

One of the most severe problems retarding progress in the area of microwave plasma research is that few investigators really know how much energy is being absorbed by the plasma (54). Absorbed microwave power per unit volume of plasma is the parameter of greatest importance, yet it is difficult to measure directly. It is not simply the difference between the forward and reflected power meters since this does not account for any power lost as heat. Another big problem with many generators is that the forward and reflected power meters built into the generators often can not be trusted. They provide their measurement of power either from a scaled reading of the magnetron anode current or from a microwave diode located in the output side of a direction coupler. The magnetron anode current is not a reliable method unless there is no reflected power, and it gives no indication of reflected power. Microwave diodes characteristics change over time because of heating

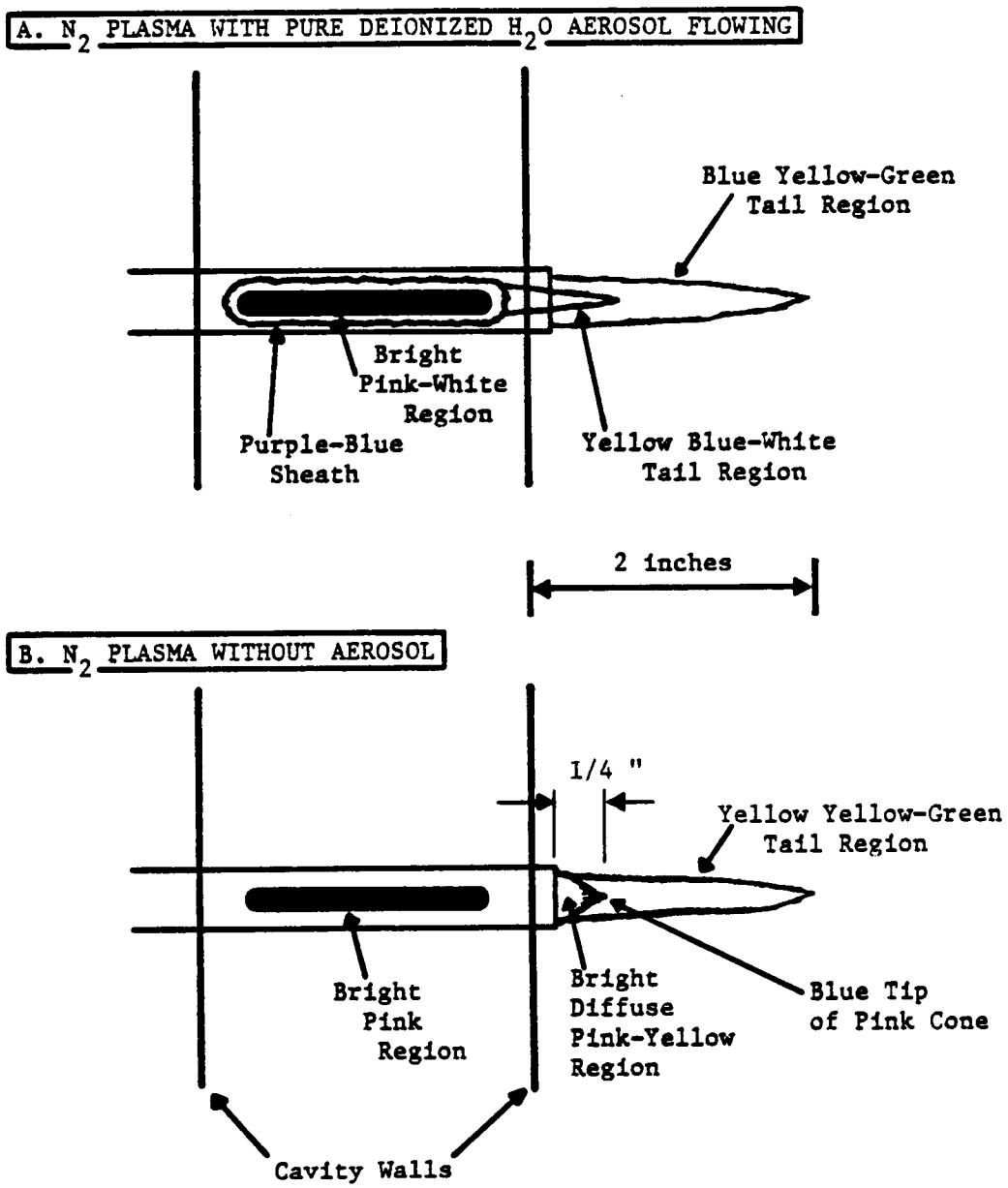

Figure 10. Appearance of the Nitrogen Plasmas

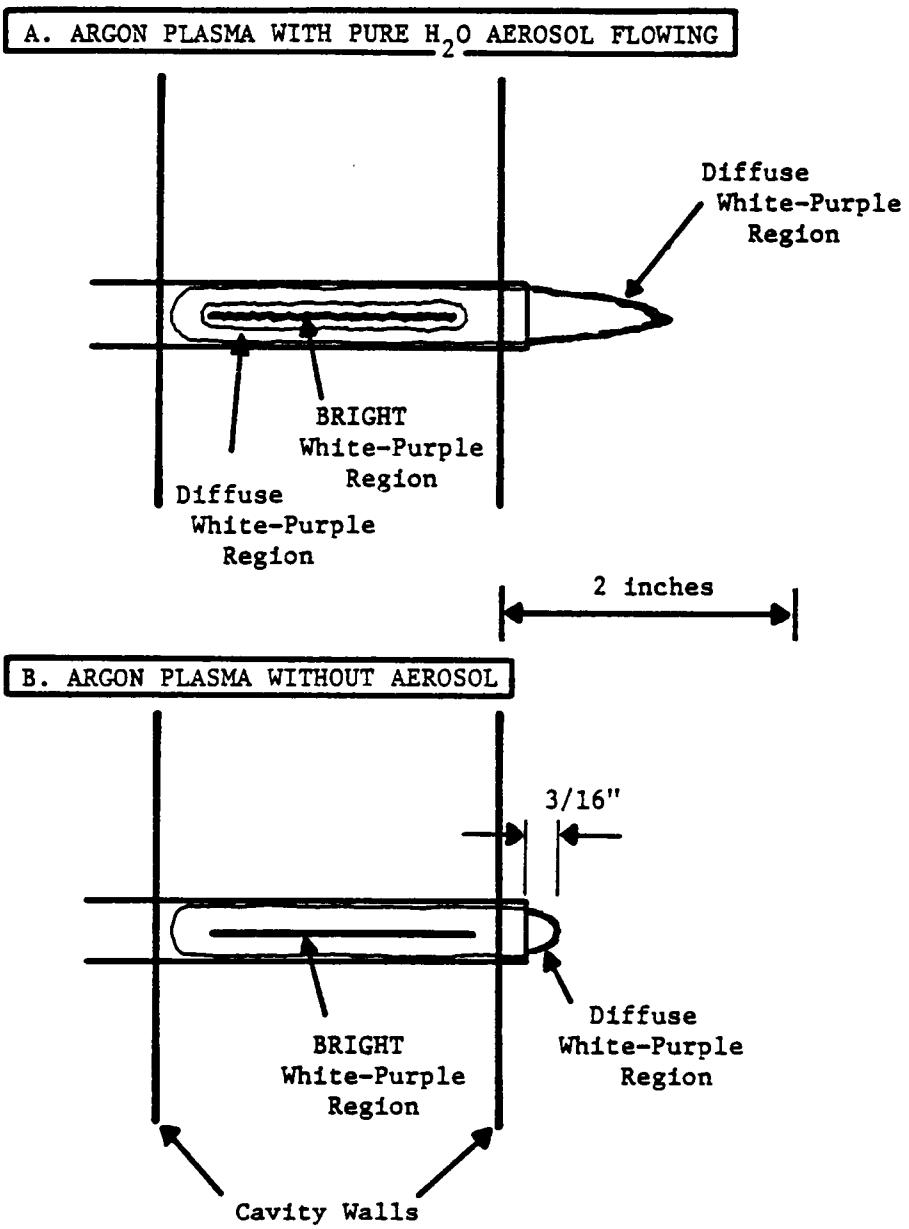

Figure 11. Appearance of the Argon Plasmas

effects and transients, thus their calibrations cannot be relied upon (54). In general, the generator calibrations cannot be assumed to be steady over a long period of time, particularly if no external protection devices such as a circulator are used to protect the magnetron.

In this work, the improved circuitry provided accurate readings of both forward and reflected power. The reflected power meter was a new Bird in-line wattmeter, factory-calibrated shortly before experimentation began. This meter was used to calibrate the generator forward power meter. The generator calibration was found to be constant and stable throughout all experimentation.

Power transfer efficiency for transmission lines is measured by electrical engineers in terms of the power transfer factor, expressed in dB's; i.e., 10[LOG(forward power/reflected power)]. In typical microwave systems 15-20 dB transfer is considered good. When the best tuning and matching conditions are used in the present cavity, a 35 dB transfer factor is typical. The reflected power can be reduced to 3-4 orders of magnitude lower than the forward power, being 50 mW or less for a 53 Watt plasma.

In Table 1 on page 61, input power characteristics are used to compare the performances of the various MIPs. The table clearly illustrates the significant improvement in operating characteristics obtained with the HEMMP cavity for nitrogen. The HEMMP cavity ordinarily needed no cooling. With no reflected power the cavity ran cold to the touch for hours.

Although some literature studies use higher input powers, it is questionable whether these other investigators are really getting substantially more power actually transferred into the plasma. The excitation temperature studies presented later in this chapter support this.

Table 1. Power Transfer Characteristics - Different Molecular MIPs

Input Power	Device Type	Experimental Conditions	Ref.
53-180 Watts	High-Efficiency TM-010 Cavity	1 Atm. 1.5 L/min.	This Work
120-250 Watts	Beenakker Cavity	1 Atm. 1.75 L/min.	(50)
300-500 Watts	Beenakker Cavity	1 Atm. 2.2 L/min.	(31)
560 Watts	Single Electrode Torch	1 Atm. 6-11 L/min	(47)
420 Watts	1/4-wave Coaxial Cavity	650 Torr 1-5 L/min	(47)
700 Watts	RF Torch	1 Atm. 15 L/min	(42)

Microwave Antenna Probe Studies

A straight wire probe was used when the cavity was first assembled. Sheet metal shims were used to set the probe penetration depth at 66%. With 0.030 inch shims the probe depth could be changed in increments of about 10% of the total cavity depth. The plasma worked quite well the first time, giving stable nitrogen plasmas at 1 atmosphere. It was serendipitous that the perfect probe penetration depth was chosen at the very start. This was not known until probe optimization studies were done later.

In late 1984, Dr. Boss reported that changing the area of the probe tip significantly improved the power transfer characteristics of the highly-efficient TM-010. Although the present work had already demonstrated excellent power transfer to the plasma (38 watts minimum power required for a stable N_2 plasma at 1 atmosphere), new studies on plasma stability and power absorption as a function of probe tip area and geometry were initiated. The geometries of the various probes are illustrated in Figure 12 on page 63. These probes were each fitted into the impedance matching slider mechanism illustrated in Figure 3 on page 40. The results of the probe studies are presented in Table 2 on page 64 through Table 5 on page 67.

The antenna probe results obtained here are in direct contrast to those obtained by Boss (57) and Burns (58). The focus of that work had been on improving the power transfer efficiency of argon and helium monatomic plasmas. In Boss's studies the circular disc probe, which is the most capacitive (i.e., largest probe area, with the maximum penetration depth possible, ca. 95 percent) was found to give the most stable plasma and the most efficient power transfer characteristics. In the present studies the straight wire probe, which has the least capacitive and most inductive probe, (i.e., smallest probe area, 66% probe penetration depth), was the most satisfactory.

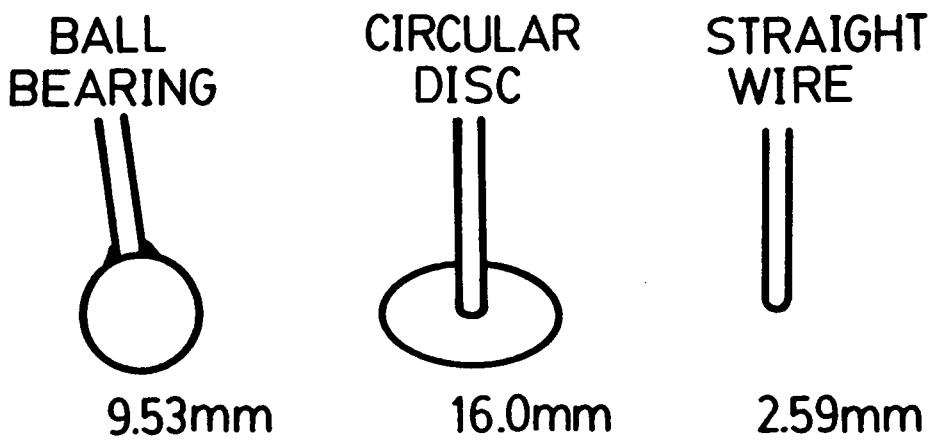

Figure 12. Antenna Coupling Probe Design Characteristics

NITROGEN PLASMA ANTENNA PROBE STUDIES - 8 mm TORCH

STRAIGHT WIRE PROBE - 10 GAUGE WIRE

Table 2. Straight Wire Antenna Probe Study - 8 MM Torch N2-MIP Cavity

Probe Penetration	Results
93%	Unstable at Mixtures Greater than N_2/Ar = 1 : 1.4 PLASMA COULD BE CENTERED.
83%	Unstable at Mixtures Greater than N_2/Ar = 1 : 1.5 PLASMA COULD BE CENTERED.
66%	VERY STABLE AND CENTERED IN PURE N_2.
57%	Unstable at Mixtures Greater than N_2/Ar = 2 : 1 PLASMA COULD BE CENTERED.

NITROGEN PLASMA ANTENNA PROBE STUDIES - 8 mm TORCH

9.53 MM BALL BEARING MOUNTED ON 10 GAUGE WIRE

Table 3. Ball Bearing Antenna Probe Study - 8 MM Torch N2-MIP Cavity

Probe Penetration	Results
93%	Unstable at Mixtures Greater than N_2/Ar = 1 : 1.5 COULD NOT CENTER PLASMA.
83%	Unstable at Mixtures Greater than N_2/Ar = 1 : 1.5 COULD NOT CENTER PLASMA.
66%	Unstable at Mixtures Greater than N_2/Ar = 1 : 1.4 PLASMA COULD BE CENTERED !!
57%	Unstable at Mixtures Greater than N_2/Ar = 1 : 1.4 COULD NOT CENTER PLASMA.

NITROGEN PLASMA ANTENNA PROBE STUDIES - 8 mm TORCH

16 MM CIRCULAR DISC MOUNTED ON 10 GAUGE WIRE

Table 4. Circular Disc Antenna Probe Study - 8 MM Torch N2-MIP Cavity

Probe Penetration	Results
93%	Not Very Stable in Pure Ar COULD NOT CENTER PLASMA. WOULD TOLERATE NO N_2 !!
83%	Not Very Stable In Pure Ar ALMOST CENTERED PLASMA. WOULD TOLERATE NO N_2 !!
66%	Unstable at Mixtures Greater than N_2/Ar = 1 : 1.8 PLASMA COULD BE CENTERED. WITH 5% N_2 ADDED CAVITY HEATS UP !!
57%	Unstable at Mixtures Greater than N_2/Ar = 1 : 1.8 PLASMA COULD BE CENTERED. WITH 5% N_2 ADDED CAVITY HEATS UP !!

NITROGEN PLASMA ANTENNA PROBE STUDIES - 6 mm TORCH

STRAIGHT WIRE PROBE - 10 GAUGE WIRE

Table 5. Straight Wire Antenna Probe Study - 6 MM Torch N2-MIP Cavity

Probe Penetration	Results
93%	Unstable at Mixtures Greater than N_2/Ar = 1 : 2.3 COULD NOT CENTER PLASMA. CAVITY OVERHEATS !!
83%	Stable and Centered in Mixtures Up to N_2/Ar = 1 : 1 CAVITY OVERHEATS !!
74%	Stable and Centered with Pure N_2. CAVITY OVERHEATS !!
64%	Unstable in All Mixtures PLASMA COULD BE NOT CENTERED. CAVITY OVERHEATS !!
57%	Stable and Centered with Pure N_2. CAVITY OVERHEATS !!

The reason for this dichotomy is the large differences in the conductivities of the monoatomic argon and helium plasmas and a molecular nitrogen plasma. Electron attachment to molecules in a molecular plasma is known to be a very important effect (59). Nitrogen is a low-conductance plasma, i.e., there are relatively few free electrons. Indeed, Goode and Otto have found that nitrogen-doped atmospheric pressure argon plasmas tolerate only 5 to 7 % nitrogen before extinguishing, presumably because of plasma electron depletion (60). A dynamic double-probe method was used in which the current is measured as the voltage is quickly ramped. The dynamic resistance is then converted to an electron density. Unfortunately, electron densities measured with this method differ as much as 4 to 6 orders of magnitude from electron densities measured using the standard method (Hydrogen-beta-line broadening), making absolute comparisons impossible. Regardless, the important facts obtainable from Goode and Otto's double-probe electron density experiments are that the electron densities drop more than 2 orders of magnitude when as little as 7% nitrogen is added. And as the applied microwave power is increased, more nitrogen is tolerated since electron density increases as power increases.

How the conductance of a plasma enters into the energy transfer characteristics can be rationalized from how the electric and magnetic fields within the cavity interact with the conductive plasma. The following model elucidates a mechanism that accounts for the radically different probe geometry for the nitrogen plasma (61).

It is intuitive that as the applied power is increased the plasma becomes more conductive. That is, more electrons are generated, (electrons are primarily responsible for the conduction of current in these plasmas since the ions are so slow-moving). The magnetic field circulates around the axis of the discharge tube. The electric field is a standing wave perpendicular to this axis. As the conductivity of the plasma increases, the current through the cavity increases. Imagine the conducting plasma to be a piece of wire carrying current. One can see that as the current through the cavity increases, the magnetic field intensity inside the cavity increases, in accordance with Ampere's Law. Thus the ratio of the electric

field to the magnetic field (abbreviated "E/H") decreases. The function of introducing more dielectric into the cavity is to store more energy in the electric field within the cavity structure. As the power input to the cavity increases, the conductance increases, and for very large changes in input power, more quartz needs to be introduced into the cavity to store more energy in the electric field. This allows the ratio of E/H to be returned to 50 ohms, which is the necessary condition for maximum power transfer, i.e., critical coupling. Crudely speaking, it is as though the increase in the plasma conductivity, (current streaming out of the cavity), causes the electric field to be "drawn out" of the cavity by the streaming plasma. And to re-store the electric field density within the cavity more dielectric must be introduced.

From the paragraph above, it is clear that more conductive plasmas have a smaller E/H ratios than less conductive plasmas. Hence, in a highly conductive plasma, energy is less effectively coupled into the electric field. For a highly conductive plasma (such as argon) a coupling probe with a great deal of capacitance is needed. A nitrogen plasma is considerably less conductive, hence a less capacitive, more inductive probe is needed. The straight wire probe is the most inductive probe and gives the best results for nitrogen at one atmosphere. It provides the best overall performance in terms of ease of ignition, stability, and power transfer to the cavity.

Excitation Temperature Studies

Excitation temperature studies were performed to allow comparison of the Highly-Efficient Nitrogen MIP with other MIP sources. These measurements will also help explain the profiles found in the spatial characterizations of LIF and AES. They may also contribute to a better understanding of analyte decomposition and excitation.

Excitation temperature studies were done using the Fe emission lines. The excitation temperature is also known as the spectroscopic temperature because it is the equivalent

thermal temperature needed to excite spectral lines of a particular element. The theoretical basis of the temperature measurement method used here lies in the fact that the relative emission intensities of increasingly energetic atomic lines will show a population decrease, as predicted from the Boltzmann equation.

Spectroscopic temperatures were calculated using the slope method (34). In this method:

$\log \frac{(g \times A \times \lambda)}{c \times I}$ is plotted versus E_q

where g = Excited State Degeneracy

A = Transition Probability

λ = Wavelength of the Transition

I = Intensity of Transition

c = Speed of Light

E_q = Energy of Transition in Wavenumbers

The slope of this curve is then 1/kT.

Transition probability data were taken from two sources: NBS Atomic Transition Probability Tables and from Reif, Fassel et al (34). The NBS data gave temperatures which were consistently lower than those obtained using Reif's data. Reif's data is considered by most spectroscopists to be more accurate than the NBS data. The former data was collected with closer attention correct being paid to experimental constraints: i.e., the atoms must reside in an isothermal environment in local thermodynamic equilibrium, temperatures must be measured accurately, integrated line radiances must be measured accurately and in such a way that self-absorption does not occur. A complete theoretical description can be found in reference (34). The exact Fe emission lines used for calculating excitation temperatures in this work can be found in the computer program in Appendix A.

Temperature measurements were done using lateral viewing of the Fe emission to avoid self-absorption. 1000 ppm solutions were used in order to have enough emission intensity at

the narrow slits needed to define the emission lines well. Emission signal emission intensity was always at a premium, particularly at low MIP power levels. This caused great fluctuations in the temperatures obtained. All values plotted are the average of at least 3 to 5 separate spectral scans. Excitation temperatures are notoriously variable for low-temperature flames and plasmas, which are seldom, if ever, at perfect local thermodynamic equilibrium (LTE). Excitation temperature measurements are performed more for the purpose of comparison with other, similar types of plasmas, rather than for any rigorous theoretical purposes.

The slope method of calculating temperatures showed some inherent limitations. When signal-to-noise ratios were very small the temperatures calculated reached an asymptotic limit of 6700 degrees Kelvin. This occurred when the relative ratios between the largest and the smallest peaks fell below 2 or the S/N ratio fell below 4. This is clearly illustrated in Figure 19 on page 79. Slopes and correlation coefficients were calculated using linear regression.

Because Fe emissions were very weak, the observation height with the maximum intensity was chosen for all microwave power and gas composition studies. This observation height was always as close to the cavity wall as the detection system could permit without obscuring the optical signal. This is true for all temperature studies except the MIP power experiment in pure N_2, which was run at a 6 mm observation height in order to keep all peaks on scale and to use the same slit widths for all spectral scans within that data set. Temperature profiles as a function of observation height are reported for the nitrogen plasma at 150 Watts only. Signal intensities were too low using powers lower than 150 watts, and the MIP cavity began to overheat at higher powers.

The observation height profiles in argon had S/N problems. Not enough signal was present to obtain reliable results at any other observation height other than that of maximum intensity. For all temperature experiments, weak signal intensities set lower limits on the applied microwave power that could be used, and upper limits on the observation height.

Because of the problems encountered with low signal intensities, noise, and departure from thermodynamic equilibrium, spectroscopic temperature measurements do not provide a lot of insight into these plasmas. This is true even when the temperatures are an average of many spectral scans. However, they are useful for comparing general features of the plasmas using the various gases and cavities.

Excitation temperatures as a function of gas composition were reinvestigated after the emission, laser induced fluorescence, and laser enhanced ionization experiments (to be discussed later) were completed. The region of 0% to 40% nitrogen in argon was investigated more closely. In the AES, LIF and LEI experiments, as support gas composition was varied a sharp peak in intensity was observed around 10% nitrogen in argon. This was noted for Na atomic emission, Ba ionic LIF, Ba atomic and ionic emission, and Na laser enhanced ionization, (See Figure 50 on page 166, Figure 51 on page 167, and Figure 127 on page 330). It was thought that excitation temperature measurements could provide some insight into this phenomena. However, from the absence of a peak at or around 10% in Figure 17 on page 77, it can be concluded that the excitation energy of the plasma, as measured by the spectroscopic temperature, is not responsible for the maxima peaks noted in the emission, fluorescence, and ionization studies.

Spectroscopic Temperatures of Various Atmospheric Pressure MIP's:

Table 6 on page 81 compares excitation temperatures of the various atmospheric pressure MIPs. One notes the upper limits are somewhat higher for the inert gas plasma (Ar and He) than for the molecular gas plasmas. The inert gas plasmas do not necessarily possess more energy for transfer to the analytes. Excitation temperature is a measure of the electronic metastable energy states of the species in the plasma. Ar and He possess higher-lying metastables (about 11 eV and 20 eV, respectively) compared the molecular electronic metastables of nitrogen and oxygen (6.1eV for nitrogen, about 1 eV and 4.3 eV for oxygen). This gives He and Ar an advantage for analysis of elements with high excitation

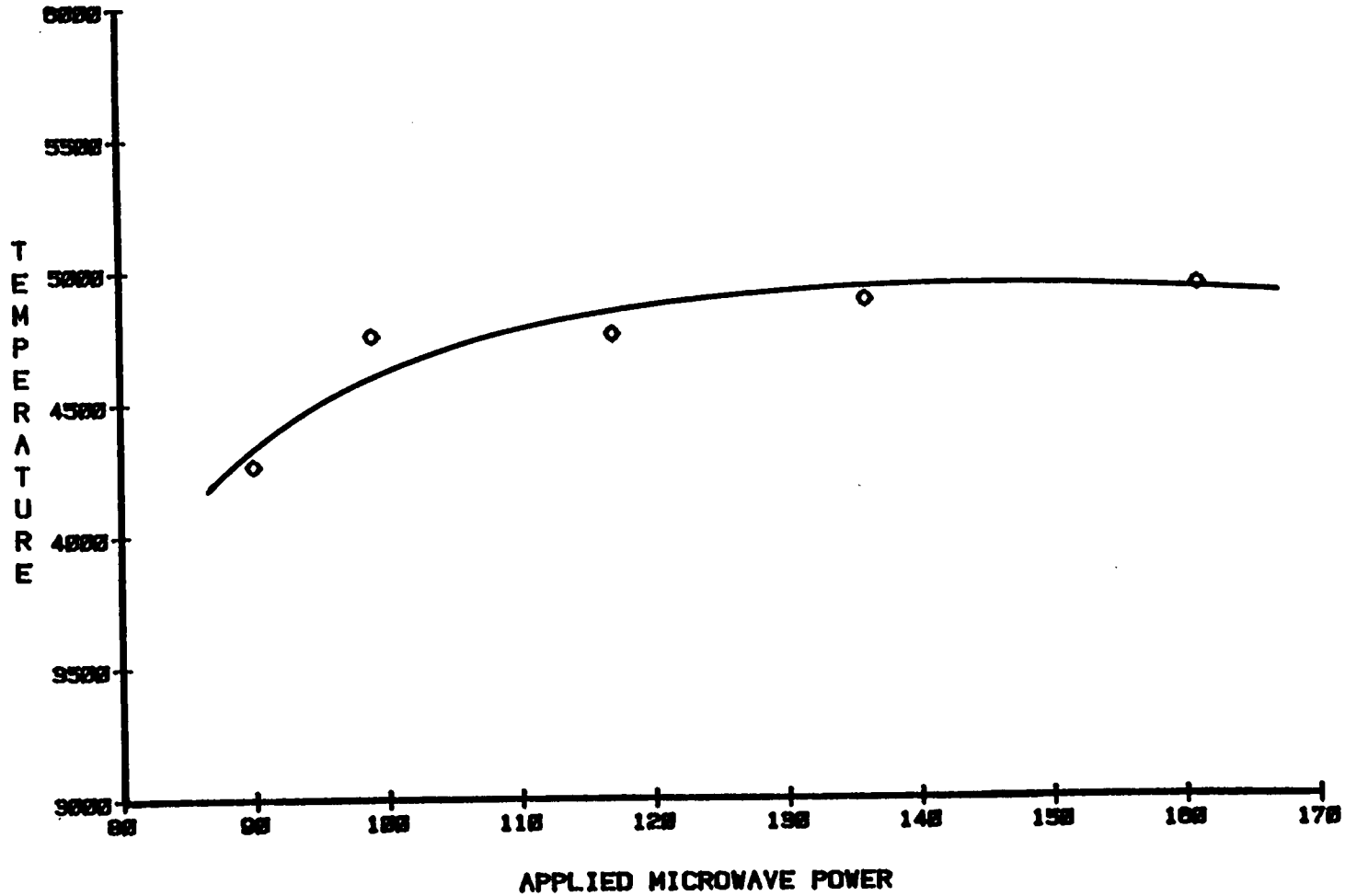

Figure 13. Excitation Temperature vs. Applied MIP Power - Pure Nitrogen

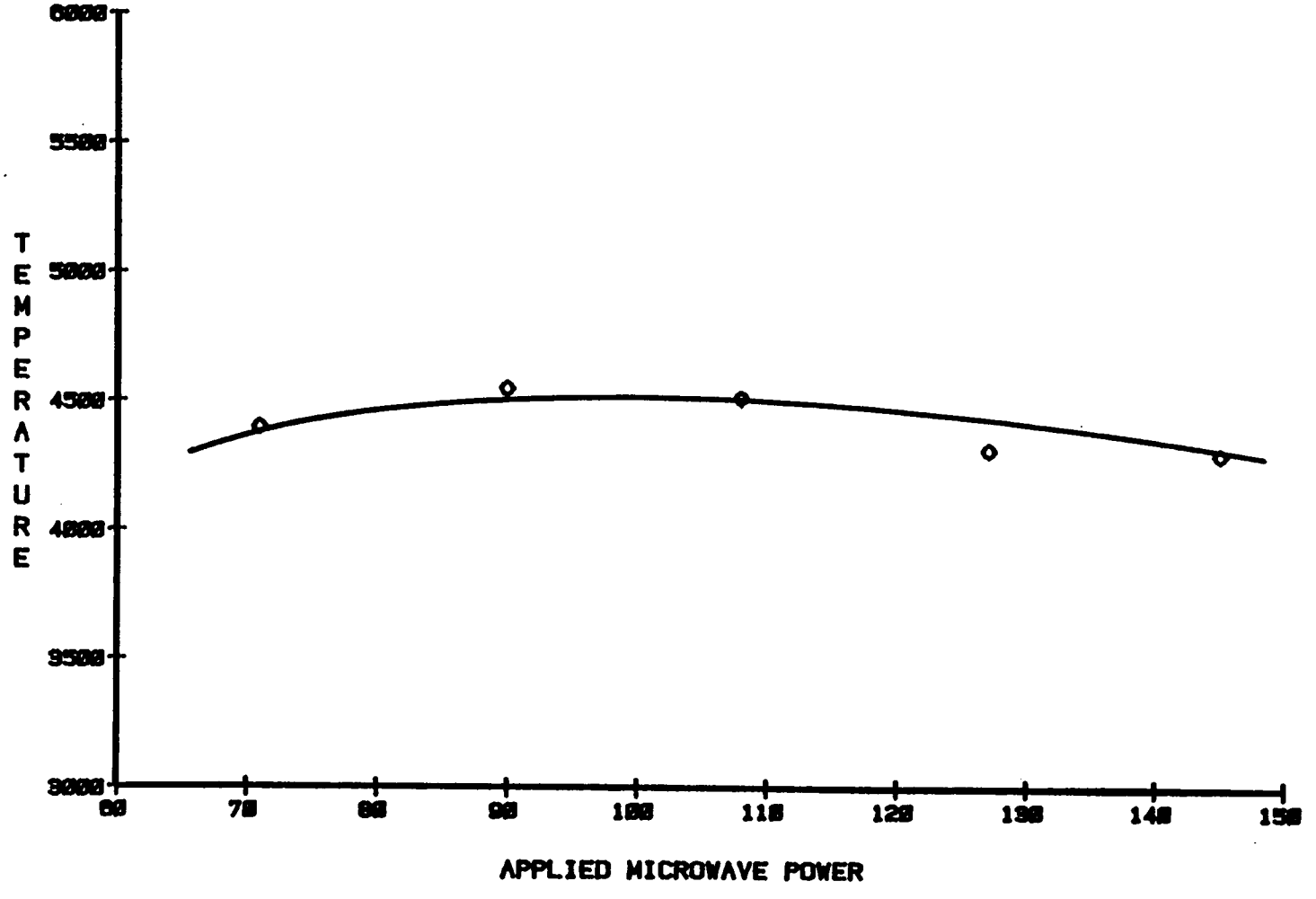

Figure 14. Excitation Temperature vs. Applied MIP Power - Pure Argon

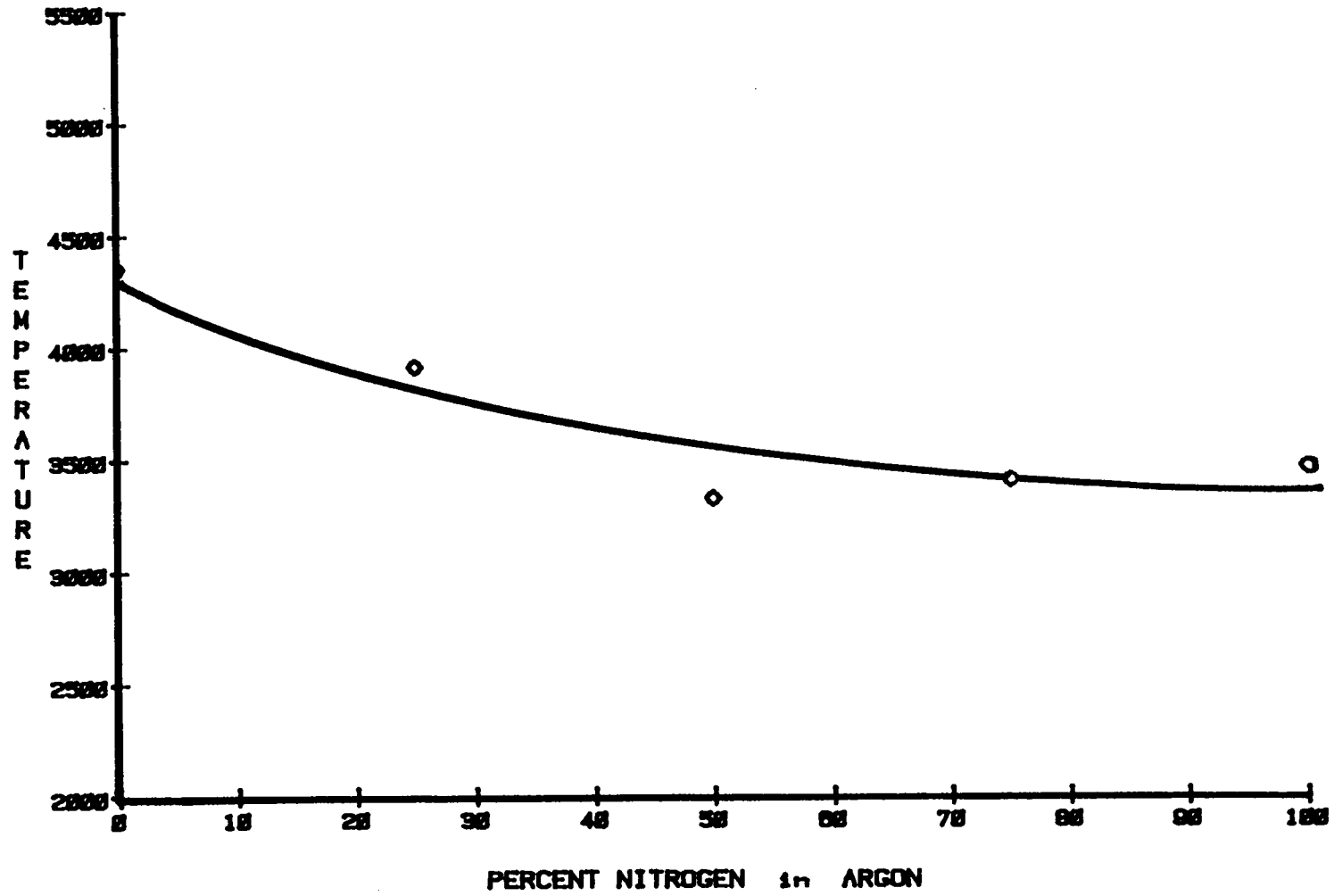

Figure 15. Excitation Temperature vs. Percent Nitrogen in Argon - 75 Watts

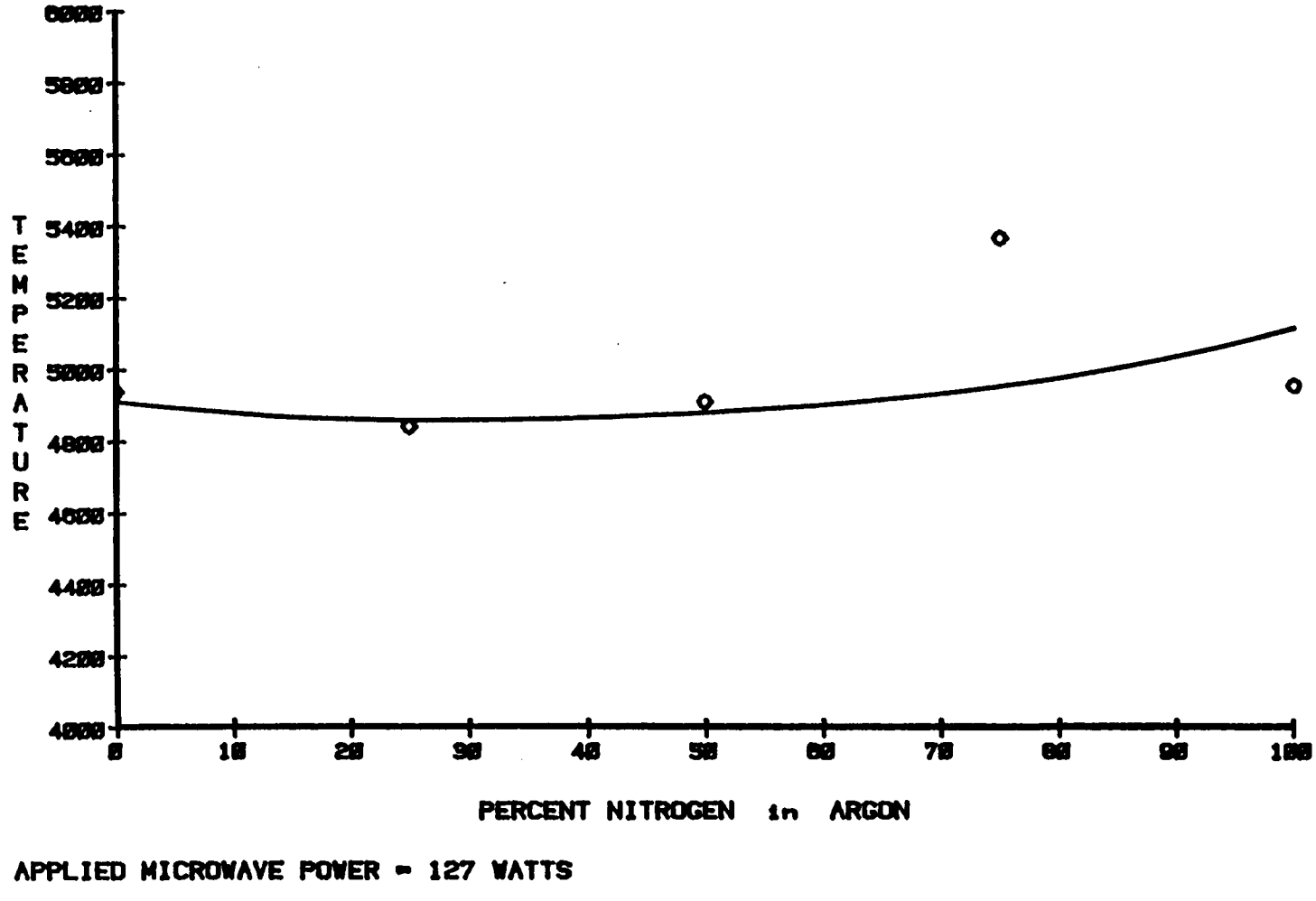

Figure 16. Excitation Temperature vs. Percent Nitrogen in Argon - 127 Watts

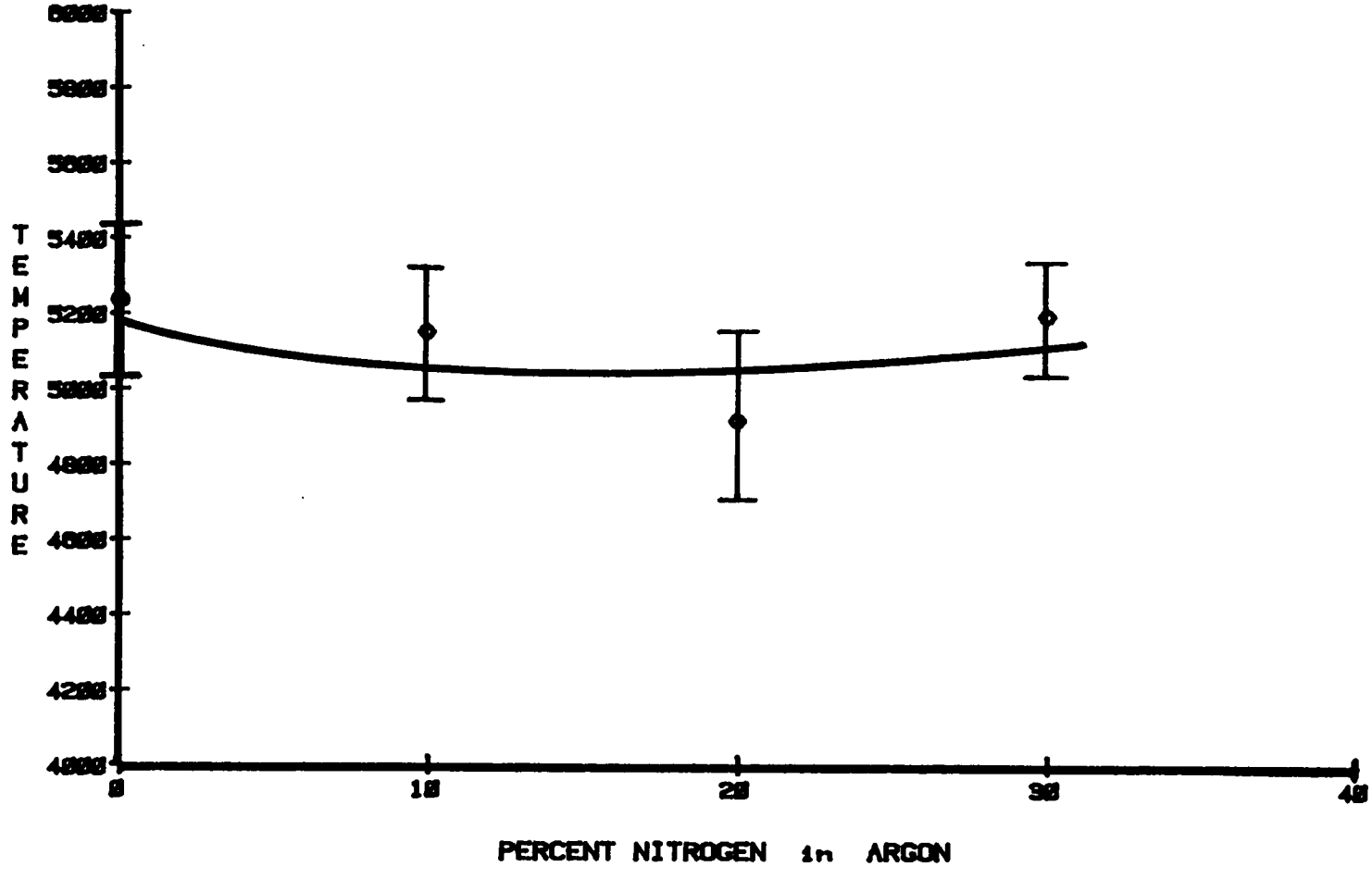

Figure 17. Excitation Temperature vs. Percent Nitrogen in Argon - 153 Watts

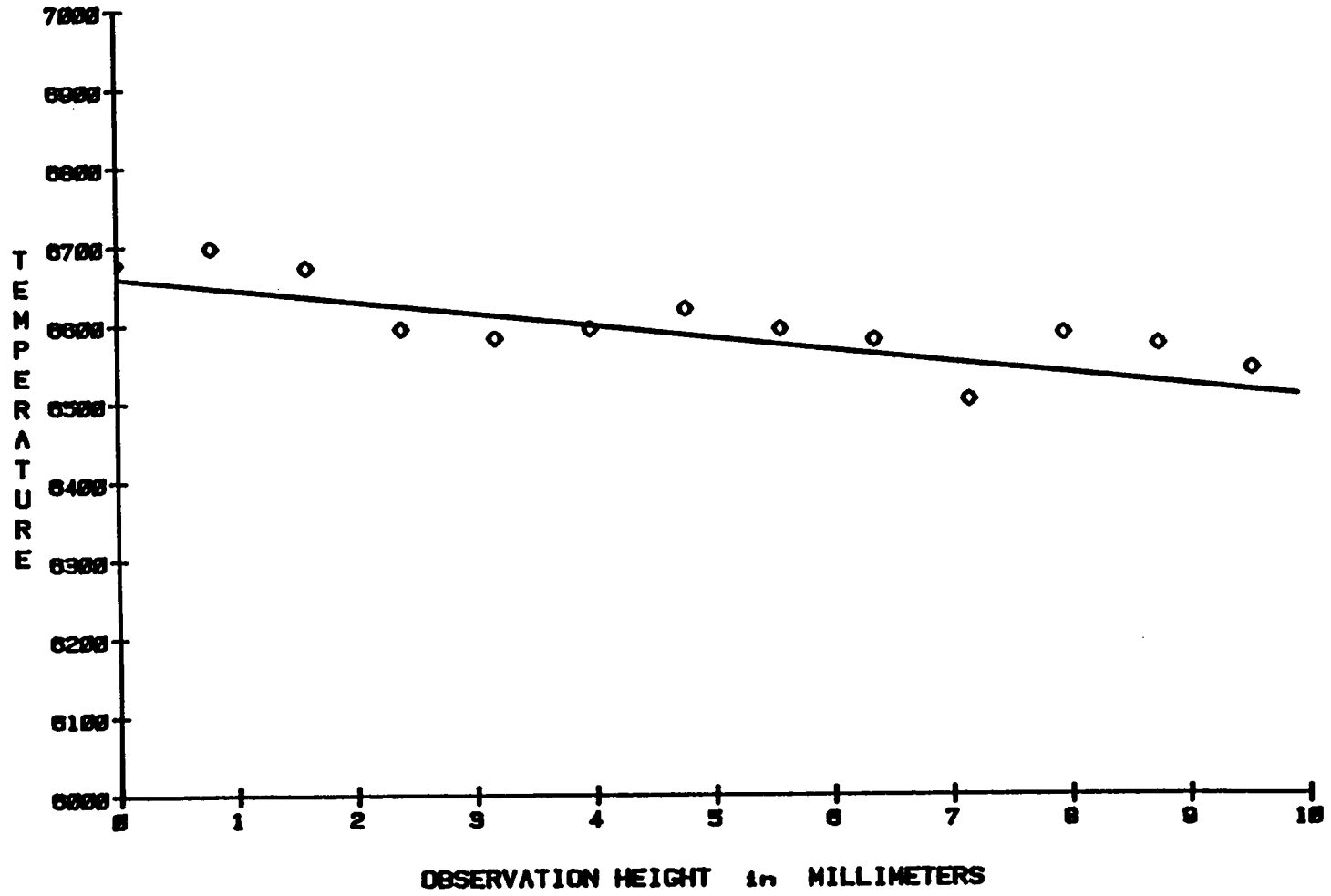

Figure 18. Excitation Temperature vs. Observation Height - - Pure Nitrogen

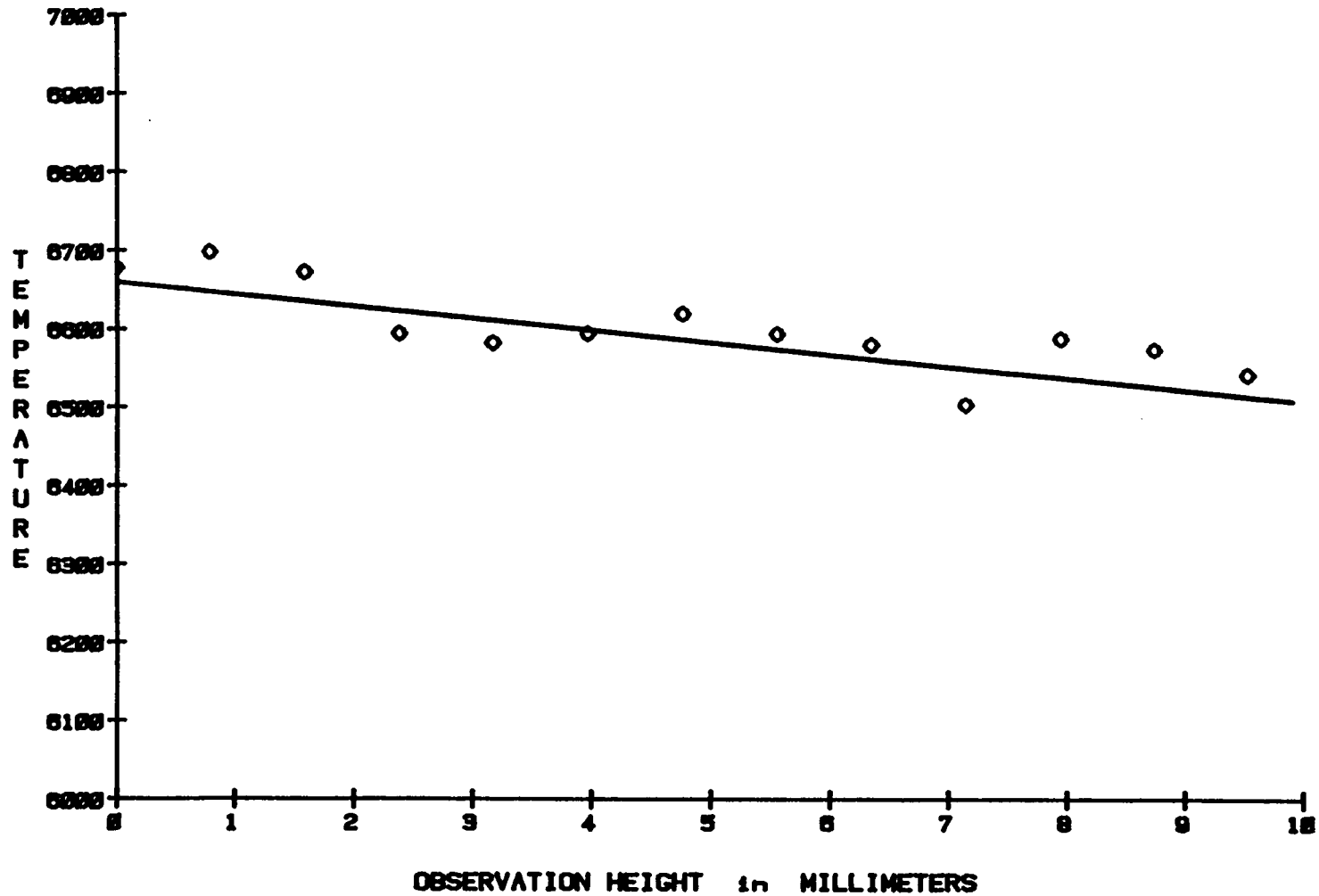

Figure 19. Excitation Temperature vs. Observation Height - Pure Argon

energies, such as the halogens, phosphorus, sulfur, and other nonmetals. However, this does not necessarily convey an advantage for elements with low to medium excitation potentials. The most common inorganic analyses are done on elements with low to medium excitation energies. Thus, a plasma with low to medium excitation energies, particularly one with a more thermalized energy distribution, may offer wider analytical applicability. Choosing a plasma for analytical purposes requires a clear understanding of these principles.

Spectroscopic Temperatures - Summary and Conclusions:

The tables show that the temperatures for the low-power N_2 -MIP compare favorably with all of the other plasmas, which require more power. One thing to notice about all of the molecular gas plasmas in TM-010 cavities is that temperatures increase with increasing applied power. But the increase is highly nonlinear. A doubling or a tripling in power produces at most a 1000 degree Kelvin increase in temperature. The graphs show that excitation temperatures are not strongly affected by increases in power, or changes in gas mixture. A relative insensitivity to changes in applied power (and flow rate) has been noted elsewhere in Ar and He MIPs (62). Matus (22) measured only a 57% increase in in plasma power for a 100% (a doubling) increase in input power. The measurements were made using thermocouples. The implication is that excitation temperatures may not greatly increase with further increases in power transfer efficiency. However, such conclusions cannot yet be made; more research with power-efficient MIP's is needed. Until experimenters are certain that all of the extra power is actually getting into the plasma, MIP power studies will not produce reliable quantitative conclusions.

Background Emission Studies

The primary purpose for the spectral characterization of the MIP support gas was to ascertain if there was a large concentration of active nitrogen being produced in the form of

Spectroscopic Excitation Temperatures - Atmospheric Pressure MIPs

Table 6. Spectroscopic Temperature Comparison - Different MIPs

Plasma Type	Excitation Temperature Degrees Kelvin	Experimental Conditions	Ref.
Capacitively Coupled High-Efficiency Cavity			
Low-Power N_2	4250-4950	90-180W 1.5 L/min	This Work
Capacitvely Coupled Single-Electrode Torch			
Air	4530-4740	400-500W 6-11 L/min	(47)
N_2/Ar	4900-6100 400W, 3.6 L/min	0% to 83% Ar	(49)
N_2	4390-5020	400-560W	"
Ar	5230-5360	" "	"
He	6030-6080	" "	"
Ar	4980	100W	(63)
N_2	6000-10,000	130-420W 10-650 Torr	(47)

Table 7. Spectroscopic Temperature Comparison - Different MIPs (cont.)

Plasma Type	Excitation Temperature Degrees Kelvin	Experimental Conditions	Ref.
High-Power Inductively-Coupled TM-010 (Beenakker) Cavities			
N_2	5800	300-500W 2.2 L/min	(31)
Air	5900	300-500W 2.2-8.6 L/min	(31)
Low-Power Inductively-Coupled TM-010 (Beenakker) Cavities			
N_2	3750-5250 4350-5850 4500-5850	140-250W,2.1 L/min 120-250W,1.75 L/min 120-250W,1.35 L.min All 1 Atm.	(64)
Ar	5100	100W	(65)
Ar	4000-6000	50-120W 2.6 L/min	(62)
He-MIP	5000-7000	70-120W	(62)
He-MIP	7250	100W	(64)
He-MIP	5700-6700	50-75W 120 mL/min	(66)

Spectroscopic Excitation Temperatures - Atmospheric Pressure ICPs

Table 8. Spectroscopic Temperature Comparison - Different ICPs

Plasma Type	Excitation Temperature Degrees Kelvin	Experimental Conditions	Ref.
ICP at 1 Atm. in Various Support Gases			
Ar-ICP	4500	1kW	(28)
Ar-ICP	4630	1kW	(41)
Ar-ICP	6000-9000	1kW	(67)
He-ICP	4100		(68)
Ar/N_2	4500-5100		(68)

the N_2 (A) state. This is the state thought to be most responsible for excitation of analytes through metastable energy transfer. This is also the 6.1 eV metastable state that was to replace one or more of the lasers in a resonance ionization spectroscopy scheme. This state is detected most easily by monitoring the Vegard-Kaplan bands, which are the bands resulting from the transitions from the first excited triplet state down to the ground state of the nitrogen molecule (see Figure 20 on page 87).

One should take note of the First Positive (1+), Second Positive (2+), and Vegard-Kaplan (VK) emission bands indicated in the molecular electronic potential energy diagram of nitrogen given in Figure 20. These are all triplet-state to triplet-state transitions. The First Positive bands arise from a C-state to B-state transition, and appear in the wavelength range 500-800 nanometers. The Second Positive bands arise from a B-state to A-state transition, and appear in the wavelength range 275-450 nanometers. The Vegard-Kaplan bands arise from an A-state to ground-state transition, and appear in the wavelength range of 210-280 nanometers. A spectral characterization revealed that not a great deal of active nitrogen was being produced by the discharge in the form of the N_2 (A) state.

Low Pressure Studies:

In Figure 21 on page 88 it can be seen that the low-pressure (10 torr) MIP discharge is producing no detectable Vegard-Kaplan (VK) bands. Another investigator has found that the VK bands do not appear at low pressure (about 1 torr) because of the increased N atom concentration, which quenches nitrogen molecule A states (69 , 70). The only detectable emissions in the range 210 nm to 280 nm are the nitric oxide bands, the NO Gamma bands, also known as the "nitrogen third positive system". The sensitivity was increased by a factor of 50 above that used in the next figure, Figure 22. There we see the intensity of the NO Gamma bands are very small compared to the nitrogen Second Positive bands. The nitrogen Second Positive bands give the plasma its characteristic blue color (71). They are the primary

feature of the spectral emissions over the entire range from 200 to 700 nm. The most intense bands are shown in Figure 22 and Figure 23. Some First Positive bands were detectable in the range of 600 to 700 nanometers, but the intensities were at least 20 times lower than the Second Positive bands. The yellow color of these bands was visible, but it was so dim that it only made the blue color of the Second Positive bands appear paler.

Atmospheric Pressure Studies:

The MIP discharges at atmospheric pressure and at low pressure illustrate basically the same features. Comparison of Figure 23 and Figure 25 will demonstrate this. The major difference in spectral characteristics at the different pressures, is that more quenching is occurring at atmospheric pressure. This can be seen by comparing the vibrational bands, 2P(1,2) and 2P(0,1). The lines also exhibit some pressure broadening.

It was thought that the maxima observed in the gas composition studies for LIF, AES, and LEI might be due to an abnormally large concentration of the $N_2(A)$ state of active nitrogen. Spectral scans were done to investigate this hypothesis. The results in Figure 26 on page 93 indicate that the N_2 (A) of active nitrogen is not primarily responsible. At 10% N_2 in Ar, (spectrum B in Figure 26) there is no unusual change in spectral appearance. Again, no Vegard-Kaplan bands are detectable. An increase in concentration of the $N_2(A)$ state of active nitrogen does not account for the peak observed at low concentrations of nitrogen in argon for the LIF, AES, and LEI experiments.

One other thing is worth noticing in Figure 26. As the gas composition is changed from pure argon to pure nitrogen, the NH bands appear and steadily increase, and the OH bands decrease relative to the NH bands. These changes are to be expected. Nitrogen is being added to the pure argon plasma so NH bands will appear. For a fixed observation height close to the cavity wall, the OH band intensity will decrease because of increased OH molecule dissociation. This is because the plasma gets thermally much hotter as nitrogen is added (35). The plasma also gets hotter as applied microwave power is increased. Figure 27 on

page 94 illustrates an OH band decrease relative to the NH band, again because of increased OH molecule dissociation.

Spectroscopic Results - Further Observations and Conclusions:

At 1 atmosphere all intensities are reduced greatly, about 5 times that at reduced pressures (10 torr). At all pressures, the Second Positive bands have the highest intensity. The First Positive bands are weak, though detectable, at low pressures, but not at 1 atmosphere. Some upper vibrational state quenching is occurring as the pressure is raised from 10 torr to 1 atmosphere. ***In all cases the Vegard-Kaplan bands are not detectable.*** Nor is there an appreciable N atom concentration, usually indicated by emission which occurs at 337 nm. This is because the N atom excited metastable states have long lifetimes (greater than 10 sec), and emission is expected to be weak. These statements are true of both the afterglow and the discharge. ***Since the spectra retain the same basic features at 1 atmosphere as at 10 torr, the plasma is basically unchanged.***

Conclusions

It is hoped that this work represents a significant contribution to microwave plasma spectroscopy. The Highly-Efficient Molecular Microwave cavity developed in these studies provides ease of operation, robustness, insensitivity to aerosol introduction, low gas consumption relative to an ICP, and freedom from all external tuning and impedance-matching devices. Cavity tuning and impedance matching are fairly insensitive to microwave power and flow rate changes. Small changes in applied power and flow rate do not significantly alter the optimum positions of the impedance matcher or tuning rod. This highly power-efficient atom source provides a plasma with the same excitation energies as MIP cavities which require 2 to 3 times more applied power. The decreased diameter provides closer frequency matching, hence greater plasma stability. The isolator/circulator circuit greatly stabilizes the generator

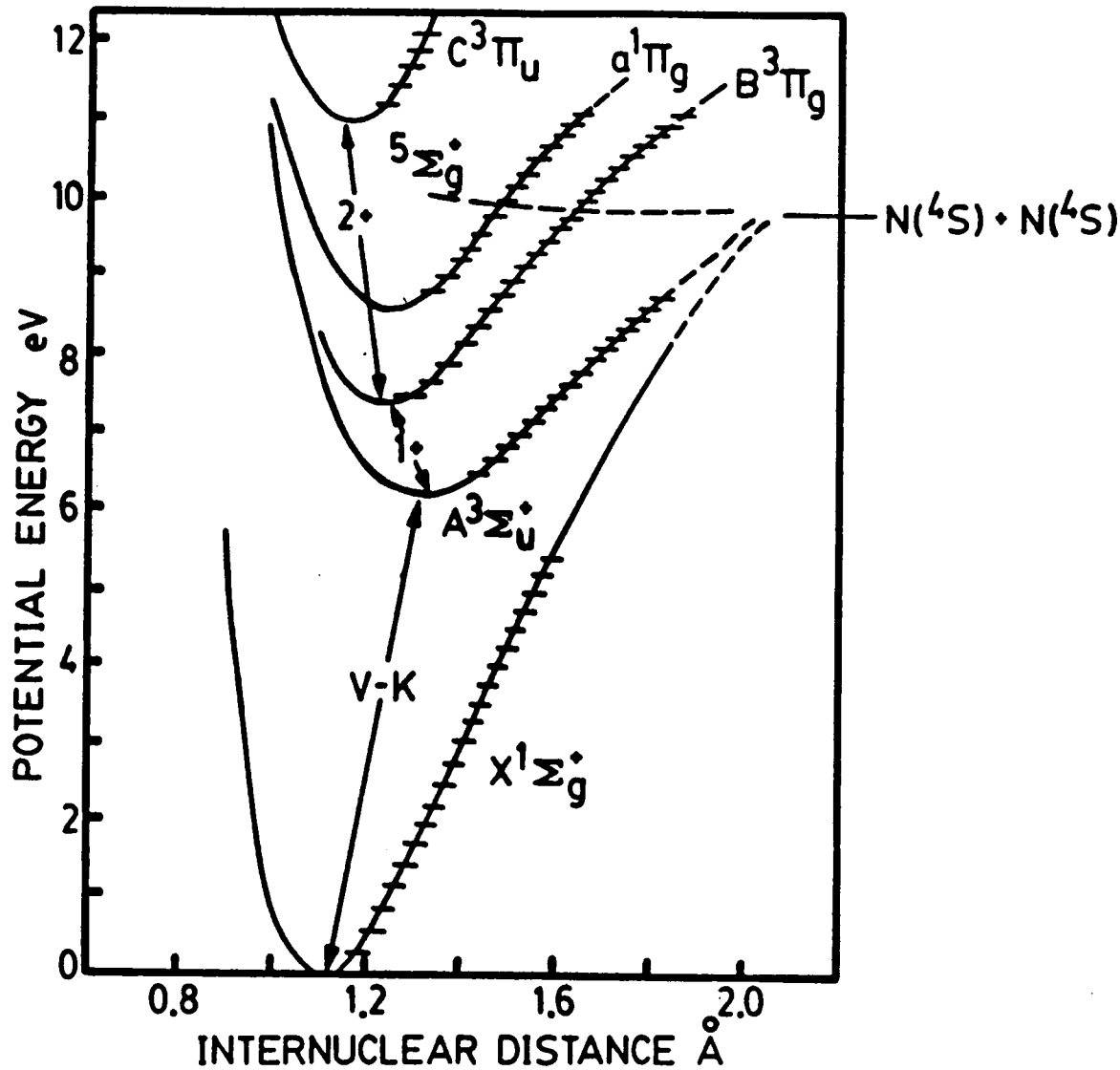

Figure 20. Excited States and Transitions of the Nitrogen Molecule: This figure was taken from Reference (72.).

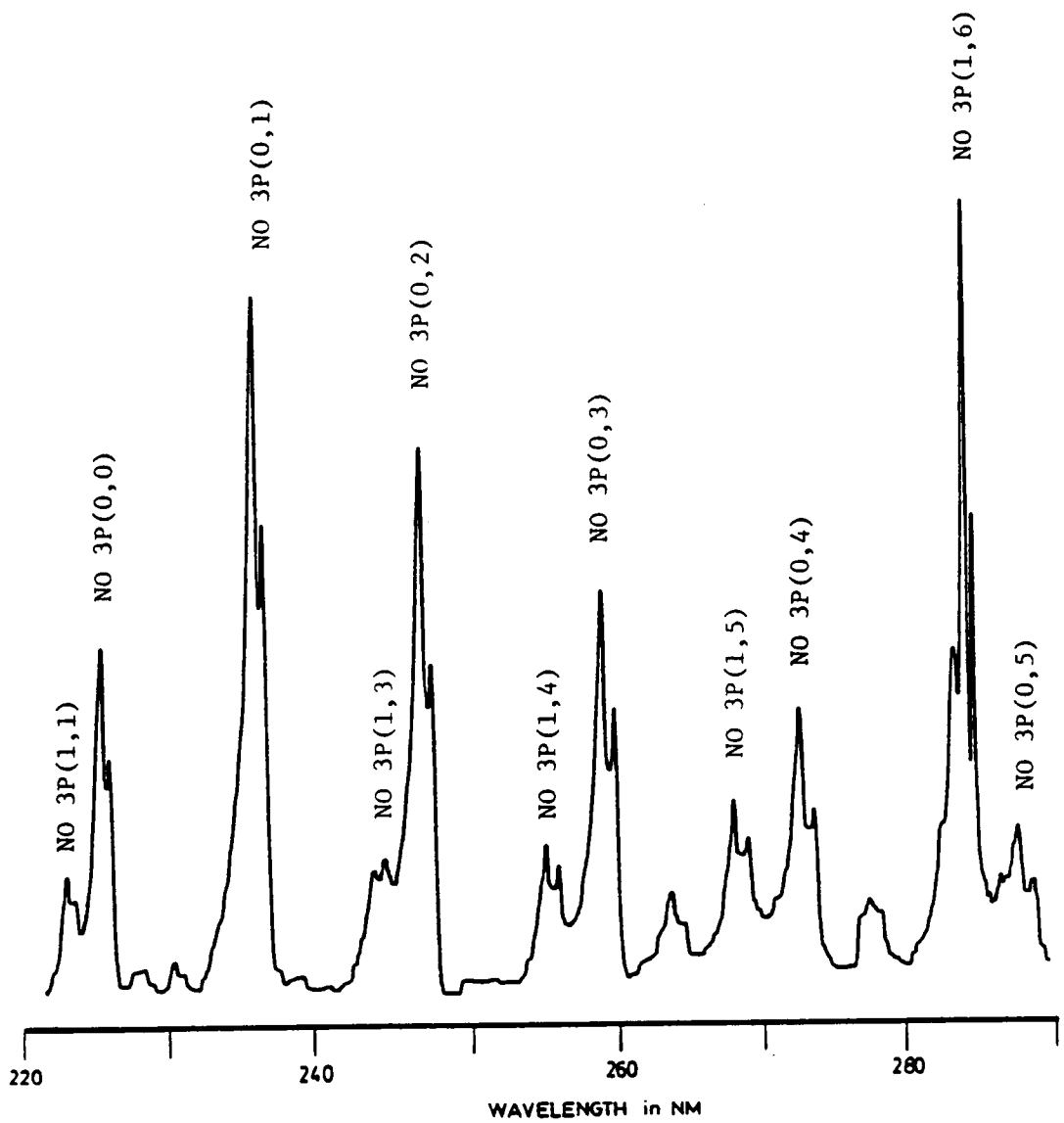

Figure 21. **N2 Plasma Spectrum - Direct Discharge at Low Pressure - UV:** Experimental Conditions: Forward Power = 12 Watts, Reflected Power = 4 Watts, Pressure = 10 Torr

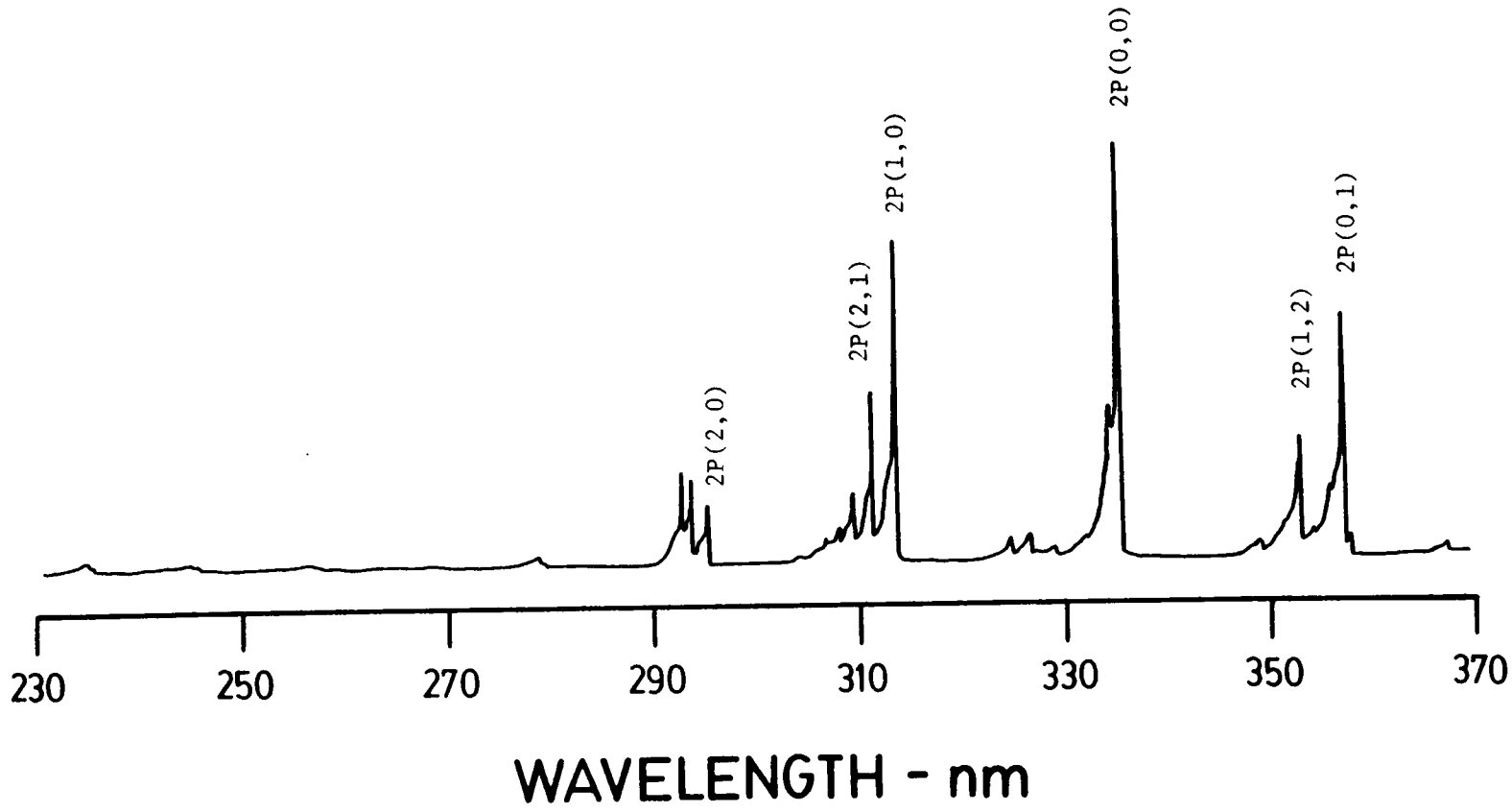

Figure 22. Nitrogen Plasma Spectrum - Direct Discharge at Low Pressure - Ultraviolet Region

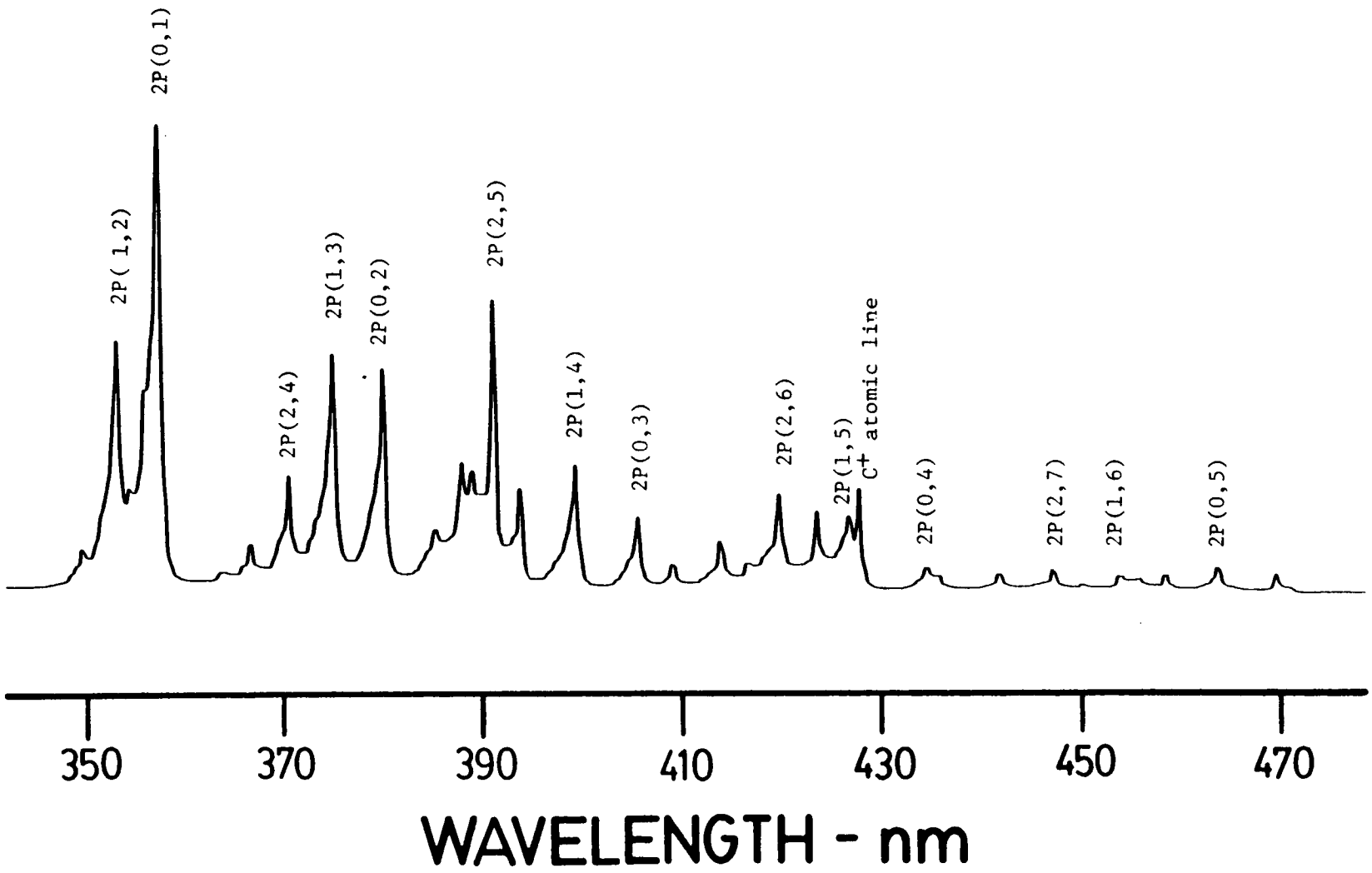

Figure 23. Nitrogen Plasma Spectrum - Direct Discharge at Low Pressure - Visible Region

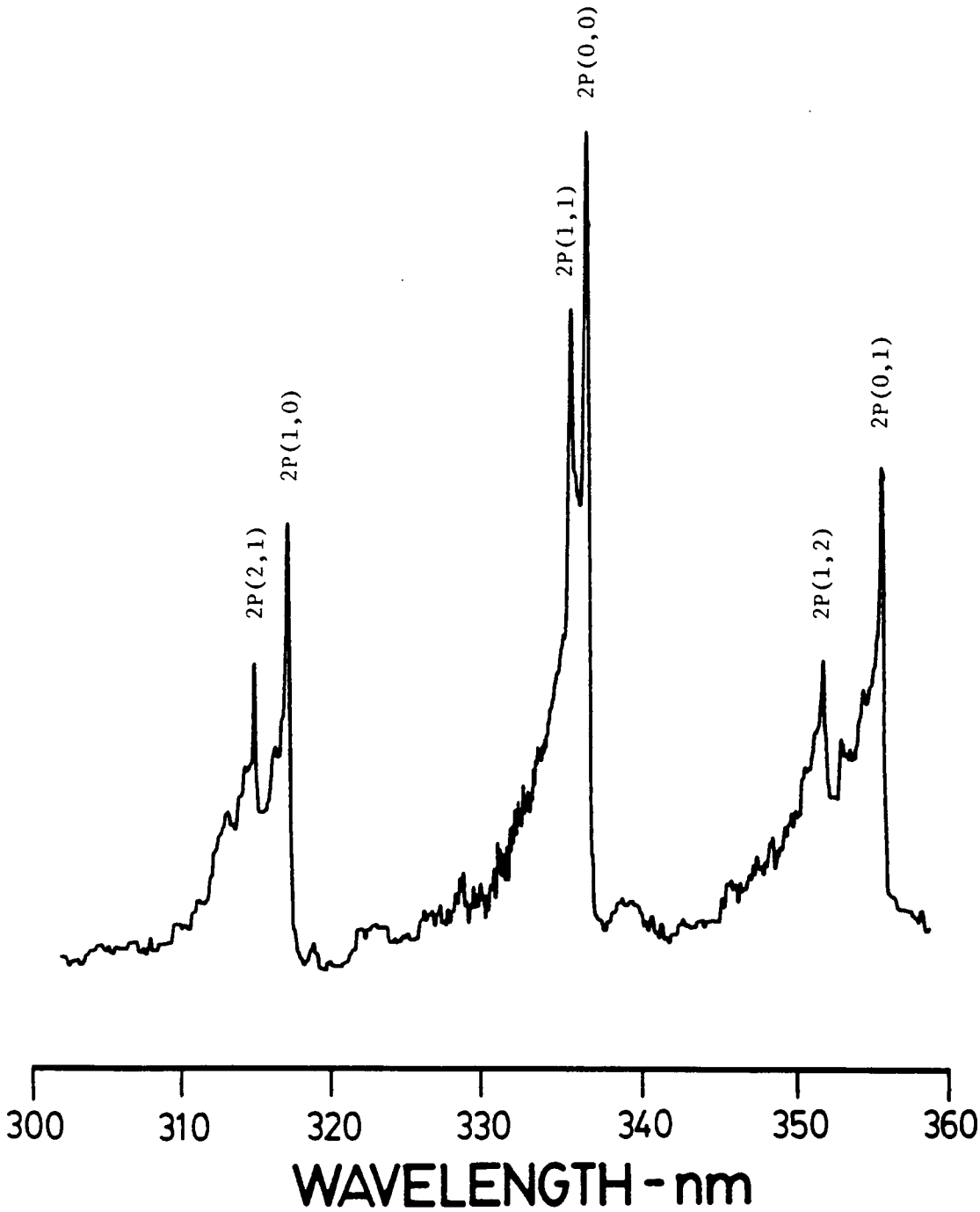

Figure 24. **N2 Plasma Spectrum - Direct Discharge at High Pressure - UV:** Experimental Conditions: Forward Power = 40 Watts, Reflected Power = 1 Watt, Pressure = 1 Atmosphere

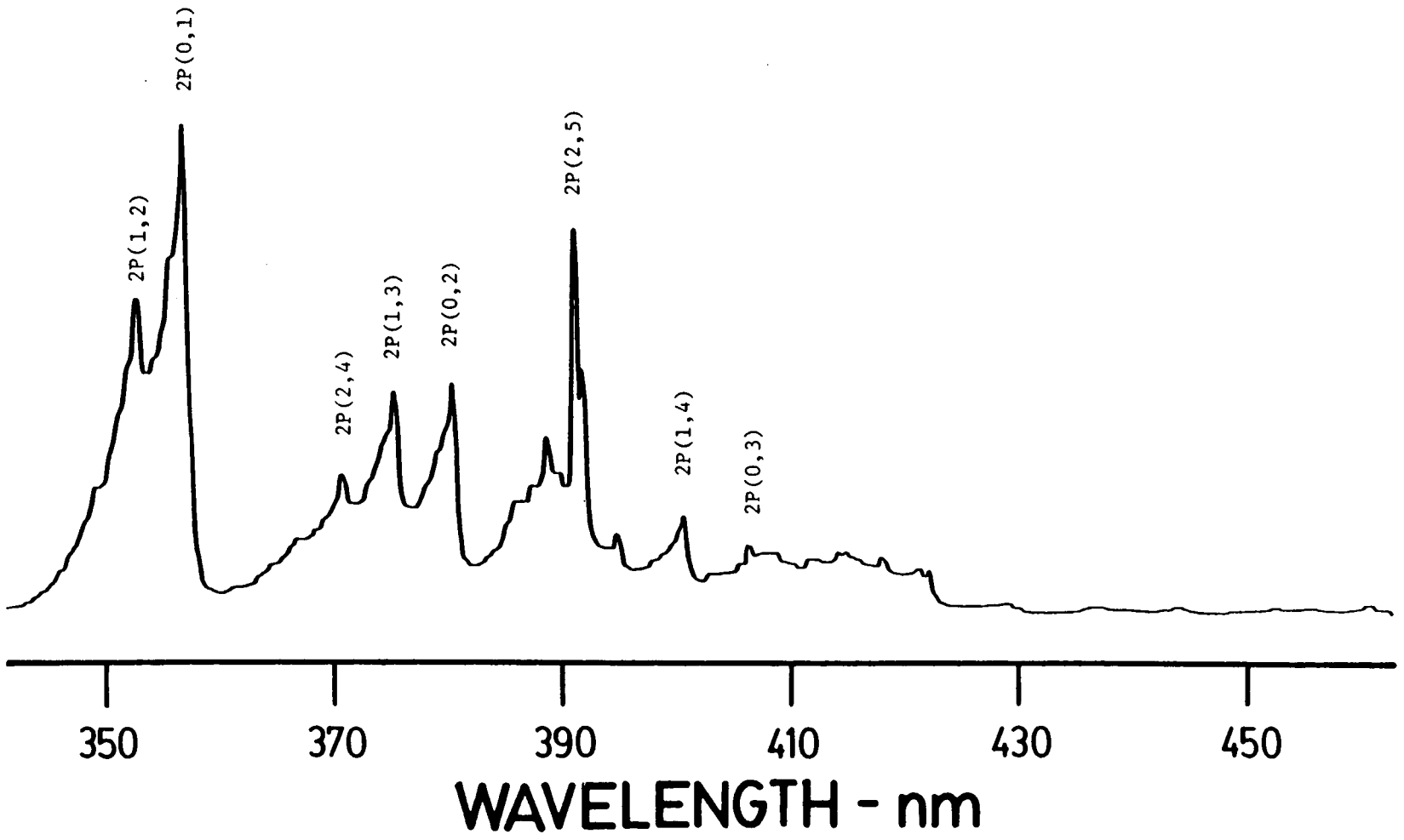

Figure 25. Nitrogen Plasma Spectrum - Direct Discharge at High Pressure - Visible Region

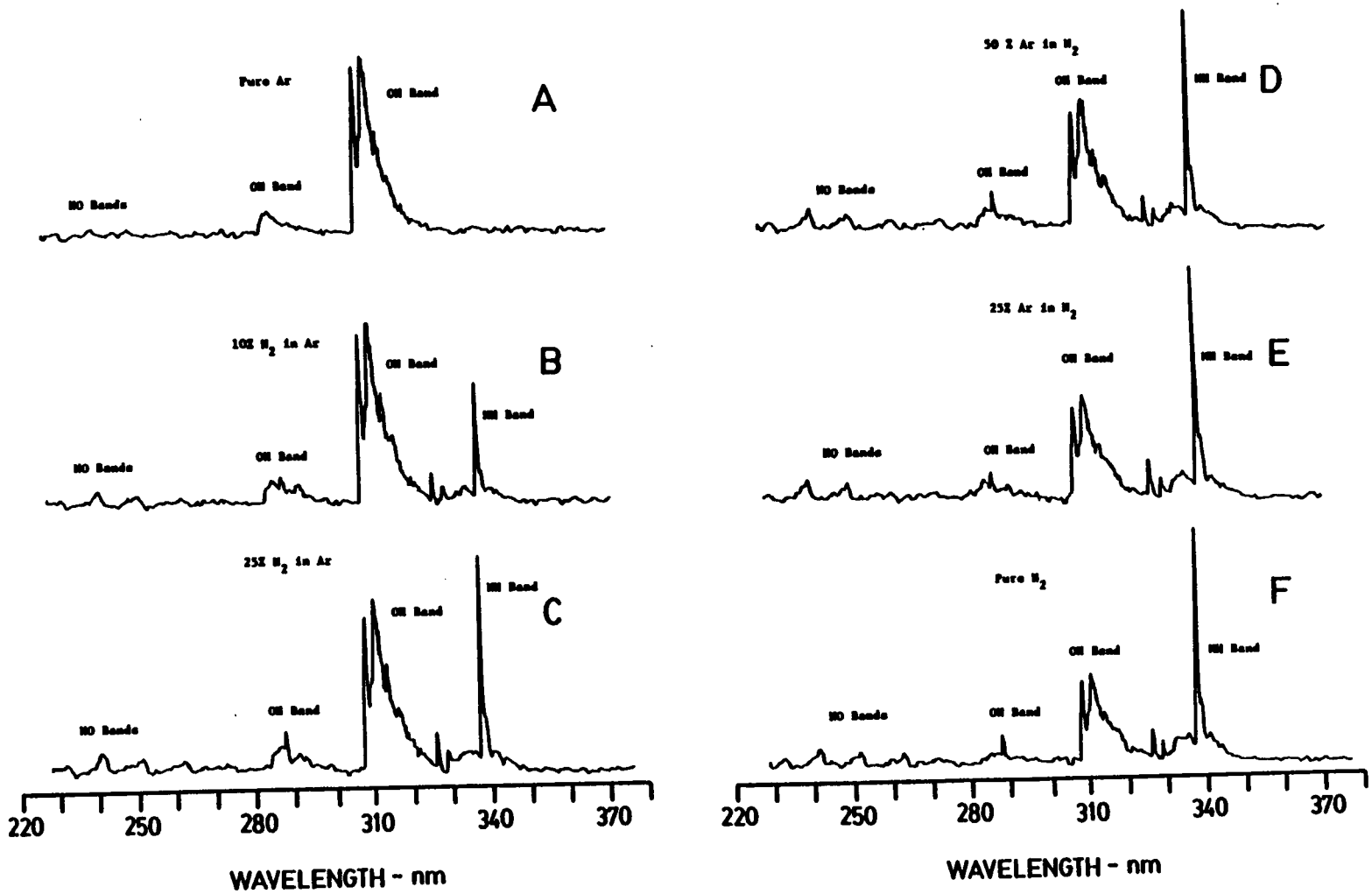

Figure 26. Nitrogen Plasma Spectrum - Ultraviolet Afterglow with Aerosol Flowing

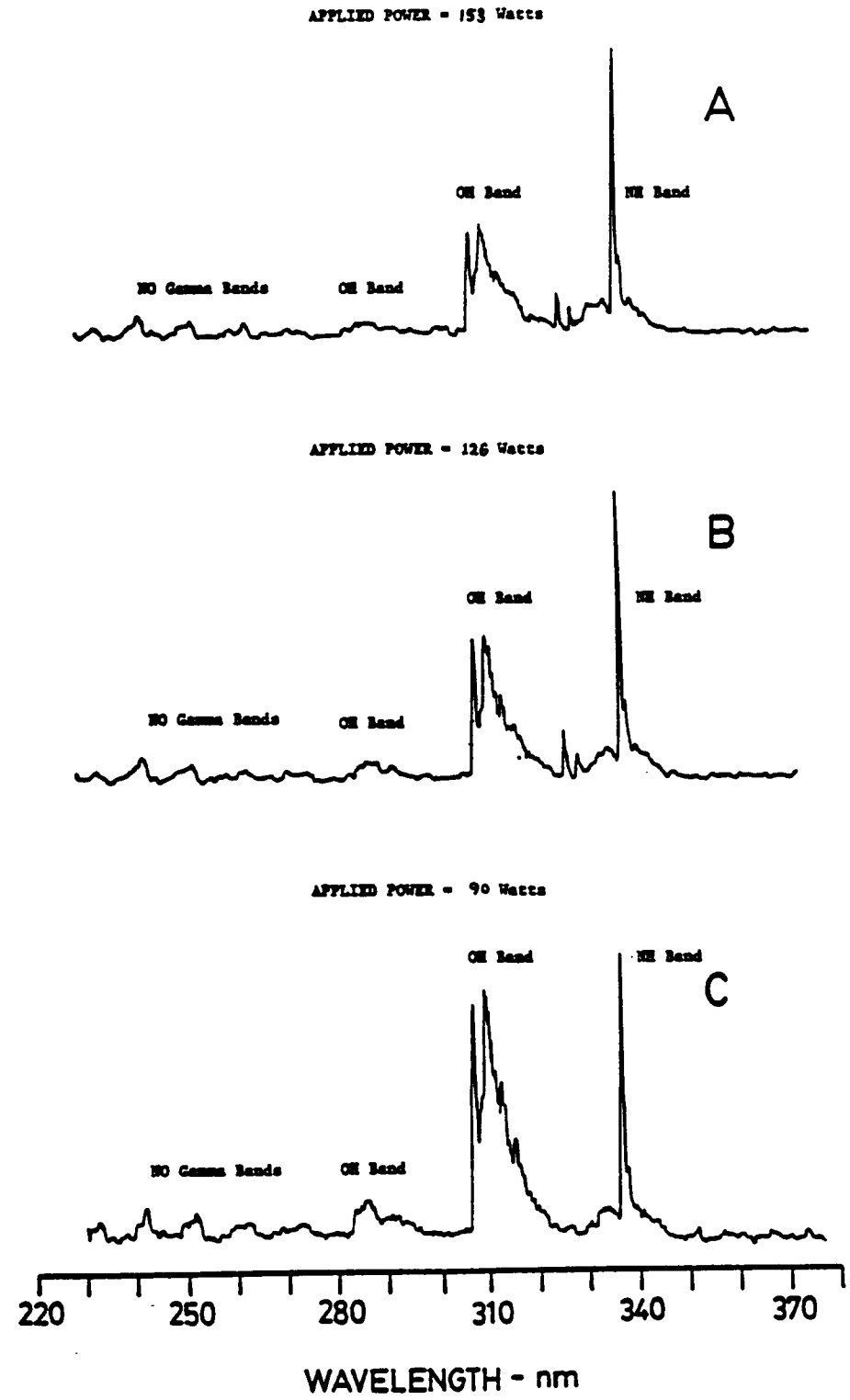

Figure 27. **N2 Background Spectra - UV Afterglow with Aerosol Flowing:** Experimental Conditions: Pressure = 1 Atmosphere, with aerosol flowing.

by eliminating spurious modes of magnetron oscillation due to reflected power perturbing the magnetron. The straight wire probe gives the best performance in terms of ease of ignition, stability, and power transfer to the cavity. All of these improvements on the original Beenakker design together have greatly improved the power transfer characteristics to the N_2 -MIP.

With further development and application of these MIP systems it is conceivable that they may have capabilities that compete with or surpass the ICP. Its small size, low power and gas consumption, low cost, and safety are distinct advantages over the ICP, with atomization efficiencies that favorably rival the ICP. Further work on increasing power transfer efficiency into the plasma may raise the excitation energies to equal that of the ICP. The analytical utility of these plasmas depends upon what mode of spectroscopic detection is used, and what element is considered, as will be seen in the next chapter on spectroscopic applications of the MIP.

III) LASER-INDUCED FLUORESCENCE IN MICROWAVE-INDUCED PLASMAS

A) HISTORICAL SECTION

An exhaustive review of the history and theory of AFS in flames and plasmas is unnecessary and would be redundant. Excellent reviews of the area have been published. The most recent and definitive by Omenetto and Winefordner in 1979 (8) includes references to analytical and diagnostic studies, and summarizes the primary results up until that time. Specific details on instrumentation, experimental conditions, and methodologies are contained in the monograph by Sychra, Svoboda, and Rubeska (73), and the earlier reviews by Browner (74), West (75), and Wineforder (76). Short reviews focussing on pulsed laser-excited AFS have been published by Weeks and Winefordner (77), and Omenetto (78). A short review by Van Loon points out some critical areas needing research (79). The reader is referred to these sources for an exhaustive coverage of the theory and applications.

The purpose of this chapter is to outline the major points needed to understand the experimental results presented in the next chapter, and to show the relationship of this experimental work to previous work.

A short definition of fluorescence will be presented first, followed by a very brief history of AFS up to the present time. Then a description of fluorescence instrumentation will be presented, along with some key concepts that are important for a finer understanding of fluorescence measurements. After that, these concepts will be used in a discussion of the AFS applications most directly related to LIF in MIP's. This will clarify the relationship between laser-induced fluorescence in microwave-induced plasmas (LIF/MIP) and other techniques.

What is Atomic Fluorescence Spectroscopy ?

Atomic fluorescence occurs when an atom absorbs radiation of a particular energy and then emits the radiation as light. If the emitted photon has the same energy as the absorbed photon, this process is called resonance fluorescence. Energy can be lost or gained in collisions with surrounding atoms. If the emitted photon has less energy than the absorbed photon, the process is called Stokes fluorescence. If the emitted photon has more energy than the absorbed photon, the process is called anti-Stokes fluorescence. A pictorial representation of these processes is given in Figure 28 on page 98. It should be remembered that the lowest level (labeled "M") can be an atomic ground state, a thermally-populated excited state, or an excited state populated by another laser photon.

Early History of Atomic Fluorescence Spectroscopy

Atomic fluorescence was first studied by physicists in the late 19th century. The first half of the 20th century focussed on discovering the fluorescence lines of more elements in the periodic table. In 1956, Boers, Alkemade, and Smit (80) first used atomic fluorescence to study fundamental physical and chemical processes in flames. And in 1962 Alkemade (81)

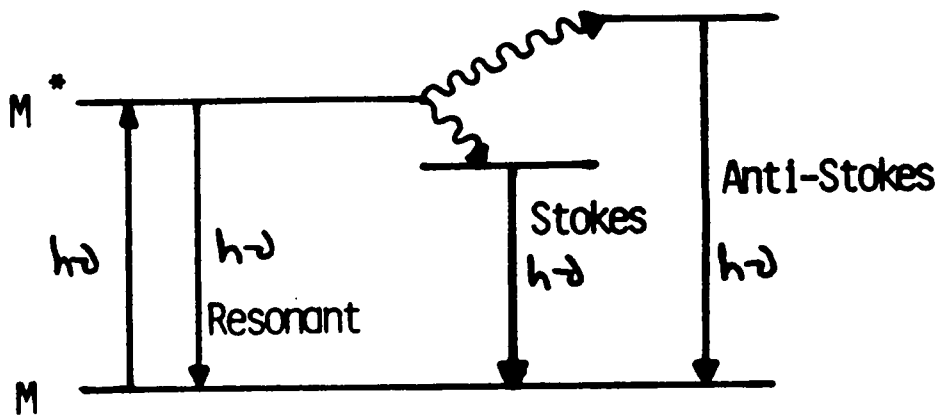

Figure 28. Fluorescence Processes

suggested its use in analytical chemistry. The demonstration of the utility of flame atomic fluorescence for chemical analysis was done by Winefordner and Vickers in 1964 (82).

The development of AFS has been slow relative to atomic absorption and atomic emission spectroscopy. AFS came after these other techniques and is generally used for the same classes of problems. These other techniques developed in the late fifties, when there was a great impetus to find a sensitive, simple, and broadly applicable method of analysis. However, since its introduction, fluorescence has grown from just a tool for research work, to a standard method of analysis for many routine analytical labs.

Besides analytical applications, AFS is used for flame and plasma physical diagnostic studies: excited state lifetimes (83), temperature profiles (84 , 85), number density (86 , 87), fluorescence quantum efficiency (88), and flow velocity measurements (89). These studies are done for both support gas and analyte species (atoms, molecules, and ions). Many theoretical and experimental details of these techniques are given by Omenetto and Winefordner (8), Bradshaw et al (90), and references therein. An extensive review of molecular LIF techniques was written by Demtroeder (91). Lasers have greatly advanced the state-of-the-art for these fluorescence applications.

Laser-induced fluorescence (LIF) is one of the two techniques used to do single atom detection (92). The other is resonance ionization spectroscopy, abbreviated RIS (93), A explanation of this technique can be found in Appendix C. The single-atom-detection technique is ahead of its time and is slowly finding more uses. As state-of-the-art lasers advance, it will be possible to perform such ultra-sensitive measurements for more elements, in more varied applications.

Instrumentation Used in AFS

The instrumental configuration used in AFS is shown in Figure 29 on page 101. Light from the excitation source (1) passes through a modulator (2) into the atom source (3). The atoms absorb the radiation and emit fluorescence in all directions. Fluorescence is observed at a right angle to the illuminating source to avoid direct viewing of the excitation source. This viewing angle also minimizes source scatter. The fluorescence passes through the collection optics (4) into a radiation filtering device, usually a set of optical bandpass filters or a monochrometer. After the fluorescence wavelength of interest is filtered, the photons are converted into an electrical signal, usually using a photo-sensitive electron tube (5). The signals are subsequently amplified (6), displayed, and recorded (7).

Features of AFS

One of the unique features of AFS is that it is a "self-filtering" technique, i.e., only while the excitation source is shining into the atom source is fluorescence present (ignoring the very short fluorescence decay times). Thus the pure fluorescence signal can be isolated by modulating the excitation source, detecting during the period while the atoms are being illuminated, and then subtracting the atom source emission background which occurs during the period of non-illumination. AFS has a significant advantage over atomic absorption techniques because it consists of measuring a large signal on top of a small background; atomic absorption measures a small signal on top of a large background.

The three factors crucial to producing intense fluorescence signals are:

- High Excitation Source Intensity at the Wavelength of Interest
- High Atomizer Efficiency and Performance
- Freedom from Noise Sources

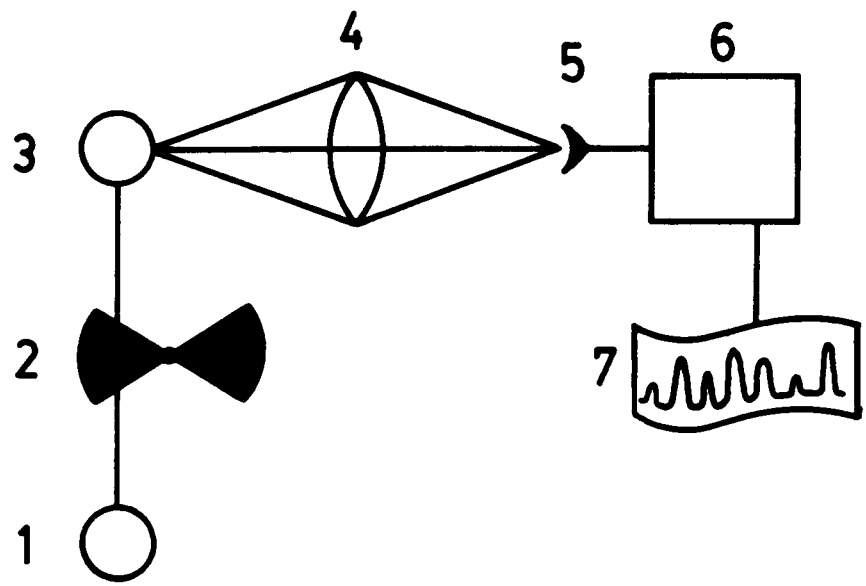

Figure 29. Instrumentation Used in Atomic Fluorescence Spectroscopy

Excitation Sources

The lack of availability of suitable excitation sources initially slowed the application and acceptance of AFS for routine analytical applications. However, the search for better fluorescence sources has led to major advances in excitation source technology. The following brief outline will help inform the reader about the important variables to consider when for choosing a source for AFS.

- High Intensity at the Wavelength of Interest **
- Freedom from Stray Light and Spectral Interferences **
- Good Short and Long Term Stability
- Simplicity of Operation
- Output at All Excitation Wavelengths
- Short Warmup Time
- Low Total Cost and Long Lifetime

The types of sources that have been used for AFS are:

- Pulsed and Continuous-Wave (CW) Lasers
- Xenon Arc Lamps with Bandpass Filter or a Monochrometer
- Microwave-Excited Electrodeless Discharge Lamps, including Metal Halide Lamps
- Radio Frequency Plasmas
- Hollow-Cathode Lamps

At present, none of these sources satisfy all of the requirements listed above. A critical discussion of each type of source will clarify the many tradeoffs to consider when selecting one of them.

Pulsed dye lasers and continuous-wave (CW) dye lasers are the best sources when considering intensity and spectral purity alone. They are the highest intensity sources and possess the highest spectral purity available. However, lasers have not yet met the promise of their potential. Lasers cost considerably more than all other sources. The laser dyes

degrade rapidly, are rather expensive, and are not presently available at all wavelengths of interest. The ultraviolet region is still difficult to access without frequency doubling and tripling crystals. Tuning etalons must be employed to narrow the output bandwidth, but then very narrow linewidths (0.01 angstroms) are possible. However, the intensity and spectral purity lasers offer far exceeds those of all other sources.

Microwave-excited and radio-frequency electrodeless discharge lamps, containing either pure metals or metal halides are excellent line sources. These line sources have high intensity outputs and good spectral purity. The lamp lifetimes are long, the problems with line self-absorption are minimal, and the cost approximate that of hollow cathode lamps. However, the stability is poor compared to other sources, particularly the xenon arc lamps, hollow cathode lamps, and CW lasers. Very close attention must be paid to their preparation and operating conditions. Commercial lamps sometimes lack sufficient stability and intensity. They can be made in the laboratory, but this approach is often tedious. They are not tunable; a different lamp is needed for each element. However, the lamps are easily interchanged. Lamps can be prepared for almost every element, and progress is being made in fabrication of multi-element lamps. These are the most studied of all excitation sources for AFS.

Hollow-cathode lamps exhibit good short and long term stability. They are similar to electrodeless discharge lamps in many respects; they are simple to operate, lamps exist for many elements, their intensities are greater than that of xenon arc lamps, and there are not a lot of problems with stray light and spectral interferences. Because they are single element lamps they provide excellent spectral selectivity. The major disadvantages of these sources is that lamps are expensive and line intensities are low. However, analytical limits of detection for these sources are still substantially better than that for continuum sources.

Continuum sources such as xenon arc lamps have some advantages over other sources. Multielement analysis is possible just by changing filters or changing the monochrometer wavelength. They have a long lifetime (1200-2000 hours), cost less than other sources, are

simple to focus and operate, and have good long and short term stability. Problems with continuum sources include:

- Low intensities at any one particular wavelength
- Required optics quality for beam focussing is critical since the the arc spot size is small.
- Arc-wandering can be excessive during burn-in time.
- Spectral interferences and stray light are considerable unless a monochrometer and spatial filtering are used.

Clearly an ideal AFS excitation source does not yet exist.

Atomizers

Sample introduction is known to be the least well-developed aspect of analytical spectroscopy. Indeed, improvements in atomizer technology have not kept pace with advances in optical and electronic components (94). Atomizers are generally the weakest part of an analytical instrument.

The desirable characteristics for an atomization cell for AFS are (8 , 73):

- High Density of Atoms
- Long Residence Time of Analyte Atoms in the Optical Path
- Low Background Emission
- Freedom from Physical and Chemical Interferences
- High Volatilization Efficiency (to avoid light scatter)
- Low Quenching Properties
- High Stability and Reproducibility
- Simplicity of Operation
- Low Cost

The most commonly used atom sources for AFS are:

- Chemical Flames
- Hot Wire Filament Devices
- Furnaces Atomizers
- Cathodic Sputtering Devices
- Inductively Coupled Plasmas
- Atom Cells

All currently used atomization systems require tradeoffs between important characteristics. Some of these tradeoffs can best be illustrated by contrasting a few of the most commonly used atomizers - ICP's, furnace atomizers, and chemical flames. The ICP provides the greatest freedom from chemical and physical interferences, but background emissions limit the ultimate sensitivities attainable, and its initial and operating costs are prohibitive for many laboratories. Furnace atomizers have provided the best possible sensitivities when they are used in an atom cell configuration, but they also possess the worst chemical and physical interferences. Atom cells are also not very practical because they are tedious to operate.

Chemical flames are low in cost, and are simple and easy to operate. However, there are problems with sample matrix interferences, background emissions are strong, as is flame flicker noise. Residence times in the optical path are short. Species such as carbon monoxide, carbon dioxide, and nitrogen molecules are effective quenchers and lower fluorescence yields. Reducing flames are needed to minimize refractory metal oxide formation, but they are also very luminous.

The temperature of the atomizer accounts for many of these characteristics. Generally a very hot atomizer provides efficient atomization and freedom from chemical and physical interferences but suffers from high background emission. Low temperature atomizers have the lowest background emission but have great problems with chemical and physical interferences.

Some of the other design constraints for existing sampler/atomizer systems are in conflict with each other. The sample flow rate through the system should be minimized to maximize residence time in the optical path, and temperatures should be maximized to minimize physical and chemical interferences. However, higher flow rates are normally needed to effectively cool the hot atomizer; this is particularly true for a continuous sample introduction system where there is no time for a cooling cycle. One would like to minimize spectral background and fluorescence quenching effects by working in an inert gas atmosphere. Yet these gases are expensive and it is most economical if flow rates are minimized. However, the high temperatures required to minimize interferences establishes a lower limit on the minimum flow rates. These tradeoffs between analytical and economic factors seem unavoidable with all present-day sample atomization systems.

Detection Systems

The following detection systems are commonly used for fluorescence measurements:

- Phase-Sensitive Detection
- DC Amplifier
- Boxcar Averager
- Photon Counting

Phase-sensitive detection and DC amplifiers are employed with continuous-wave excitation sources. Boxcar averaging is used for pulsed excitation sources. Photon counting systems have been employed with both CW and pulsed sources.

Phase-sensitive detection is by far the most common detection system for instruments with continuous-wave excitation sources. This technique, also commonly called lock-in detection, modulates the excitation source, which produces modulated fluorescence signals. The modulated signals are then amplified, synchronously demodulated, and then low pass

filtered (95.). The end result is that only signals at modulation frequency (fluorescence signals) are amplified; all other frequencies are left unamplified and are filtered out. Most lock-in amplifiers have an additional tuned amplifier to provide further noise rejection. Lock-in amplifiers are easy to use, provide automatic background subtraction and give signal-to-noise ratios close to the theoretical limit. The primary problems are not with lock-in detection but with excitation source and atomizer drift.

Another type of detection system not used much anymore is a ***DC amplifier*** with an unmodulated excitation source. Its primary advantages are very large dynamic range (10-15 decades is not unusual) and very wide bandwidth. These systems are usually have severe long-term drift and gain instability, and require manual background subtraction. These systems are still useful for special situations where the very high-speed and wide dynamic range are needed.

Boxcar averaging (gated detection) must be used for very fast pulsed excitation systems (usually lasers) since the fluorescence pulse exists for only a short time after the excitation pulse. The primary problem with this approach is excitation source drift in the form of poor shot-to-shot reproducibility.

Photon counting employs high-sensitivity photomultiplier tubes to produce a current pulse at the anode for every photon that impinges upon the photocathode. Pulse-height discrimination can be used to set a minimum threshold for signal detection. The principle disadvantages of photon-counting systems are the inability to distinguish between photomultiplier dark-current pulses and signal pulses, and the limited dynamic range due to the pile-up of pulses at high counting rates. However, they are very useful for extremely low-level light measurements and provide a signal-to-noise improvement of approximately two over analog systems such as lock-in detection and DC amplification (8).

Key Concepts in Atomic Fluorescence Spectroscopy

Optimal AFS measurements are made by minimizing signal interferences and sources of noise. The following sections are intended to impart an understanding of the most common signal interferences and types of noise, their sources, and, how they can be most effectively eradicated.

Scattering Problems

Light scattering constitutes the major limiting factor in AFS. The two major types of scatter are Rayleigh scatter and Mie scatter. Rayleigh scatter is due to source scattering from atoms and molecules; it constitutes the fundamental limit of AFS. However, it is ordinarily not a problem, even for high-power pulsed lasers used for resonance fluorescence (8). Rayleigh scatter is only a problem for ultra-high sensitivity measurements. Mie scatter is due to source scattering from unvaporized particles and aerosol droplets. It is the **MOST** significant practical limitation for AFS methods, particularly when resonance fluorescence is used. It can be reduced most effectively by increasing nebulization efficiency and using non-resonant transitions.

Nonresonance Fluorescence Advantages:

A nonresonant fluorescence transitions occurs when the fluorescence wavelength is different from the excitation wavelength. Mie scatter occurs at the excitation wavelength only, and is eliminated by employing nonresonant transitions. Reflections in the optical components are also eliminated. Nonresonance fluorescence can also be used to study the collision dynamics of states involved in fluorescence processes, relaxation rates, energy transfer mechanisms and cross sections of fluorescence processes.

Saturated Atomic Fluorescence Advantages:

Saturated fluorescence occurs when, for a two-level atomic system, the population of the two states (initial and final) become equal, i.e., just as many photons being absorbed by the system as are being emitted. A full theoretical treatment of saturation was done by van Dijk, Omenetto, and Winefordner (96). The main advantages gained by achieving saturation in AFS are (97 , 98):

- Extended linear range of analytical working curves
- Freedom from laser intensity fluctuations
- Freedom from excited state quenching

Another way of stating saturation is that "the absorption coefficient, which is proportional to the ***difference*** between the atomic populations of the levels, approaches zero" (78). The analyte medium becomes transparent, hence analyte self-absorption effects disappear. Self-absorption effects are the cause of the "bending-over" of analyte fluorescence and absorption working curves at high concentrations. Since these effects are eliminated, the analyte working curve will remain linear up to higher concentrations.

High-powered pulsed lasers exhibit shot-to-shot intensity fluctuations. Under saturation conditions the atomic system no longer absorbs additional radiation, so the fluorescence signal does not reflect the intensity fluctuations. The analyte atoms are the "limiting reagents" in this photophysical process. That is, every time an atom emits a photon there is another photon waiting to be absorbed by that same atom. Photons are the limiting reagents under non-saturation conditions. Freedom from excited state quenching occurs under saturation conditions because the system is then "radiationally controlled" by the laser, rather than by thermal, chemical or decay processes (98).

There are some problems with operating in a saturated mode. Scattering increases in direct proportion to laser power, hence detection limits eventually suffer and power is wasted

(99). Also, the laser intensity can be so great that multiphoton and ionization processes will begin to occur. At high photon fluxes Stark broadening will begin to affect line widths. Thus, in certain cases, near-saturation conditions may be preferable to full saturation.

Signal Interferences

Signal interferences arise from many sources; spectral, physical, and chemical interferences.

Spectral Interferences:

Spectral interferences are primarily due to excitation source scatter, overlap with atomic fluorescence and molecular fluorescence bands, and thermal emission background from the atom source. The result is an analyte signal that is too large.

Minimizing excitation source (Mie) scatter by using non-resonant transitions and efficient sample vaporization has already been discussed. However, elements such as Zn and Cd have no non-resonant transitions, and resonant transitions must be used. In such cases, excessive excitation source scatter can be eliminated by paying careful attention to proper shielding, baffling, and atom cell design.

Atomic line and molecular band background fluorescence can be compensated for by scanning the fluorescence spectrum in the vicinity of the analytical line and subsequent subtraction (89). Elimination of such interferences is not always possible if there are peaks which severely overlap. Sometimes a reduction in spectrometer bandpass will eliminate the problem, but this may also decrease an already-too-weak analyte signal. In such a case going to another fluorescence line may avoid the problem. Thermal emission from the atom source is a problem for DC detection systems. This is easily eliminated using by modulating the excitation source and using synchronous detection.

Physical and Chemical Interferences:

Physical factors can interfere with sample transport, efficient nebulization and solvent evaporation. The method of atomization is most critical (8). Delivery of solution to the atomizer must be constant. Nebulization and solvent evaporation are affected by the solution viscosity, surface tension, and vapor pressure (73). These factors are all influenced by matrix (chemical) effects.

Chemical interferences affect the rate of analyte particle volatilization and ionization. Chemical interferents alter the solid (usually molecular) phase formed after solvent evaporation, giving it a different thermal stability in a flame or plasma. Releasing agents such as EDTA suppress formation of refractory materials (35).

AFS exhibits generally the same interferences as atomic emission and atomic absorption. This is not surprising since the interferences depend primarily upon the chemical properties of the analyte and the interferent. These interferences are well documented (100 , 101.). Low temperature flames and atomizers can have severe problems with such interferences. MIP's and ICP's have less severe problems with volatilization interferences because of their higher temperatures (8 , 35).

Ionization interferences can be caused by the presence of easily ionizable elements (EIE's). EIE's release electrons into the chemical system, which shift the equilibrium to favor atom formation, giving a net atomic signal enhancement. These effects are present in flames, ICP's, and MIP's to varying degrees, and can be eliminated by adding an ionization suppressant (an excess of another EIE) such as cesium, to both standard and blank solutions (35).

Noise Sources

Types of Noise:

The two general classes of noise are additive noise and multiplicative noise. Additive noise simply adds to the signal and does not increase with signal increases. Multiplicative noise increases with signal increases; it is much more difficult to locate and deal with.

Specific classes of noise are:

- White Noise
- Flicker Noise
- Shot Noise
- Discrete Frequency Noise

White noise is noise with "all colors", i.e., it is equally distributed over all frequencies. Flicker noise is commonly called "one-over-f" (1/f) noise since it decreases as frequency increases. Shot noise is due to the inherently random behavior of quantum systems such as electrons, atoms, and photons. Discrete frequency noises occur only at fixed frequencies and are usually due to interfering electrical signals.

White noise is found in excitation sources, atom sources, and detection systems. Excitation sources exhibit white noise due to the random nature of photon emission from a light source (this also applies to flame and plasma background emission, and is referred to as background emission shot noise). Atom source white noise is due to the random motion of analyte atoms as they absorb and emit radiation. Detector white noise is due to shot noise caused by the movement of electrons across semiconductor junctions and anode-cathode electrode surfaces that comprise detection circuitry. Johnson noise is similar to white noise and is due to the movement of electrons in conductors without junctions, such as wires and bulk semiconductor.

High sensitivity measurements are ultimately limited by the background emission shot noise and detector shot noise (8). This random noise (due to atom and electron quantum behavior) exists in excitation sources, atom sources, and detection systems. It remains after all other noise sources have been eliminated (through proper baffling, the use of non-resonance fluorescence transitions, a high-efficiency atomizer, photmultiplier tube cooling, and other expediencies). Shot noise due to light scatter from unvaporized particles can become the most significant source in AFS systems; this is why atomizer efficiency is of paramount importance.

Flicker noise is often referred to as low frequency drift noise. It can arise in excitation sources, atom sources, monochrometers, filters and other optics, and detection systems. Excitation sources exhibit drift due to power supply current changes, temperature changes, and source spot "wandering" (in particular, continuum arc sources, electrodeless discharge lamps, and pulsed dye lasers). Excitation source flicker can become dominant since it can be magnified throughout the AFS system; this is particularly true for lasers. It is a multiplicative noise source, and can contribute to atom cell scatter, analyte fluorescence flicker, and detector flicker. ***Atom source flicker-noise*** is usually due to both short and long-term fluctuations in power and flow rates, sample delivery, and background emission. Local spatial density fluctuations of emitting and fluorescencing species is another source of flicker noise that occurs in atom cells, particularly at high analyte concentrations. Monochrometers, optical components, and detectors can all exhibit flicker noise due to temperature changes and vibration. Detectors can also exhibit flicker noise due to power supply current fluctuations.

Another class of noise is "pink noise", which is a combination of white noise and flicker noise. It shows a $1/f^n$ dependence, where n is between 0 and 1. It is still low frequency noise but the noise power spectrum does not fall off (as frequency increases) as fast as 1/f noise. The most common sources of this higher frequency drift are fluctuations in sample introduction and mechanical vibrations.

Discrete frequency noise is the last class of noise sources to consider. The two most common sources of discrete frequency noises are interference noise from power lines (60 Hz line frequency noise and harmonics) and whistle noise from flow turbulence effects (so named because of whistling noises made by flames and plasmas). These noise sources, once they are located, can be eliminated with band-reject filters.

Continuous Wave (CW) Lasers versus Pulsed Lasers

Continuous-wave (CW) lasers and pulsed lasers are historically the two major classes of lasers. Each class offers particular advantages over the other. Figure 30 on page 115 allows easy comparison of these two classes. This table was taken from Reference (102).

CW lasers offer particular advantages over pulsed lasers:

- Lower cost
- More stability, no problems with nonrepeatable pulse amplitudes
- No RF noise generated in the laboratory
- Very narrow bandwidths and accurate wavelengths
- Easier data handling than with low duty-cycle pulsed output
- Frequency modulation can provide greater background discrimination
- Greater maximum average power output (except for flashlamp-pumped dye laser)

The main advantages of pulsed lasers are derived from the high power advantage. It is easier to achieve saturation, which extends linearity of working curves and gives freedom from quenching effects. There is so much power that wavelength doubling and tripling crystals can be used to obtain continuous tunability below 200 nm, while still maintaining sufficient output power. And the very short pulses make it easier to do time-resolved spectroscopy. Pulsed-laser-pumped dye lasers also have the practical advantages that wavelength ranges can be changed quickly and easily by changing dye cuvettes, and they require much smaller volumes of dye solution than CW or flash pumped dye lasers. The main

Table 1
CHARACTERISTICS OF TYPICAL DYE LASERS

Type	Wavelength range (nm)[a]	Power (W)		Resolution (nm)		Pulse width (ps)	Pulse repetition rate (pps)
		Peak	Average	No etalons	With etalons		
Continuous wave dye	≃400—950	—	≃0.02—3	≃0.1—1	0.01—0.001	CW	CW
Synchronously pumped mode-locked dye	≃400—700	≃100—2000	≃0.08—0.1	≃0.1—1	≃0.01—0.001	≃0.5—10	≃100 MHz
Synchronously pumped mode-locked cavity-dumped dye	≃400—700	1—5 kW	≃0.03—0.1	≃0.01—1	0.01—0.001	≃1—20	≳1 pps—10 MHz
Ring dye	≃400—800	—	≳1—3	≃0.1—1	0.01—0.001	CW	CW
N_2-laser-dye	≃210—1000	≃1—300 kW	≃0.01—0.1	≃0.01	≳0.001	≃3000—8000	1—1000
Nd-laser-dye	≃250—1000	≃10 MW	≃0.5	≃0.01	≃0.002	≃10000	≃10
Excimer laser-dye	≃210—1000	≃1—5 MW	≃0.1—0.5	≃0.01	≳0.001	≃10000	≃1—1000
Flashlamp dye	≃260—365; 420—1000	≃10 kW—5 MW	≃0.3—10	≃0.03—5	≃0.1—0.001	≃10^6	≃0.1—30

[a] The range 210 to 360 nm must be obtained by frequency doubling.

Figure 30. Comparison of Different Types of Lasers Exerpted from "CRC Criical Reviews in Anal. Chem. Vol. 14, 231 (1981)".

disadvantage of pulsed lasers are the poor pulse-to-pulse repeatability that requires the use of expensive high-speed pulsed laser detection electronics. These can cost almost as much as the pulsed laser itself.

In general, laser methods possess characteristics not achievable with other atomic spectroscopic methods. The spectral selectivity achievable with lasers greatly exceeds other atomic methods. This is entirely due to the narrow bandwidths possible. Spectral resolutions (1*E+5 to 1*E+6), comparable to the very best spectrographs are possible (103). This resolution is sufficient to perform highly specialized analyses of isotopic and hyperfine structures, or collisional and radiative broadening of spectral lines (8).

Laser-Induced Fluorescence in Flames and Other Plasmas.

A short review of the LIF literature citations most pertinent to laser-induced fluorescence in microwave-induced plasmas will be given. The review will be broken down according to the type of atomizer used, since this often represents the weakest part (hence the most distinguishing characteristic) of an AFS system. Atomizers employed thus far for diagnostic and analytical atomic fluorescence studies include:

- Flames
- Inductively Coupled Plasmas
- Furnace Atomizers (graphite,carbon rod)
- Direct Current (DC) Plasmas
- Pulsed Glow Discharges

Flame atomizers have been applied most often. Excitation sources used with these atom sources have included pulsed and CW lasers, and hollow-cathode lamps, electrodeless discharge lamps and ICP plasmas.

Flame Atomizers:

Flame atomic fluorescence spectroscopy (FAFS) has been done with continuum and line sources (104 , 105), pulsed lasers (106), and CW lasers (103 , 107).

Pulsed Laser Excitation:

L.M. Fraser and J.D. Winefordner performed the first LIF experiments in flames with pulsed lasers (106). Limits of detection were generally of the same order of magnitude or better than all previous AFS work with line and continuum sources, but still inferior to those obtained with flame atomic emission. Working curve linearity was three to four orders of magnitude for all elements studied.

Weeks, Haraguchi, and Winefordner (108) made improvements to the optical train by using light traps, baffles, apertures, focussing lenses, and optimization of the monochrometer slit widths for highest S/N ratios. Working curve linearities were extended to five orders of magnitude for most elements examined. Detection limits were improved 10-200 times (0.08-30 ppb are now typical), to the point where they compared favorably with all previous atomic spectroscopic methods.

An important discovery made in these studies was that "spectral resolution (in AFS) depends upon the spectral bandwidth of the laser output, not upon the spectral bandwidth of the monochrometer". The nitrogen-laser-pumped dye laser is particularly suited for fluorescence because of its ease of use, wide tuning range (220 nm to 950 nm), and high peak spectral irradiances. Suggestions were made on how to improve limits of detection and linear dynamic ranges up to four orders of magnitude. Further optimization of the optical train, laser beam output, nebulizer, flame stability and burner configuration, and the detection system were suggested.

Currently, Pulsed-laser flame AFS is competitive with or, in some cases, detection limits exceed those found using flame atomic absorption spectrosopy, ICP or DCP atomic emission spectroscopies. It now is being improved and extended to include more elements (109).

CW Laser Excitation:

In 1976, Green, Travis, and Keller (103) performed the first CW-laser-excited flame AFS studies. They concluded that, "with exception of nonresonant detection and saturation contributions to reduced quenching, higher laser powers common to pulsed sources are of no advantage and, in fact, are detrimental to sensitivity" (103). The first experiments produced limits of detection of 2 ppb for sodium and barium. This corresponded to flame concentrations of 10 million atoms. A linearity of 3.5 orders of magnitude were obtained for sodium. The loss of linearity at high concentrations was attributed to analyte self-absorption. It was noted that the optical and electrical low-noise and the narrow bandwidth (0.005 nm) characteristics of CW lasers offer a distinct practical advantage.

In 1977, Smith, Blackburn, and Winefordner (107) found the best detection limits to be 0.1 ppb for sodium and 40 ppb for barium. The CW dye laser's narrow range of tunability (530-650 nm) greatly limited it usefulness. However, this limitation was partially offset by the use of lower excited states and nonresonance processes. Measurements performed on 9 other elements, some of them excited state transitions, gave LOD's which ranged from 0.1 ppm for strontium to 500 ppm for uranium. Signal intensities greatly depended upon the lower excited state energies, the state degeneracies and oscillator strengths for the transitions, and their populations in the 2500 degree Kelvin flame. A dove prism was used to rotate the image of the fluorescence in the flame to coincide with the monochrometer slits over their full length. This improved signal-to-noise ratios by 2 orders of magnitude. The principal obstacles encountered with this method were the flame flicker noise due to (1) flame background emission instability (in the case of nonresonant processes, and (2) laser scatter shot-noise due to unvolatilized particles (in the case of resonance fluorescence).

Not much work has been done using CW-laser-excited flame AFS over the past decade. Recently, Hovis and Gelbwachs (110) performed CW-laser-excited flame AFS on barium at trace levels. The same instrumental setup was used to make a direct comparison of LOD's for atomic and ionic LIF. Barium ion LIF gave a better detection limit (0.7 ppb) than barium atom LIF (3 ppb). This is comparable to ICP ionic emission spectroscopy (0.1 ppb), and barium ion ICP-LIF (0.5 ppb). The similarly low detection limits were explained by a similar extent of ionization in the two sources. This seems unlikely since temperatures are much higher in the ICP. Working curve linearity extended over 4 orders of magnitude.

Inductively Coupled Plasma Atomizers

Hollow Cathode Lamp Excitation:

Demers and Allemand (111) used hollow cathode lamp (HCL) excitation to do AFS with an ICP as an a atom reservoir (HCL-ICP-AFS). Detection limits for 23 elements (ranging from 0.08 ppm for Ca, to 200 ppm for As) were comparable to flame atomic absorption. Results for refractory elements were as much as two orders of magnitude poorer (range 20 ppm for Al, to 3000 ppm for W). No reason was given for these poorer detection limits. Working curve linearities were typically 4-5 orders of magnitude. Detection limits peaked gradually with decreasing RF power and with increasing observation height. Background spectral interferences due to emission line overlap, molecular absorption and fluorescence were fewer and less severe than for atomic absorption or ICP atomic emission. This was attributed to narrow hollow cathode lamp line widths.

A multielement HCL-ICP-AFS instrument has been commercially marketed by Baird Corporation since 1982 (112.). Up to 12 elements can be analysed simultaneously. Detection limits are comparable to atomic absorption for all elements except refractories. One unique aspect of the instrument is that interference filters are used for spectral separation. The hollow-cathode lamps are pulsed at 500 Hz, and fluorescence signals are monitored using

phase-sensitive detection. This approach obviates the need for multiple chopping wheels and still provides the noise-rejection properties of lock-in detection.

Laser-Induced Fluorescence in ICP's

CW Laser Excitation:

The first LIF-ICP-AFS experiments used a CW laser and were performed by Pollard et al (113.). Initially, temperatures were found to be so high that background and analyte emission degraded S/N ratios. Decreasing the RF power dramatically increased S/N ratios. The ICP was operated at 600 watts for LIF analytical measurements. A nonthermal excitation mechanism was confirmed for the ICP under such conditions by comparing atomic and ionic line emission intensities. Atomic barium LIF signals were not detectable, presumably because most barium existed as the ion, for which a detection limit of 6 ppb was observed (ICP-AES limit of detection for Ba was 0.1 ppb). Sodium gave an LIF limit of detection that was roughly equivalent to ICP-AES (0.1 ppb). The limited wavelength range of the CW laser was stated as the major drawback of the system. Studies of LIF as a function of RF power, carrier gas flow rate, and vertical observation height were not published. No other CW laser LIF-ICP-AFS studies have been reported.

Pulsed Laser Excitation:

Epstein et al (114.), performed the first pulsed-laser LIF-ICP-AFS experiments. A flashlamp laser-pumped dye laser and a nitrogen laser were used; results were similar for each of the two lasers. Detection limits were approximately two orders of magnitude worse than the best ICP-AES results at that time (1980). The background emission shot-noise limited region of the ICP discharge was found to be the optimal region for high S/N ratios. Increasing the throughput of the optical system was suggested as a way to further improve S/N ratios.

Uchida, Kosinski, and Winefordner (115) employed pulsed-laser-excited AFS in the ICP (LIF-ICP-AFS) to study the vertical distributions of calcium and yttrium ions and atoms. Ionic and excited state fluorescences were strong. The spontaneous transition probability value of the fluorescence line and the lower state population were found to be the dominant factors in predicting signal intensities. Increases in (analyte) carrier gas flow rates decreased the temperatures experienced by the analyte, thus increasing calcium atom ground state density (which also increased atomic Ca AFS signals and broadened their vertical distributions). Thermally-assisted (non-resonance) fluorescence of yttrium was shown to occur with up to 1.2 eV of "thermal assistance" coming from the plasma. Collisional redistribution of radiatively-excited analyte energy levels was shown to be non-Boltzmannian; radiatively excited levels were found to be overpopulated. The absence of molecular species in the ICP support gas was stated as the reason. Molecular species can easily depopulate highly-excited states and assist in equilibration of all species in the plasma.

Detection limits were poor compared to ICP emission results for the same instrument, (calcium was the best: 8ppb for LIF-ICP-AFS, 0.4 for ICP-AES; thallium was the poorest : 8000 ppb for LIF-ICP-AFS, 60 for ICP-AES). Measurements were made in the analytical region (10-25 mm above the coil) where the high temperatures cause excessive analyte excitation, strong background emission, and noise problems. The poor detection limits were explained by these factors. It was suggested that an extended torch be used to make the lower temperature regions high above the ICP coils (50-80 mm) more accessible. This also eliminates the problems of analyte atom diffusion and plasma turbulence caused by the surrounding atmosphere.

Omenetto et al (116) measured the observation height profiles of Ba atoms and ions in the ICP. The purpose of the work was to show the information capability of such technique, rather than to provide extensive mechanistic interpretations. The direct measurement of species distributions, without the need for tedious deconvolution techniques (Abel inversions), was noted as a powerful advantage of the LIF technique. Absolute analyte concentrations

(free from quenching effects) can be obtained if laser saturation conditions are employed. Volumes resolutions of 0.2 cubic millimeters were obtained. The atom and ion distributions complemented each other. Huang, Yeah, and Winefordner (117) measured observation height profiles for calcium, copper, and manganese atoms and ions in the ICP. LIF profiles of ionic and excited atomic states resembled each other. Profiles obtained with laser-induced fluorescence agreed with those obtained using spatial emission profiles followed by the Abel inversion technique.

ICP results with Extended Torch:

Kosinski, Uchida, and Winefordner (118) tested an ICP with an extended-sleeve torch and used a nitrogen laser-pumped dye laser for excitation. Radial and observation height profiles, power studies, and interference studies were performed. Interelement interferences could be minimized by optimizing RF powers and carrier gas flow rates. Fluorescence quenching due to entrained air was greatly reduced with the extended torch. Limits of detection for 20 elements were almost equivalent to those obtained for hollow-cathode lamp excitation, but still inferior to those with ICP atomic emission.

Optimization of LIF-ICP-AFS Measurements:

Omenetto and Human (119) discussed general considerations and experimental parameters important for obtaining good results with pulsed lasers as the excitation source for AFS. Factors important to obtaining saturation were discussed in detail. These are laser power, pulse duration, focussing, and radiative absorption rates per unit spectral irradiance. Theoretical arguments for proper selection of the excitation lines, and excitation and detection optics are given. Detection system gate width optimization with relation to laser pulse widths were discussed, along with the effects of these operational parameters on noise.

Only flame, furnace, and ICP atomizers were considered, although the general conclusions should also hold for other atomization systems. This is because furnaces and

flames represent the two extremes of low and high spectral background noise levels, respectively. The ICP offers advantages over flame atomizers since it has greater freedom from formation of refractory oxides. Excited atom and ion lines can be used in the ICP. It also has a higher quantum efficiency for several elements because less quenching occurs in the inert gas atmosphere. However, for high sensitivity measurements, the electrothermal atomizer is preferred because of its very low spectral background.

A followup paper by Omenetto and Human (120) focussed on the analytical characteristics of the ICP as an atom/ion reservoir. The choice of elements was biased toward the refractory elements to ascertain the real advantages that the ICP offers for these elements. Detection limits were measured for 14 elements and were found to be in the range 0.4 to 20 ppb. In all cases this was an improvement over "standard" tabulated ICP emission lines. For Ba, Ti, U, V, Y and Zr, the highest sensitivities were obtained for ionic lines, while atomic lines gave higher sensitivities for Al, B, Ga, Mo, Pb, Si, Sn, and Tl. Minimum detectable quantities using a carbon rod electrothermal atomizer were determined for Pb (6 femtograms) and Tl (100 femtograms).

Advantages of the LIF-ICP-AFS technique were stated to be good sensitivity and detection limits, and extremely high selectivity. The quantum efficiency of the ICP (due to reduced quenching in the Ar atmosphere) was found to be advantageous. Also, the use of other spatial regions of the plasma offers more freedom from interference effects (if the highest sensitivity is not required). The disadvantages of the technique were stated as the inability to do multielement analyses (the single-element selectivity inherent in a laser turns into a disadvantage), and the cost and complexity of the combined ICP/laser system. The frequent replacement of the laser dyes was also stated as a serious obstacle to routine analyses. The final conclusion in the paper was "The development of a simpler and more versatile atom source (temperature about 5000 degrees Kelvin) deserves the attention of spectroscopists in the field."

Other Excitation Sources in the ICP:

Montaser and Fassel (121) employed a microwave-excited, electrodeless discharge lamps (EDL's) as the primary excitation source for exciting AFS in an ICP. The optimum observation height for AFS was found to be 45 to 64 mm above the load coil. A conventional torch was used. They measured AFS and AES detection limits for Cd, Zn, and Hg and found the AFS values were better than the AES values by factors of 2 to 8.

Kosinski, Uchida, and Winefordner (122) employed tandem ICP's for AFS, one as the excitation source, the other as the atom reservoir. The ICP is an excellent high-intensity excitation source that does not promote spectral interferences, and is relatively free from self-reversal, The purity of the ICP line source depends on the purity of the solutions employed. Elements are changed simply by changing elemental solutions. The detection limits measured were 1 to 2 orders of magnitude poorer than those obtained in other ICP-AFS systems. Long and Winefordner (123) re-examined the ICP-ICP AFS system. They employed more efficient light collection optics, optimized the RF power with respect to the fluorescence signal, and installed RF interference filters in the power supplies of the RF generator and the detection electronics. This improved detection limits by 1 to 2 orders of magnitude.

Furnace Atomizers:

As early as 1973, Neumann and Kriese (124) had achieved detection limits of 0.2 pg for lead using a graphite rod atomizer. This was at least an order of magnitude lower than any previous spectroscopic method. These early measurements were plagued by large noise sources (37% RSD for 10 measurements).

By 1977, Balykin, Letokhov, Mishin, and Senchishen (125) had measured detection limits of 1*E-2 atoms/cc for Na in a vapor cell (up to 1*E+8 absorption/fluorescence cycles/atom/second are possible using saturation conditions for a system which is resonant with the radiation field). However, vapor cells are not practical sampling devices, and not all atoms can provide the detection limits of two-level resonant systems such as Na.

Nonresonant systems with intermediate metastable levels can accumulate atoms on the metastable levels; this greatly diminishs the number of photons that each atom can radiate.

In 1981, Bolshov, Zybin, and Smirenkina (126) made significant progress in the analysis of real world samples in a graphite cup atomizer. With improvements to the detection system, lowered noise background levels and scatter elimination, the detection limits dropped to 1.5 femtograms for Pb. Limits of detection for 9 other elements were also significantly improved. Precision values were typically in the range of 10-15% for aliquots prepared from wheat, potato, and grass mixture samples.

Recent work by Wittman and Winefordner (127) characterized figures of merit for graphite atomizer systems and Mn, Na, and Sn analytes. Sodium gave the best results; it gave an absolute limit of detection of 3 picograms, a linear dynamic range of 5.5 orders of magnitude, a relative standard deviation of 6%, and a slope sensitivity of 0.77. Scatter noise limited the LOD's for resonant processes (Na and Mn), and OH emission shot noise limited the LOD for Sn. Quantum efficiencies were characterized by measuring the relative quenching ratios (fluorescence intensity in nitrogen/fluorescence intensity in argon) for Sn (0.80) and Mn (0.61). Each element has a characteristic quenching cross section in argon and in nitrogen which accounts for the different fluorescence intensities.

Direct Current Arc Plasma:

Hendrick, Seltzer, and Michel (128) performed the first studies using the direct current plasma (DCP) as an atom cell for LIF. It was employed as a diagnostic tool to study analyte population enhancement effects due to easily ionizable elements (EIE). In a mechanism proposed by Miller (129), EIE's are postulated to affect the rates at which radiative and collisional redistribution occur within the DCP. The purpose of the LIF/DCP work was to confirm an important aspect of Miller's mechanism: that EIE enhancements would not be observed under conditions of saturation by laser radiation, and would be observed under non-saturated laser excitation conditions.

It is known that during saturated LIF, laser excitation rate constants can be at least 3 orders of magnitude greater than quenching rate constants (8). If EIE's do affect radiative and collisional redistribution rates, then under conditions of LIF saturation the collisional coupling effects would be obliterated by the much faster radiative excitation process. In other words, "the EIE cannot be expected to populate the level in question faster than the laser is able to do the same thing by saturation."

Their postulate was confirmed; the enhancement effect disappeared with saturated laser excitation of the barium transition, showing that the collisional rate effect was obliterated by the saturated laser excitation rate. This is a delightful example of the diagnostic power of LIF in plasmas.

Hendrick, Seltzer, and Michel have performed the only analytical studies of LIF in the DCP to date (130). Detection limits ranged between 3 ppb (calcium) and 72 ppb (iron). These were 1-2 orders of magnitude poorer than LIF in flames or ICP's. Linear dynamic ranges spanned just over four orders of magnitude. In their earlier publication (128), working curves showed good linearity for barium from 1-1000 ppm. Graphs reporting the effects of EIE interferences on working curve linearities for barium were published, as were graphs showing the effects of EIE's on barium and calcium LIF fluorescence intensities as a function of observation height. Their conclusion was that considerable improvements in sample introduction would be needed before the DCP would be broadly applicable as an atom cell for LIF. The major factor raising the detection limits of the LIF/DCP technique was the high continuum background inherent in the DCP (this is also true for the ICP).

Pulsed Glow Discharge Atomizer:

Smith, Omenetto, and Winefordner (131) published results on LIF in a planar geometry glow discharge. The discharge was pulsed at 20 Hz with 600 volts; the nitrogen laser-pumped dye laser was triggered 300 microseconds after the discharge was extinguished. This allowed the background emission to disappear so that a stable state ground population of atoms could

be observed free from spectral interferences. They had done previous studies observed the behavior of the decaying atom population (132). Analytical studies for aqueous lead solutions gave a detection limit of 20 picograms, and a linear dynamic range spanning 5.8 orders of magnitude. Such sputtering discharge atom sources are stable, reproducible, low-background atom reservoirs for analytical and diagnostic LIF measurements.

Summary:

In general, the significant increases in sensitivity expected from laser induced fluorescence have been reached only in systems with low background emission, high atomization efficiency, and low background scatter. The limitations and finer points of performing such measurements in flames, ICP's and furnace atomizers are only now beginning to be understood. Laser AFS in flames is limited by the low temperature and high flame luminosity; detection limits are not significantly better than other atomic spectroscopic methods. ICP's possess sufficiently high temperatures to excite and ionize analytes, a property not always desirable for AFS. And detection limits are not significantly better than flame AFS or ICP-AES, because of background noise sources inherent in the ICP. Furnace atomizers provide extremely low detection limits when noise sources are properly eradicated. However, the nature of these discrete sampling devices make them difficult to use with continuous sampling plasmas such as flames and ICP's.

Further research into new atom sources may combine the aspects of low background emission and scatter, and high atomization efficiency. Hopefully, that will provide low detection limits, along with easy operation. The next sections describe the efforts made in the present work to develop and explore a microwave plasma source having such characteristics.

B) EXPERIMENTAL APPARATUS

Overview - Block Diagrams and Functional Descriptions

The High-Efficiency MIP cavity was incorporated into an instrument composed of a laser, sampling system, flow system, scanning monochrometer, detection circuitry, and computer. A schematic diagram of the system used for LIF and AES measurements is shown in Figure 31 on page 130. For AES measurements, the system differed in two primary aspects: 1) no laser was used, 2) the chopping wheel was placed in front of the entrance slits of the monochrometer to modulate the emitted light.

Gas Handling System:

Figure 31 shows the gas plumbing connections used for the MIP system. Three separate flows fed into the MIP torch. One flow fed into the center tube of the torch. The sampler flow combined with the auxiliary (sampler bypass) flow and fed into the side arm of the torch. The auxiliary flow was a make-up gas that brought the total MIP flow rate up to at least 1 L/min. This was required to prevent overheating of the MIP torch when no sampler flow was used.

A gas manifold was constructed which allowed mixtures of up to 3 different gases to be made. A total flow meter (Matheson, Model 603) measured the flow rate after mixing of the 3 gases. The mixed support gas was divided 3 ways and then fed into the MIP flow system described above. Separate metering valves were then used: one for the MIP torch center flow, another for the MIP torch auxiliary flow, and a third for the sampler flow. The auxiliary flow and the sampler flow had their own flow meters. The MIP center torch flow was set and left fixed at the beginning of the day.

MIP Cavity and Torch System:

The MIP cavity and tangential flow torch design characteristics were described in detail in Chapter II of this document. The cavity was mounted with the plasma plume mounted horizontally (perpendicular to the monochrometer slits), at a height convenient for viewing with the monochrometer mounted on a translation stage. Monchrometer height is the parameter which dictated the placement of all other components. The laser beam was raised up approximately two inches using two flat mirrors (this can be seen as two 90 degree bends of the laser beam in Figure 31 on page 130).

Flow Meter Calibrations:

No calibrations were available from the manufacturers for the argon/nitrogen mixtures. These were done by volume displacement of water. A 100 mL volumetric flask was filled with water, inverted in a 4 liter beaker, and the amount of time required for the gas to displace the water was measured with a digital stopwatch. This method permitted accurate flow rate measurements up to approximately 8-9 liters per minute. The resulting calibration curves are shown in Figure 32 on page 131.

Sampling System

The problem of sample introduction in atomic spectroscopy is traditionally one of the toughest. The MIP has problems because large volumes of water are not tolerated; all water must be introduced as a finely nebulized aerosol. The approach used most often in the past has been sample desolvation prior to introduction into the MIP. This minimizes plasma quenching during sample analysis.

Microarc Sampler:

The first approach used by the author involved a microarc sampler (9). This device is

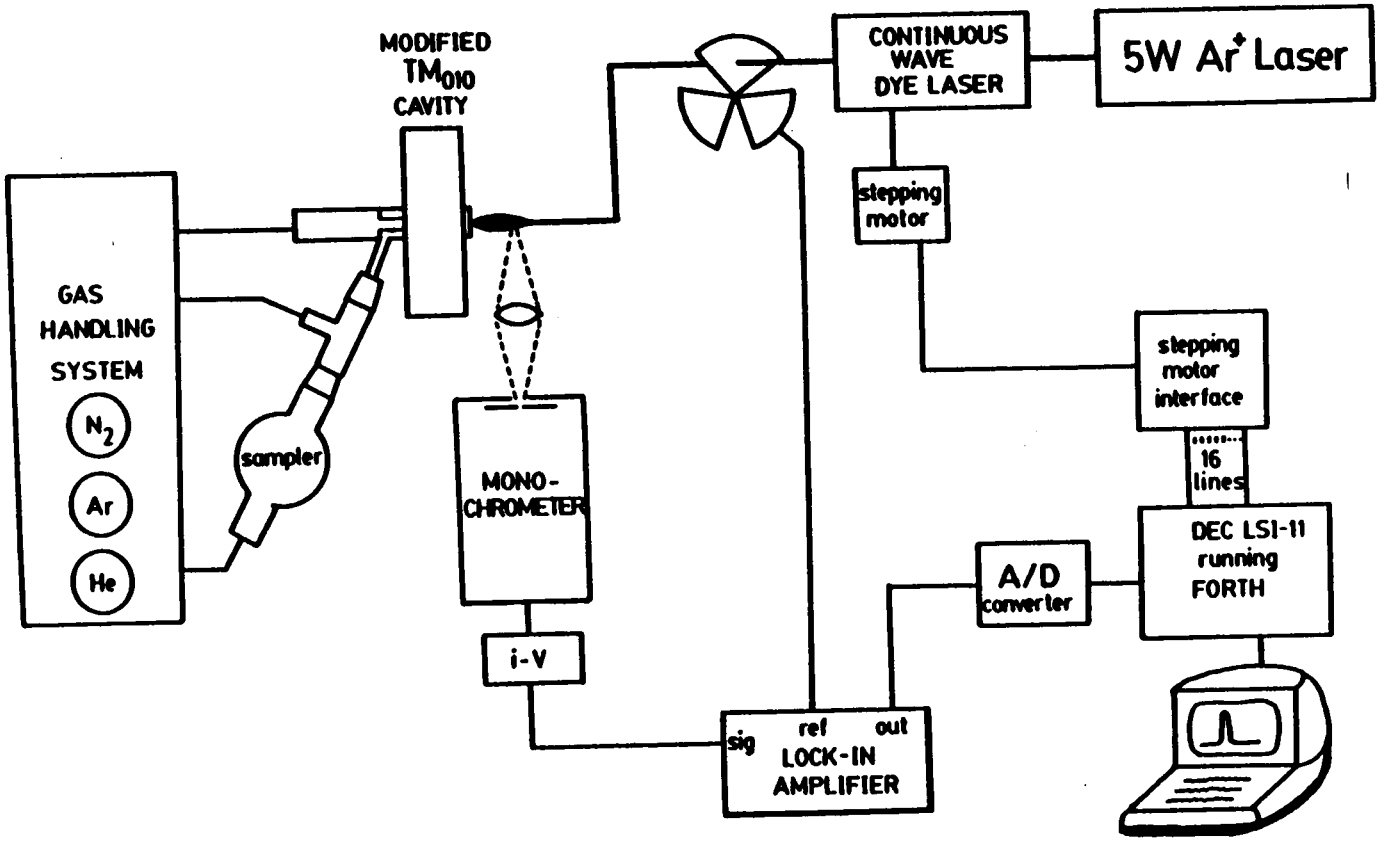

Figure 31. Instrument Schematic for Laser-Induced Fluorescence in MIP

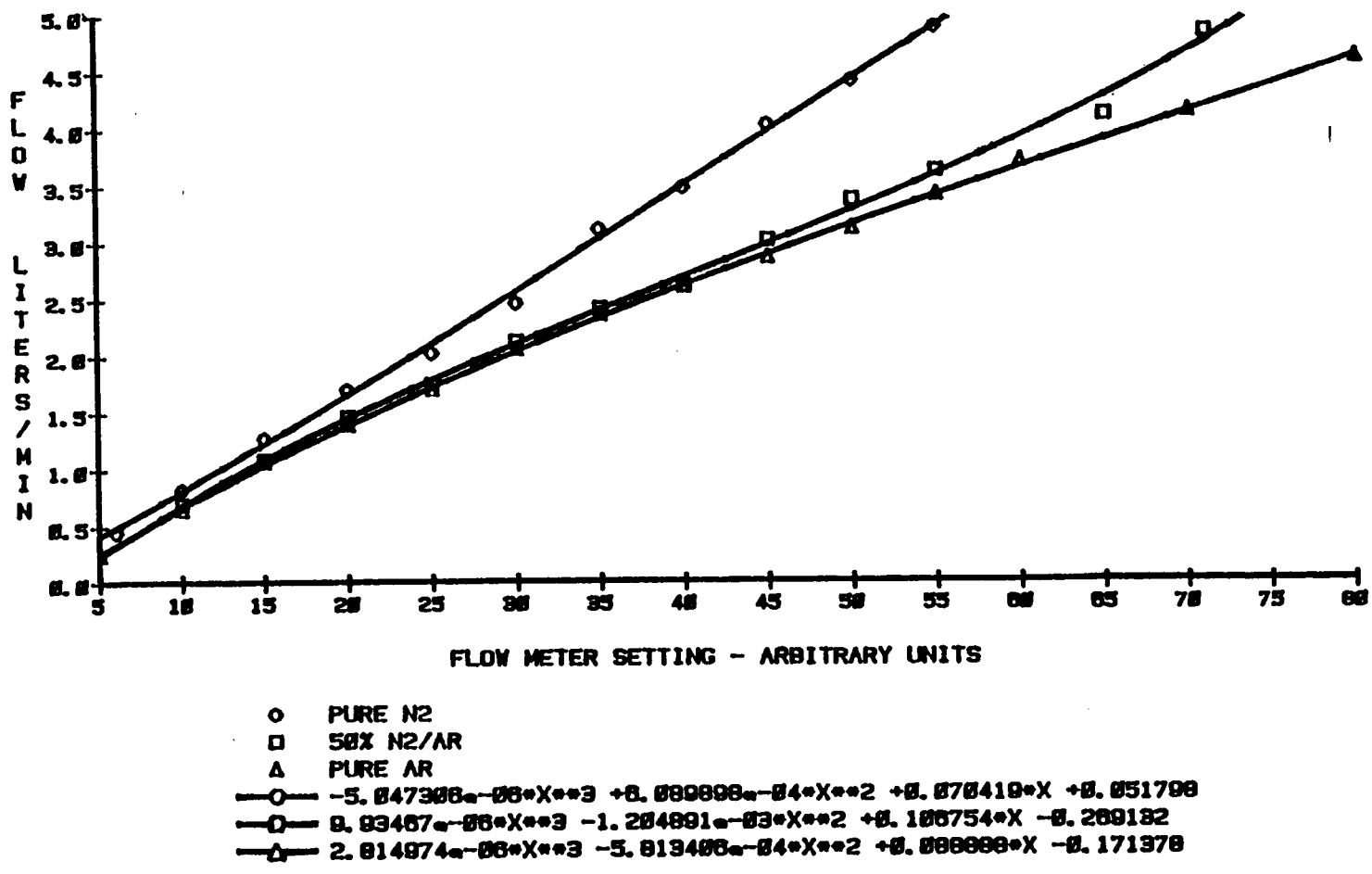

Figure 32. Calibration Curve for Flow Meters

Table 9. Experimental Components

Microwave Plasma Components		
Component	**Model/Size**	**Manufacturer**
Microwave Cavity	High-Efficiency TM-010 Cavity	Laboratory Built
Microwave Generators	Model 2150 0-180 Watt	Holaday Industries Edina,MN
	0-125 Watt	KIVA Instrument Corp. Rockville,MD
Coaxial Cable	RG 214/U (50 ohm)	Times Fiber Communications Wallingford, CT
Microwave Circulator	Model 300303 125 Watt CW	RYT Industries Santa Clara, CA
Termination Load	Termiline 5 Watt	Bird Electronic Corp. Cleveland, OH
Attenuator	50 Watt, 10 dB	Lectronic Research Labs Camden, NJ
Reflected Power Meter	Model 43	Bird Electronic Corp. Cleveland, OH
Glass Frit Nebulizer	20 mm Diameter 4-5 micron pores	Laboratory Built
Support Gases	Prepurified Nitrogen Prepurified Argon	Airco Murray Hill, NJ

Table 10. Experimental Components (cont.)

Detection System Components		
Lockin Amplifier	5101	EG + G Princeton Applied Research Princeton, NJ
Chopping Wheel Motor	75A121	Globe Industries Dayton, OH
Chopping Wheel	24 Tooth 5″ Diameter	Laboratory Built
Monochrometer	98G (0.5 meter)	Perkin-Elmer Danbury, CT
Stepper Motor Interface	12-bit resettable Counter/Driver	Laboratory Built
Photomultiplier Tube	1P28	RCA Sommerville, NJ
Focussing Lens	UV Glass, Bi-convex	Melles Griot Irvine, CA
Amplifier	i-V Converter	Thorn EMI Gencom, NY
High Voltage Power Supply	HV-1572 1-1500 Volt, 50 mA	Power Designs Pacific Palo Alto, CA
Data Collection Minicomputer	LSI-11/03 Corporation with ADV-11 A/D Convertor	Digital Equipment Maynard, MA

Table 11. Experimental Components (cont.)

Laser System		
Argon Ion Laser	Model 165	Spectra-Physics Piscataway, NJ
CW Dye Laser	Model 375	Spectra-Physics Piscataway, NJ
Laser Dye	Rhodamine 6G	Exciton Chemical Co. Dayton, OH

Table 12. Experimental Operating Conditions

Typical Experimental Operating Conditions	
Microwave Frequency	2450 MHz
Forward Power Reflected Power	20-180 Watts 0-55 Watts
Argon Flow Rate Nitrogen Flow Rate	0.75-5.0 L/min 0.75-5.0 L/min
Nebulizer Type	Glass Frit
Nebulizer Solution Uptake Rate	0.2-1 mL/min
Plasma Viewing Mode	Radial
Monochrometer Slit Widths	0.02-2 mm

a low-power (200 watt), high-voltage, pulsating dc current glow discharge which operates at atmospheric pressure. It is a discrete sampler that separates the desolvation step from the atomization step. First, 0.1-10 microliter aliquots of sample are deposited onto the filamentary cathode. The filament is heated slightly to speed up desolvation. Once desolvation is complete, the high-voltage discharge is initiated, causing very complete sample atomization. Figure 33 on page 137 shows the microarc sampler.

Atomization in the microarc sampler occurs by electron sputtering of sample atoms from the cathode. Sputtering efficiency greatly depends upon the surface conditions of both electrodes. Electrode contamination causes it to fire erratically. The distance between the two electrodes was only 0.5 mm. Contamination of the anode with sample solution accidentally occured a few times. Consequently, the sampler was particularly erratic and required many rinse and fire cycles to restore reproducible operation. Sampler firing was erratic with highly concentrated solutions (greater than 200 mg/mL). This was similar to that the erratic firing which occurred when the sampler was contaminated. It is believed that distortion of the electric field and insulation of the electrodes by samples caused these problems with erratic sampler operation. Sampler performance degraded very much after about 60-90 minutes of operation. After that, the only way to achieve reproducible firing of the sampler was to rebuild it. The microarc sampler caused many problems because it was so noisy and required too much rebuilding. It was abandoned in favor of a fine aerosol generator.

Glass Frit Nebulizer:

Experimenters in Dr. Gary Long's laboratory found that the high-efficiency MIP cavity constructed by this author would tolerate aqueous aerosol introduced directly into the MIP at low power (133). That was one of the first times that aqueous aerosol had been introduced directly into an atmosphere pressure low-power molecular MIP. At first a glass-frit nebulizer described by Layman and Lichte was used (134). Later, it was found that a Meinhard pneumatic nebulizer works just as well as the glass frit nebulizer (133). The droplets from a

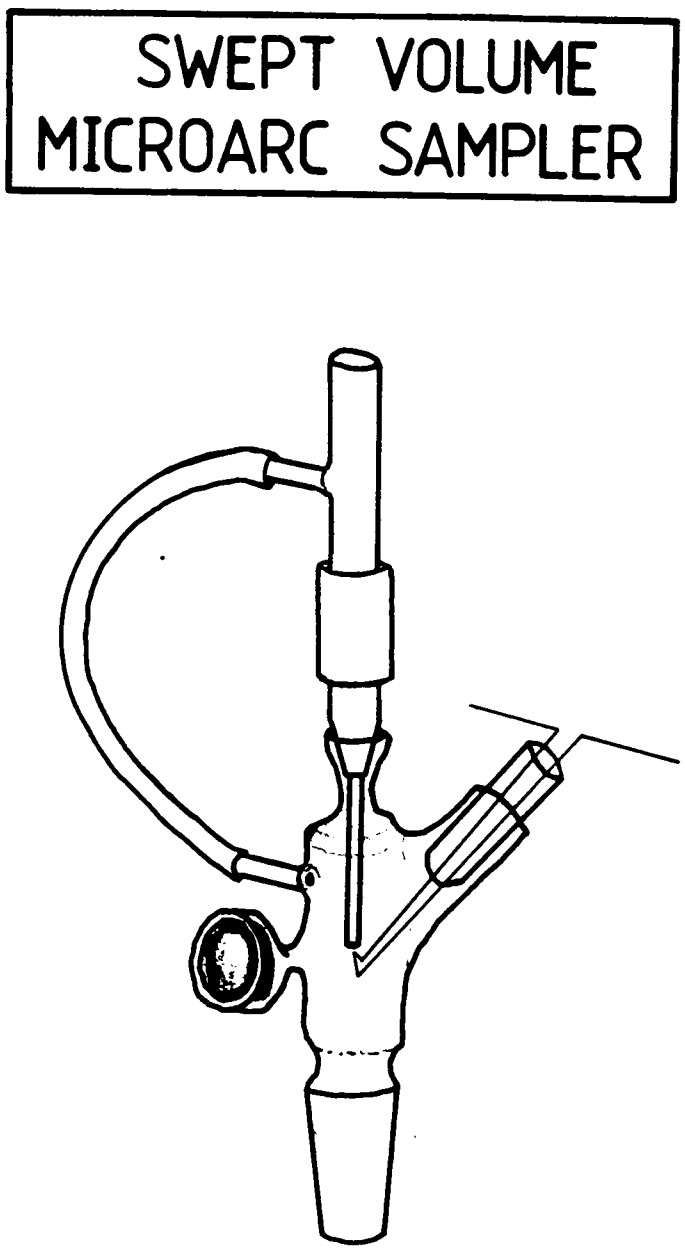

Figure 33. Microarc Sampler

Meinhard nebulizer are larger than from a glass frit nebulizer, which are typically around 0.1 microns in diameter. Both types of nebulizers have problems with clogging when high salt concentrations are used. The glass frit nebulizer was used for all experiments described in this manuscript. The glass frit nebulizer is shown in Figure 34 on page 139. Also shown is the aerosol ballast that provided a more stable flow of small aerosol droplets to the MIP torch.

One of the strong points of the glass frit nebulizer/MIP combination used here is that the nebulizer was designed so that the full supply of gas going to the torch could first pass through the nebulizer. This eliminated dilution of the aerosol flow to the plasma. Dilution of aerosol flow to the plasma is a major problem with flame nebulization systems.

Glass Frit Nebulizer Characterization Experiments:

Experiments were conducted to characterize frit nebulizer efficiency. This allowed selection of the best conditions for sampler operation with the MIP. Sodium atomic LIF was selected to characterize nebulizer efficiency since the atomic fluorescence was sufficiently intense to allow signal collection at all flow rates.

As the nebulizer gas flow increases the amount of water in the aerosol steadily increases, up to the point where so much gas is flowing through the glass frit that the liquid applied to the underside of the frit stops wetting it and is just blown off by the gas flow. At that point the aerosol flow ceases. The maximum possible nebulizer flow rate increases as the rate of sample solution applied to the underside of the glass frit increases. This is shown in Figure 36 on page 141.

The glass frit has problems with memory effects when analyte solutions are changed frequently. That was not a problem in this work since the same solution was used for all physical studies. A long rinse cycle with pure deionized water was used between solutions for the analytical studies.

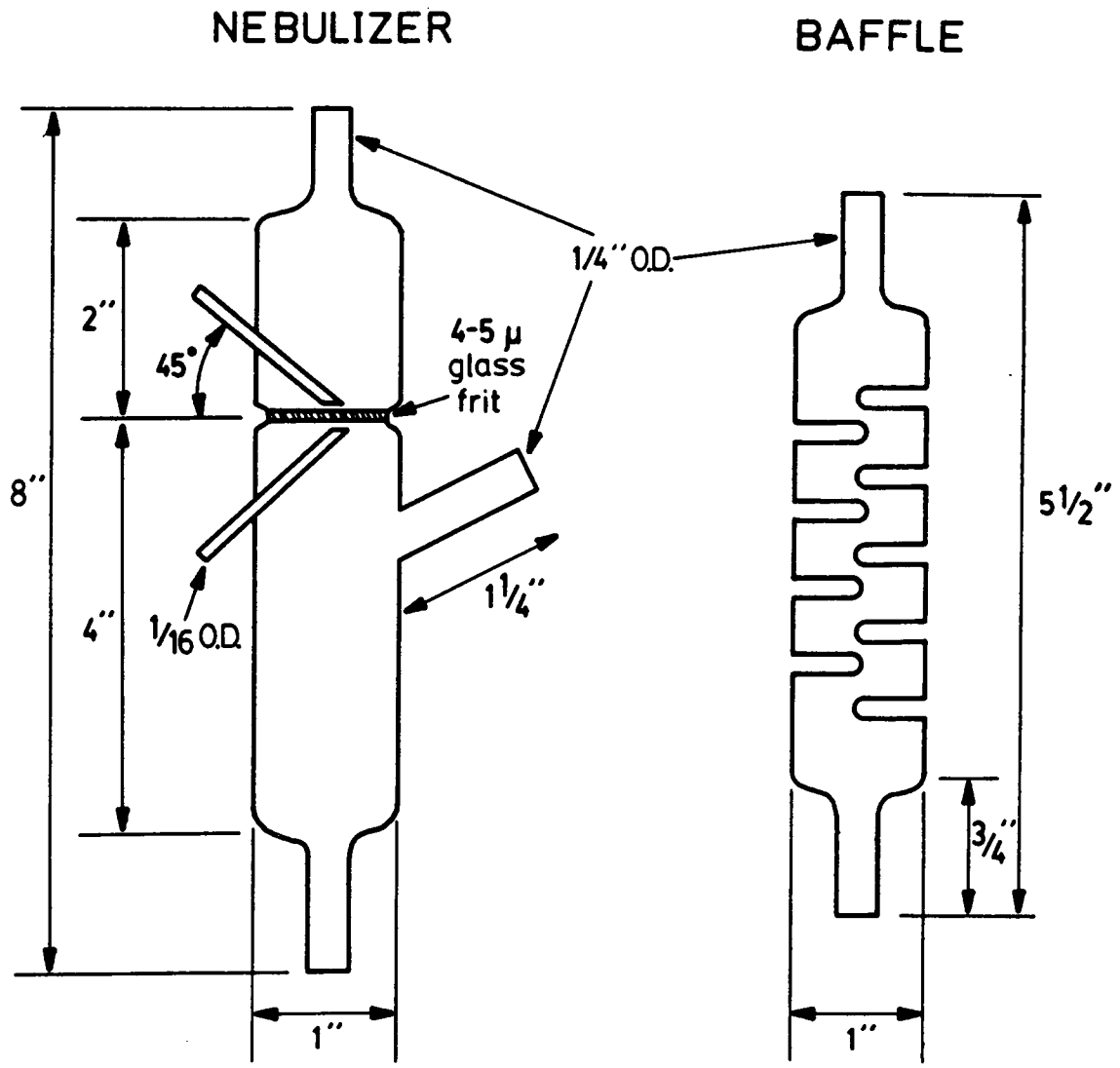

Figure 34. Glass Frit Nebulizer and Aerosol Baffle

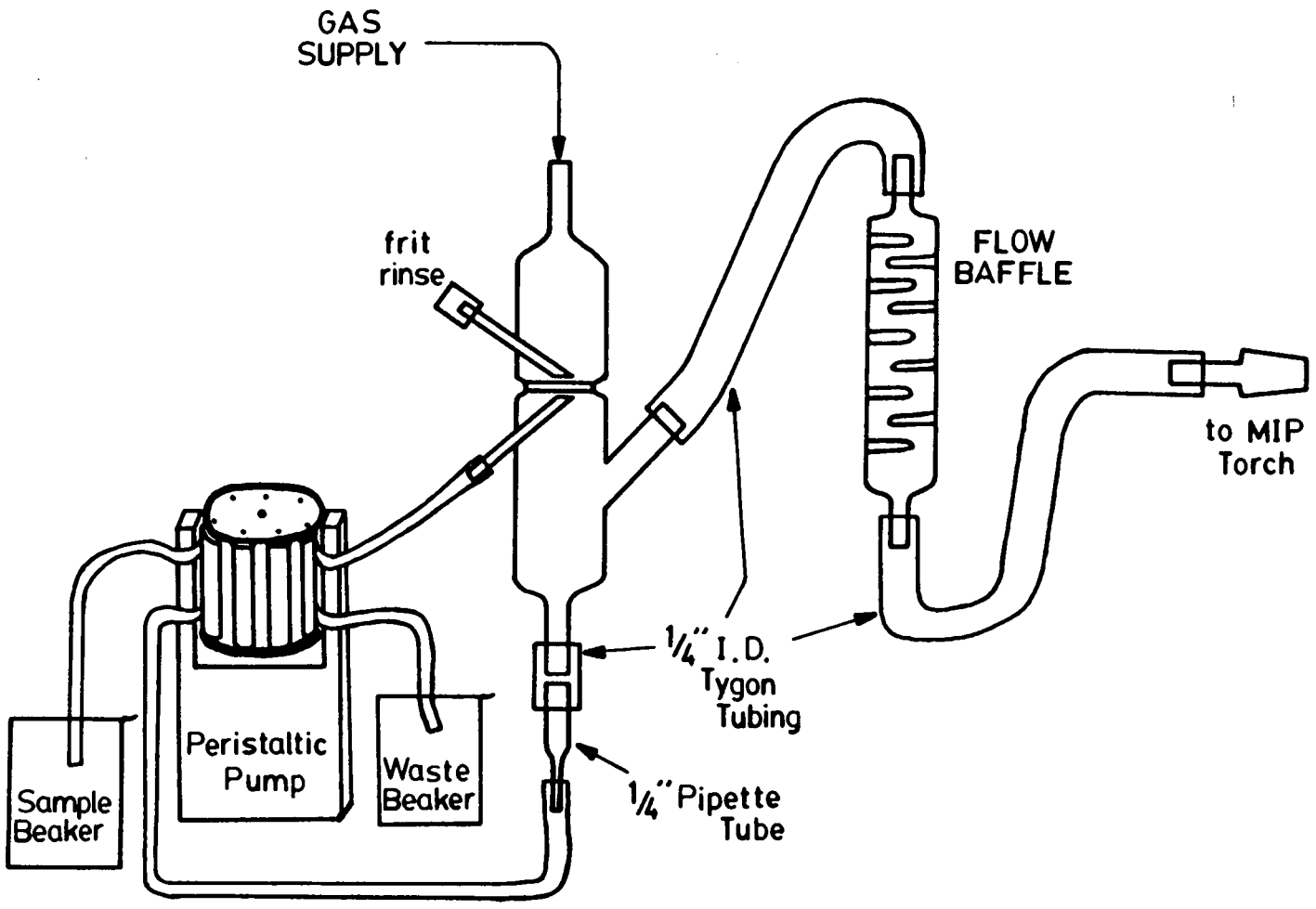

Figure 35. Schematic for the Sample Introduction System

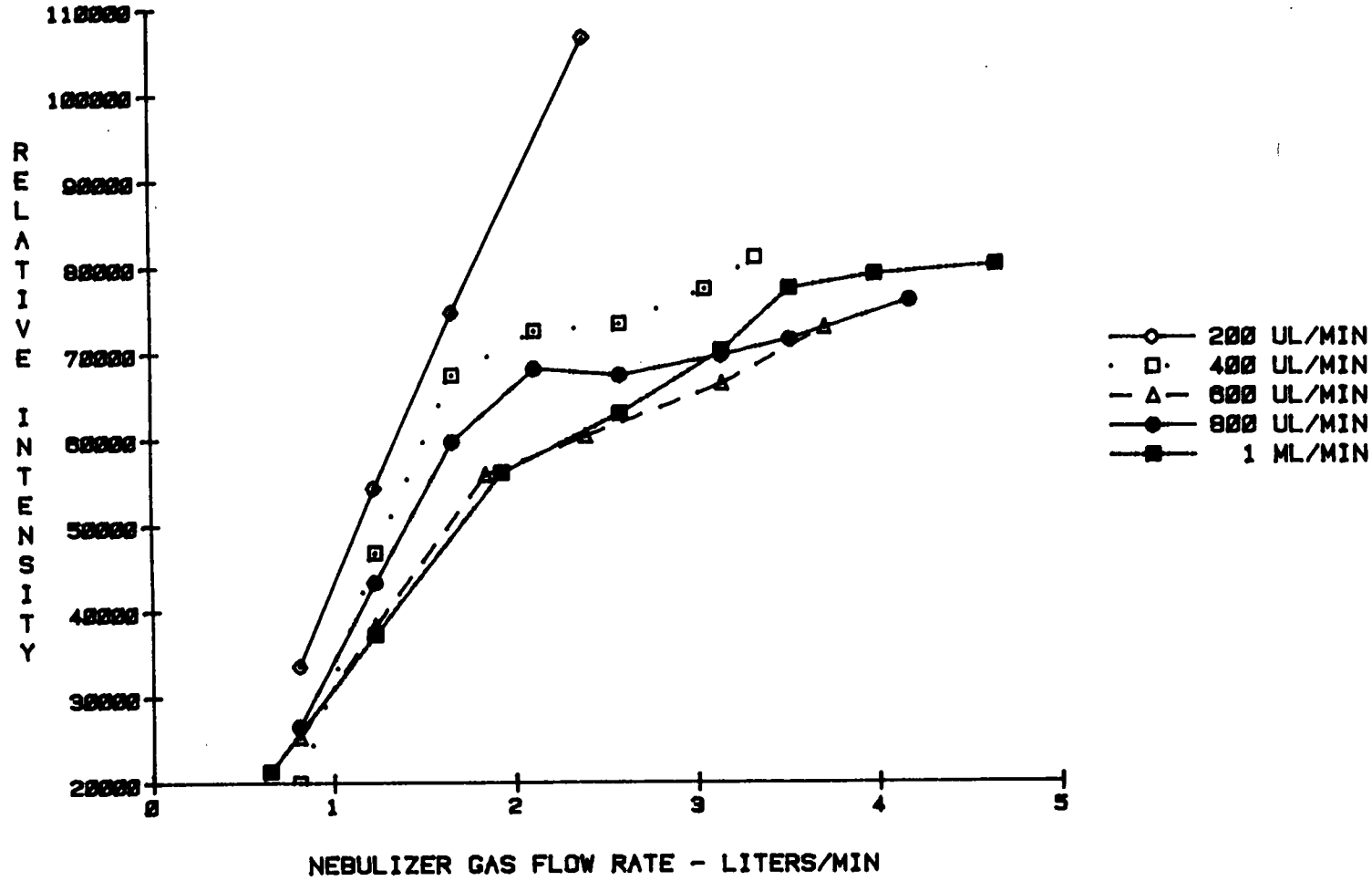

Figure 36. Glass Frit Nebulizer Characterization

Detection Electronics:

Even with a noisy sampling system, the LIF signals were plentiful and could be extracted with a lockin amplifier using phase-sensitive detection. The output of this detector was interfaced through an analog-to-digital converter to a digital computer, which did signal smoothing and integration.

Instrument Automation

Scanning Monochrometer Automation:

The scanning monochrometer was automated to make nitrogen plasma spectrum collection easier. A digital stepping motor interface was designed and built by the author. The initial hardware design came from James T. Currie (135). It was modified to incorporate electromechanical limit switches. This prevented the stepper motor from driving the monochrometer past the full travel of the wavelength drive mechanism, which would damage the gear trains of both the monochrometer and the stepper motor.

The software scanned the monochrometer while a D/A converter (DEC AAV-11) drove an X-Y recorder. The signals from the monochrometer phototube were fed through a current-to-voltage converter to the recorder's Y-input. The programs were written in MACRO-11 assembler programming language running under RT-11 operating system on the DEC LSI-11/03 minicomputer. The full details of the hardware and software used to automate monochrometer wavelength drive are given in Appendix A1.

Fluorescence and Emission Measurement Automation:

Data collection, processing, and reporting were performed online. Software routines were written using the FORTH programming environment, i.e., both a programming language and an operating system (136). FORTH was used to create an applications-oriented language that was specific for the operation of the instrument measurement system.

Data was plotted using the RS/1 data management system running on a DEC/VAX computer. RS1 is a collection of research software tools for data management, plotting, statistics, and curve-fitting. This greatly facilitated organizing and managing the 30,000+ data values collected over the full course of experimentation.

All data values consist of the average of five data runs, each run being the average of 25 A/D samplings taken at 100 Hz. This method of signal averaging gave freedom from rapid short-term fluctuations in the analyte signal.

Appendix A2 contains listings of the data collection, processing, and reporting routines. Instrument operations are fully documented there. Various instrument operations included data collection, data display on an oscilloscope, and data storage and retrieval using floppy disks.

C) EXPERIMENTAL RESULTS

1) INTRODUCTION

The following are the physico-chemical studies needed to characterize the MIP for use as an atom source for atomic spectroscopy, specifically for laser-induced fluorescence (LIF). Results for the atomic emission spectroscopic (AES) studies are included here for completeness, and to allow easy comparison of results with the LIF results.

The AES studies were done for several reasons:

1) Atomic emission constitutes the primary background for LIF.
2) Atomic emission in the low-power N_2-MIP has never been studied before.
3) Physical insights into the plasmas may be gained that are not evident using LIF.
4) AES studies allow data sets from this system to be compared with other MIP systems.

Both LIF and AES are useful as tools to investigate the characteristics of the pure nitrogen and nitrogen/argon mixed plasmas. Together they provide complementary information so that a more complete picture can be drawn for the separate processes of atomization, ionization, and excitation.

Two representative elements were chosen to physically characterize the plasmas. Sodium and barium were selected because they readily fluoresce, with an intensity detectable to the unaided eye. The sodium atom and barium ion fluorescences provide much insight into the atomization and ionization processes occuring in the plasmas.

The experimental variables that most influence measured LIF and AES signal intensities are the following: 1) applied microwave power, 2) support gas flow rate, 3) support gas

composition, 4) signal observation height. Experiments measuring the effects of these variables on LIF and AES signals were performed. LIF signal intensity is also greatly influenced by the incident laser power. This variable was explored to determine if saturation was occuring. LIF background noise and signal-to-noise experiments were performed to confirm that noise is not significant in the low-power MIP. These experiments also provide information useful for selection of the best conditions for analytical work. LIF and AES analytical feasibility studies were performed which give limits-of-detection (LOD's), and linear dynamic ranges (LDR's). Analytical working curves were also constructed (these results are given at the end of this chapter). Experiments were also performed to study the influence of applied microwave power and gas composition on LOD's and LDR's.

The physical and diagnostic studies are presented and discussed first. The microwave power and gas composition studies allow statements about plasma equilibrium and plasma excitation mechanisms to be made. These begin discussions since they lay a groundwork for later discussions. Flow rate studies follow next. They allow a deeper understanding of the differences between the nitrogen and argon plasmas. Next, the observation height studies and their interpretations allow further statements about equilibrium in the plasma to be made. The physical and diagnostic studies in the HEMMP cavity constitute the major portion and principle emphasis of the experimental work.

The laser fluorescence studies exhibit slightly more signal variations and noise variations than the emission studies. There were temporally intermittent wavelength instabilities due to instabilities in the optical train inside the dye laser cavity. The manufacturers informed the author that this particular model was never intended to be used for applications requiring bandwidths on the order of an atomic linewidth, particularly not without an expensive birefringent filter tuning assembly costing $1400. However, after realigning the entire dye laser optical train three times, the dye laser was stable enough to allow experimental runs of 10 to 30 minutes. This was long enough to collect the data sets

required. A more complete discussion of the instabilities, and the dye laser realignment procedure are given in Appendix B.

2) RESULTS

Microwave Power / Gas Composition Studies

In all cases power studies were done between two experimentally imposed power limits. The low limit was the lowest power setting for which a stable plasma could be generated. The high limit was the highest power setting for which the reflected power remained less than 55 watts. At 55 watts reflected power the cavity became very hot after 15 minutes of operation, too hot for extended operation without a danger of the torch overheating and melting. Power applied to the pure nitrogen plasmas was typically at least 180 watts before there was 50 to 55 watts of reflected power. Total flow rates through the torch were typically 1.5-1.8 L/min. This was the sum of the sample nebulizer flow and the auxiliary flow. Sample nebulizer flow rates were typically 0.75 L/min. Interactions between power and flow rate are quite strong: results can be found in the (later) section on flow rate studies.

Since a plasma with as little as 5 to 10 percent of a molecular gas added behaves as though it were a molecular plasma, the cavity needed to be set up and optimized for nitrogen. A straight wire probe was used for all of these studies. An examination of nitrogen, argon and nitrogen/argon mixtures, using the same instrumental system and excitation conditions, was desired. This allowed a direct comparison of the plasmas to be made.

The argon plasmas were just as stable with the straight wire probe as with the circular disc probe. The low power stability limit was 15 watts forward power for both probes. The reflected power levels in the upper power ranges were also approximately the same for Ar

plasmas with both antenna probes, about 50 watts reflected power with 145 watts applied power.

1) Laser-Induced Fluorescence as a Function of MIP Power:

Sodium fluorescence intensity decreases with increasing MIP power, as shown in Figure 37 on page 148 through Figure 40 on page 151. This is because the sodium atom population decreases. Plasma conditions are simply too energetic to allow free sodium atoms to exist at higher microwave input powers. Sodium atoms are being excited from the ground state and are unavailable for atomic fluorescence. This is true for all the gas compositions studied, from pure nitrogen to pure argon.

Argon support gas gives particularly strong sodium LIF signals in the MIP under the conditions used; this is shown in Figure 40 on page 151. There are a few possible explanations for this increase. The first and most probable explanation is that nitrogen has much more thermal energy available for excitation and ionization than argon, and therefore much more sodium excitation and ionization is occuring in the nitrogen-containing plasmas than in the argon plasma.

Another possible explanation is that the coupling of energy from the cavity to the argon plasma is less efficient than that for the nitrogen plasma. This is supported by the fact that there is substantially more reflected power for pure argon plasmas than for nitrogen plasmas under the same input power conditions. Hence less energy goes into the plasma, possibly reducing the amount of ionized sodium. Less ionized sodium means more atomic sodium available for LIF. However, much less energy is needed to ignite and sustain a pure argon plasma. The excess energy can go into providing more atomization and excitation capability for analytes. Thus these two effects, poorer power transfer into the argon plasma, and less energy needed by argon, would be expected to balance each other out to some degree. The net effect would be fairly small. Poorer power transfer alone probably does not account for the observed difference.

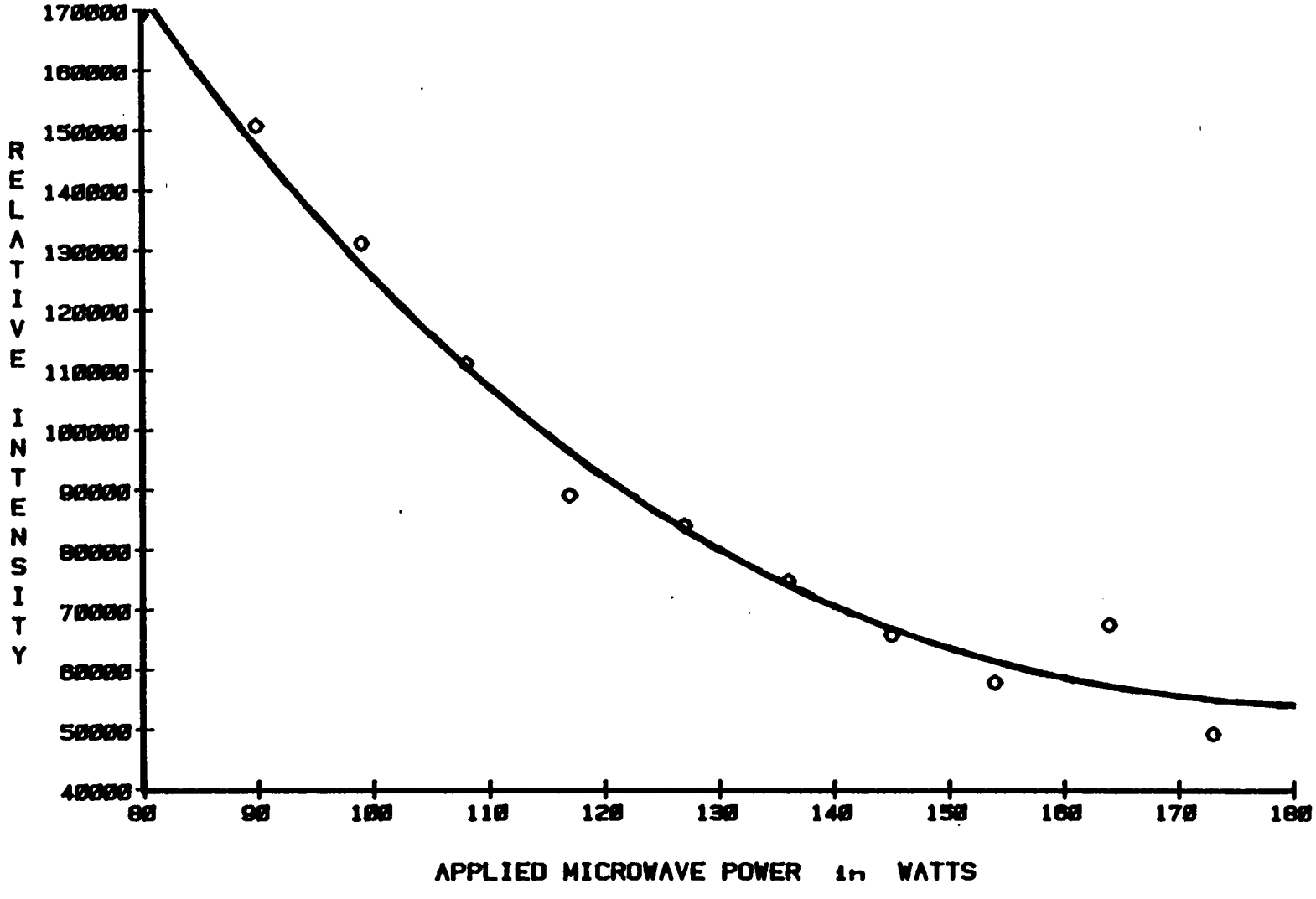

Figure 37. Sodium LIF Intensity vs. Microwave Power - Pure Nitrogen Support Gas

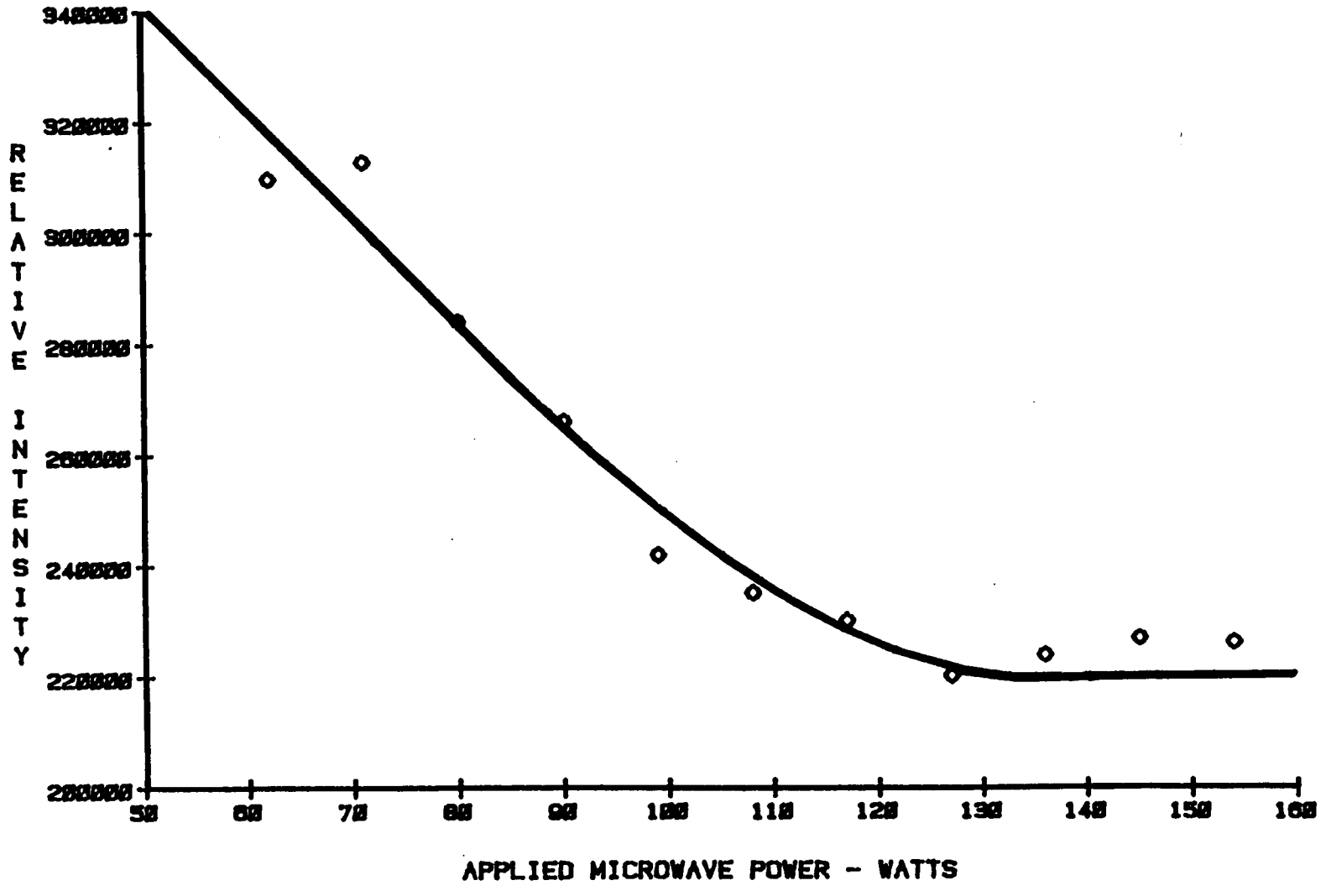

Figure 38. Sodium LIF Intensity vs. Microwave Power - 50% Argon in Nitrogen Support Gas

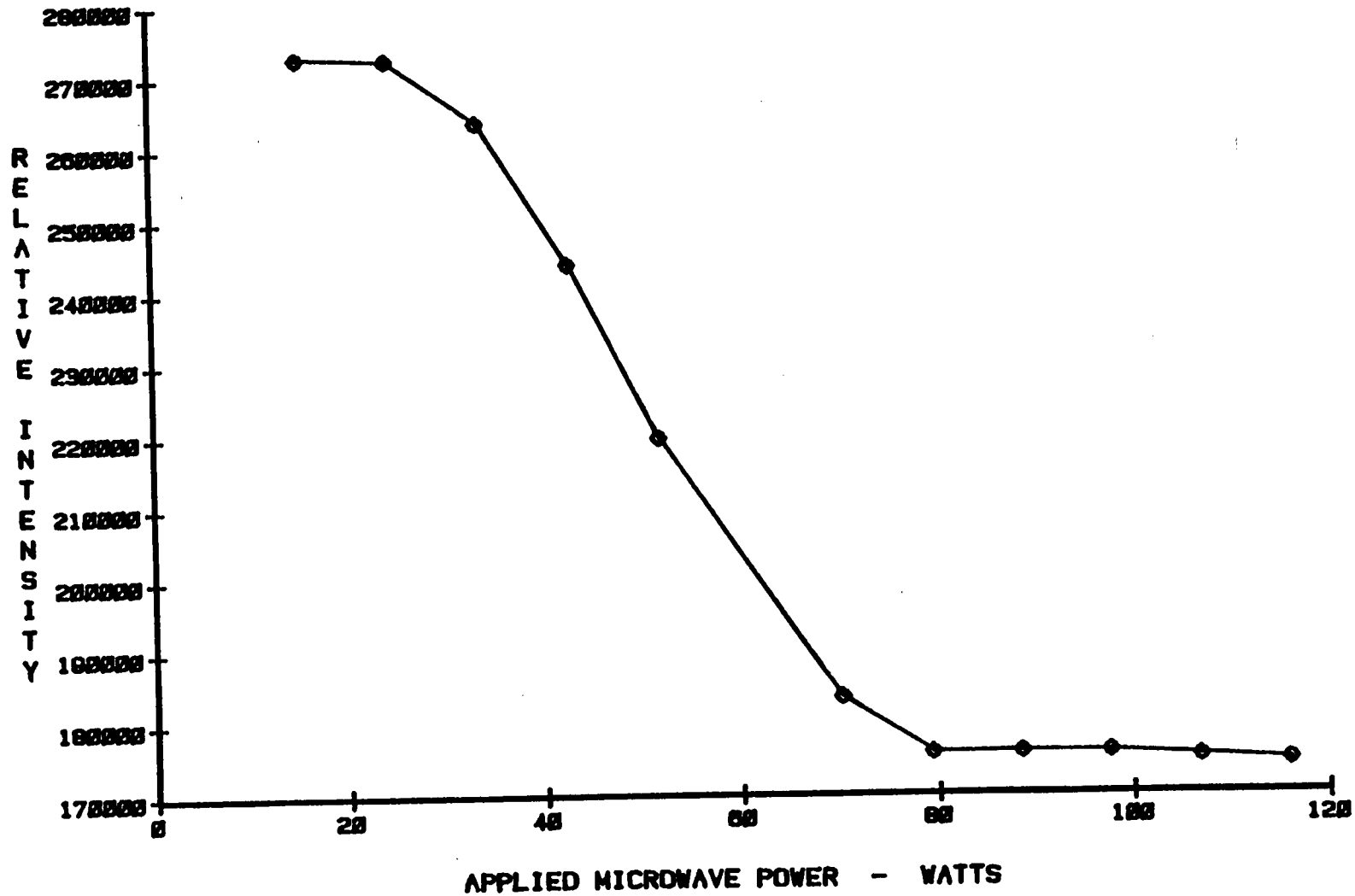

Figure 39. Sodium LIF Intensity vs. Microwave Power - Pure Argon Support Gas

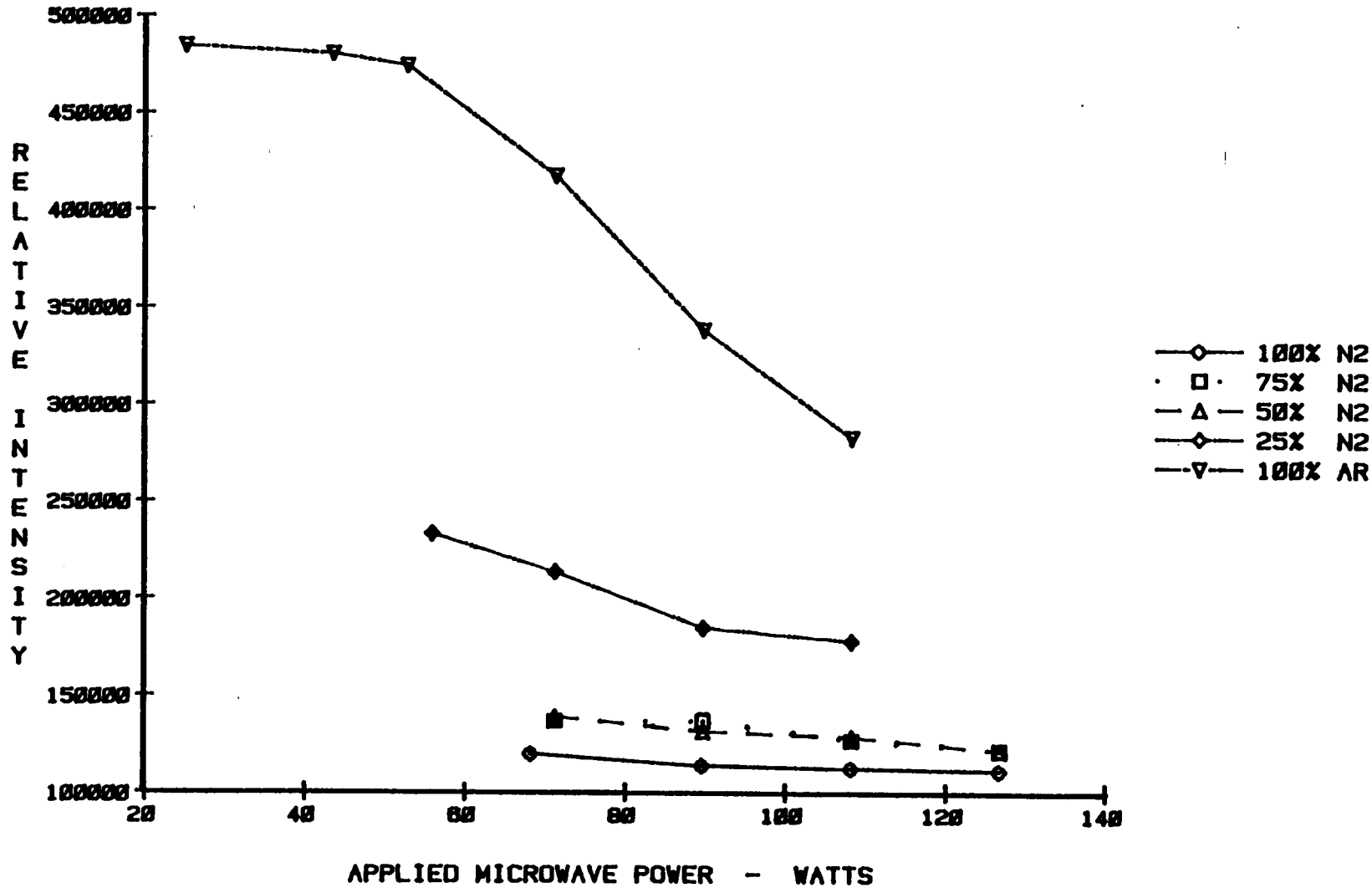

Figure 40. Sodium LIF Intensity vs. Microwave Power - Mixed Argon/Nitrogen Support Gas

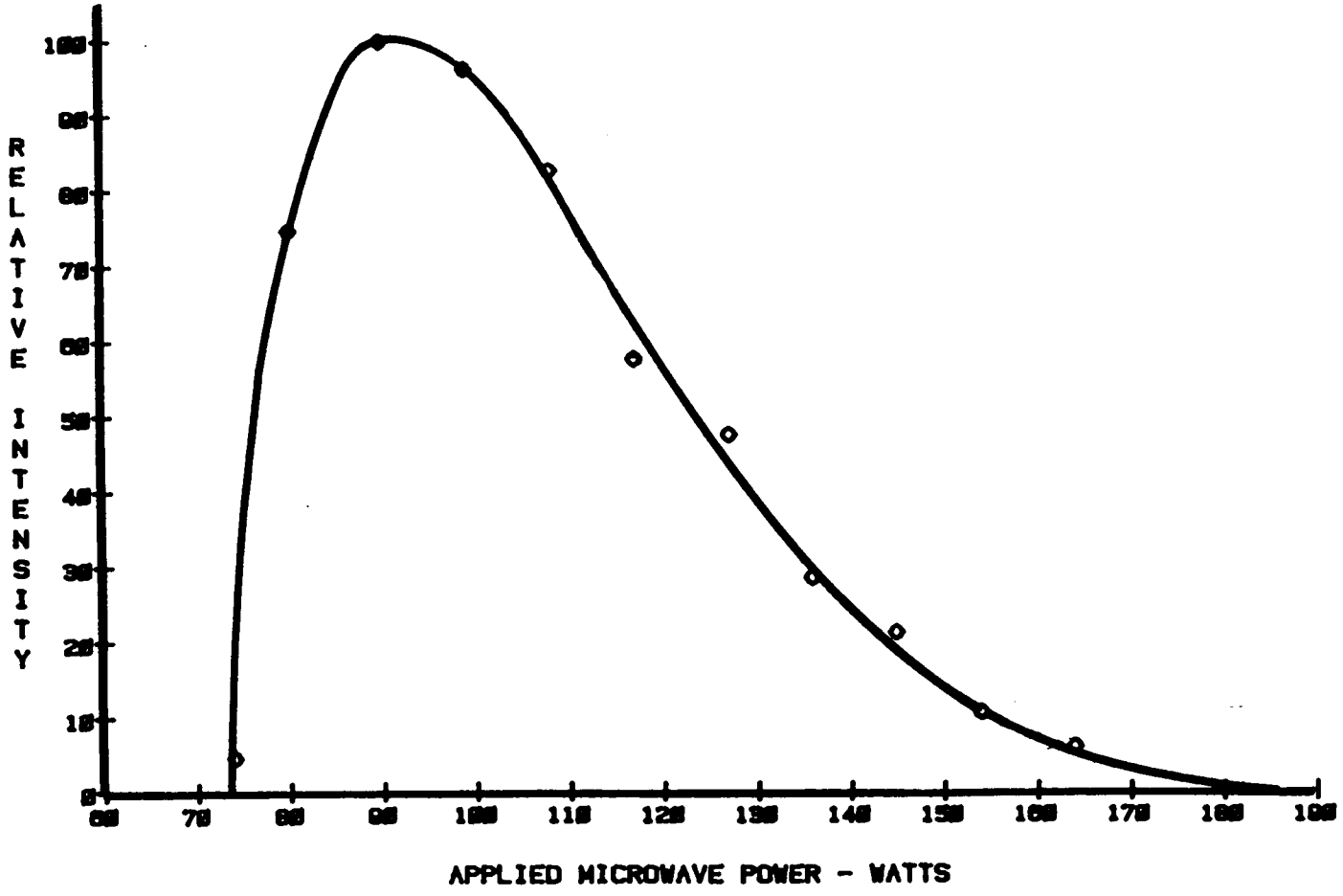

Figure 41. Barium LIF Intensity vs. Microwave Power - Pure Nitrogen Support Gas

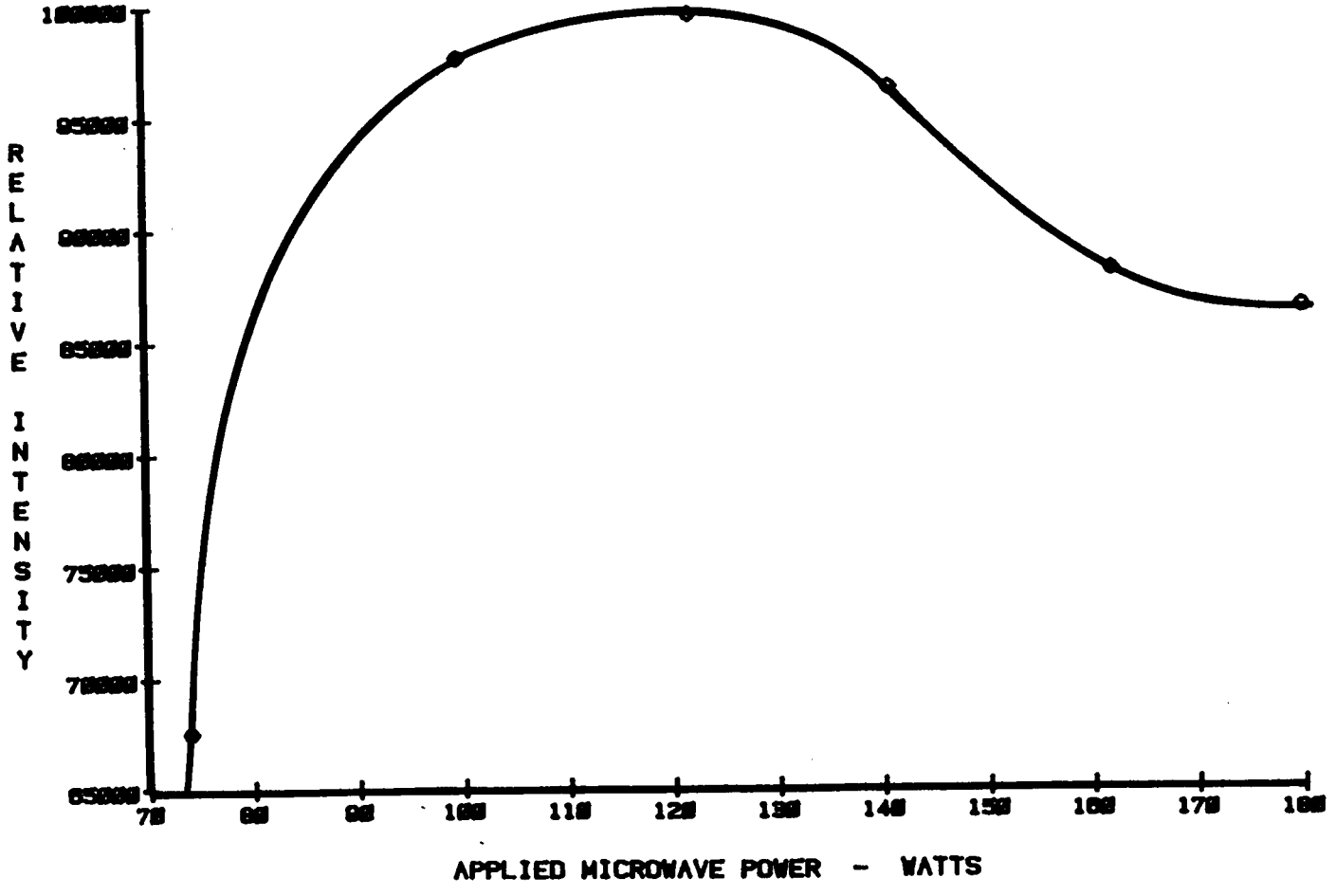

Figure 42. Barium LIF Intensity vs. Microwave Power - 50% Argon in Nitrogen Support Gas

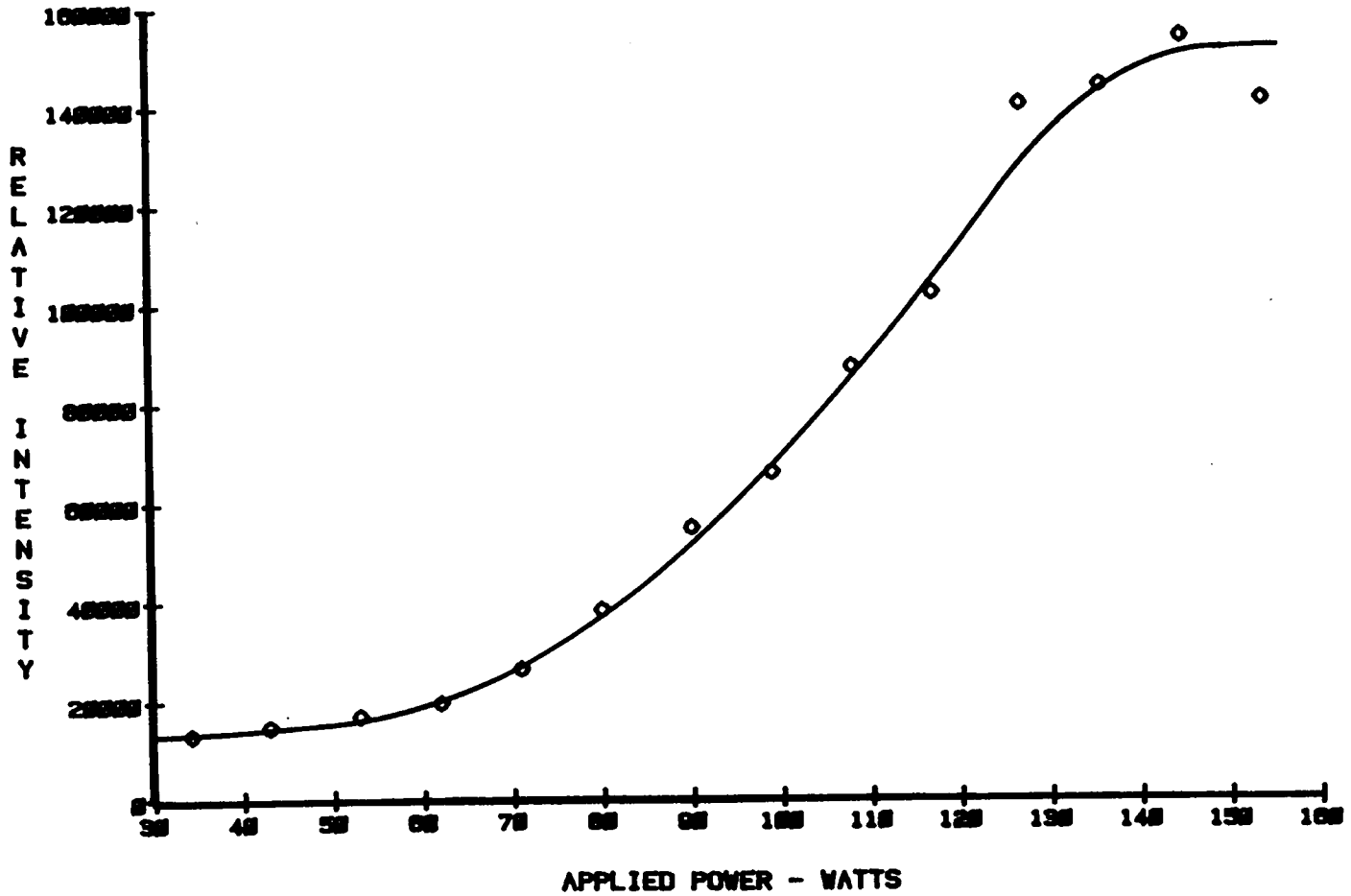

Figure 43. Barium LIF Intensity vs. Microwave Power - Pure Argon Support Gas

There is clearly more energy for excitation in nitrogen-containing plasmas than in pure argon plasmas. This is implied by the degree of analyte excitation and ionization observed in the various plasmas. Fluorescence intensities reflect the population of the lower energy state involved in the fluorescence transition. Evidence which supports there being more excitation in the nitrogen plasmas can be seen in Figure 41 on page 152 through Figure 43 on page 154. Figure 41 shows barium fluorescence in the pure nitrogen plasma; barium ion fluorescence goes through a sharp maximum at 100 watts applied power. This demonstrates that the population of the lower excited ionic state of barium (0.75 eV above the ionic ground state) goes thru a maximum as the power is increased. That is, at higher powers barium ions are promoted to higher energy states from which they do not fluoresce at 455 nm (see Figure 45 on page 160 for an illustration of the barium states involved in the ionic transitions). In the mixed Ar/N_2 and pure argon plasmas the barium ionic fluorescence maximum is reached at a higher power, and in neither case is it a sharp maximum (see Figure 42 and Figure 43).

Since the maximum occurs both more sharply, and at a lower input power in the nitrogen plasma, it is concluded that ionic analyte excitation occurs more readily in the pure nitrogen plasma. And if the excited ionic states of barium are more readily populated, it is logical that the ground ionic state is also more readily populated in the nitrogen-containing plasmas. This implies that more analyte excitation and more analyte ionization is occuring in the nitrogen-containing plasmas. Studies with nitrogen-containing ICP's and other RF plasmas done by other investigators also support this conclusion (23 , 36 , 41 , 42). **Increased excitation and ionization energy in nitrogen plasmas, plus their close approach to LTE (concluded in the experimental chapter on MIP's), support the conclusion that they possess more thermal energy than pure argon plasmas.**

Another factor contributing to analyte ionization in molecular plasmas in that they are much less conductive than atomic plasmas. This is because the electron affinity of molecules is much greater than that of atoms (59). This results in a much larger fraction of the electrons

in the plasma being unavailable to neutralize ions in the plasma. For the case of a fairly non-conductive molecular plasma, (the nitrogen plasma), the production of analyte ions from analyte atoms can actually be promoted by the LeChatelier principle (137). The relative deficit of electrons in the low-conductivity plasma favors a shift toward ionization of atomic analytes. The nitrogen-containing plasmas are near LTE, thus LeChatelier's principle is still expected to hold. The net effect of LeChatelier's principle in these plasmas is probably small, yet not insignificant, compared with the excess ionization and excitation energy in nitrogen-containing plasmas.

These explanations clarify why sodium LIF appears to be increased in the argon plasmas, and why more intense barium ion LIF is seen in nitrogen plasmas. **Overall, the dominant factor which accounts for the increased atomic LIF signals in pure argon plasmas, and increased ionic LIF signals in nitrogen-containing plasmas, is plasma thermal energy.**

With fluorescence, the atomization, ionization, and excitation pathways may be separated from one another. Thus excitation can be studied independently of the other two steps. See Figure 44 on page 157 for clarification of the steps leading to atomization. Conclusions can be drawn about atoms and ions in nitrogen and argon plasmas by studying atomic and ionic spectral changes as a function of the experimental variables. From the very large atomic sodium LIF and Ba ionic LIF signals in Figure 37 through Figure 43 on page 154, it can be concluded that atomization and ionization readily occur in MIP's. The ionization energy of these elements is approximately 5 eV. It is energetically more favorable for atomization and ionization to occur as separate steps. It is safe to say that these steps occur sequentially, rather than simultaneously (which would require a three-body process). Sequential atomization and ionization in atmospheric pressure plasmas has been postulated by other investigators (25).

Fluorescence makes it possible to examine atomic and ionic processes individually. When emission methods are used the separate steps cannot be resolved directly since the

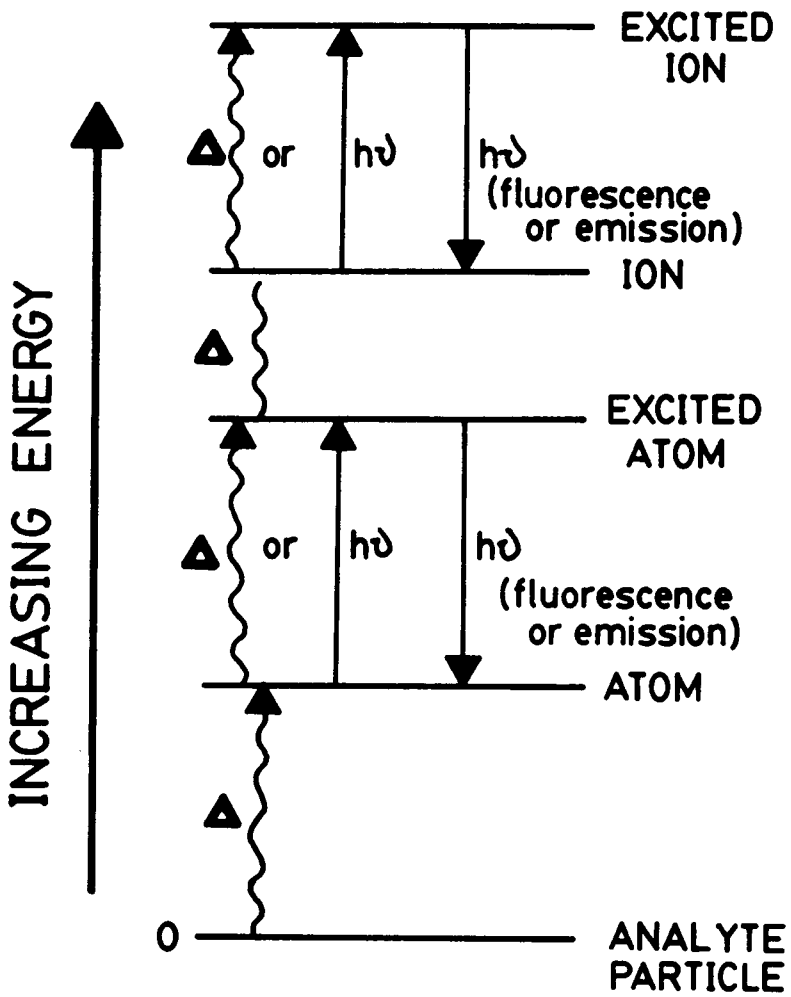

Figure 44. Stages in Excitation and Ionization of Analytes

plasma must supply energy for all of the steps. The next section looks at the information that can be provided by studies of emission processes.

2) Atomic and Ionic Emission as a Function of MIP Power:

Atomic and ionic emission intensities all increase with increasing microwave power. This is shown in Figure 46 on page 161 through Figure 48 on page 163. The slopes of the atomic emission curves indicate atomic emission is beginning to reach a plateau more quickly than ionic emission. In neither case is a plateau reached, indicating that more energy would be needed before the atomic or ionic states begin to be depopulated. Deutsch found that AES signals increased in his moderate-power nitrogen MIP up to the limit of his microwave cables and instrumentation, 250 Watts (35). For purposes of increasing signals it would be useful to have a moderate-power or high-power generator. But, this might surrender the advantages of low power, low gas consumption, and low cost in the present system. And, as will be seen later in this work, the noise levels start to increase as one moves into the moderate power range, $>$200 Watts, (see Figure 93 on page 236). At that point the very low noise background inherent in these systems begins to be lost.

From the Na fluorescence results in Figure 37 on page 148, it is seen that atomic state depopulation occurs quite readily if the microwave power is increased above its lowest level of 70 watts. The results from the barium ion fluorescence shown in Figure 41 on page 152 show that at higher MIP powers barium ions are made unavailable for fluorescence. At higher MIP powers, the most probable channel for state depopulation is excitation to a higher energy atomic or ionic state.

In emission, the excitation energies for the observed transitions, acquired from the plasma, range from 2.1 eV for the sodium 589-nm line to 2.7 eV for the barium ion 455-nm line. These systems are quantized and do not possess a continuous range of energies above the ground state that can continuously absorb energy from the plasma. Either the excitation

energy (greater than 2 eV) is present in the plasma as thermal energy, or a particular species in the plasma provides it.

In the barium ion there are excited states at 0.6 and 0.7 eV, above the ground state. The thermal energy of the plasma has no problem populating these lower excited states. If the plasma were in thermodynamic equilibrium, the 5000 degree Kelvin N_2-MIP excitation temperatures reported by the author in Chapter II would represent a thermal energy of only 0.5 eV. It is conceiveable that thermal energy alone could bring the ion to these lower excited states. And then the energy of high-energy electrons could bring the Ba ion to the upper excited states (approximately 2 eV), from which they can emit radiation at 455, 489, 585, and 614 nanometers. But, in the case of sodium, there are no excited atomic states below 2.1 eV. The temperature would need to be ca. 20,000 degrees Kelvin if this 2-3 eV of excitation energy were to come from plasma thermal energy alone. Clearly some non-thermal process is occuring.

There is little argument that atomization and ionization are sequential processes. Saying whether ionization and excitation are separate processes, and whether they are sequential or simultaneous is more difficult. It is only possible to say what are the most likely predominant processes. The possibility of a single-step, simultaneous ionization and excitation process seems to be ruled out, at least on the basis of plasma energetics alone. The ionization potential of barium is 5.21 eV. The lowest excitation energies of the Ba ion range from 2.0 to 2.7 eV. A single-step simultaneous ionization/excitation process would require about 7 eV (see Figure 44 on page 157 for an illustration of the energies involved). This energy is clearly above the 0.5 eV thermal energy of the plasma. ***The conclusions are that the ionization step is separate from the excitation step, and that non-thermal processes are occuring.***

3) GAS COMPOSITION STUDIES AT VARIOUS POWERS:

Sodium fluorescence decreases rapidly as nitrogen gas is added to a pure argon plasma

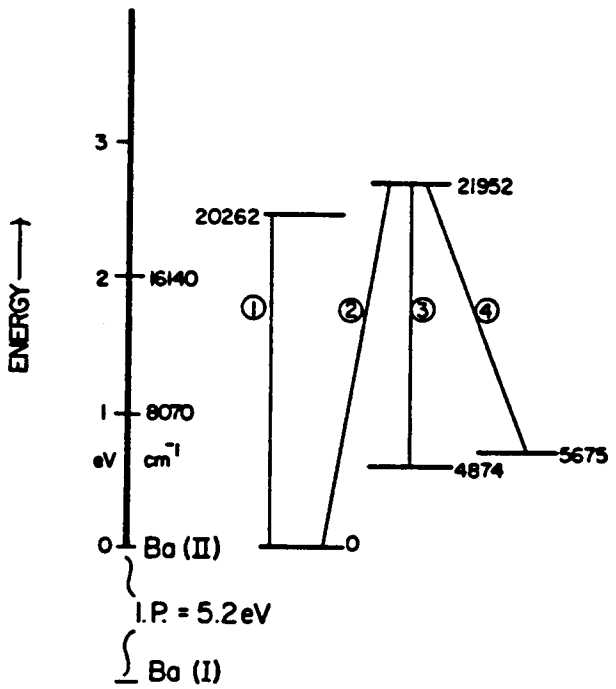

FIG. 5. Barium ion energy level diagram.
Transition (1): $\lambda = 493.4$ nm; $gA = 0.19 \times 10^8$ s^{-1}
Transition (2): $\lambda = 455.4$ nm; $gA = 0.90 \times 10^8$ s^{-1}
Transition (3): $\lambda = 585.3$ nm; $gA = 0.19 \times 10^8$ s^{-1}
Transition (4): $\lambda = 614.2$ nm; $gA = 0.38 \times 10^8$ s^{-1}

Figure 45. Barium Ion Energy Level Diagram: The Transitions Involved in Fluorescence and Emission. This diagram was taken from Appl. Spectrosc. Vol. 35, 5 (1979).

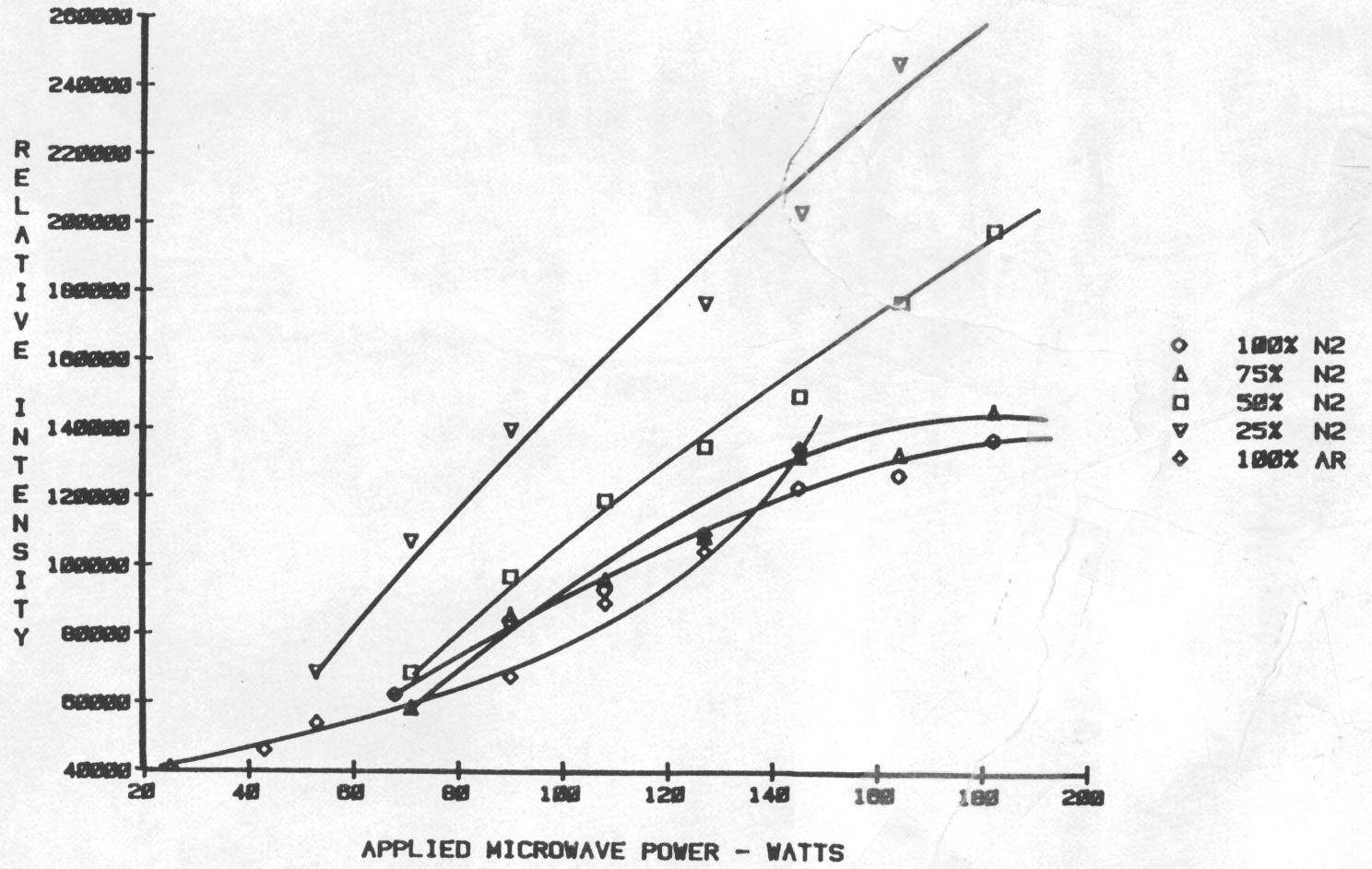

Figure 46. Sodium Emission Intensity vs. Microwave Power - Mixed Argon/Nitrogen Support Gas

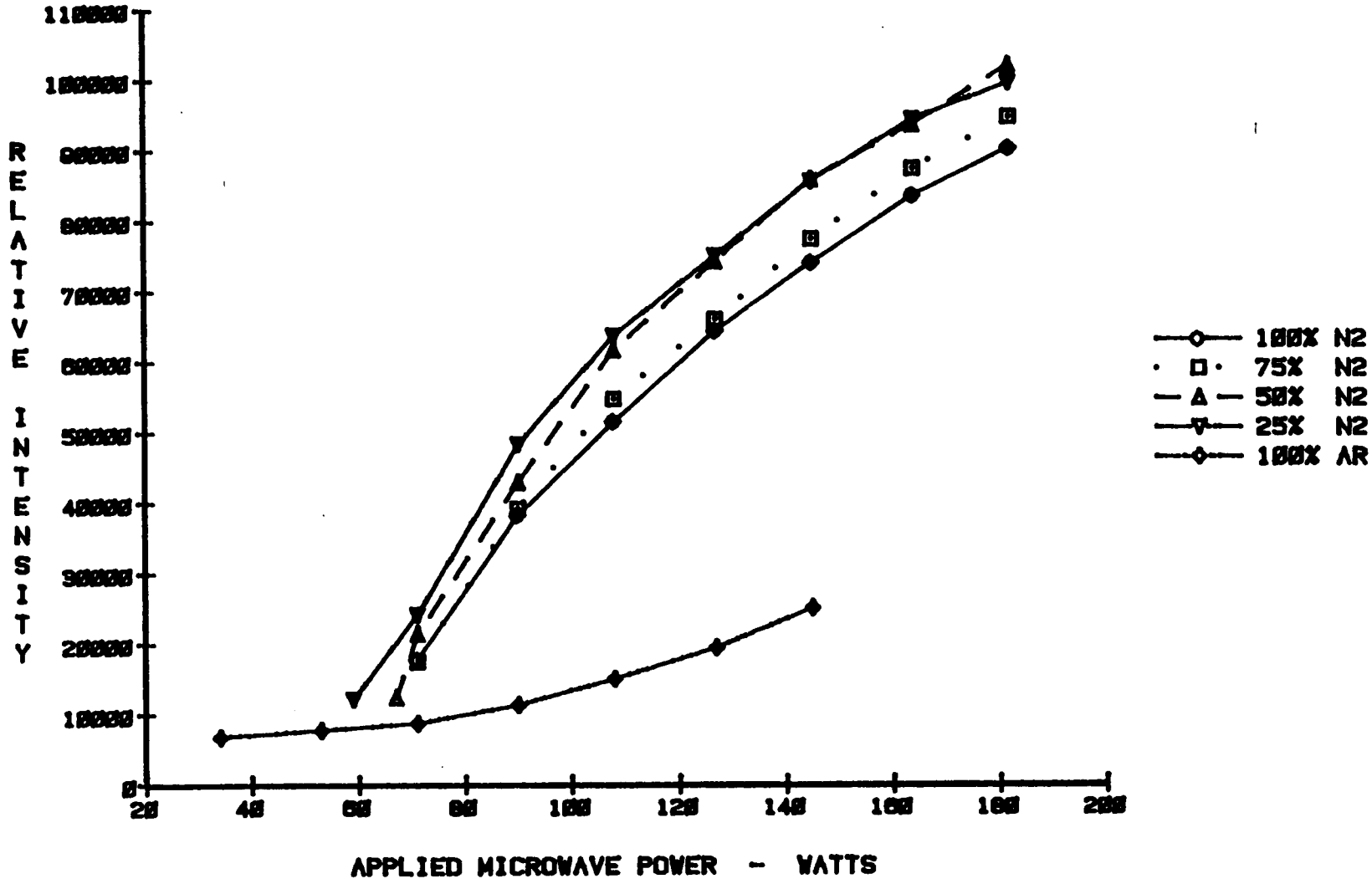

Figure 47. Barium Atom Emission Intensity vs. Microwave Power - Mixed Argon/Nitrogen Support Gas

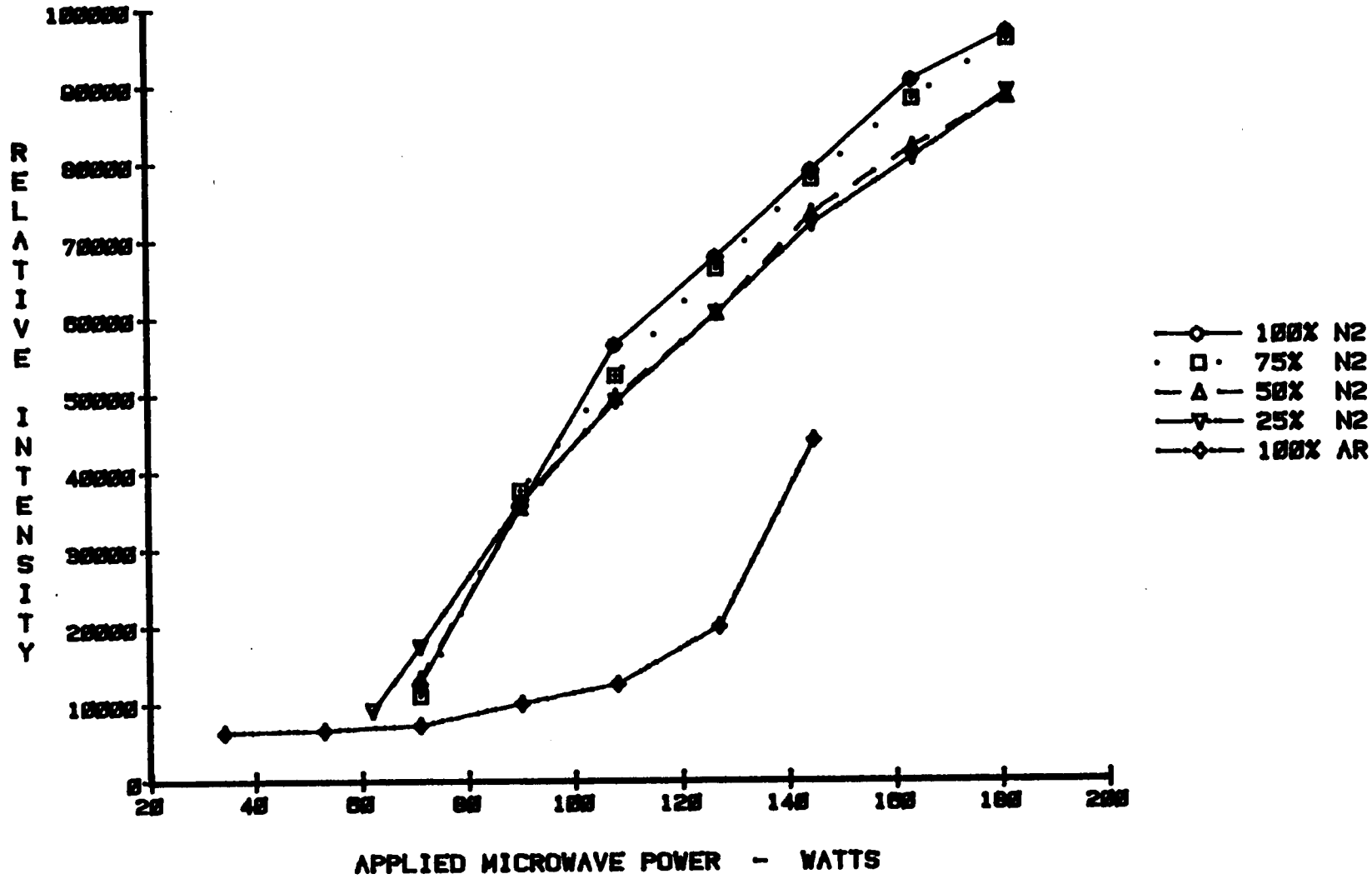

Figure 48. Barium Ion Emission Intensity vs. Microwave Power - Mixed Argon/Nitrogen Support Gas

(See Figure 49 on page 165). The most rapid decrease occurs from 0-20% addition of nitrogen, and is particularly pronounced at low powers (< 150 watts). This indicates that fewer ground state sodium atoms are present for excitation by the laser as the nitrogen content of the support gas is increased. This is probably because more sodium is being excited and ionized due to the higher thermal energies present in the nitrogen plasmas.

The results for the remaining gas composition studies are markedly different and present an interesting phenomena. In all cases, the fluorescence and emission intensities are dramatically altered when low percentages of nitrogen are used (See Figure 50 on page 166, through Figure 52 on page 168).

For Ba ion LIF, Ba atom and Ba ion emission, the pure argon plasma has the lowest signal intensity. As nitrogen is added to the support gas, the signal increases greatly in the range 1% to 50%.

Na atom emission signal intensity exhibits a very sharp peak at 10% nitrogen-in-argon, with a long tail as more nitrogen is added to the support gas. Signal intensities in pure nitrogen are generally 50% to 100% larger than in pure argon. See Figure 50 on page 166.

For Ba ion LIF, there is a sharp increase up to a peak at 10% nitrogen in argon; from 10% to 100% nitrogen-in-argon the decline in signal intensity is less steep, (see Figure 51 on page 167). The signal intensity in pure nitrogen is about twice that in pure argon.

For Ba atom emission, there is a steep rise in signal intensity as more nitrogen is added up to a peak at 30%, where the signal magnitude falls gradually to twice its value in a pure argon plasma. See Figure 52 on page 168.

Ba ion emission signals exhibit a fairly gradual increase, up to a broad peak at 30% to 50% nitrogen-in-argon. The signal then decreases almost imperceptibly as the nitrogen

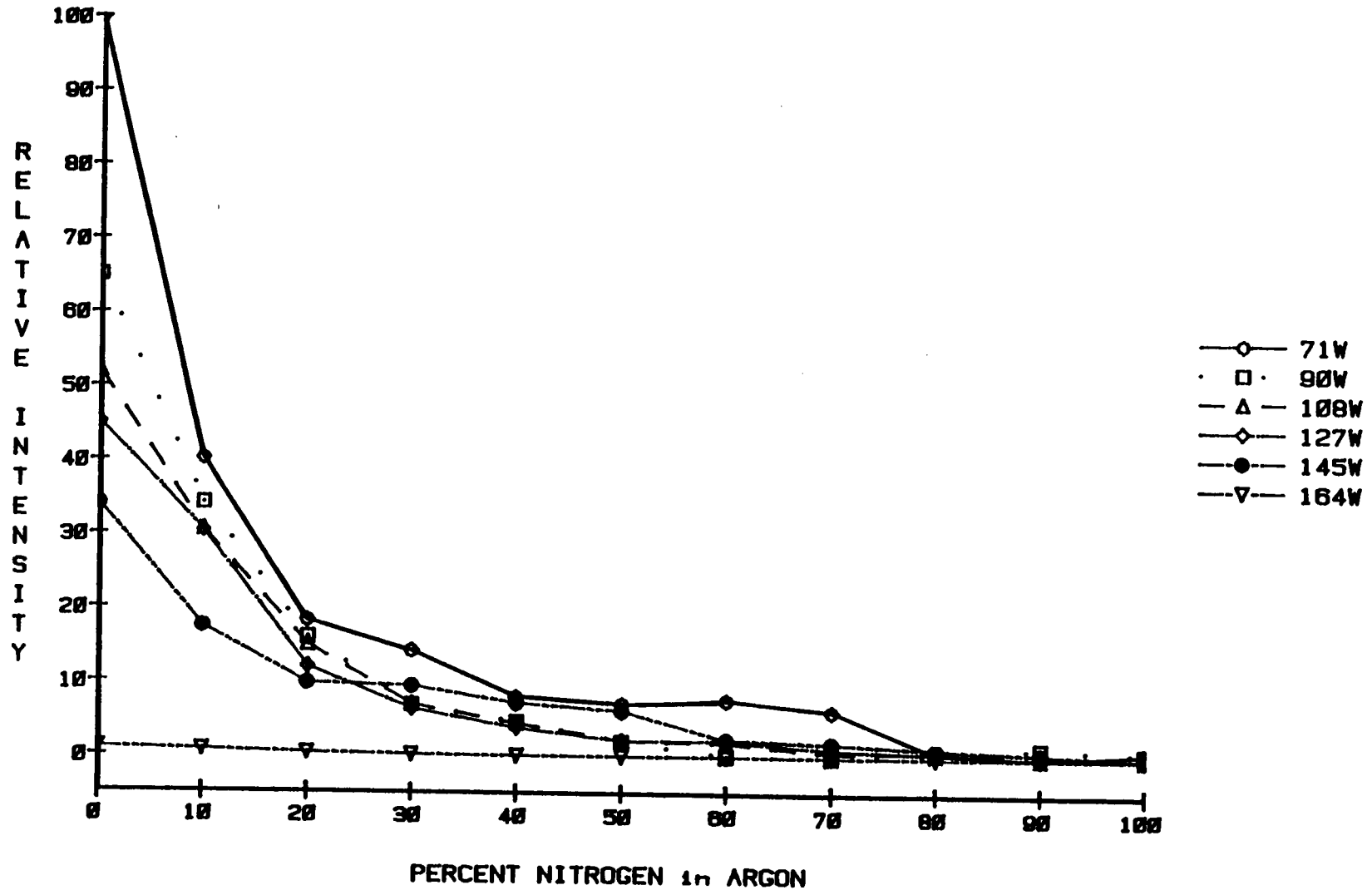

Figure 49. Sodium LIF Emission Intensity vs. Gas Composition - at Various Powers

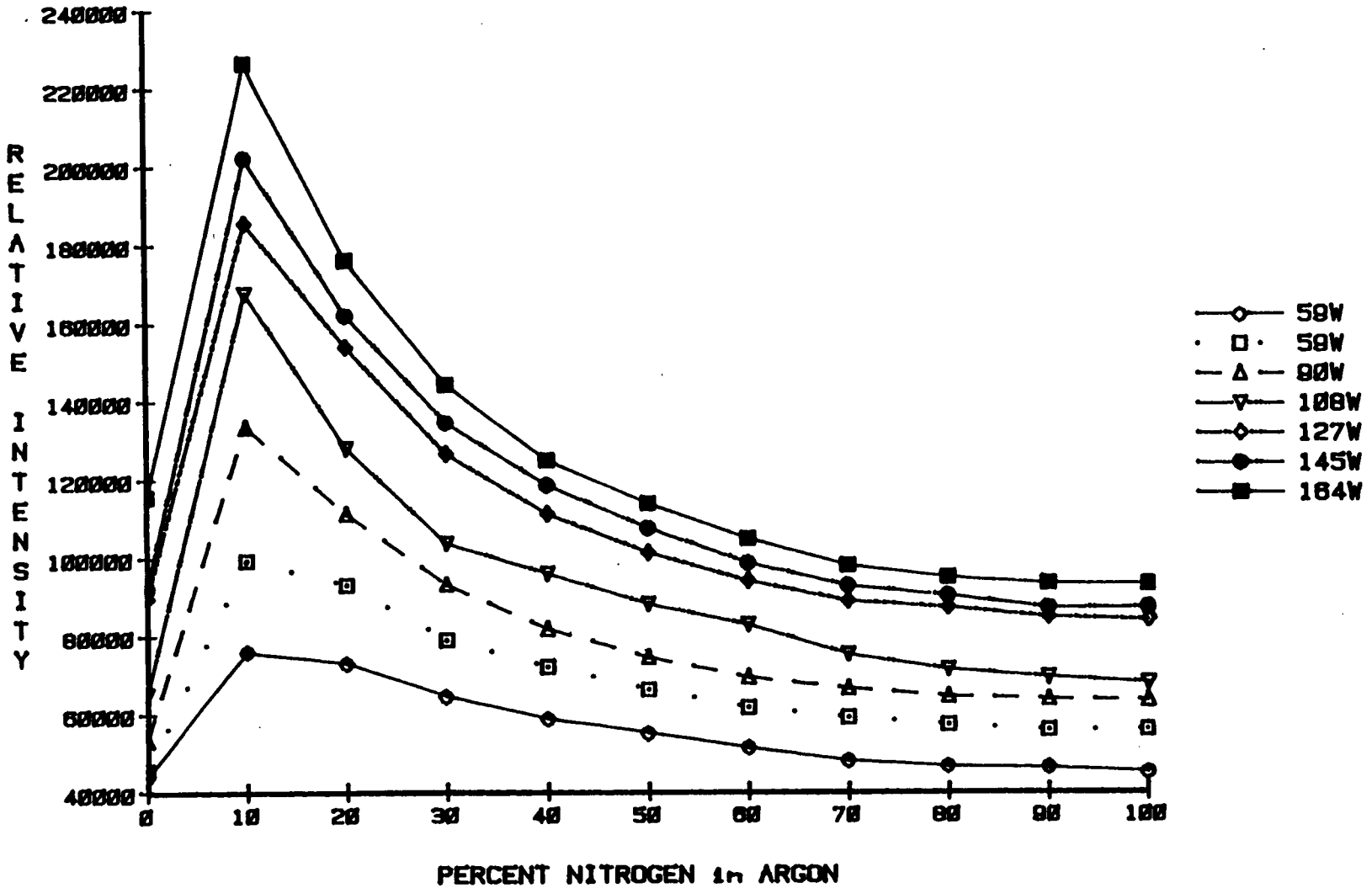

Figure 50. Sodium Atom Emission Intensity vs. Gas Composition - at Various Powers

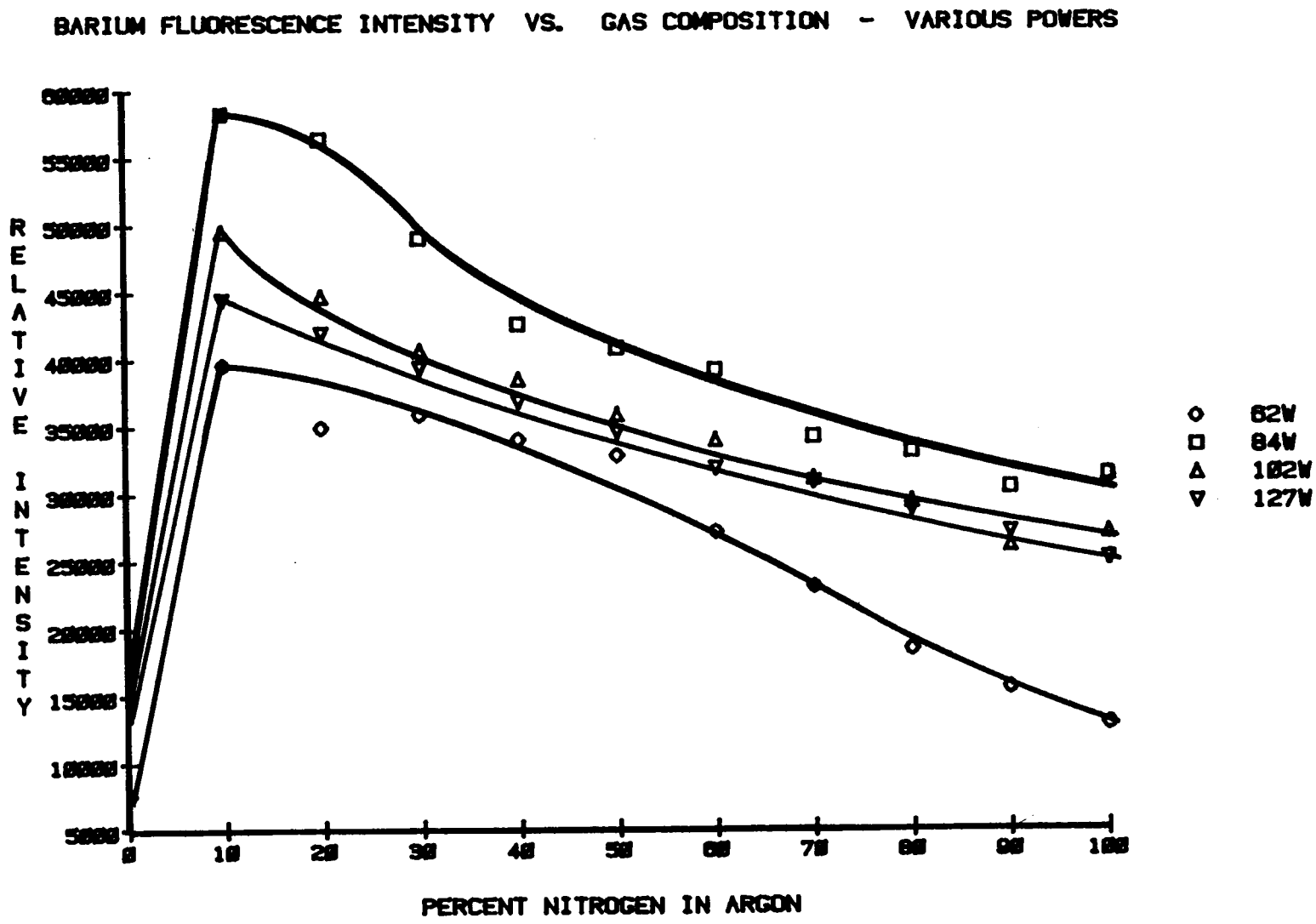

Figure 51. Barium Ion LIF Intensity vs. Gas Composition - at Various Powers

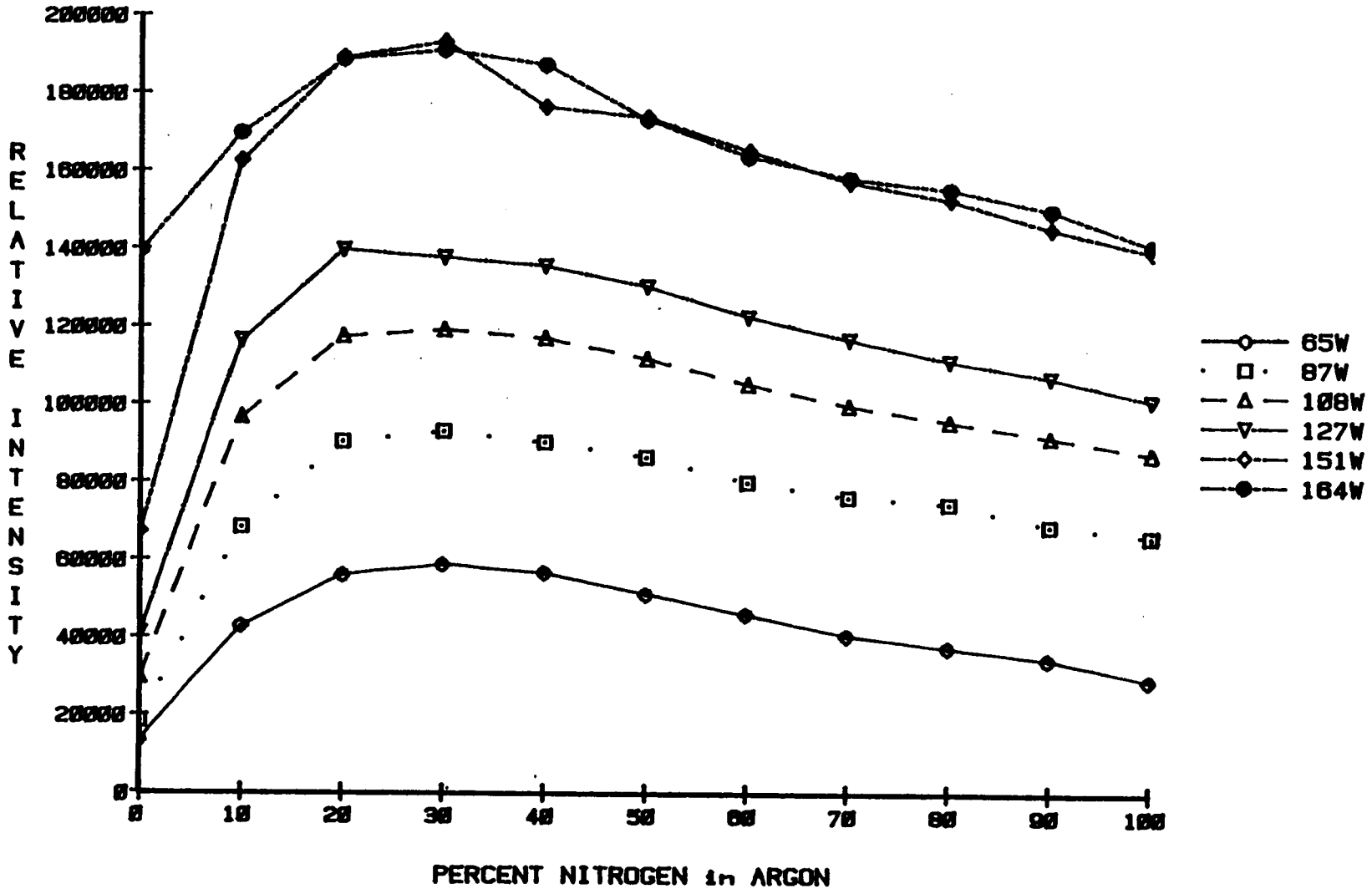

Figure 52. Barium Atom Emission Intensity vs. Gas Composition - at Various Powers

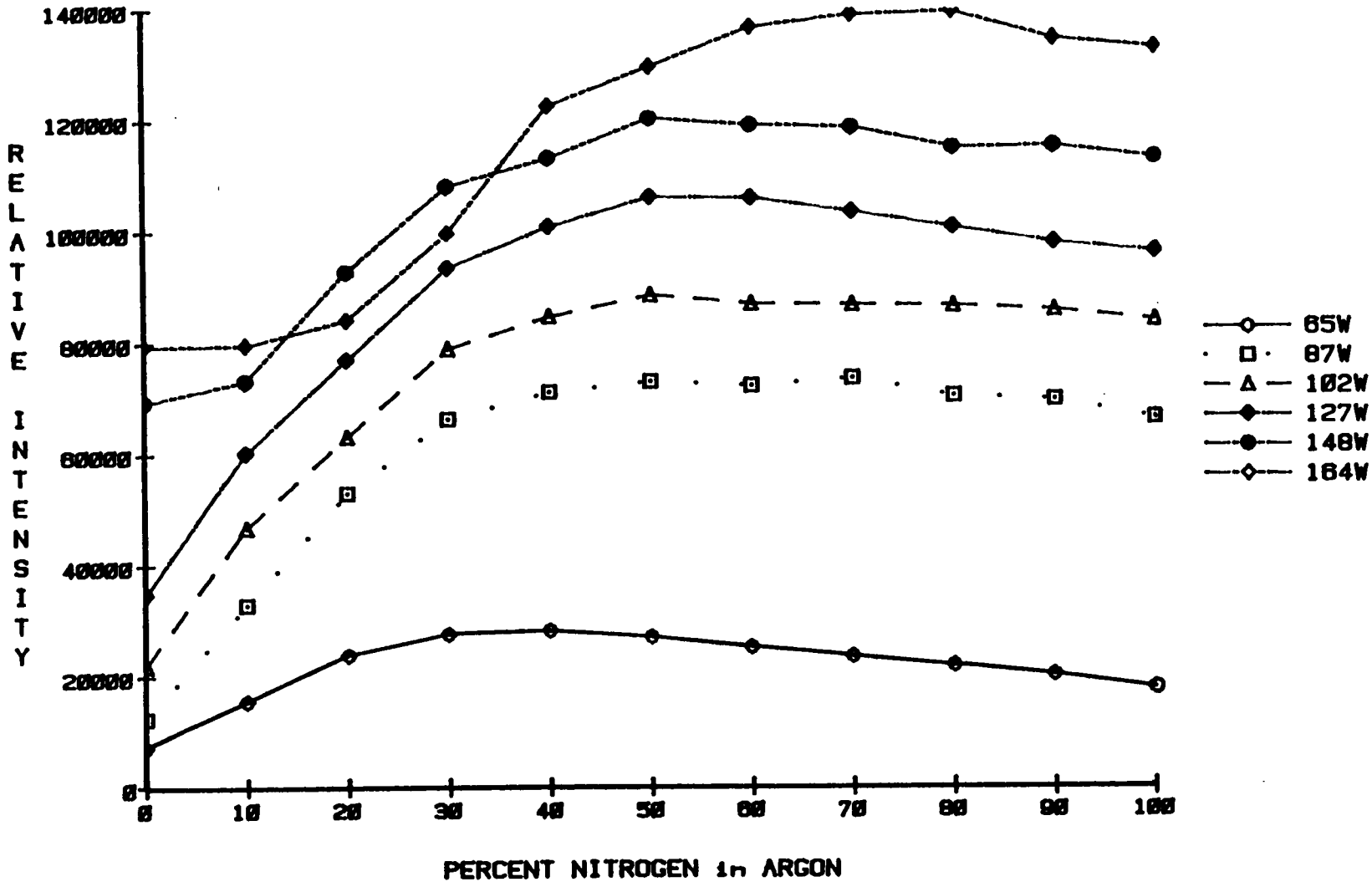

Figure 53. Barium Ion Emission Intensity vs. Gas Composition - at Various Powers

support gas concentration increases to 100%. Again, the signal in pure nitrogen is twice that in pure argon. See Figure 53 on page 169.

A similar peak shape has been observed in cadmium atomic emission in an ICP when low percentages of nitrogen in argon is used as the support gas (39).

Plasma Nonequilibrium:

The N_2 -MIP is very much like a chemical flame. In both types of plasma there are excited and ground state forms of atoms, molecules, molecular and atomic ions. The major difference between a chemical flame and the N_2-MIP is the electric field, which rapidly accelerates free electrons to very high speeds. However, this difference is very significant. It produces two groups of electron kinetic energy profiles, a low-energy group [like in a chemical flame], and a high-energy group [like in a low-pressure electrical discharge], (10). Adding nitrogen to an inert gas plasma has little effect on the electron energy profiles. Goode and Otto reported that electron densities decrease about two orders of magnitude when 7% nitrogen is added. This decrease will equally affect the population of both the high-energy and the low-energy group of electrons. Thus, the maximum electron temperatures remain relatively unchanged as nitrogen is added (60).

Deutsch reported that the moderate-power pure nitrogen MIP has excitation temperatures of 4000 to 5500 degrees K, ionization temperatures of 5000 to 5500 degrees K, and rotational temperatures of 4400 to 5000 degrees K (35). He indicated that the plasma was very close to LTE since these temperatures are nearly equal. However, no electron temperatures were reported by Deutsch. Goode and Otto studied an argon/nitrogen MIP system at atmospheric pressure and reported electron temperatures in the range 21,000 to 25,000 degrees K, which corresponds to an energy of 1.5 eV (60). The study used 100 watts applied power and up to 7% nitrogen in argon. Increasing applied power increased the electron temperature.

In the present studies the power transfer characteristics and appearance of the nitrogen-in-argon plasma changed most radically in the range 0 to 5%. Additional nitrogen did not significantly change reflected power (less than 2% of total applied power for of all powers used). Since plasma conductivity is the most important factor that can change cavity power coupling performance, observed power transfer characteristics very likely reflect changes in plasma conductivity. A logical conclusion from the constancy of the reflected power with additional nitrogen (>5%), is that plasma electron density and electron temperatures do not change appreciably as more nitrogen is added.

Plasma Excitation Mechanisms:

The excitation step can be simply explained by the presence of some plasma species which absorbs energy from the microwave field and then transfers it to the analyte. Both highly-energetic free electrons and metastable atoms and molecules have been postulated as the primary energy carriers in microwave plasmas (64). Active nitrogen is most certainly a factor, shown by the visually observable First and Second Positive emission bands present in the tail-flame. The energy states involved in the generation of these bands are above the $N_2(A)$ metastable (lifetime = 2.1 seconds) state, hence some cascade to the $N_2(A)$ state does occur. This metastable state is the one thought to be most responsible for excitation by "active nitrogen" (45).

The peaks in LIF and emission observed at low concentrations of nitrogen in argon are due to changes in concentration of the primary plasma energy carrier responsible for analyte excitation. The concentration of that energy carrier is maximized at low nitrogen compositions, hence analyte excitation is maximized.

If metastable nitrogen molecules are responsible for analyte excitation, the peak at low N_2 compositions can be explained in the following manner. At constant energy input there is an optimum gas mixture which favors the production of N_2 metastables. At low nitrogen compositions there is little quenching due to N atoms, which are the principle quencher of N_2

metastables. A N_2 plasma requires considerably more energy to sustain than an argon plasma. At low N_2 concentrations not as much power is absorbed by the N_2 support gas. Thus, the energy absorbed by the plasma goes into making as many metastables as possible, and not as many N atoms are produced. Since fewer N atoms are being produced, less quenching occurs that is due to N atoms. Less quenching of N_2 metastables by N atoms means more N_2 metastables available for analyte excitation.

This same mechanism can also be thought of in terms of a gross physical effect. The effect of operating in an atmosphere of 10% N_2 is to effectively operate the discharge at a partial pressure of 1/10 atmosphere (76 torr). As pressure is reduced there is a distinct maximum in the absolute number of N_2 metastables produced. The maximum typically occurs between 10 and 300 torr (138 , 69 , 70). This optimum pressure occurs because there is an equilibrium between nitrogen atom production and recombination, hence N_2 metastable state destruction and production.

Spectroscopic experiments were conducted by the author to prove whether or not metastable atoms and molecules are the principle energy carriers in the nitrogen plasma. A complete spectral characterization is described at the end of the Chapter II, Section C. The wavelengths for the spectral emissions of the N_2 (A) metastable states were scanned. The most prominent N_2(A) metastable emissions are in the UV, known as the Vegard-Kaplan Bands. High pressure conditions are favorable for observation of these bands, since the concentration of N atoms (the principal quencher of nitrogen molecular metastables) is reduced at high pressure. Collisions with the walls of the discharge tube are also reduced in number.

The Vegard-Kaplan bands were so weak that they were not detectable in these studies, at either low pressures or high pressures. This indicates that the concentration of active nitrogen is below 1E+10 particles/cc. This is too small to be able to excite analyte concentrations of 1E+14 analyte atoms/cc, which is the approximate concentration of a 10 ppb

gaseous solution of Na atoms in the plasma. Granted, there may not need to be unit excitation efficiency, i.e., every analyte gets excited. However, this disparity in exciter/excitee concentrations is quite large. So large that multiple analyte-excitation cycles might be needed to make the overall metastable energy transfer process efficient enough to explain the linear dynamic ranges (about 4 ppb to 100 ppm) and limits of detection (1ppb) measured and reported at the end of this chapter. N_2 (A) metastables are not in great abundance in the plasma. This rules out a dominant contribution from these species. Thus, **metastable energy transfer from the N_2(A) states is not the predominant mechanism for analyte excitation in the low-power nitrogen plasma.**

Another possible explanation is that changes in plasma conductivity (i.e., electron density) are responsible for the maxima seen in the gas composition studies. According to such a scheme, at low % N_2 concentrations a pure Ar plasma has a much higher conductivity than a nitrogen plasma. As N_2 is added to an argon plasma, the plasma conductivity goes down since more free electrons are taken up by the electrophilic N_2 molecules.

However, if electron collisions were predominantly responsible for atomization this would not explain why the most intense Na fluorescence occurs at the highest electron concentration, i.e., at 100% argon. It is more probable that the microwave field is responsible for atomization by heating of solvated analyte particles and atoms. And, if electron collisions caused analyte excitation, sodium atoms would be expected to emit more strongly in an environment where they were undergoing more collisions with high-energy electrons, again at 100% argon, rather than at 10% nitrogen-in-argon (see Figure 50 on page 166).

Another piece of evidence which does not support electron collision as the dominant mechanism is seen in Figure 50 on page 166, through Figure 53 on page 169. One would expect the maxima for Na and Ba emission to occur at lower % N_2 concentrations since electron concentration goes up at these lower nitrogen concentrations. The observed effect

is in the opposite direction. Thus, **electron collision is not the dominant mechanism for analyte excitation in MIP's.**

To establish the exact role of electron transfer in the mixed argon/nitrogen plasmas would require electron density measurements. The most common technique for doing this is Stark broadening measurements of the hydrogen Balmer line. Increases in the local charge density around an atom due to plasma electrons increases the local electric field experienced by the atom, causing Stark broadening of spectral emission lines. Data on Stark-broadened hydrogen atom profiles have been extensively tabulated and are used to determine electron density concentrations. (139).

Electron density measurements using Stark broadening were attempted in our laboratory, but no H atom emission was detectable in the low-power HEMMP cavity. Nitrogen gas with 1% hydrogen gas added was used, as was aqueous aerosol. Deutsch also tried to do the same measurements in the moderate-power N_2 -MIP, and no H atom emission was observed there either (35). Without sufficient H atom emission in these plasmas this technique is not feasible.

Even if enough H atom emission were present it is doubtful whether Stark broadening would be observed. Plasma electron densities of 1E+14 to 1E+16 electrons/cc are the lower limit for the detection of Stark broadening measurements for electron density calculations. Stark broadening methods are useful for the range $1E+14 < N < 1E+20$ electrons/cc. They are generally applicable to plasmas near thermodynamic equilibrium at high temperatures greater than 5000 degrees Kelvin (140). At a density of 1E+14 electrons/cc, the Stark half-width for a 5000 degree Kelvin arc plasma is 0.25 Angstroms. This is below the resolving power of the 1/2 meter monochrometers available in the laboratory.

In any case, the most probable mechanism responsible for the observations involves the concept of plasma thermal energy. As more N_2 is added to the Ar support gas the thermal

energy of the plasma increases. Nitrogen gas has a much higher heat capacity than argon because of the extra degrees of freedom in which it can store energy. As the concentration of nitrogen in the support gas increases, more energy is absorbed by the plasma; this is observed as a decrease in reflected power. Looking at Figure 50 on page 166, through Figure 53 on page 169, one can see a gradual shift in the location of the intensity maxima in the gas composition curves; from 0% N_2 for Na LIF, 10% for Na atom emission, 10-20% for Ba LIF, 20-30% for Ba atom emission, to about 50% N_2 for Ba ion emission. This is the approximate order of excitation energy increase - Na atom LIF < Na atom emission < Ba ion LIF < Ba atom emission < Ba ion emission. Since, the LIF studies demonstrated that ionization is probably a separate step from excitation, this order is very reasonable.

A thermal-energy excitation mechanism is supported by the several results observed in this work. Excess excitation and ionization energies are observed in nitrogen-containing plasmas. The intensity maxima of the gas composition curves shift to greater nitrogen concentrations (i.e., more "thermal" plasmas) for species which require more energy for excitation. The results of the observation height studies (later in this chapter) strongly support this order of excitation energies. Even though the N_2-MIP is not at thermodynamic equilibrium it is a more nearly "thermal" plasma than the argon or helium MIPs. This was confirmed by rotational, ionizational, and excitation temperature measurements performed by Deutsch (35).

Contributions due to active nitrogen metastable-energy transfer and electron-energy transfer are probably small, though should not be totally ignored. The absence of a very large concentration of the $N_2(A)$ states of active nitrogen precludes this state from being very important in excitation of analytes. The $N_2(B)$ and $N_2(C)$ states of active nitrogen are well-populated, as can be seen from their emission spectra. These high-energy states do not appear to be very important in excitation since one would expect to observe highly non-thermal excitation of analytes. The AES and LIF results from these experiments support a "nearly-thermal" mechanism. Thus, it appears that the dominant excitation mechanism is

not metastable energy transfer from support gas molecules to analytes. The electron-energy-transfer mechanism was ruled out as the dominant because of the fluorescence and emission experiments. They predict intensity maxima shifting to lower nitrogen-in-argon concentrations on the basis of an electron-transfer mechanism.

The dominant excitation mechanism in the Highly-Efficient N_2 -MIP is predominantly "nearly-thermal" excitation, with contributions from high-energy electrons, and support gas metastable-energy excitation. Investigations are going on in many laboratories to elucidate the exact mechanisms most responsible for analyte excitation in MIP's and ICP's. Although there continues to be a great deal of activity devoted to developing models, the dominant factors in analyte excitation are unknown. None of the currently proposed excitation mechanisms entirely explain all observed fluorescence and emission phenomena in these plasmas.

Support Gas Flow Rate Studies

Fluorescence and emission intensities for Na and Ba were measured as a function of flow rate. This was done for two reasons: 1) to determine the optimal flow conditions for operating the instrument, 2) to gain more insights into plasma processes.

The minimum flow rate was determined by the ability of the support gas to cool the plasma torch. One would like to operate at the lowest flow rate possible, without incurring torch damage. In all gases used the torch began to overheat at flow rates below approximately 0.75 L/min. The optimal flow rate was typically 1.2 to 1.5 L/min. The range of 1 L/min to 5 L/min had the largest effects on the observed analyte intensities. A nebulizer flow rate of approximately 0.75 L/min was used for all flow rate studies. The observation height of maximum intensity shifted slightly if very large changes in flow rate were made. All measurements were taken at the observation height which gave maximum fluorescence or emission intensity.

Introducing a few theoretical points will help clarify the discussions that follow. The time that it takes for a particle to transit the microwave cavity at the linear velocity of the support gas is called the transit time or residence time. The plasma species responsible for energy transfer to analyte particles needs time to be formed within the microwave cavity. Time is also needed to transfer this energy over to the analyte introduced into the plasma; this is the interaction time. Increasing the flow rate reduces the residence time, eventually to the point where it is too short for the efficient formation of the high-energy plasma species. And, simultaneously, the interaction time is reduced to a point where efficient transfer of plasma energy to analytes cannot occur. This is true whether the high-energy plasma species are electrons, ions, or metastables.

1) Nitrogen-Containing Plasmas:

The signal intensities decrease rapidly as the support gas flow rates increase, as shown in Figure 54 on page 179 through Figure 63 on page 188. This is because residence times decrease very quickly, to the point where there is not enough time for efficient atomization, ionization, or excitation. All fluorescence and emission studies done in nitrogen-containing plasmas follow this trend. In general, by the time the flow rate reaches 2.5 L/min, the intensities drop to less than 50% of the maximum intensity. Argon MIP's give slightly different results; these are discussed in the next section.

As noted in the section on microwave power studies, the signal intensities increase as the MIP power is increased. In the flow rate studies, the signal intensities also increase as the power is increased, giving curves shifting up and to the right. Analytes atoms acquire energy more quickly in a hotter plasma, hence the residence times can be shorter. The minimum flow rate required to cool the MIP torch also increases at higher MIP powers.

Instrumentally the Highly-Efficient N_2 -MIP cavity is "rugged" with respect to flow rate; it requires little or no change in tuning or matching elements, even with large changes in flow rate. Only very large changes in applied power require retuning. It is as if the nitrogen gas acts as a buffer to absorb large changes in electron concentration because of its strong electrophilicity. Applied power changes do not appreciably affect coupling efficiency because of the many ways nitrogen can absorb energy without ionizing.

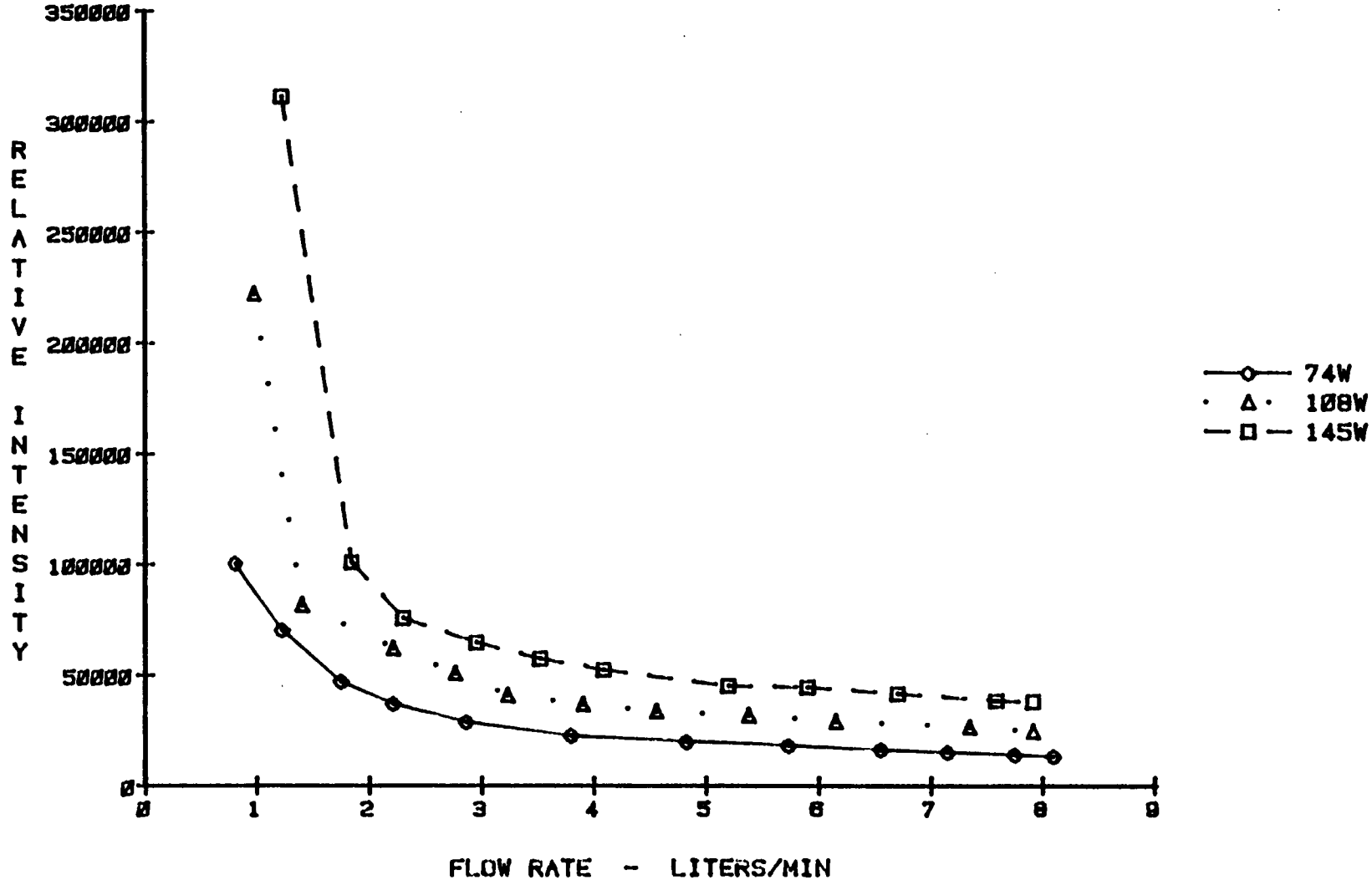

Figure 54. Sodium Atom Emission Intensity vs. Flow Rate - Pure Nitrogen Support Gas

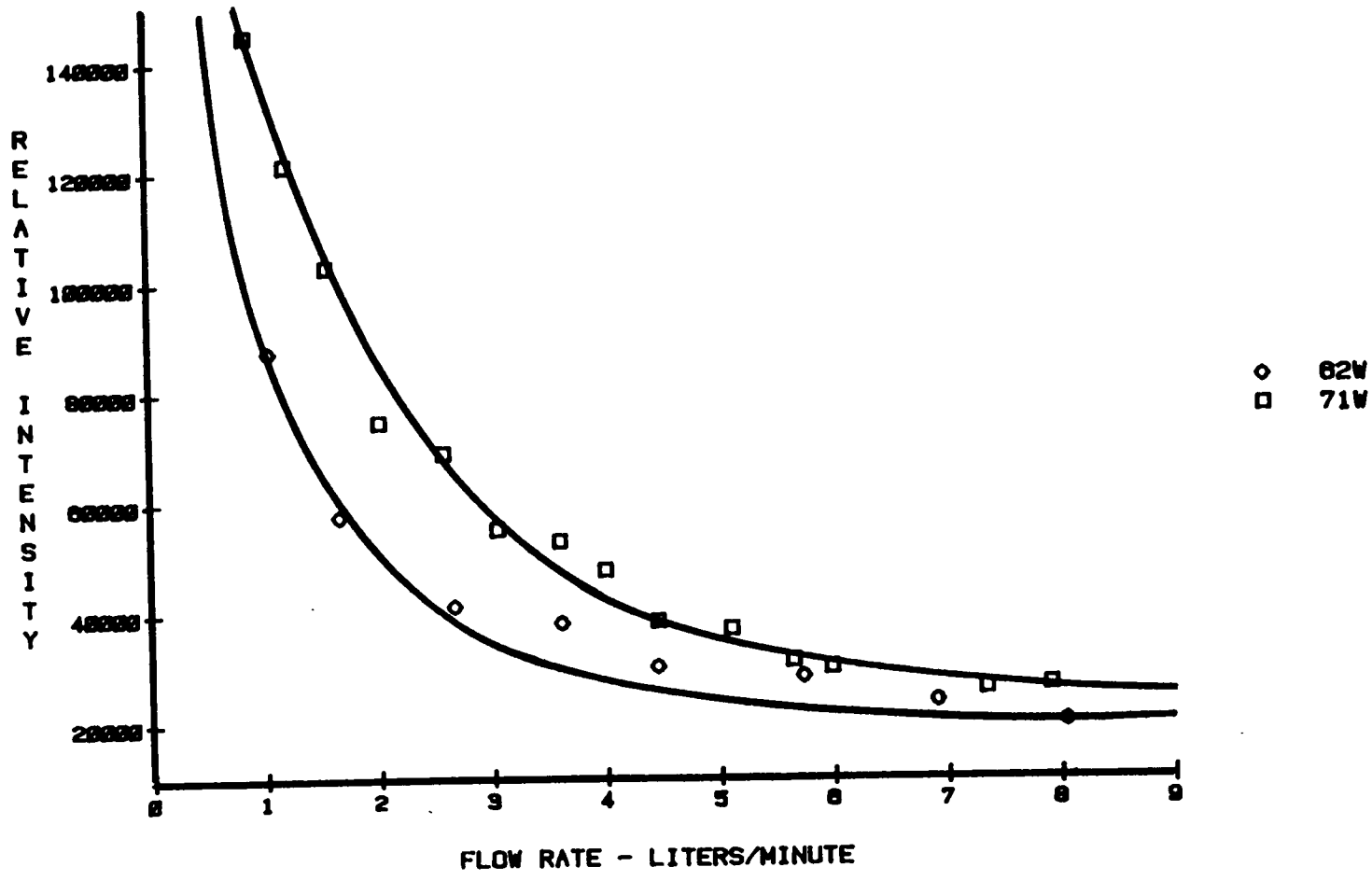

Figure 55. Sodium LIF Intensity vs. Flow Rate - Pure Nitrogen Support Gas

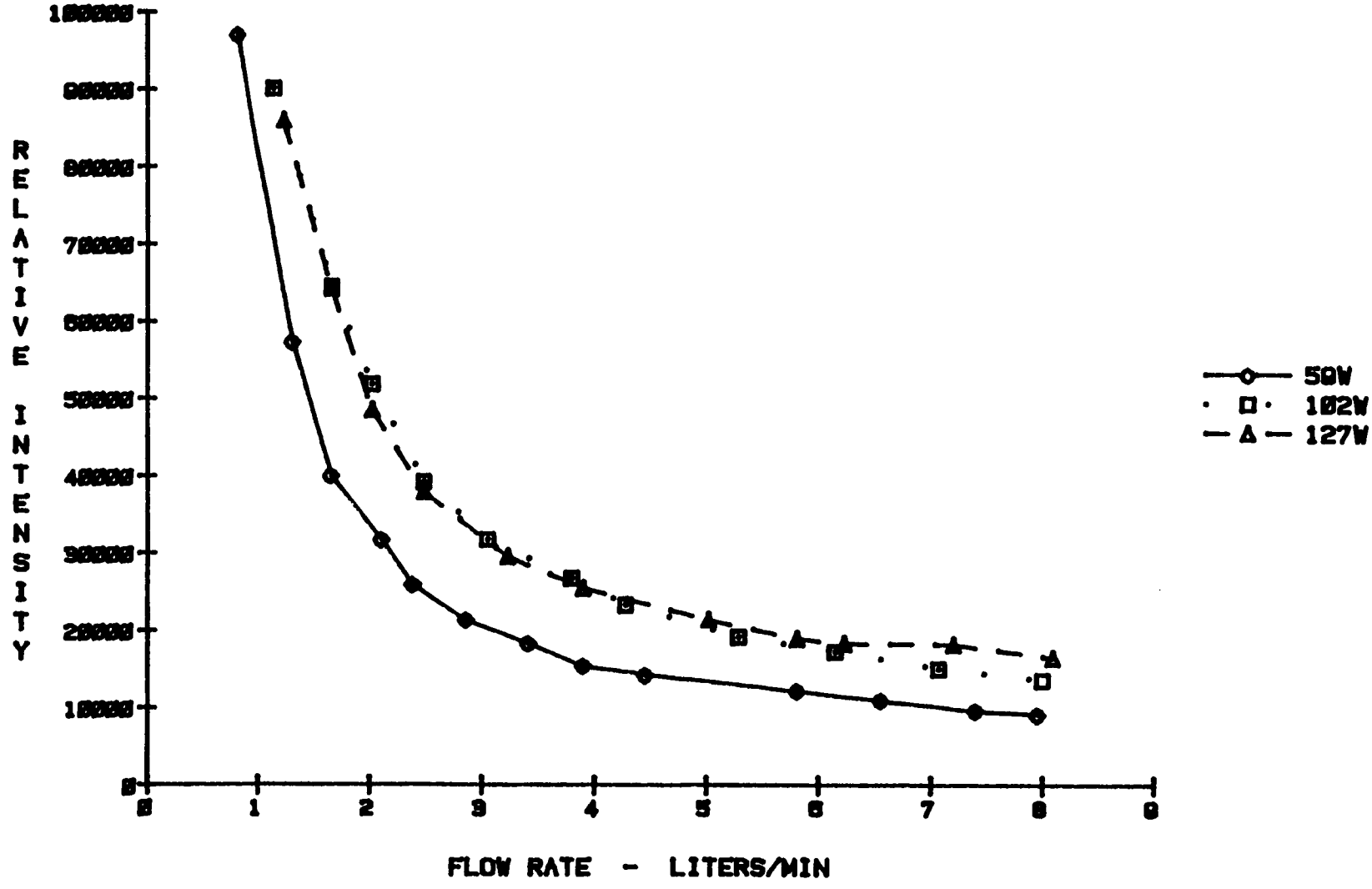

Figure 56. Barium Atom Emission Intensity vs. Flow Rate - Pure Nitrogen Support Gas

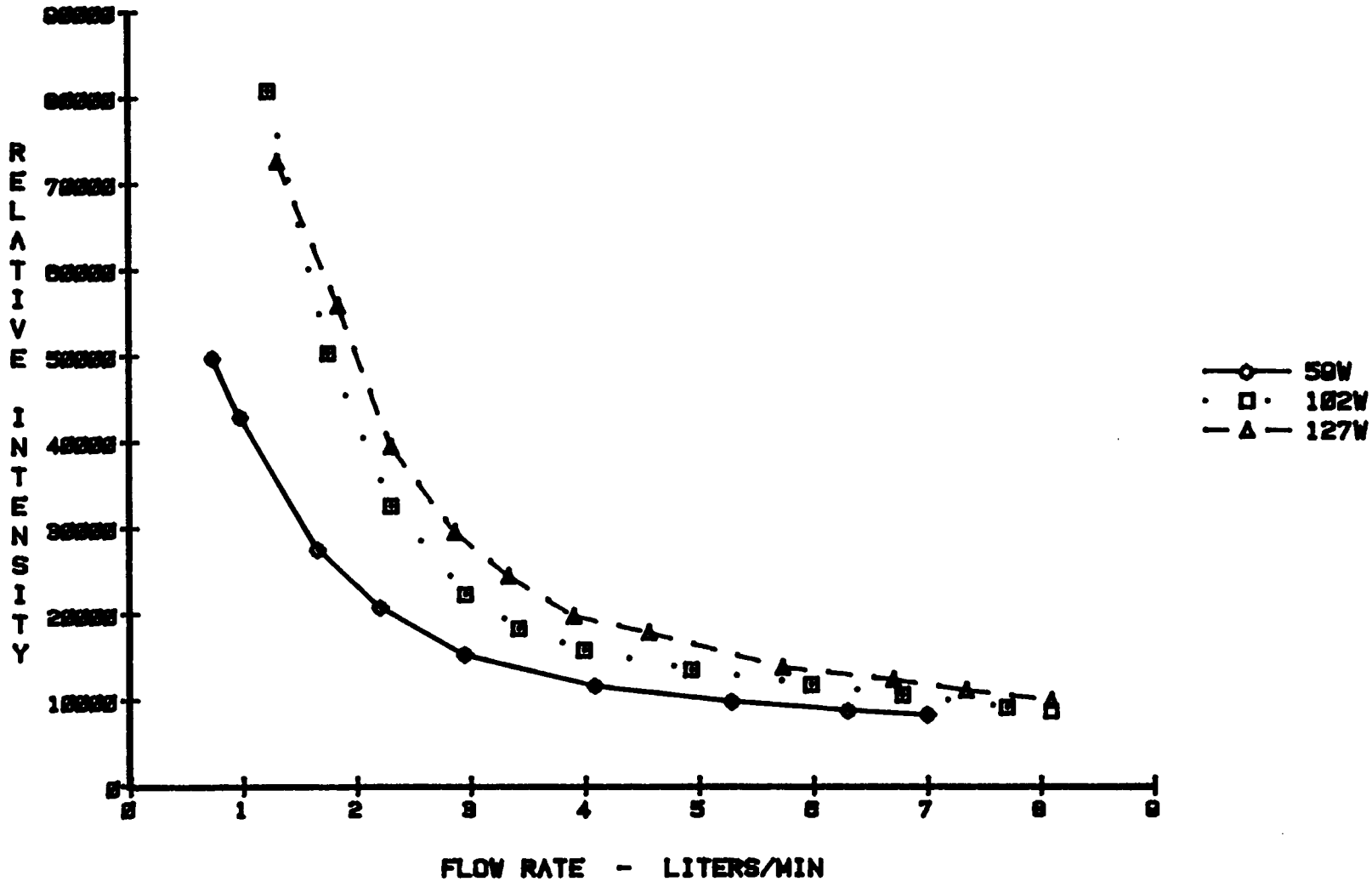

Figure 57. Barium Ion Emission Intensity vs. Flow Rate - Pure Nitrogen Support Gas

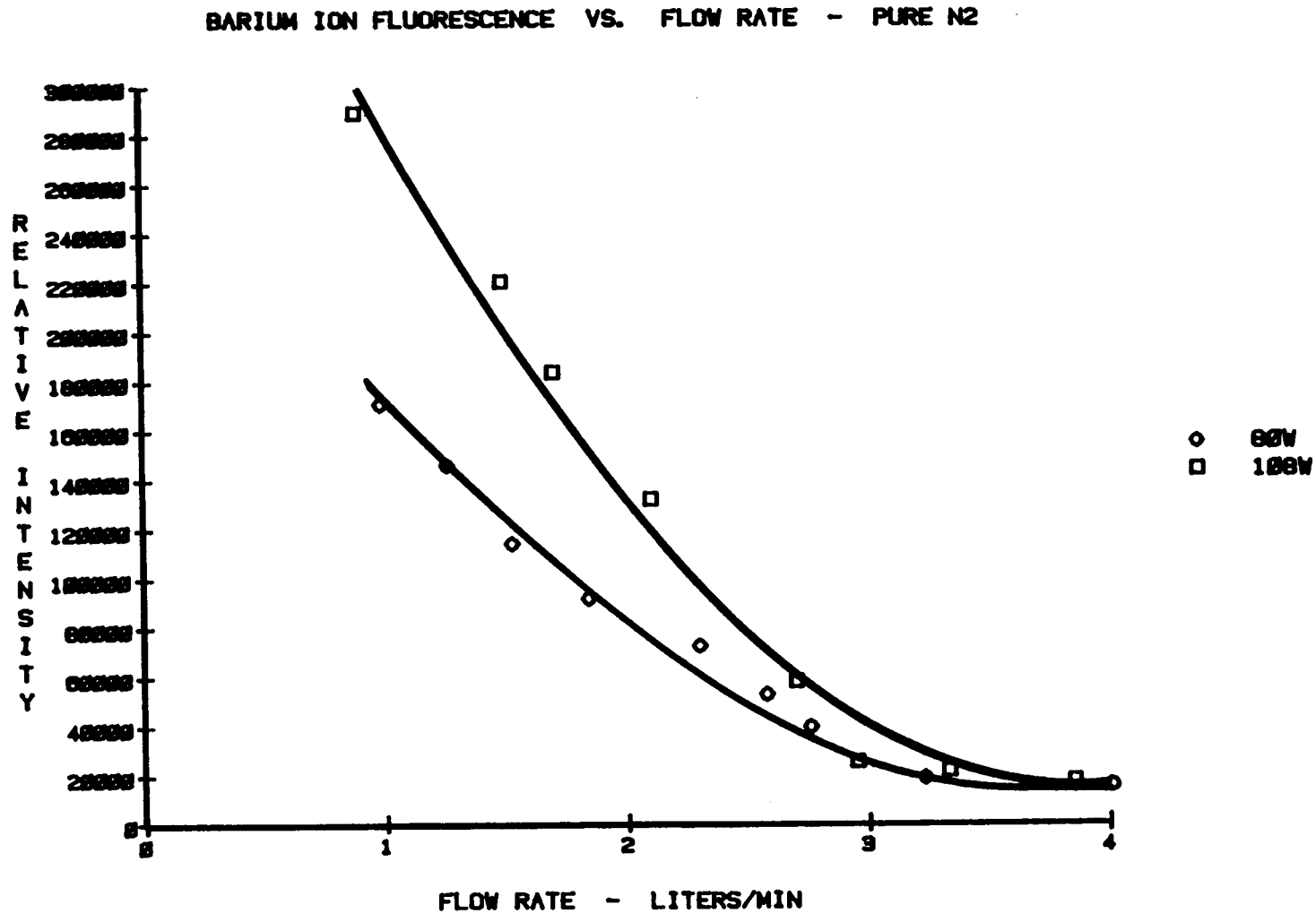

Figure 58. Barium Ion LIF Intensity vs. Flow Rate - Pure Nitrogen Support Gas

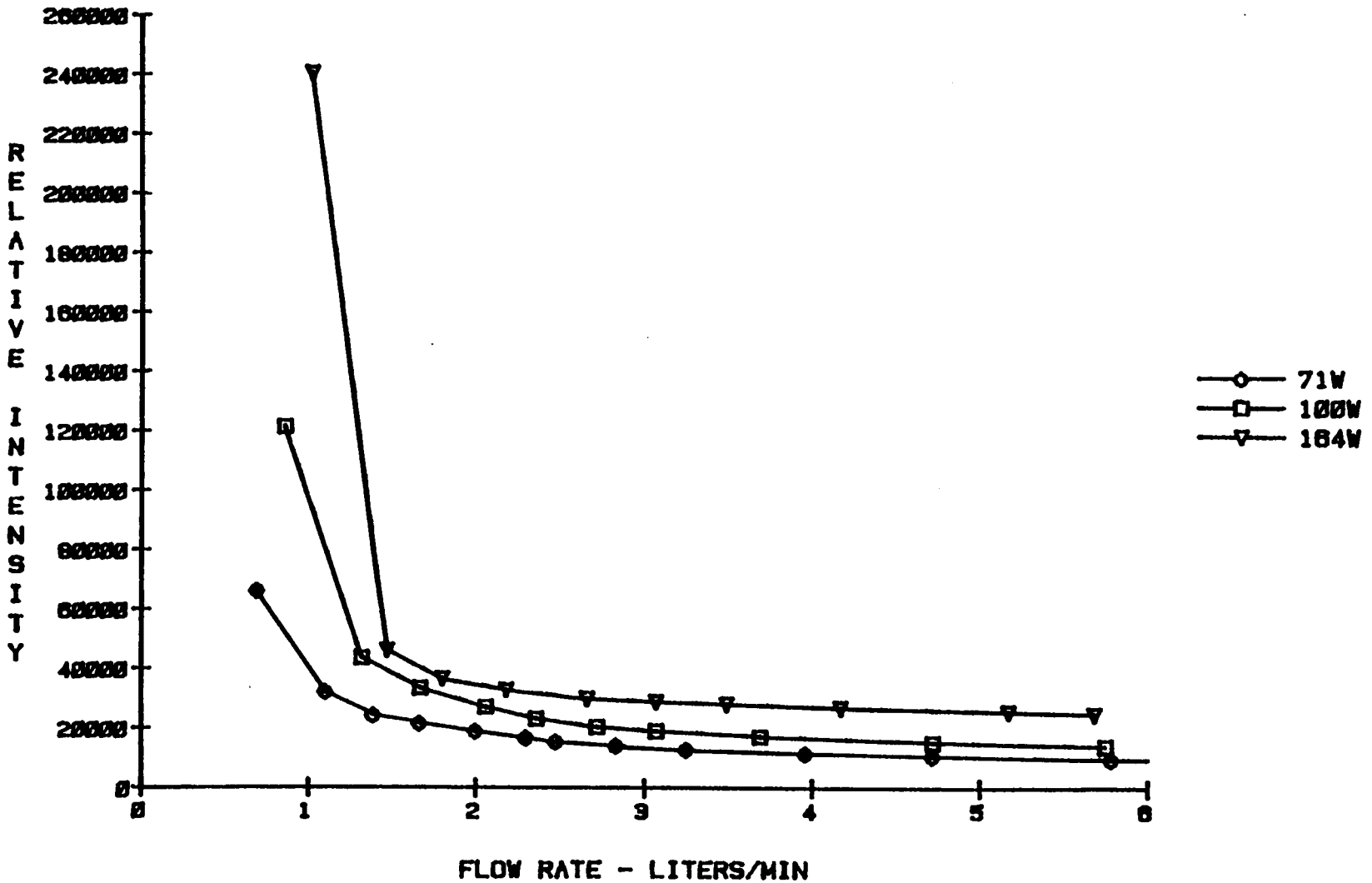

Figure 59. Sodium Atom Emission Intensity vs. Flow Rate - 50% Argon in Nitrogen Support Gas

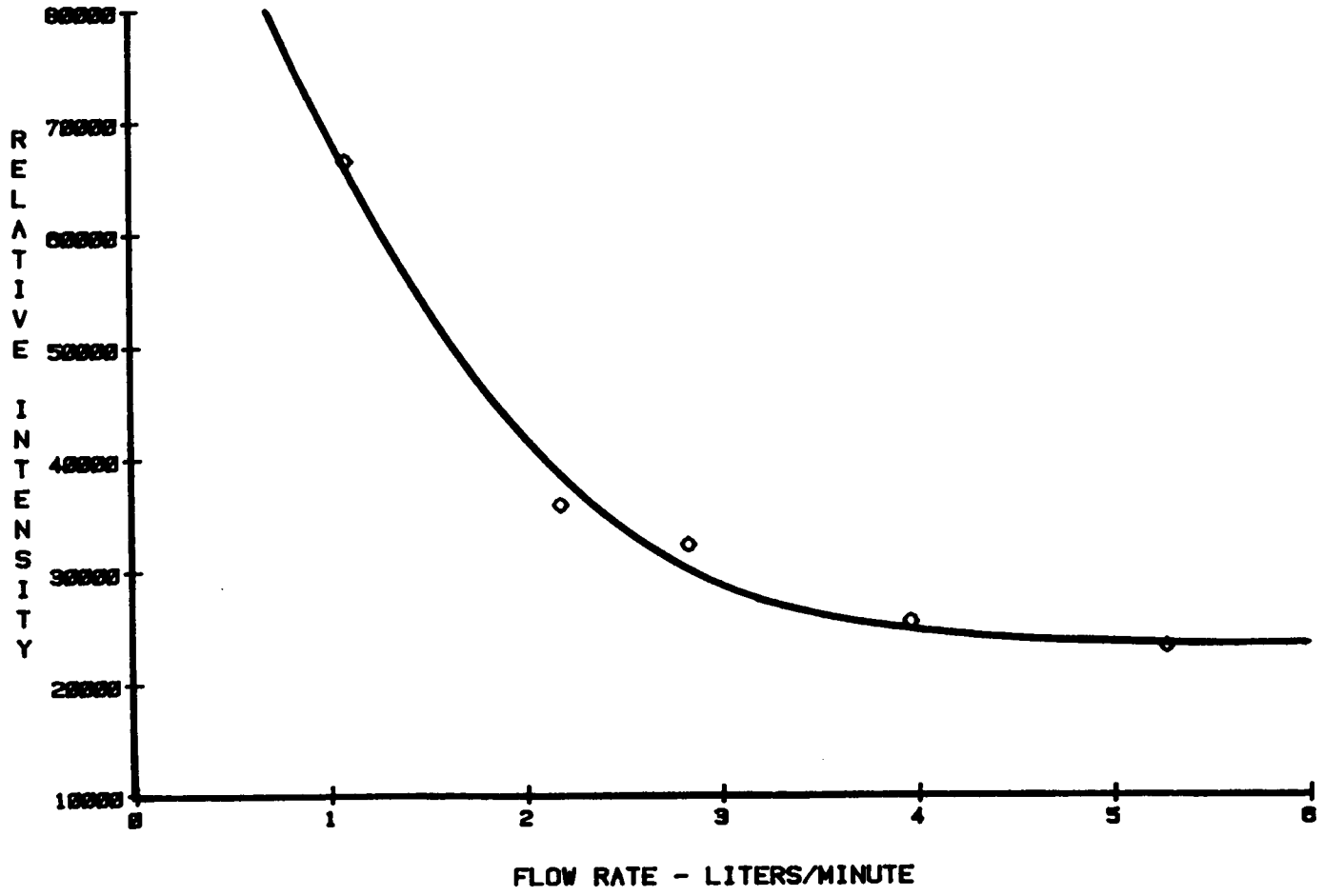

Figure 60. Sodium Atom LIF Intensity vs. Flow Rate - 50% Argon in Nitrogen Support Gas

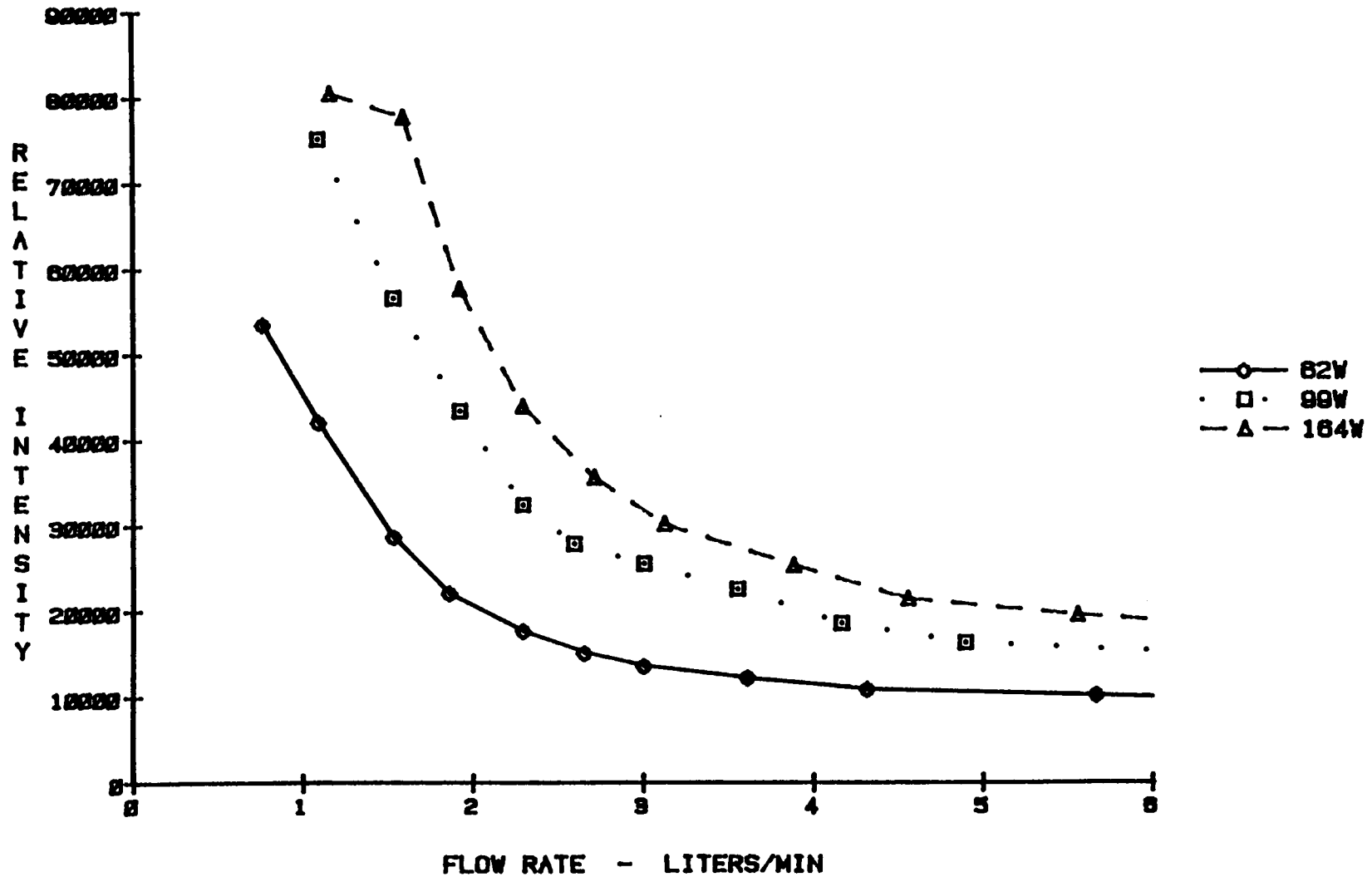

Figure 61. Barium Atom Emission Intensity vs. Flow Rate - 50% Argon in Nitrogen Support Gas

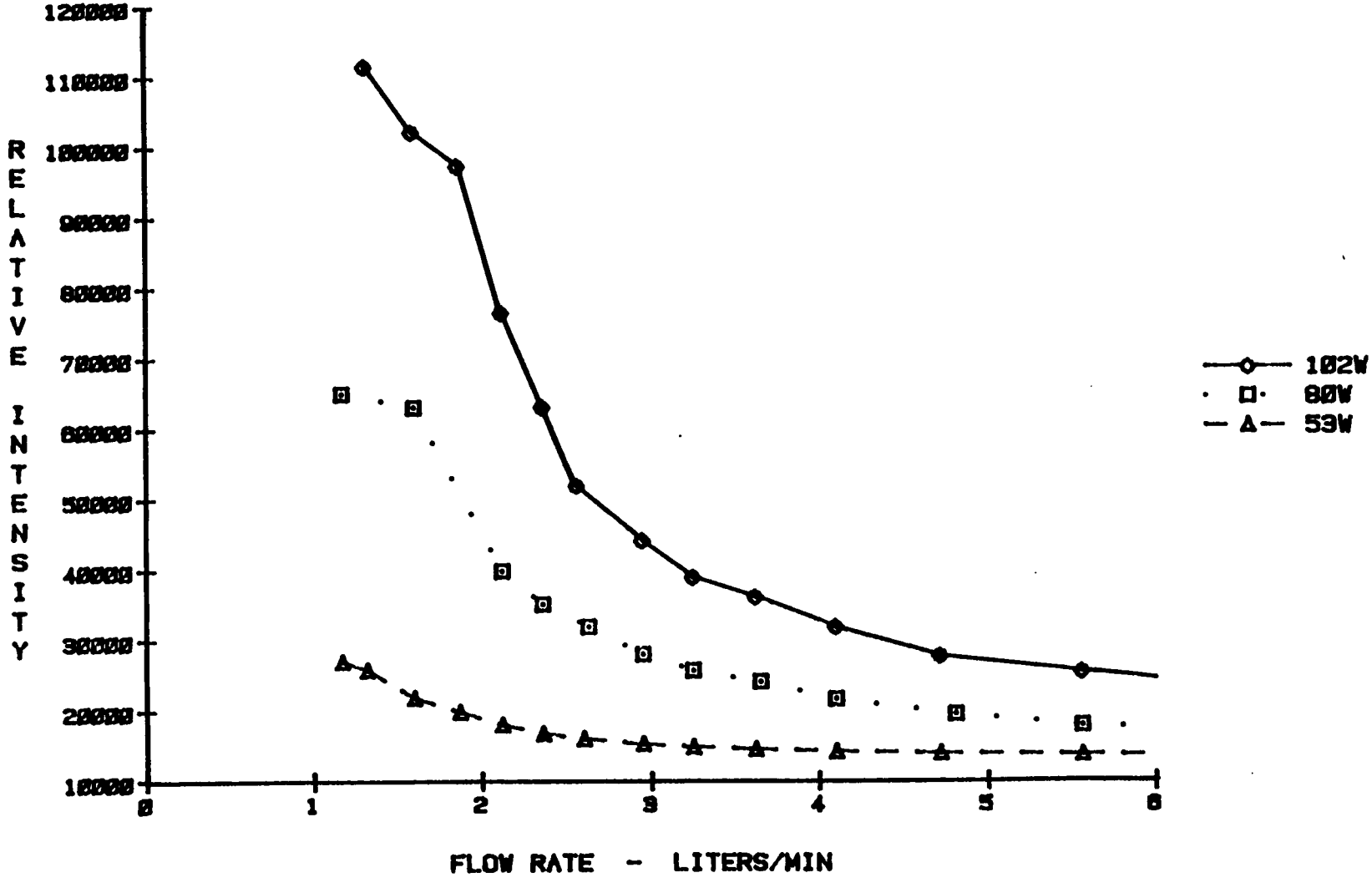

Figure 62. Barium Ion Emission Intensity vs. Flow Rate - 50% Argon in Nitrogen Support Gas

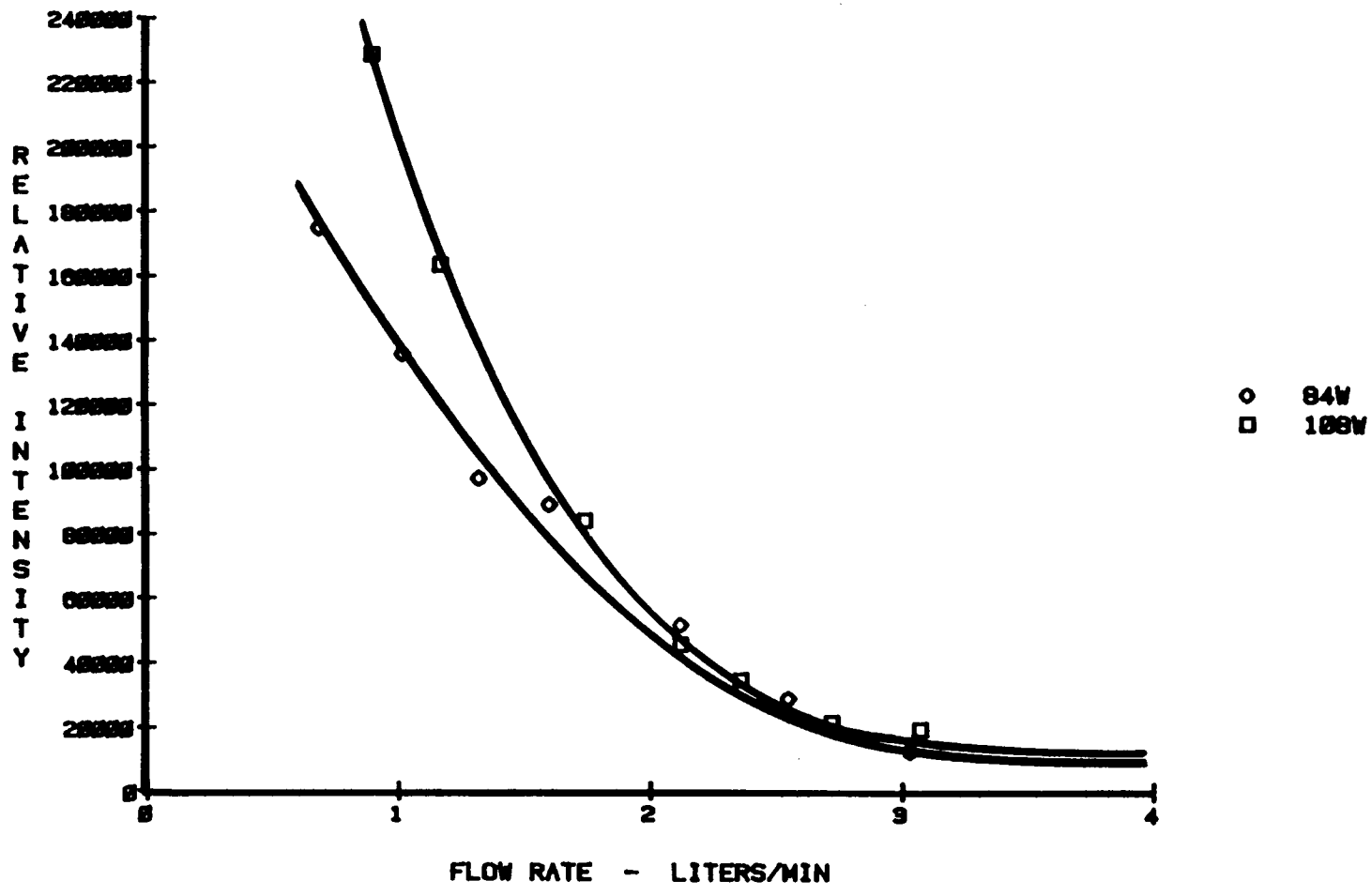

Figure 63. Barium Ion LIF Intensity vs. Flow Rate - 50% Argon in Nitrogen Support Gas

3) PURE ARGON PLASMA:

Pure argon microwave plasmas have tuning and matching properties which are significantly different from nitrogen-containing plasmas. This is primarily due to the very large difference in the conductances of argon and nitrogen-containing plasmas (i.e. atomic and molecular plasmas, respectively). The tuning and matching properties of highly-conductive argon MIPs depend very much on the flow rates and powers employed (58). Changes in flow rate significantly alter the conductance properties of the support gas, hence changes in tuning and matching elements are required. It should be noted that the present study was done using a cavity with a coupling probe optimized for nitrogen-containing plasmas. This was necessary because in a cavity perfectly optimized for argon, as little as 5% nitrogen extinguished the plasma. However, the power absorption characteristics of the Ar plasma were not altered significantly by a change from a straight wire to a circular disc probe. Plasma initiation and stabilization was more difficult with the straight wire probe, particularly until the aerosol flow was started, but once centered and stabilized the argon plasma behaved well. The tuning and matching elements were adjusted to give minimum reflected power before each experimental run and left alone during each run.

The influence of flow rate on fluorescence and emission were studied in the following manner. Starting at the lowest possible flow rate for which a plasma could be maintained without overheating the torch, the flow rate was steadily increased until the signal passed through a maximum. As the flow was further increased, the signal decreased to almost zero because residence times became too short. Reflected power changes with flow rate were considerable, particularly at higher powers, often as much as 12 watts between flow rate extremes.

The support gas flow rate greatly affects the intensities measured in both fluorescence and emission experiments in argon plasmas. An examination of the results in Figure 64 on page 192 through Figure 68 on page 196 show this. There is a optimal flow rate that must be used to obtain maximum intensities, particularly at higher powers. This flow rate corresponds

to optimal tuning and matching conditions, and to that required to maximize production of analyte-exciting species.

But, power transfer and absorption alone do not account for the maxima observed in the argon flow rate studies. The same mechanistic explanation used to account for the trends seen in the nitrogen studies are applicable here. There are optimal flow conditions that maximize production of the energy-containing species responsible for atomization, ionization and excitation of analytes. Sufficient interaction time for subsequent transfer of this energy over to analytes is highly dependent upon the flow rate. Excitation is obviously very sensitive to changes in both power and flow rate.

Comparing Figure 65 on page 193 with Figure 66 on page 194, it is seen that the maxima in the atomic emission curves occur at lower flow rates than the maxima in the atomic fluorescence curves. This is also seen to be true as one compares Figure 67 on page 195 with Figure 68 on page 196. Atomic emission requires more energy from the plasma than atomic fluorescence, hence a lower flow rate (a longer analyte residence time) is needed. However, in the case of a low excitation potential element such as sodium, if the flow rate is decreased too much, the signal will be reduced because of ionization.

In these studies the observation height was chosen that gave the greatest intensity. For the emission studies this was typically as close to the cavity wall as possible, without letting the MIP cavity wall stop any light from entering the collection optics (the so-called "vignetting effect.") For analytes of high excitation energy the region of maximum intensity may actually occur within the confines of the cavity. Figure 67 on page 195 and Figure 68 on page 196 illustrate that as lower flow rates are used the region of analyte emission recedes into the cavity, out of the viewing region of the monochrometer. Ionic spectroscopy requires more energy than atomic spectroscopy, hence a slower flow rate or a higher applied power must be used. It is therefore desireable to use a higher applied microwave power because the analyte emission region will then move outside the cavity, as seen in Figure 66 on page 194.

If excessive power is used the maximum can become very broad, to the point at which no maximum is apparent. At these higher powers, the minimum flow rate possible (without torch overheating) is always above the flow rate at which the analyte emission region begins to recede into the cavity. Saying it another way, at higher powers, the flow rate is never slow enough for the analyte emission region to wholly recede into the cavity. One can see the recession of the plasma plume beginning to happen as power is decreased in Figure 67. This is a primary reason why no strong maxima are ever seen in nitrogen and nitrogen-containing plasmas. Incidentally, the nitrogen plasma plumes are much longer than the argon plasma plumes and never recede into the cavity.

Effects of Water Vapor on the Pure Argon Plasma:

An interesting curiosity regarding the interaction of water vapor and plasma stability was observed in the argon plasma Ba emission experiments. The results are shown in Figure 69 on page 199. For this experiment a constant flow of 1.75 L/min argon flow was passed through the bypass line into the torch. A flow rate of 1.75 L/min was used because this maintained the argon plasma under a "normal" operating condition, even when the nebulizer flow was zero. The nebulizer flow was increased from 0 L/min upward, to the point where the nebulizer stopped working.

The curious fact is seen in the sharp peak in the Ba 455 nm line emission intensity as a function of aerosol flow rate. This effect was not observed with the N_2 or N_2/Ar plasmas! This is not simply an effect due to changes in nebulizer efficiency which, until failure, increases linearly with aerosol output. This seems to be a water-related effect. Unlike the nitrogen plasma, the argon plasma is very sensitive to the addition of water.

The peak can, however, be explained quite simply. At low water vapor flow rates the argon plasma plume barely extends out of the cavity. At intermediate water vapor flow rates (1.92 to 2.23 L/min) the plasma gave bright Ba emission outside of the cavity. At high water vapor flow rates the plasma became unstable and receded back into the cavity.

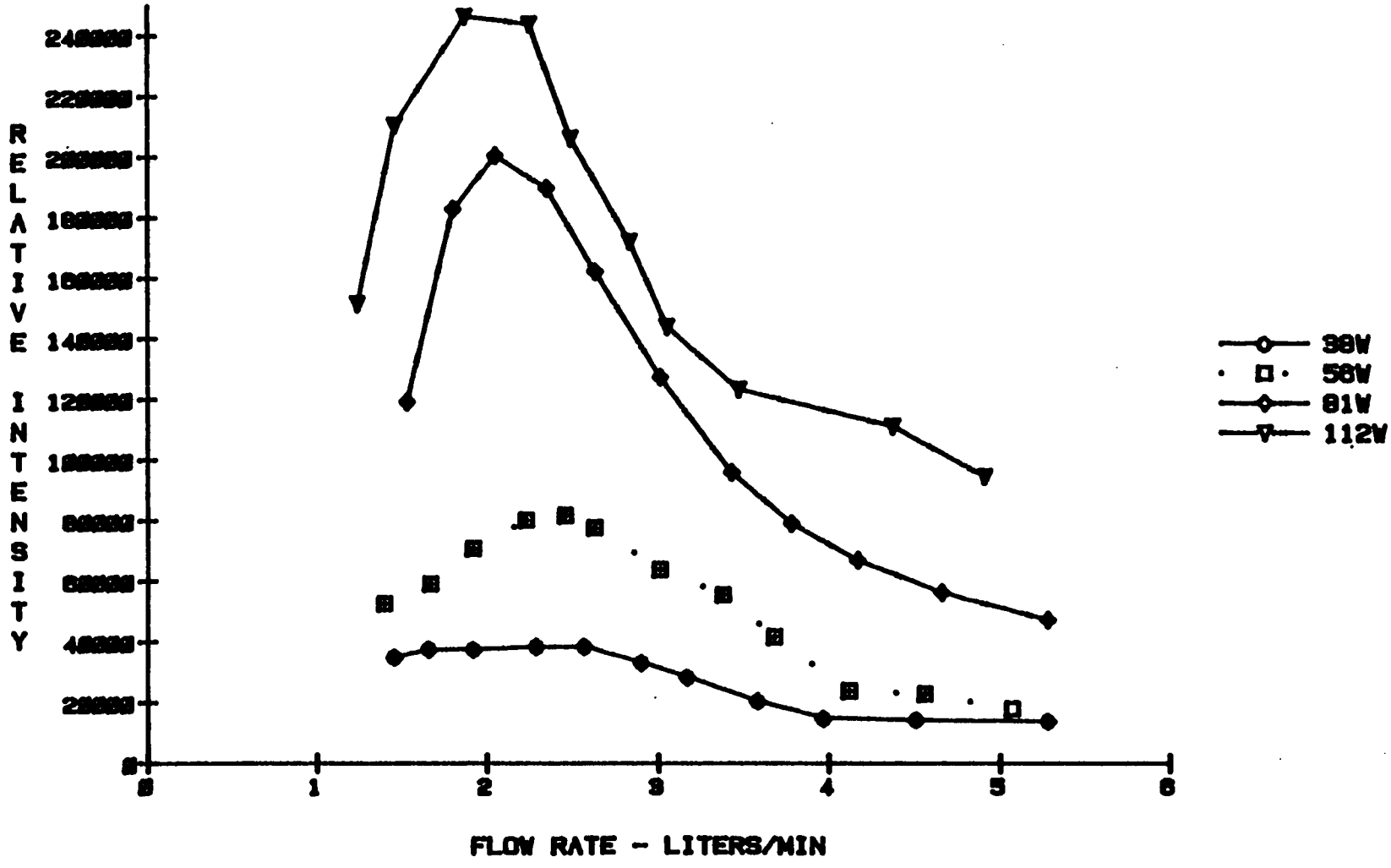

Figure 64. Sodium Atom Emission Intensity vs. Flow Rate - Pure Argon Support Gas

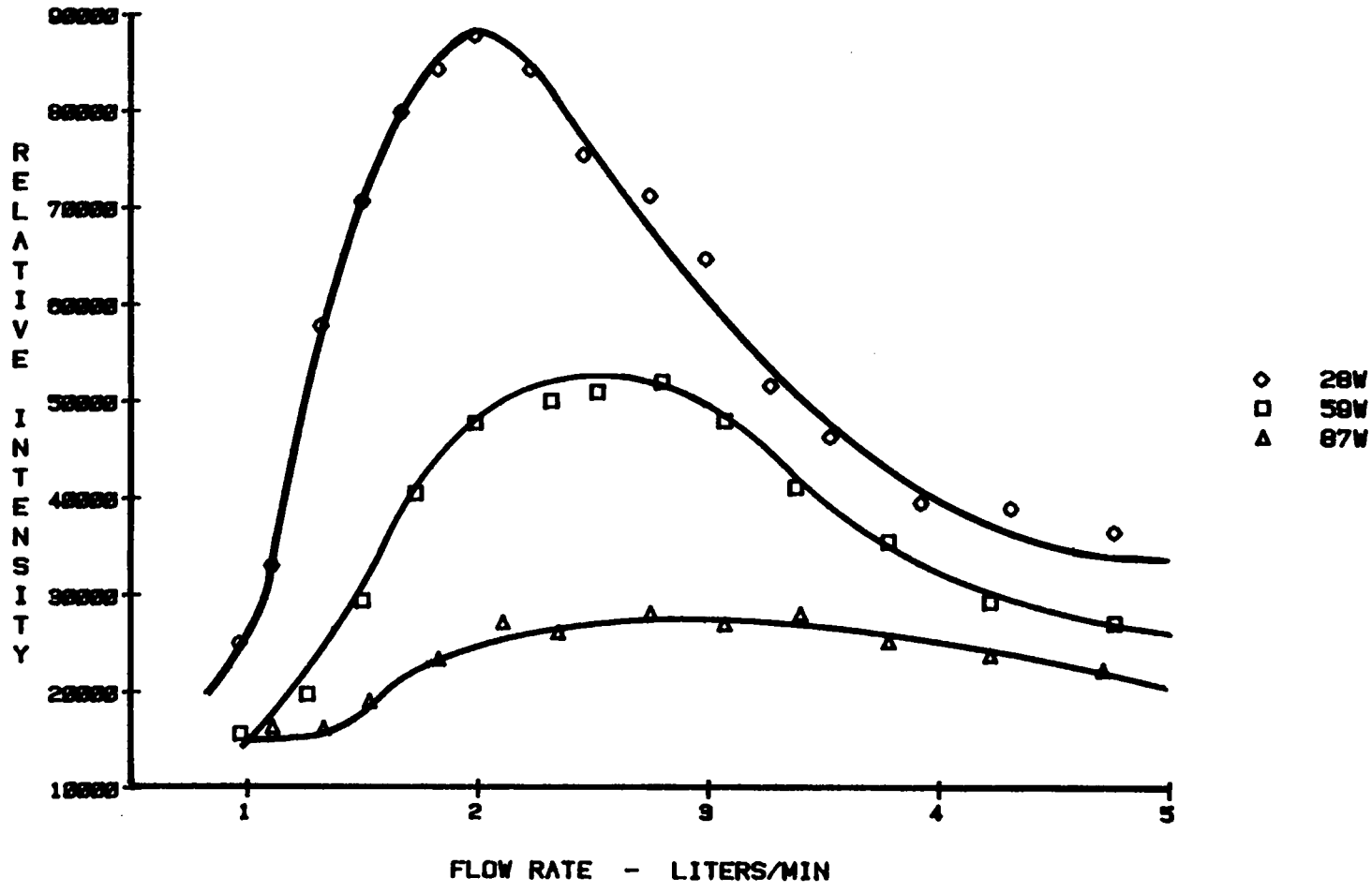

Figure 65. Sodium Atom LIF Intensity vs. Flow Rate - Pure Argon Support Gas

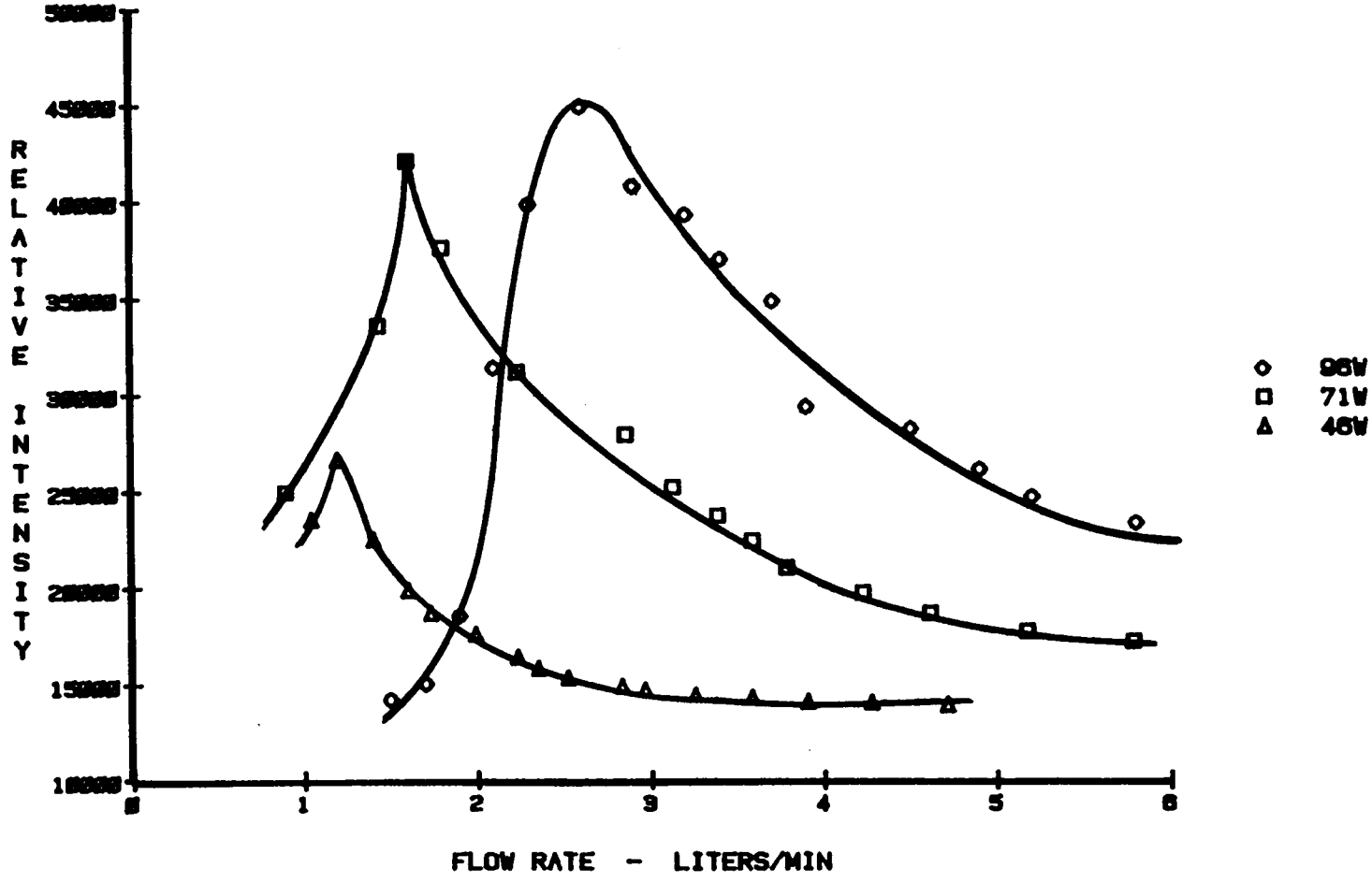

Figure 66. Barium Atom Emission Intensity vs. Flow Rate - Pure Argon Support Gas

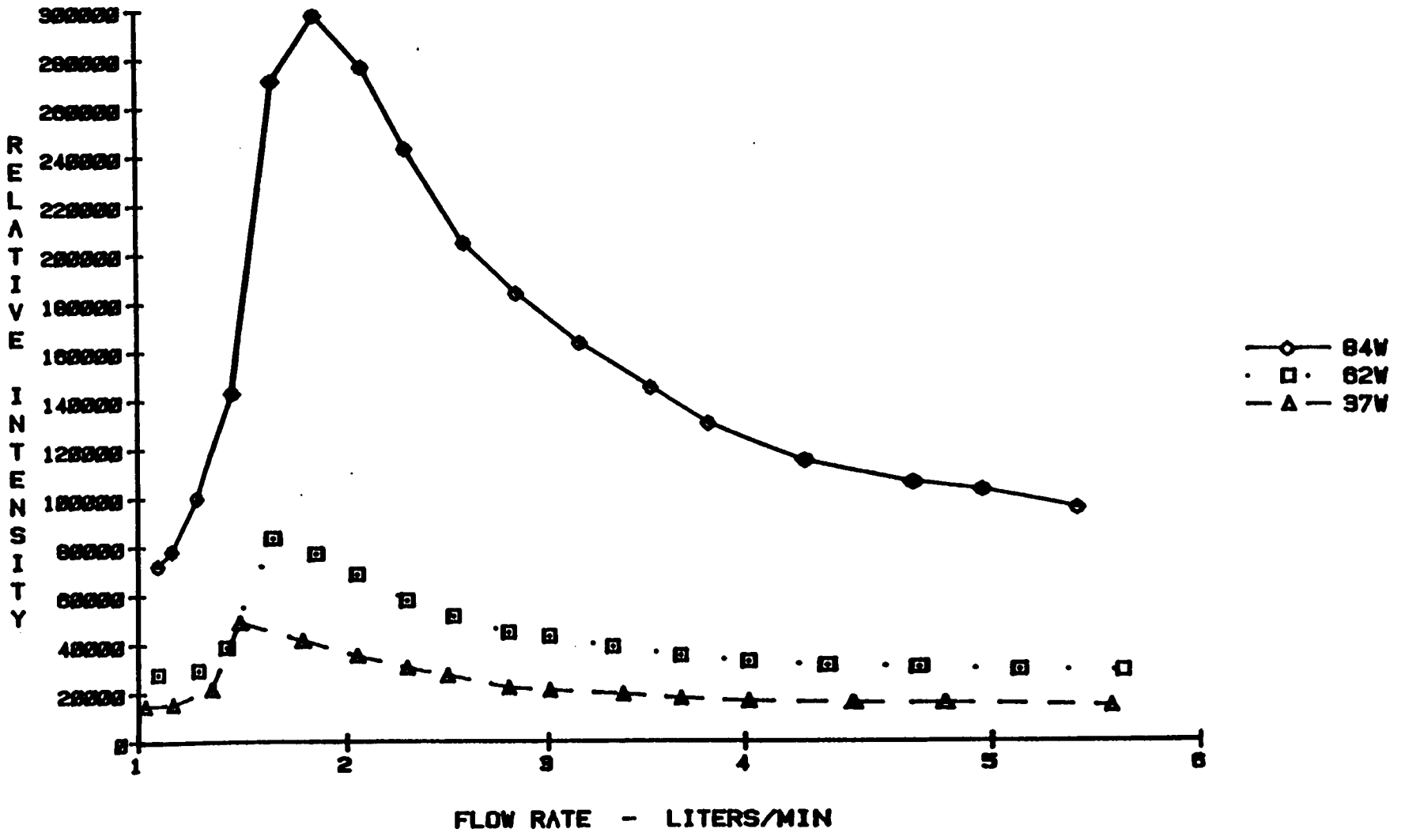

Figure 67. Barium Ion Emission Intensity vs. Flow Rate - Pure Argon Support Gas

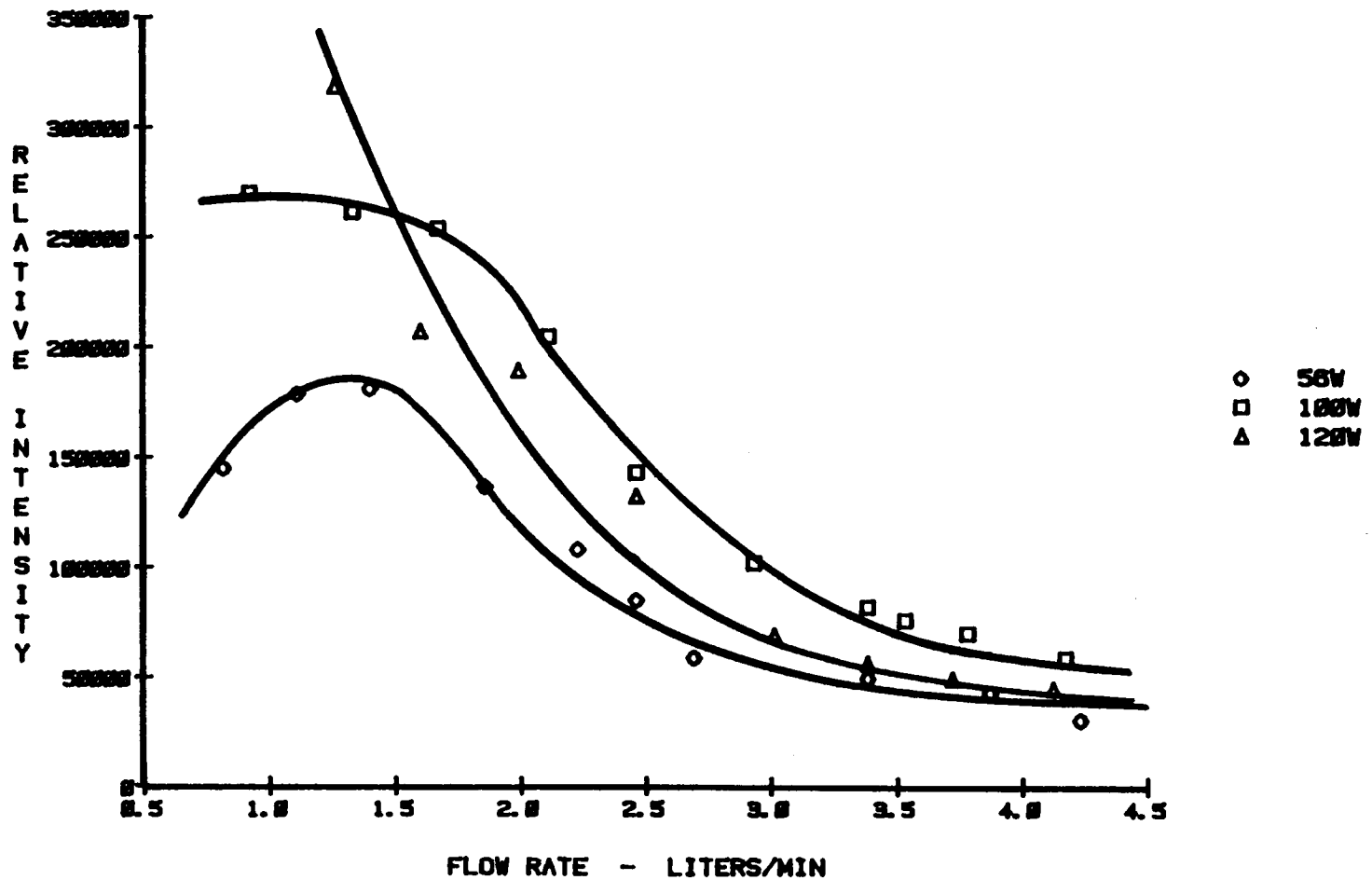

Figure 68. Barium Ion LIF Intensity vs. Flow Rate - Pure Argon Support Gas

It appears that at low water vapor flow rates, the total flow rate through the torch is too low for the plasma plume to extend outside of the cavity. The argon plasma is very cool to the touch, until a significant flow of aerosol is introduced. At intermediate aerosol flow rates the water stabilizes the argon plasma, which allows it to more effectively excite the Ba ion. When sufficient water vapor is added to the plasma, it appears to turn into a molecular plasma. It becomes longer in length, conical in shape, and very hot to the touch. At high water vapor flow rates the signal decreases for two reasons. The water begins to quench the plasma; and the total flow rate through the torch is so fast that the analyte residence time is too short to allow effective excitation. The latter reason is thought to be more important since the nebulizer was designed to allow flow rates up to 5 L/min to be used.

One interesting and important practical detail noted in the argon studies is the difference between the argon plasma structure with and without the analyte aerosol. Without the aerosol the argon plasma was very filament-like. Sometimes it appeared as two filaments on opposite walls of the discharge tube, and at other times as many as three separate filaments were noted. All of these filaments resided entirely within the cavity structure. This made it very difficult to do axial viewing studies with argon, since these filaments wander in the discharge tube. Depending upon the flow rate being used these filaments would circulate, sometimes very rapidly, causing loud acoustical noise in laboratory, which would increase in audio frequency as the circulation frequency increased. As soon as aerosol is added the argon plasma collapses into a stable and centered plasma, very similar in appearance to to the nitrogen plasma. The presence of the water "diffuses" the structure of the argon plasma, eliminating the multiple filaments, centering the remaining filament, making it more manageable for viewing with a spectrometer. Adding water also makes the plasma tail-plume extend farther out of cavity, making axial viewing much easier.

The primary points to note from the experiment with water in the pure argon plasma are that the water vapor actually stabilizes the argon plasma in the TM-010 cavity. And there is an optimal flow of water vapor through the argon plasma which helps to "tune" it. This specific

nebulizer flow rate was used for all the argon plasma experiments. These effects are not observed in the nitrogen plasma.

It can be concluded that the excitation properties of argon plasmas in the high-efficiency cavities depend greatly upon power absorbed by the support gas. The factors that most influence power absorption by the support gas and energy transfer to the analytes are flow rate and the amount of water introduced into the plasma.

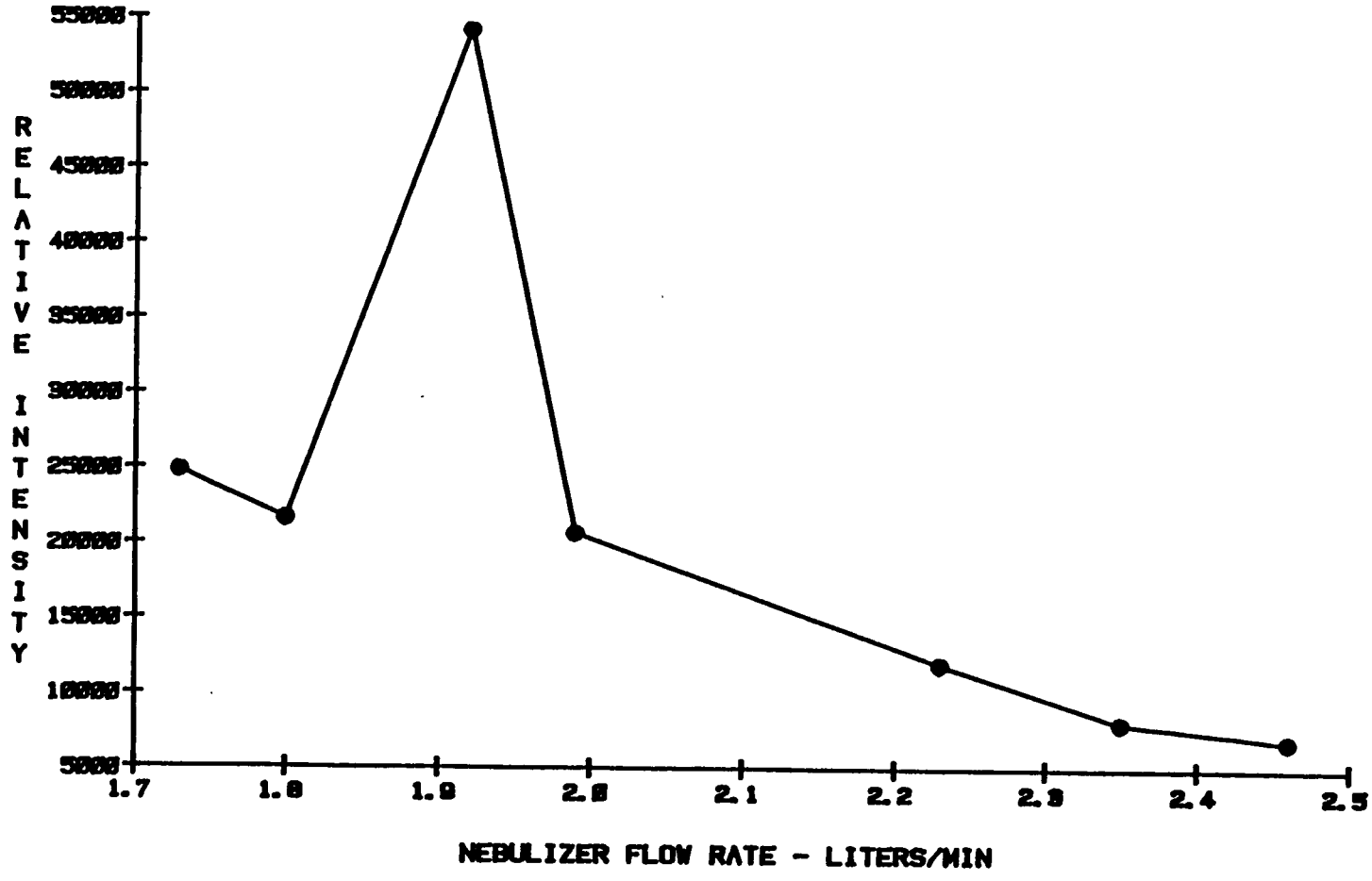

Figure 69. Barium Ion Emission Intensity vs. Nebulizer Flow Rate - Pure Argon Support Gas at 46 Watts

Observation Height Profiles at Various Powers

Plasma tail-plume length and temperatures change considerably with alterations in applied power, gas composition, and flow rate. Spatial profiling was done to characterize the useful analyte signal regions.

Intensity profiles were done as a function of the distance above the support gas exit wall of the cavity, termed the "observation height". The plasma was found to be perfectly radially symmetric. In both emission and fluorescence modes the plasma appears as a stable, centered plasma bolus existing within the cavity structure, with a symmetrical cone extending some distance beyond the exit wall. The normal condition of operation was the use of this non-circulating plasma plume. Radial profiles were deemed unnecessary. These were done by looking down the plasma axis, scanning horizontally across the width of the plasma, and measuring the variation of the analyte signal intensity. Other investigators of similar plasmas have found analyte emission from modified Beenakker-type cavities to be symmetrical across the radial face of the plasma (53). Radial, or "side-on" viewing of the plasma has the advantage that plasma or analyte self-absorption does not occur, as it can with axial viewing.

The microwave cavity was mounted so as to give the plasma plume a horizontal orientation. The monochrometer had vertical slits. This arrangement precluded the problem of longitudinal integration over the plasma plume, caused by having the slits accept light from the full length of the plasma plume. The monochrometer was mounted on a translation stage that had 1/64th of an inch (0.4 MM) resolution. This horizontal plume/vertical slit configuration gave a minimum spatial resolution of 0.4 MM. The "zero" for the observation height profiles was chosen by moving the translation stage far enough back so that all light was blocked from entering the 30 MM diameter lens used to collect light from the plasma. In this position, light from the plasma was completely obscured by the cavity. See Figure 31 on page 130 for a better understanding of the geometry.

1) SODIUM FLUORESCENCE in N2, N2/AR, and AR at VARIOUS MIP POWERS:

The results for the observation height profiles are easy to interpret. The sodium laser-induced fluorescence profiles show that as the MIP power is increased, the intensity maxima **decrease**, as was observed in the LIF/MIP power studies (See Figure 70 on page 202 through Figure 71 on page 204) The intensity maxima also shift farther away from the cavity. This is to be expected considering that the plasma energy increases when power is increased. Near the cavity wall the plasma energy is too great to allow a significant population of ground-state sodium atoms to exist. They are either excited or ionized at the lower postions in the tailflame.

The maxima in the pure Ar plasma occurs at a lower observation height than in the 50% Ar/N_2 plasma, which in turn occurs at a lower observation height than in the pure N_2 plasma. This is logical since the order of the thermal energies of these plasmas is: pure N_2 > 50% Ar/N_2 > pure Ar.

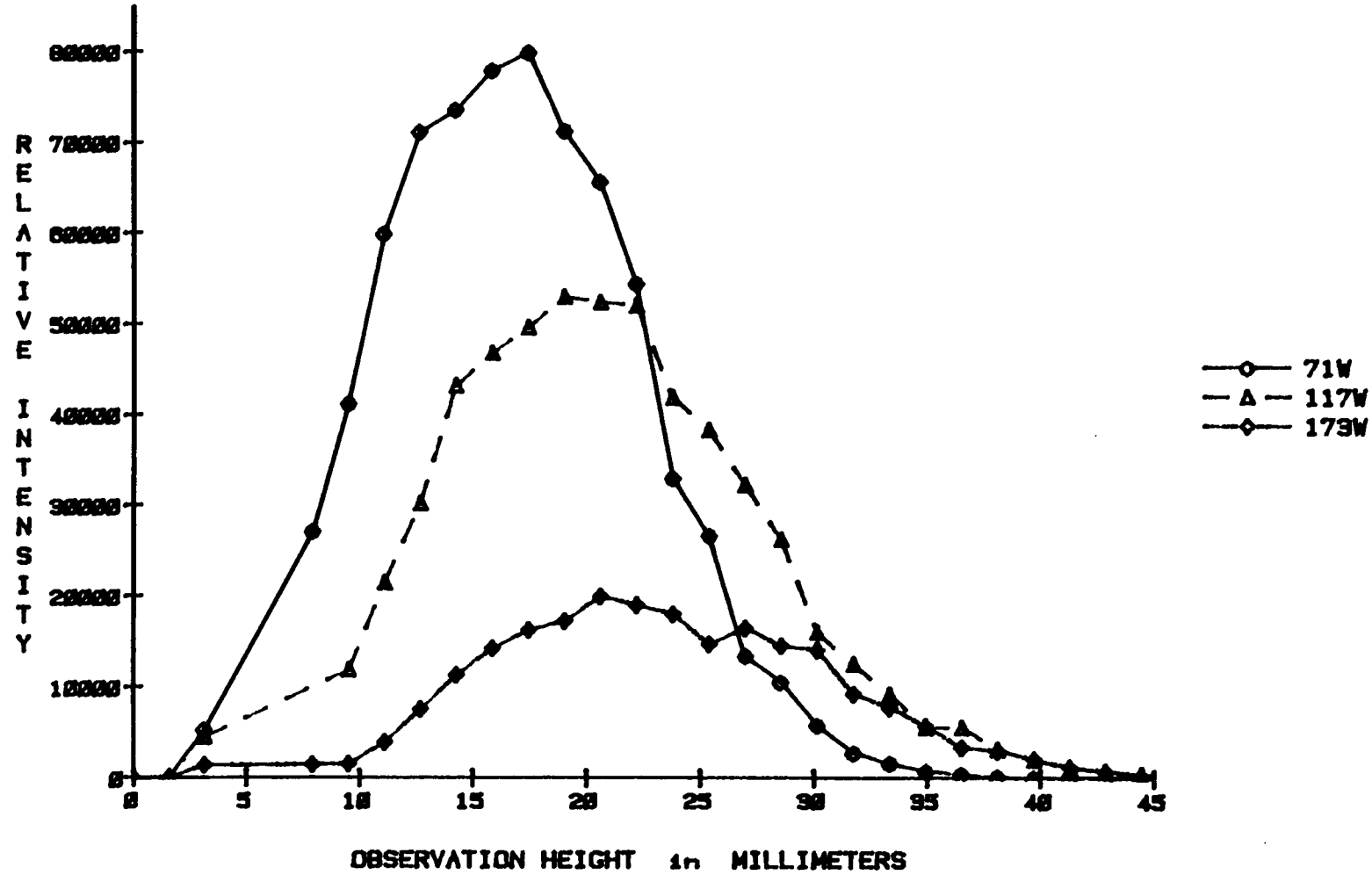

Figure 70. Sodium LIF Intensity vs. Observation Height - Pure Nitrogen Support Gas

Figure 71. Na Atom Fluorescence Intensity vs. Observation Height in Pure Ar

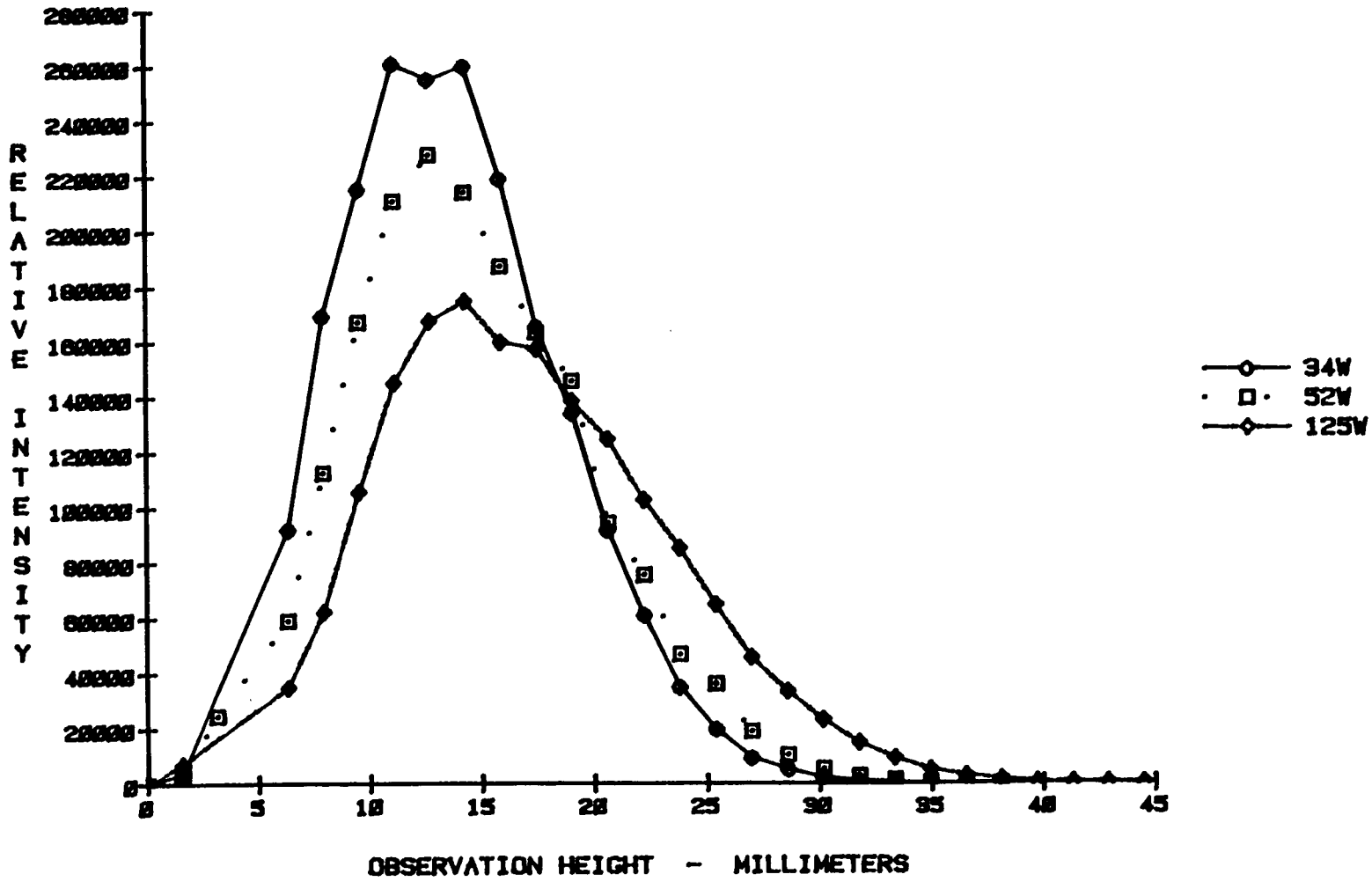
RELATIVE INTENSITY
0
5
10
15
20
25
30
35
40
45
OBSERVATION HEIGHT - MILLIMETERS
34W
52W
125W

2) SODIUM EMISSION IN N2, N2/AR, and AR at VARIOUS MIP POWERS:

The order of thermal energies stated above also explains the trends found in the sodium emission observation height profiles, (See Figure 70 on page 202 through Figure 71 on page 204). The full width at half maximum (abbreviated "FWHM") is greatest for the pure N_2 plasma, followed closely behind by the 50% Ar/N_2 plasma. In the pure argon plasma sodium emission extends a significantly shorter distance from the cavity. Emission intensities increase in magnitude in all plasmas as MIP power is increased. Also, the length of the plasma plume and the analyte emission region extend farther beyond the cavity wall. This is shown by the FWHM increase as power is increased.

The maximum always occurs at the same height, within experimental error. This is because the emission is a maximum right at the cavity wall, and is probably even more intense farther into the discharge region. Radial viewing of analyte signals has one disadvantage: elements requiring high excitation energies present their most intense signals within the discharge region, out of easy viewing range of a radially-placed spectrometer. It is possible to cut a hole in the side of the cavity to allow viewing of the discharge region from a "side-on" vantage point. Indeed, this was done by previous investigators, who found that copper emission in the Ar MIP was most intense when monitored in the interior of the cavity (26).

For the present studies a hole was not cut in the cavity for several reasons. First, the elements selected to characterize the cavity exhibit very strong LIF and AES signals outside of the cavity. Second, the possibility of microwave radiation leakage is increased, since the hole size required for radial viewing of the primary discharge is fairly large. Lastly, in theory, the total number of holes cut in the inside wall and the number of irregularities on the inside wall should be kept to a minimum since this is the surface which conducts current. Eventually the cavity efficiency will begin to drop.

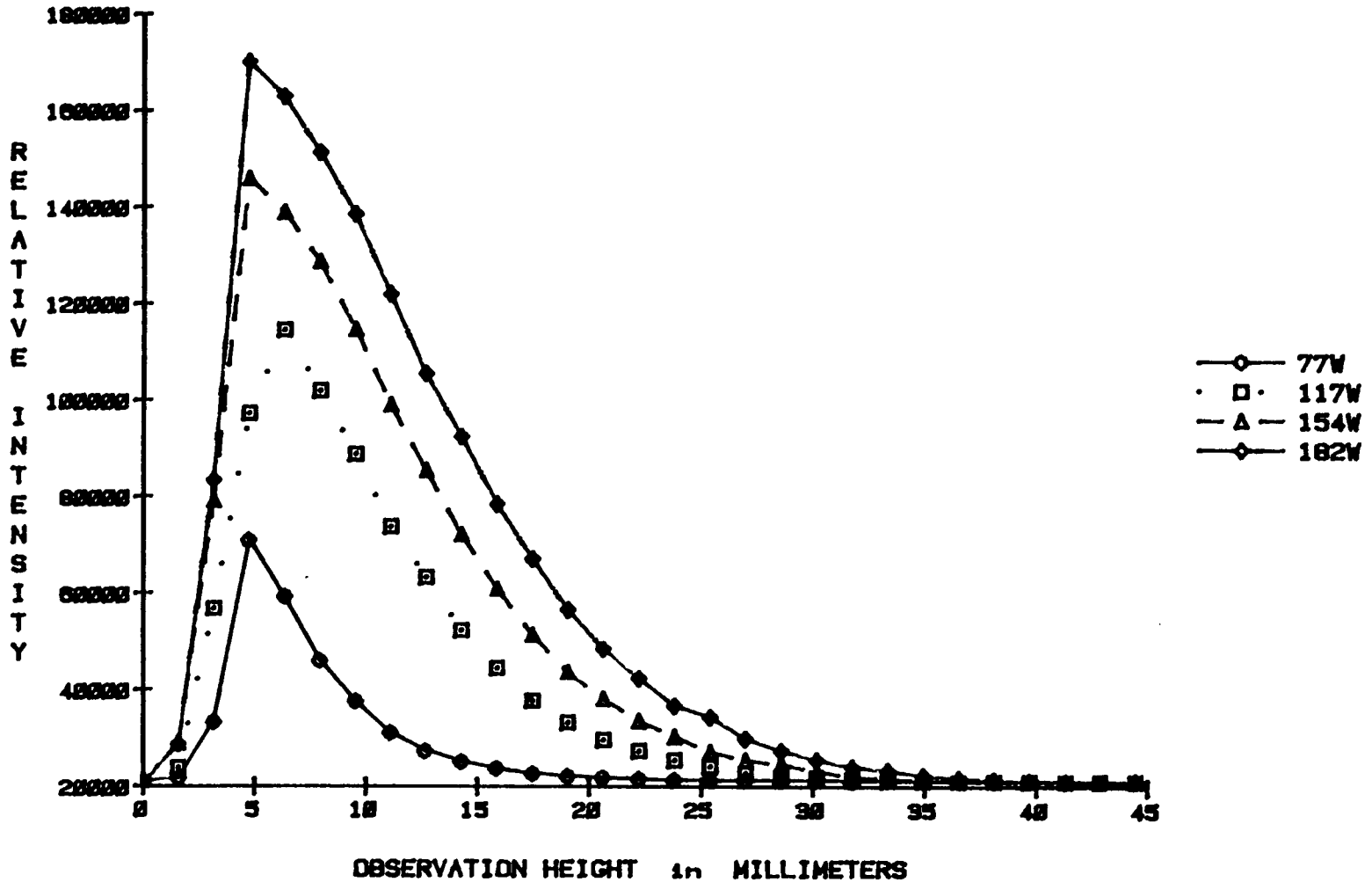

Figure 72. Sodium Emission Intensity vs. Observation Height - Pure Nitrogen Support Gas

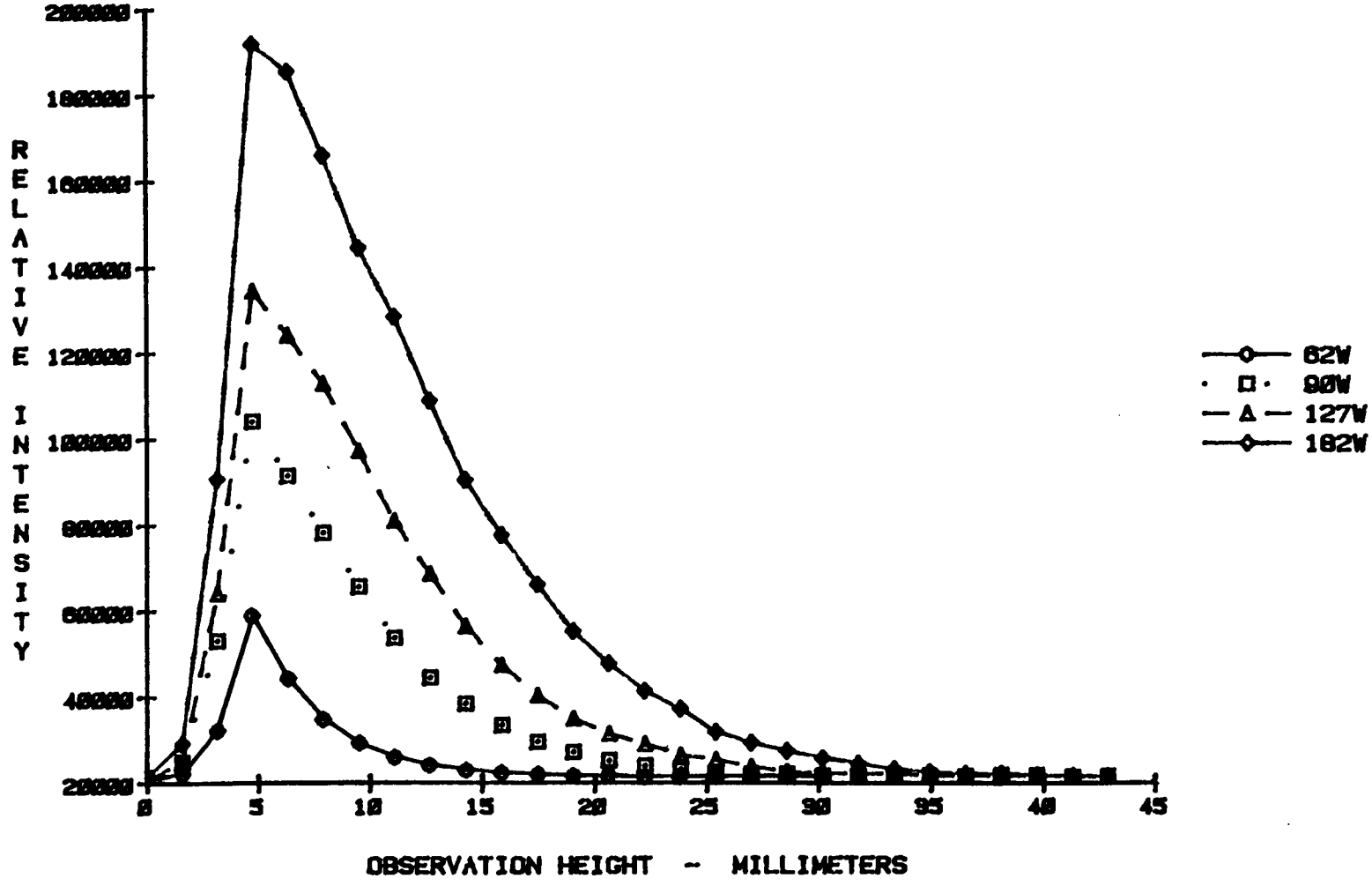

Figure 73. Sodium Emission Intensity vs. Observation Height - 50% Argon in Nitrogen Support Gas

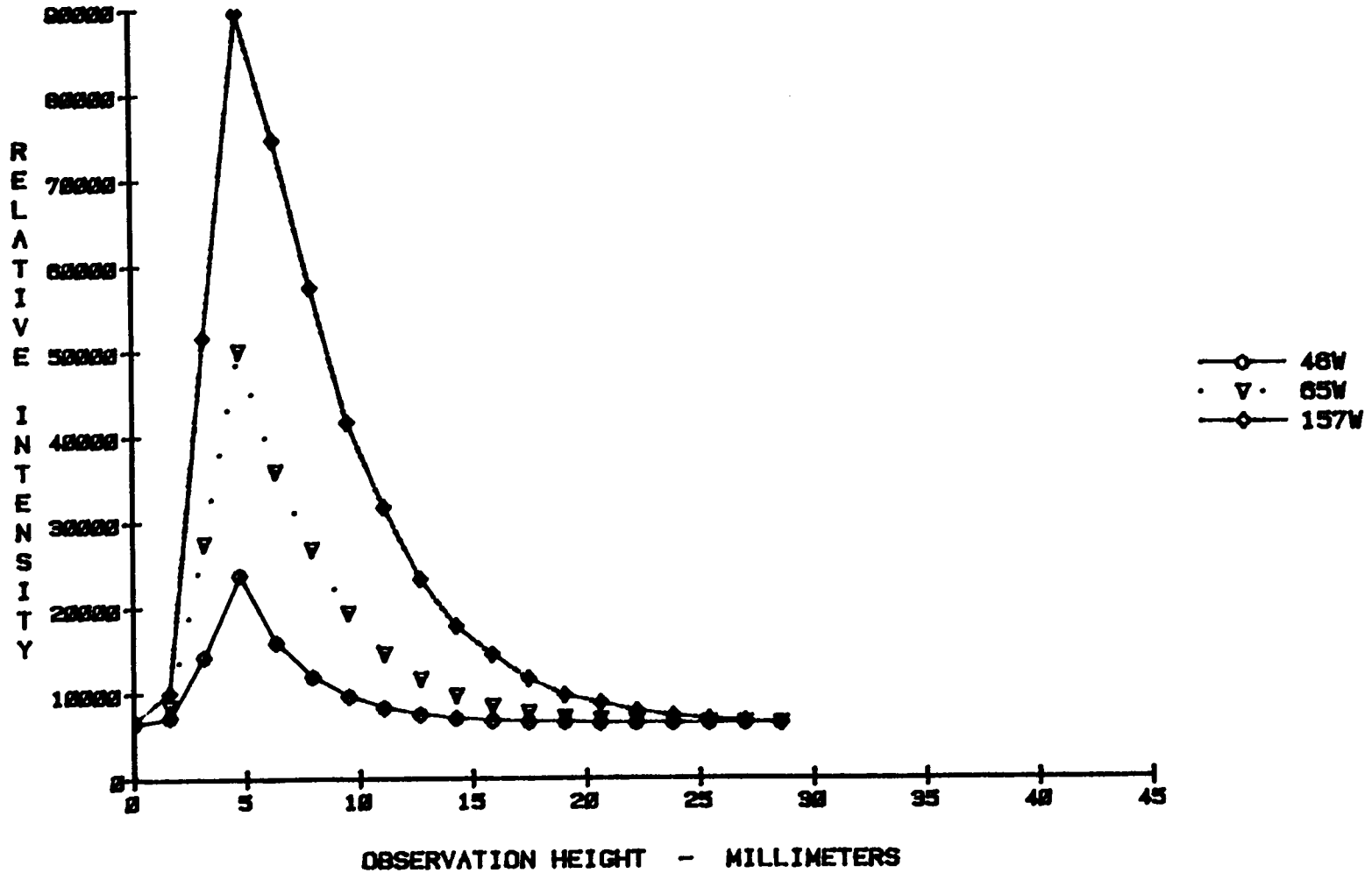

Figure 74. Sodium Emission Intensity vs. Observation Height - Pure Argon Support Gas

3) BARIUM FLUORESCENCE in N2, N2/AR, and AR at VARIOUS MIP POWERS:

The barium fluorescence experiments were somewhat more difficult than the sodium fluorescence experiments because of laser wavelength drift. The dye laser would not stay on wavelength for more than about 10 minutes. The Ba linewidths are narrower than Na linewidths. This is because the barium transitions are broad excited state ionic transitions, while the sodium transitions are sharp ground state atomic transitions. Frequency drift was therefore not as much of a problem with sodium. About ten minutes of stable operation on a Ba line was possible. Then the laser had to be reset to give maximum fluorescence intensity before the next scan. All members in these data sets required normalization, followed by scaling using appropriate factors obtained from the fluorescence intensity vs. microwave power curves discussed earlier.

There are several things to notice in the Ba fluorescence studies. First, the Ba fluorescence region is much shorter in height. It appears much closer to the cavity than sodium fluorescence, particularly at lower powers. This is because Ba ionic fluorescence requires much higher temperatures than atomic fluorescence. Finally, the FWHM follow the trends found in all the previously discussed fluorescence and emission studies.

Argon is such a thermally cool plasma (compared with the nitrogen-containing plasmas) that the Ba ionic fluorescence region does not extend very far outside of the cavity. Comparing the shapes of the fluorescence curves for the various gases demonstrates this point. The order of thermal energies discussed earlier in this chapter, (pure N2 > 50% Ar in N_2 > pure Ar), explains all of the trends.

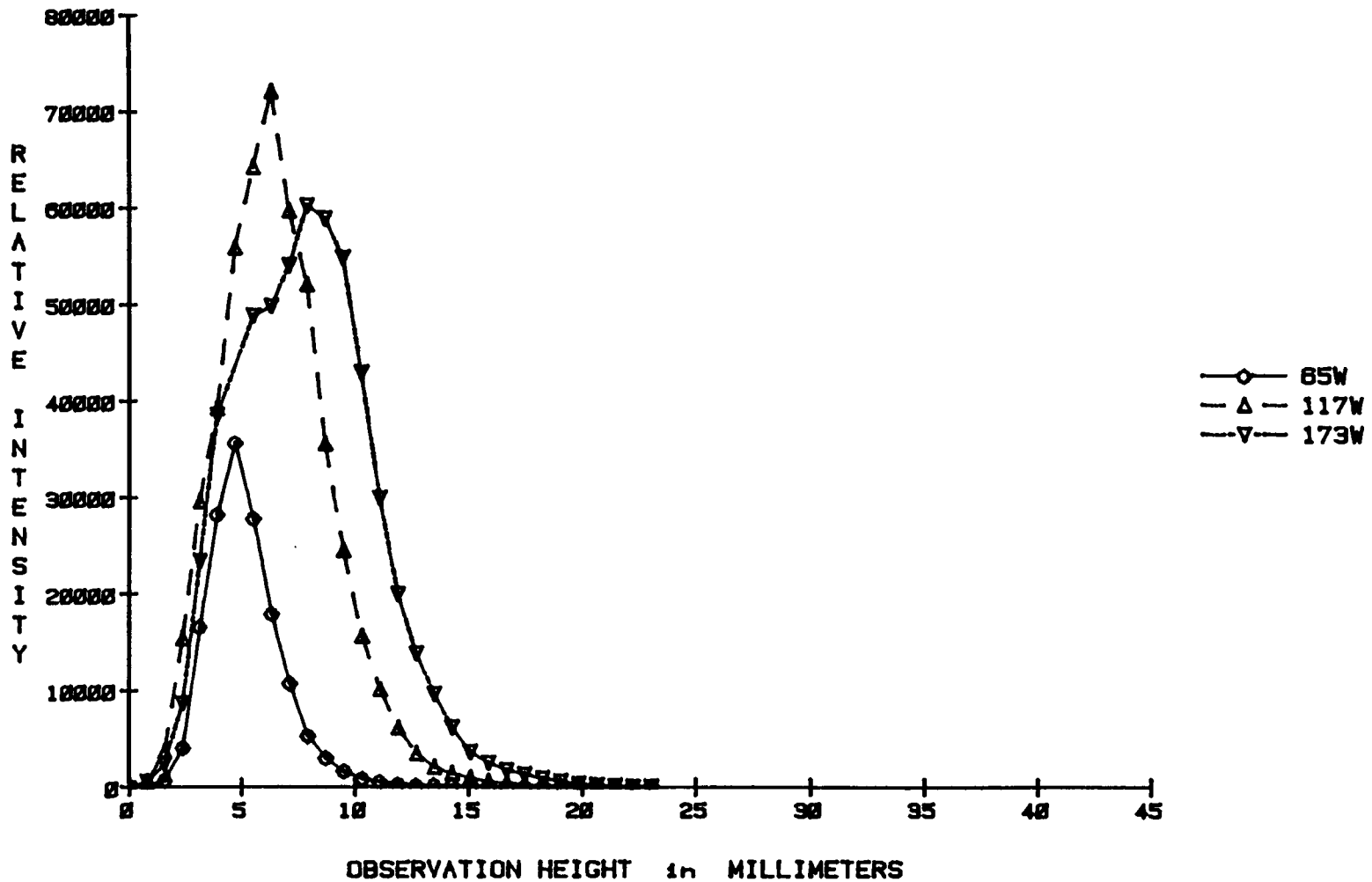

Figure 75. Barium Ion LIF Intensity vs. Observation Height - Pure Nitrogen Support Gas

Figure 76. Ba Ion Fluorescence Intensity vs. Observation Height in Pure Ar

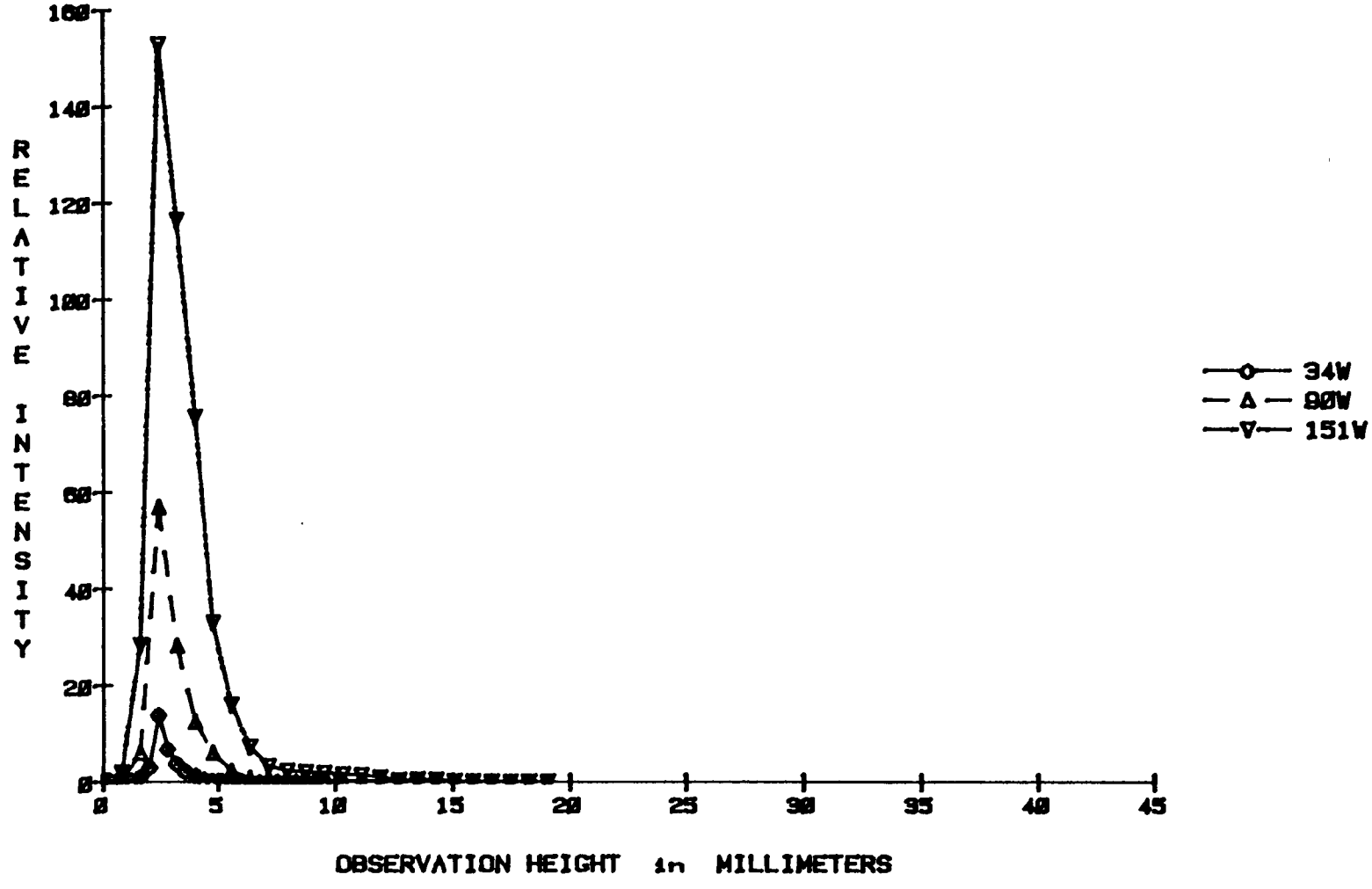
RELATIVE INTENSITY
160
140
120
100
80
60
40
20
0
0
5
10
15
20
25
30
35
40
45
OBSERVATION HEIGHT in MILLIMETERS
34W
90W
151W

4) BARIUM EMISSION IN N2, N2/AR, AND AR AT VARIOUS MIP POWERS:

Both the barium atomic and ionic emission observation height profiles follow the trends outlined previously for Ba fluorescence and Na emission - both height and width of the profiles increase as MIP power increase. The Ba atom has a higher excitation energy, (2.24 eV), than the Na atom, (2.10 eV), hence a narrower FWHM results for the Ba atom. The Ba ion has a higher excitation energy, (2.73 eV), than the Ba atom, hence an even narrower FWHM is found for the Ba ion. The FWHM for the Ba ion is not markedly narrower than that for the Ba atom, as might be expected based on the higher excitation energy of the Ba ion, and the extra energy needed for the ionization of the Ba atom (5.21 eV).

The results clearly show that the ionization/excitation process occurs in two steps, since the Ba ion emission intensity slightly exceeds that of the Ba atom. If it were a single-step process (5.7 eV) the Ba ion would be expected to have a much lower emission intensity. Several factors are responsible. First, the oscillator strength for the ionic transition is greater than for the atomic transition, (A = 1.15 E-8 for the atom, A = 1.17 E-8 for the ion). Second, the multiplicities are greater for the ion than for the atom, (g-lower = 2, g-upper = 4 for the ion; g-lower = 1, g-upper = 3 for the atom). The barium 455 nm transition also has 4 separate excitation pathways to reach its upper state (493nm, 455nm, 585nm, 614nm), all of which can result in 455 nm emission. See Figure 45 on page 160. Thus, the Ba ion 455nm emission line is much more intense than the Ba atom 553nm line.

Observation Height Studies - Conclusions:

The observation height profiles support a thermal mechanism of excitation. State populations decrease in the following manner, atomic ground states < excited atomic states < ionic ground states < ionic excited states. This is also the order of energies for the respective excitation processes. FWHM consistently decrease as excitation potentials increase. **Analytes in the tail flame exhibit intensities and FWHM's consistent with their excitation potentials and a Boltzmann distribution of plasma species.**

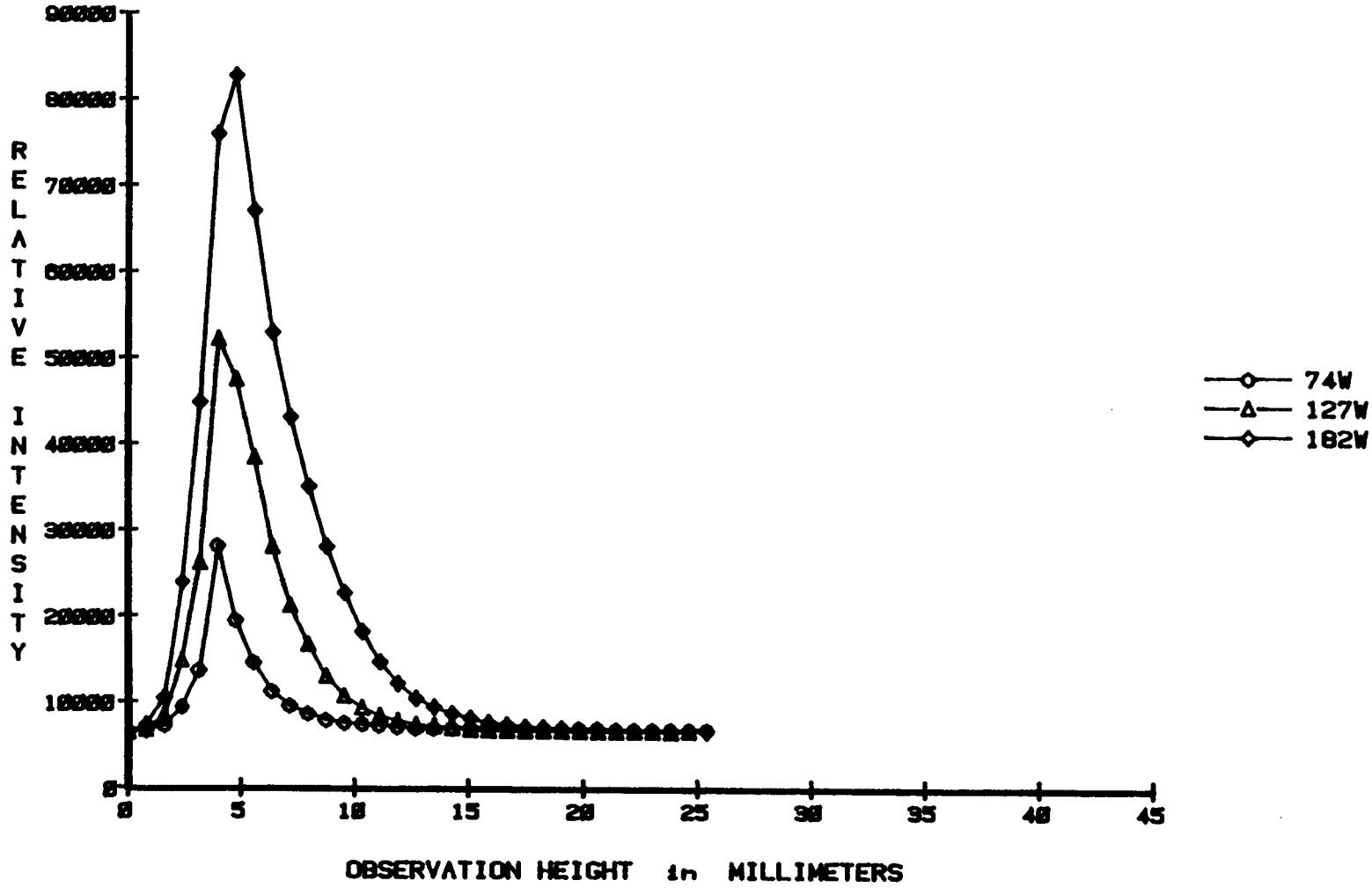

Figure 77. Barium Atom Emission Intensity vs. Observation Height - Pure Nitrogen Support Gas

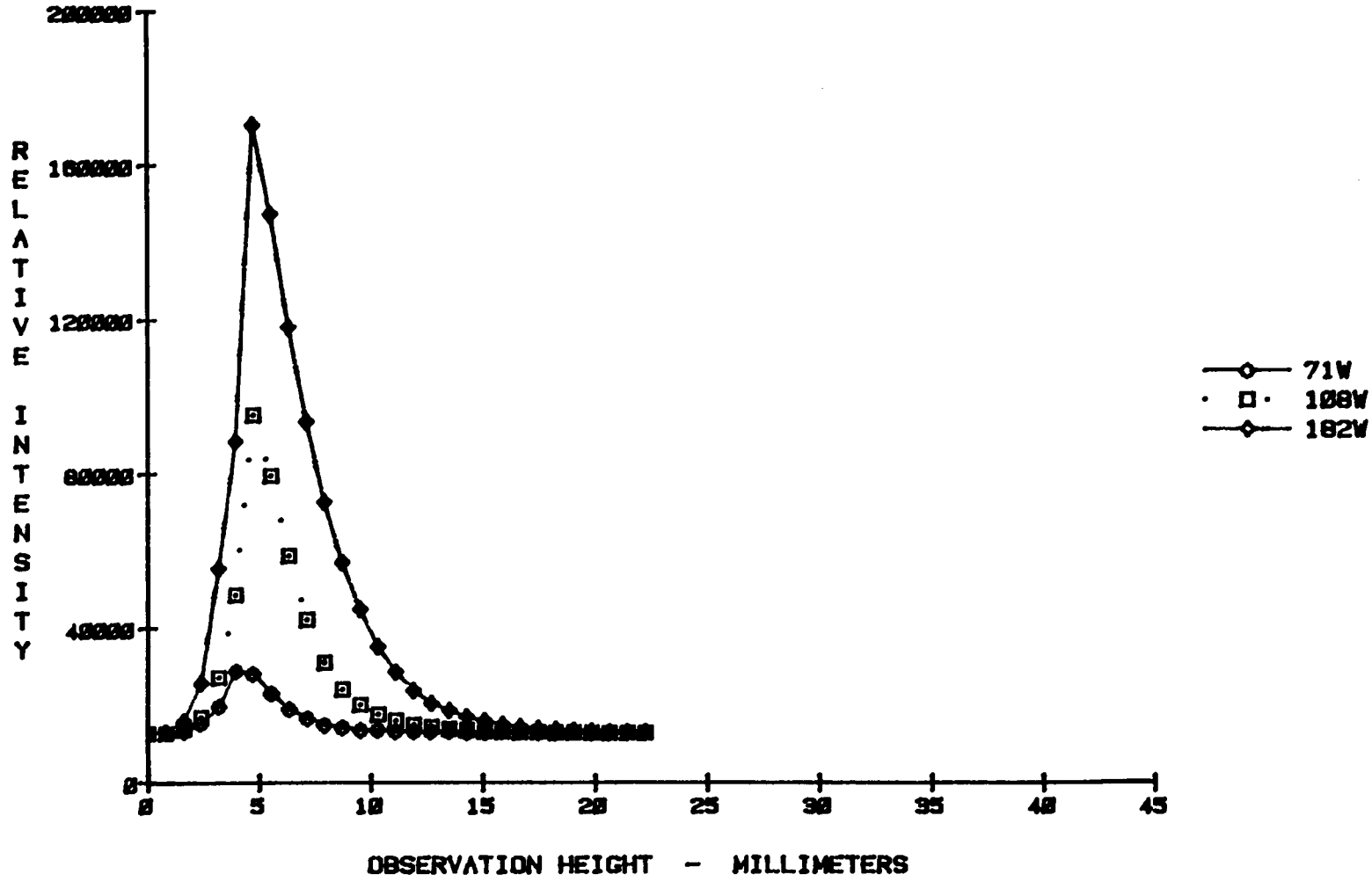

Figure 78. Barium Atom Emission Intensity vs. Observation Height - 50% Argon in Nitrogen Support Gas

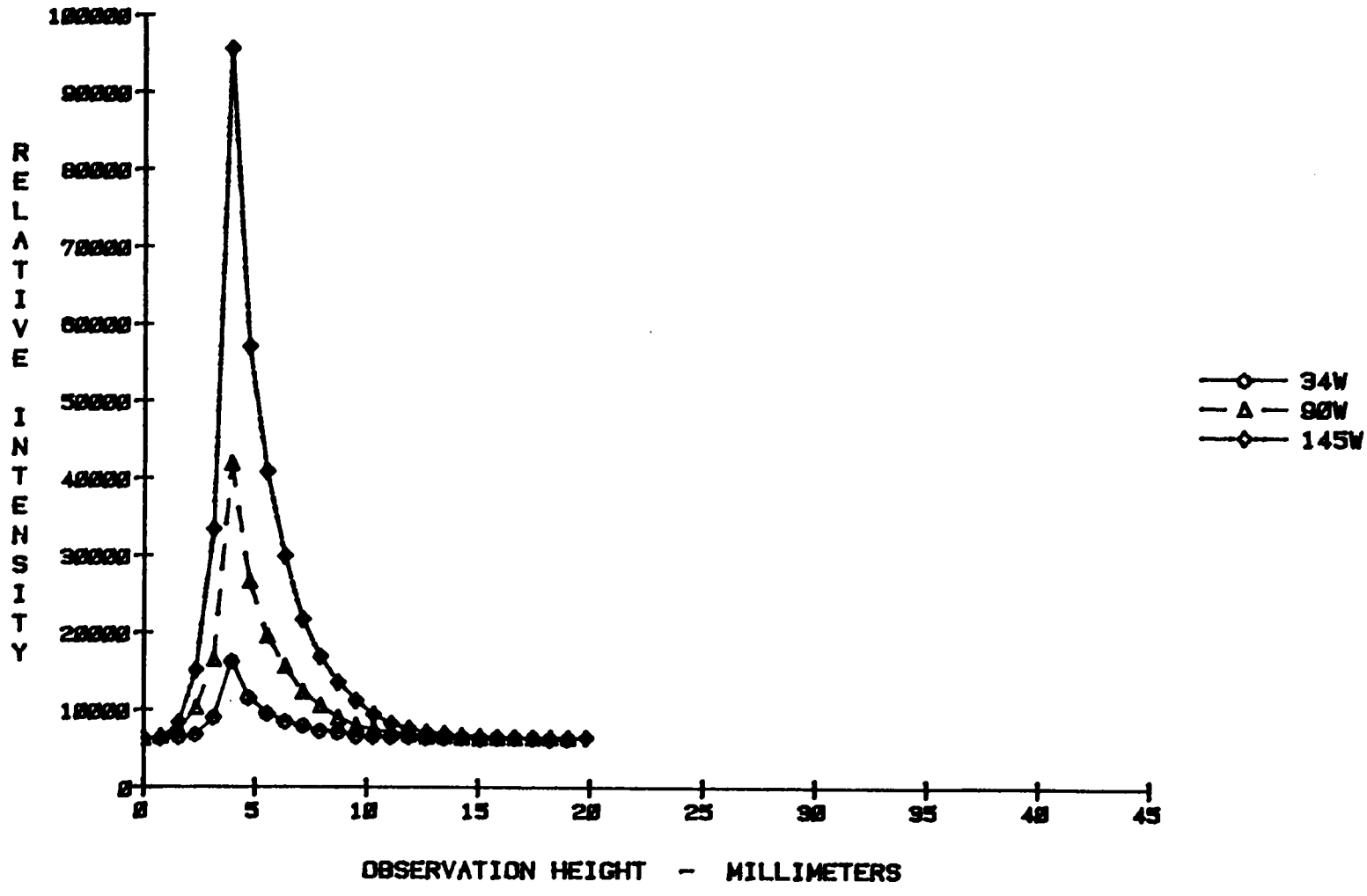

Figure 79. Barium Atom Emission Intensity vs. Observation Height - Pure Argon Support Gas

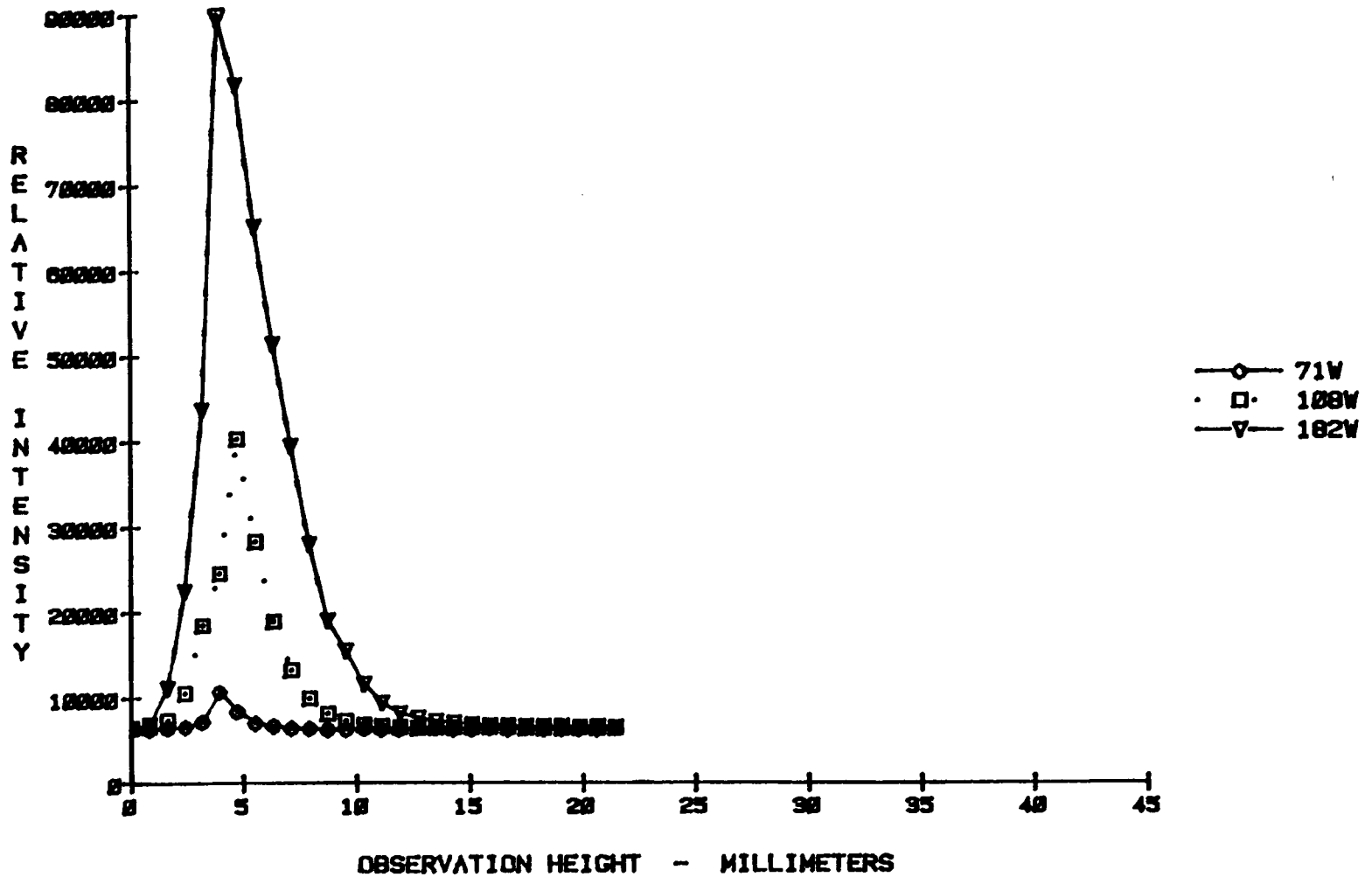

Figure 80. Barium Ion Emission Intensity vs. Observation Height - Pure Nitrogen Support Gas

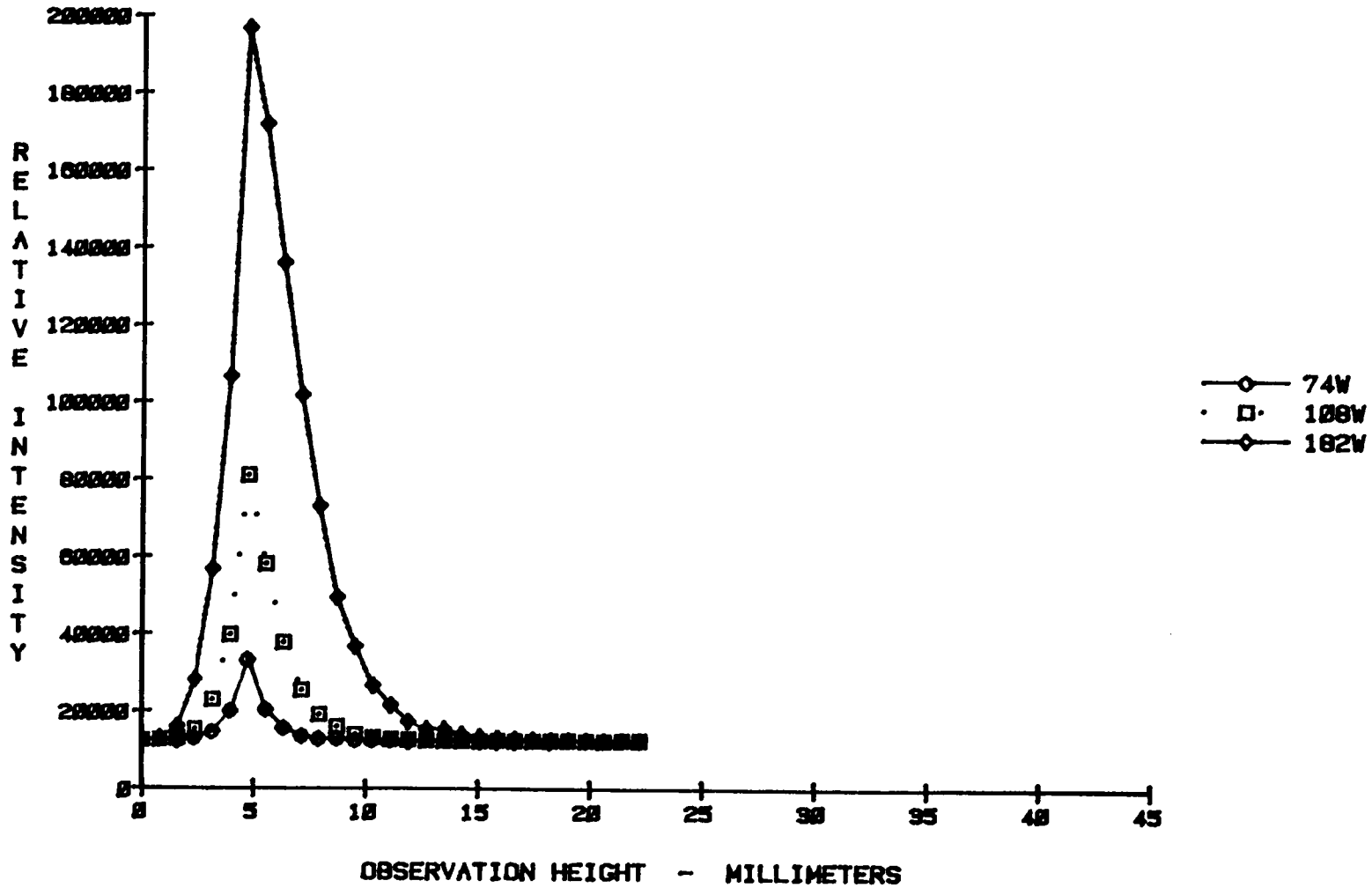

Figure 81. Barium Ion Emission Intensity vs. Observation Height - 50% Argon in Nitrogen Support Gas

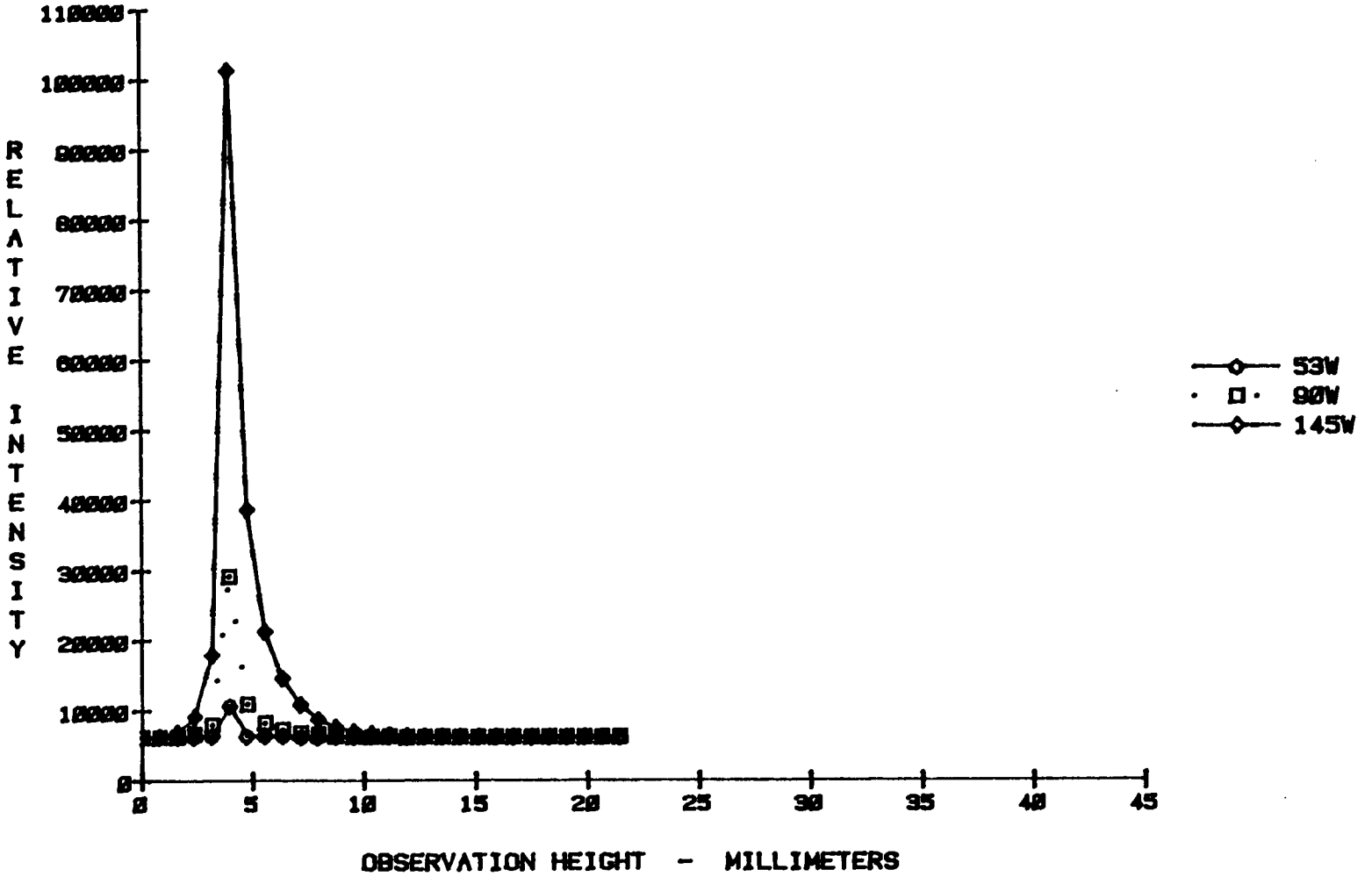

Figure 82. Barium Ion Emission Intensity vs. Observation Height - Pure Argon Support Gas

Annular Plasma - Description and Features:

For all of the experiments presented in this thesis the plasma was used in a stable and centered mode of operation. However, an annular plasma was observed when the tangential flow torch becomes unstable. It appeared as an annulus because the plasma bolus was circulating so fast around the center axis of the torch that it appeared to be a continuous, column-shaped bolus. The annular plasma developed when the cavity was tuned and matched for pure nitrogen, and pure argon was bled through the system for about 5 minutes. The torch would overheat if the condition was not corrected within a minute or so.

There is an extremely large increase in fluorescence observed when the plasma collapses into an annulus, sometimes 3 to 5 times the signal from a stable and centered plasma. It usually occurred at low flow rates, as seen from Figure 84 on page 222. The annular plasma was abnormally short in height; this can be seen by comparing Figure 71 on page 204 with Figure 83 on page 221. However, the signal increase is impressive. It is not known whether this "anomaly" may present a new, analytically useful way of using this type of torch. A further discussion of this potentially important research problem is presented in the appendix on Future Work.

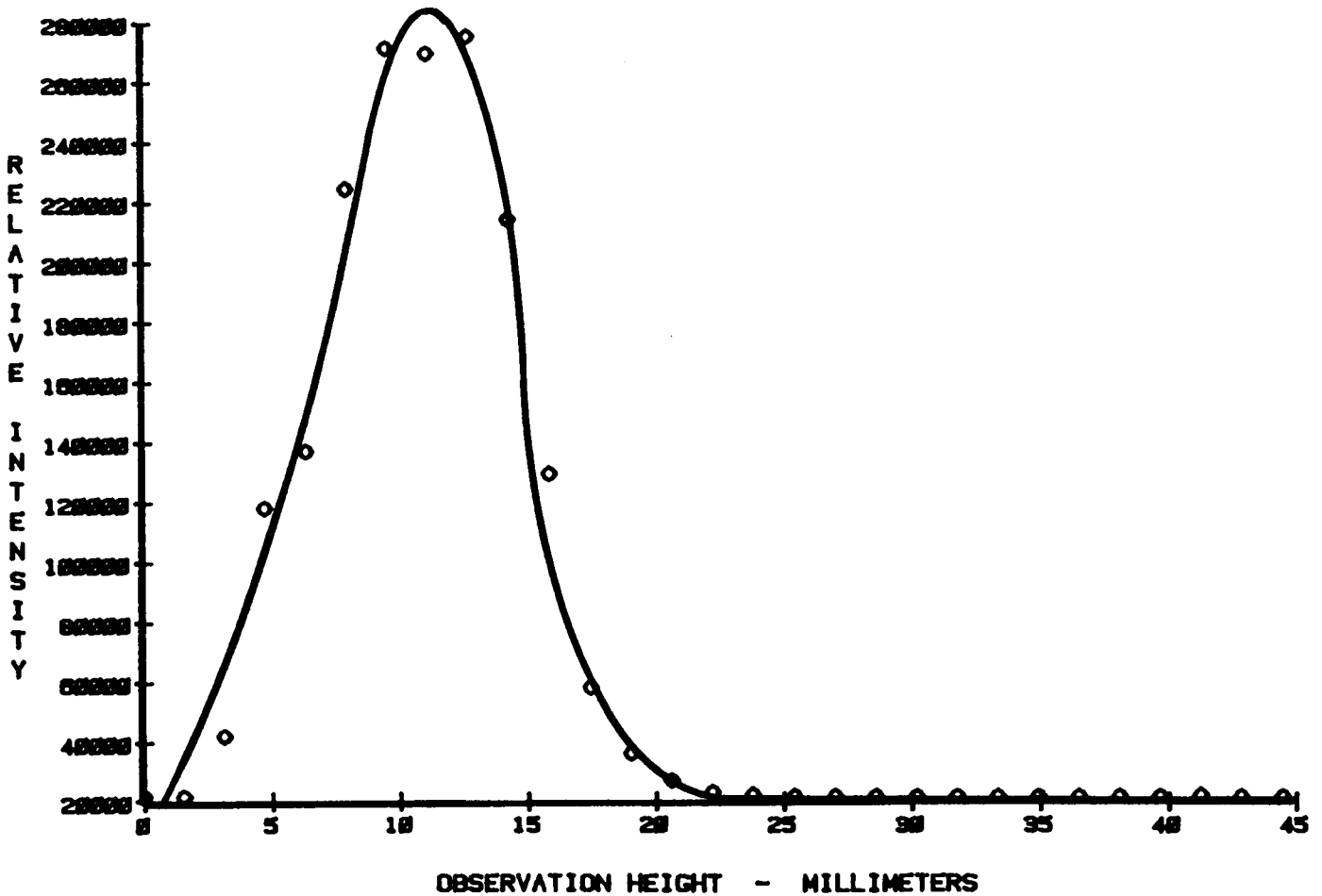

Figure 83. Sodium LIF Intensity vs. Observation Height - Annular Plasma with Argon Support Gas

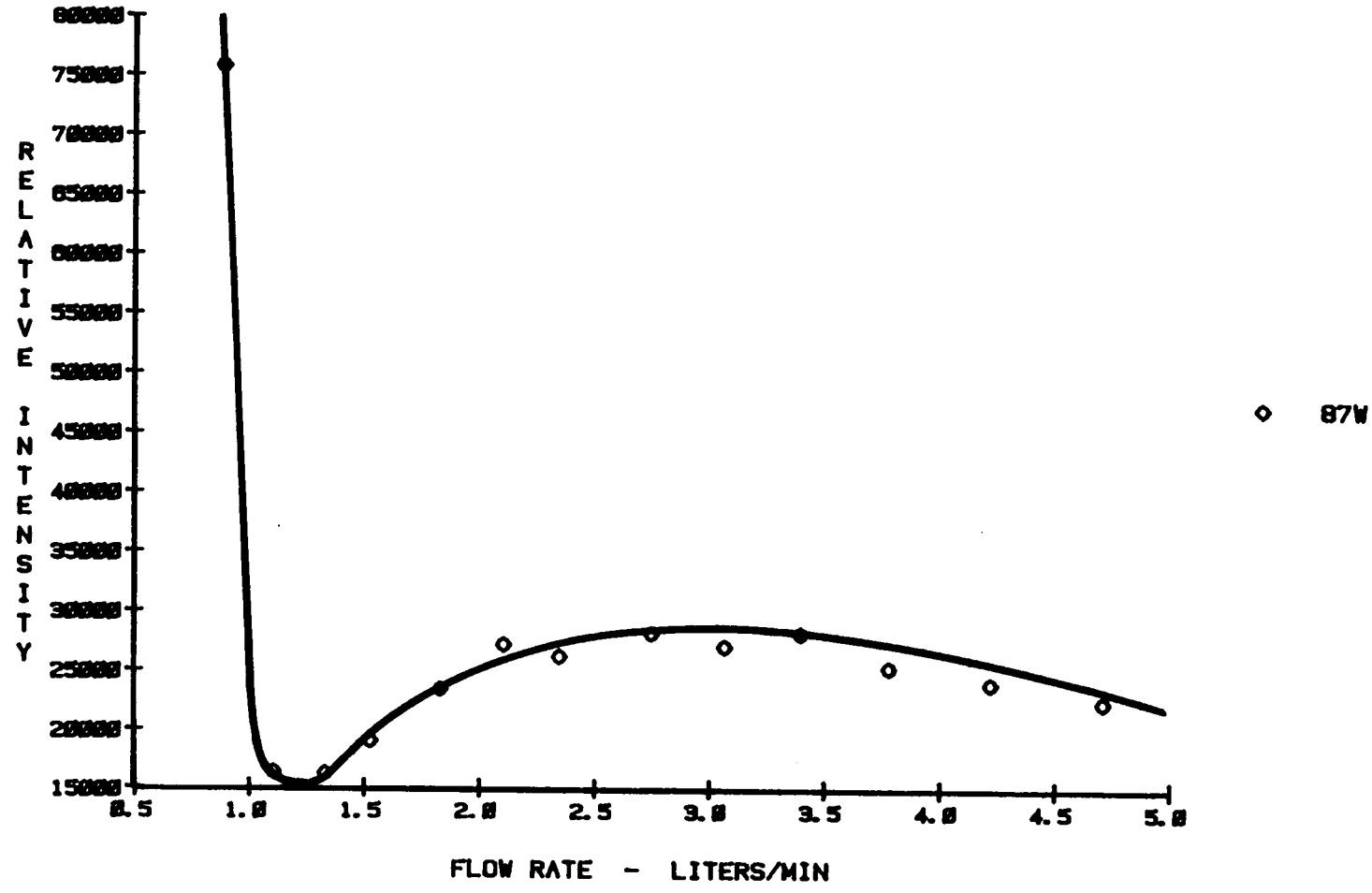

Figure 84. Sodium LIF Intensity vs. Flow Rate - Annular Plasma with Argon Support Gas

Laser Saturation Studies

Initially the Spectra-Physics Model 375 dye laser output was varied by changing the Spectra-Physics Model 124 Ar ion pump laser power. This method showed rather wide fluctuations in dye laser output power levels, as measured using a Spectra Physics Model 404 power meter. This could be attributed to several factors. The pump laser beam diameter and vertical position vary slightly with changes in power level. This can cause dye laser cavity detuning problems. It can also cause the tuning wedge and etalon to jump resonant modes, which cause further dye laser cavity detuning problems.

An alternate way of attenuating the pump laser power was sought that would keep the pump laser power fixed. Neutral density filters are not readily available which can withstand the high intensities for long periods of time (typically up to 300 mW over a 1 square millimeter area).

A simple, inexpensive attenuator was used. It consisted of a gang of 20 to 25 microscope slides, each one giving approximately 3% to 4 % attenuation because of front surface reflections. Slides were mounted on a 3" x 8" wooden, slotted jig cut on a band saw. The thickness of the band saw blade was just right to match the thickness of a single microscope slide. The slides were slid into and out of the path of the dye laser beam on this jig. The jig, full of slides, was mounted on the optical bench directly after the laser, before the chopping wheel and the mirrors used to raise the laser beam up to the height of the MIP torch, (see Figure 31 on page 130).

During the course of a single experiment the laser was left directed into the plasma as the beam was attenuated with the glass slides and the resulting signals measured with the monochrometer. After all data points were taken, the power was measured by re-directing the beam into the Spectra Physics Model 404 power meter. The microscope slides were slid out

of the path of the laser beam in the reverse order in which they were slid into the laser path. Measurements of laser power were taken at each step. This avoided the problem of exactly reproducing the setting of a 1 mm wide beam within the approximately 8 mm wide plasma plume. It also allowed every optical component to remain in use and in exactly the same position.

The major variables affecting atom population are concentration, flow rate, and applied microwave power. These were all chosen to maximize the analyte signal. Concentrations were chosen to make the fluorescence as intense as possible without easily saturating the detection system. For Na the concentration was 10 ppm. For Ba the concentration was 100 ppm. Radial viewing of the plasma involves sampling such a narrow cross-section of the plasma that self-absorption is not a problem. Self-absorption occurs when atoms at one end of a path absorb the light emitted by atoms at the other end, before detection of the light can occur. This is particularly a problem for long spectral pathlengths.

Flow rates and MIP powers were chosen which maximize the LIF signals. The total flow rate was about 1.75 L/min for both Na and Ba. The lowest MIP powers were used for Na in all support gases, and intermediate powers were used for Ba (80-120W in pure N_2, 100-150W for 50% Ar in N_2, and 90-130W in Ar).

Representative plots for Na and Ba, characteristic of experiments run at both higher and lower microwave powers, are shown in Figure 85 on page 226 through Figure 90 on page 231. The expected "bending-over" region, characteristic of a Beer's Law plot, is not present in any of the curves. In the Ar plots there are hints of saturation occuring at the highest laser power. Saturation also was not observed for the Ba ion (see Figure 88 on page 229 through Figure 90 on page 231). This is consistent with the LIF results of Hovis and Gelbwachs (110). They did flame AFS experiments using a CW dye laser for the same barium transition (614 nm excitation wavelength, 455 nm fluorescence wavelength). Saturation was not obtained with a 500 milliwatt beam until it was focussed down to a 160 micron radius. This is

approximately a factor of two greater laser power and a factor of eight tighter focussing, giving a factor of 16 greater light flux.

No matter what support gas or MIP power level was employed, saturation was not observed in any of the present experiments. Not attaining saturation can be thought of as an advantage for CW lasers, which have much lower output intensity fluctuations that greatly contribute to flicker noise. After saturation has been reached, noise due to scatter steadily increases. All extra light put into the system above the saturation level is scattered, causing signal-to-noise ratios to decrease.

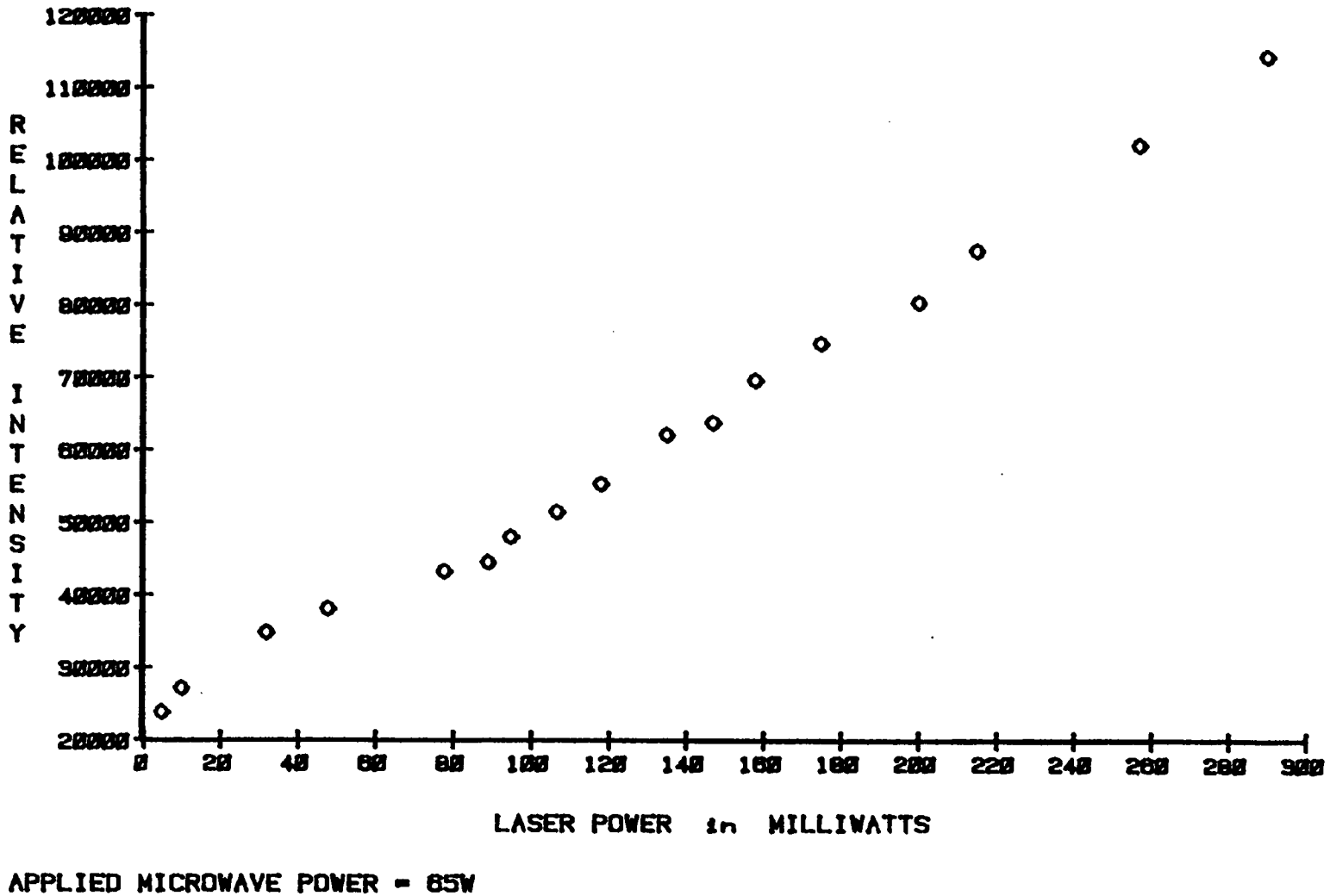

Figure 85. Laser Saturation Experiment - Sodium - Pure Nitrogen Support Gas

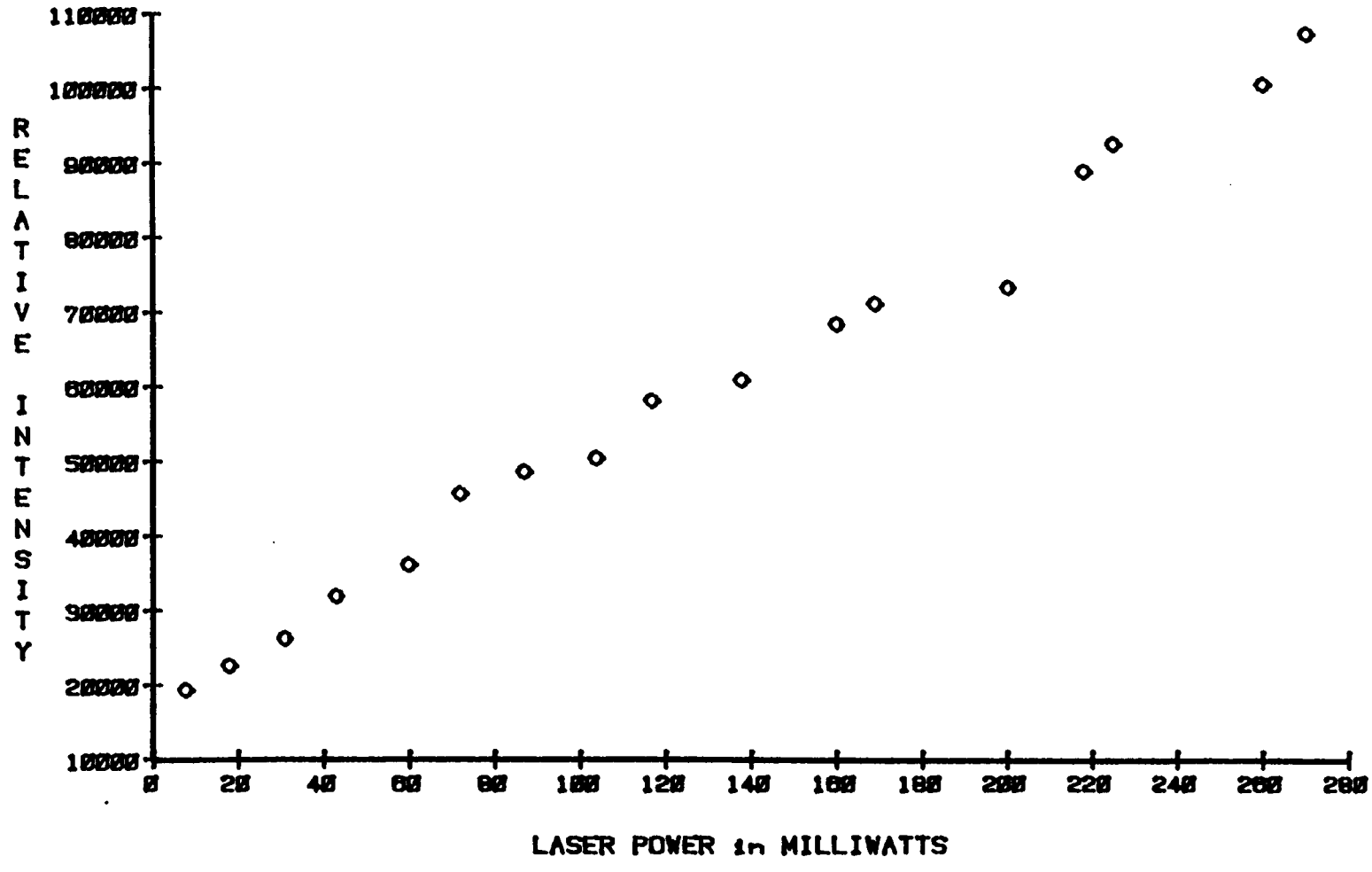

Figure 86. Laser Saturation Experiment - Sodium - 50% Argon in Nitrogen Support Gas

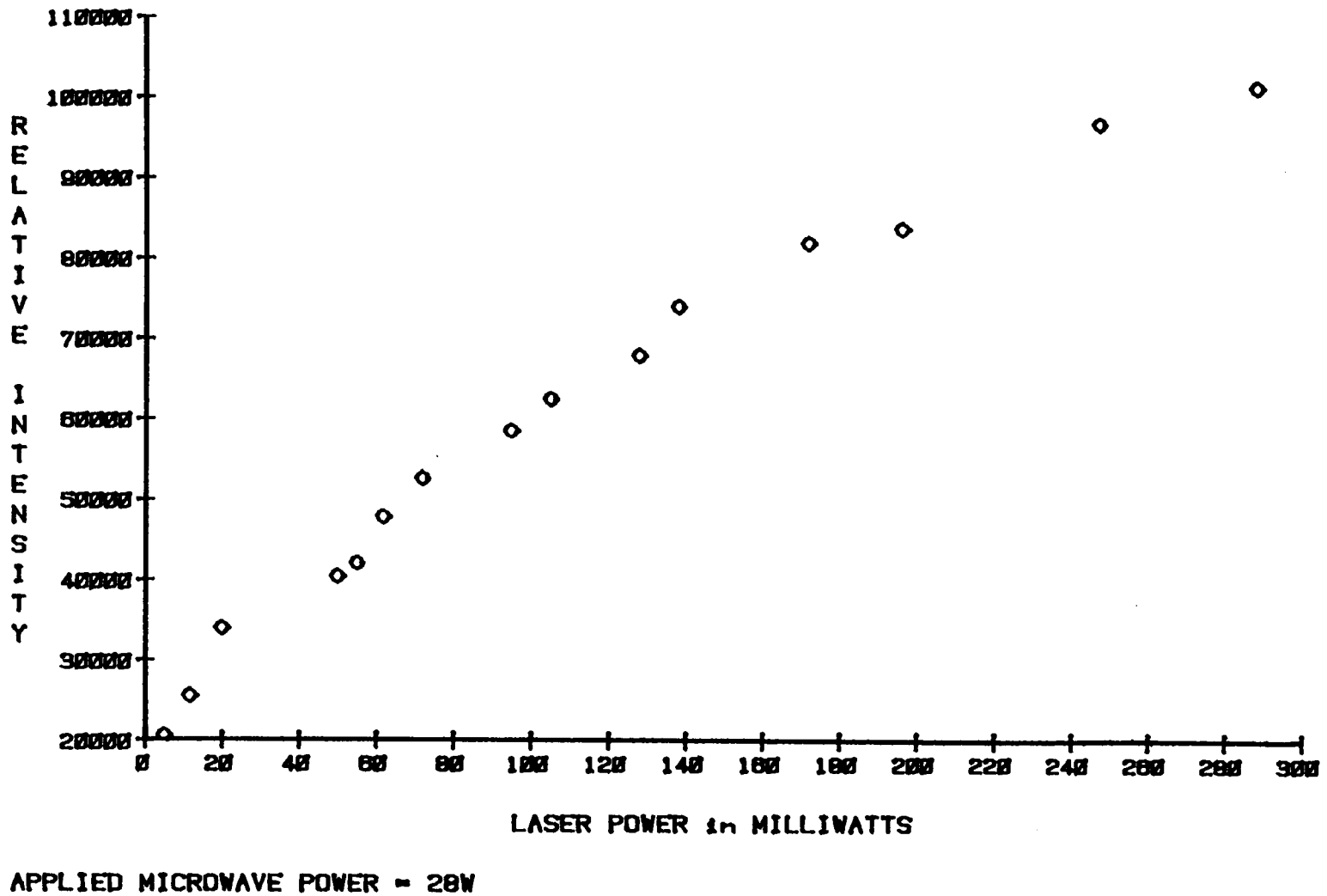

Figure 87. Laser Saturation Experiment - Sodium - Pure Argon Support Gas

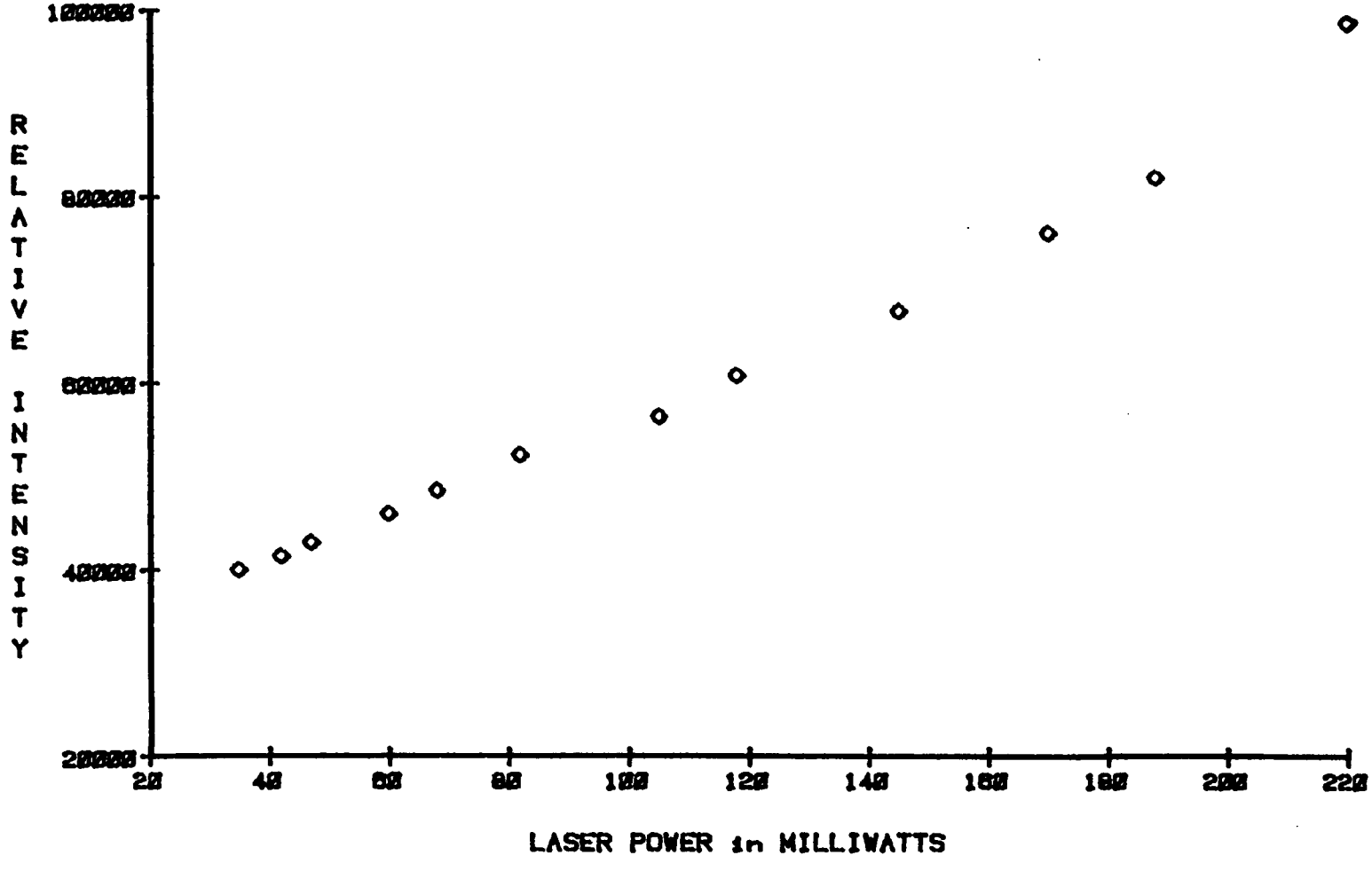

Figure 88. Laser Saturation Experiment - Barium - Pure Nitrogen Support Gas

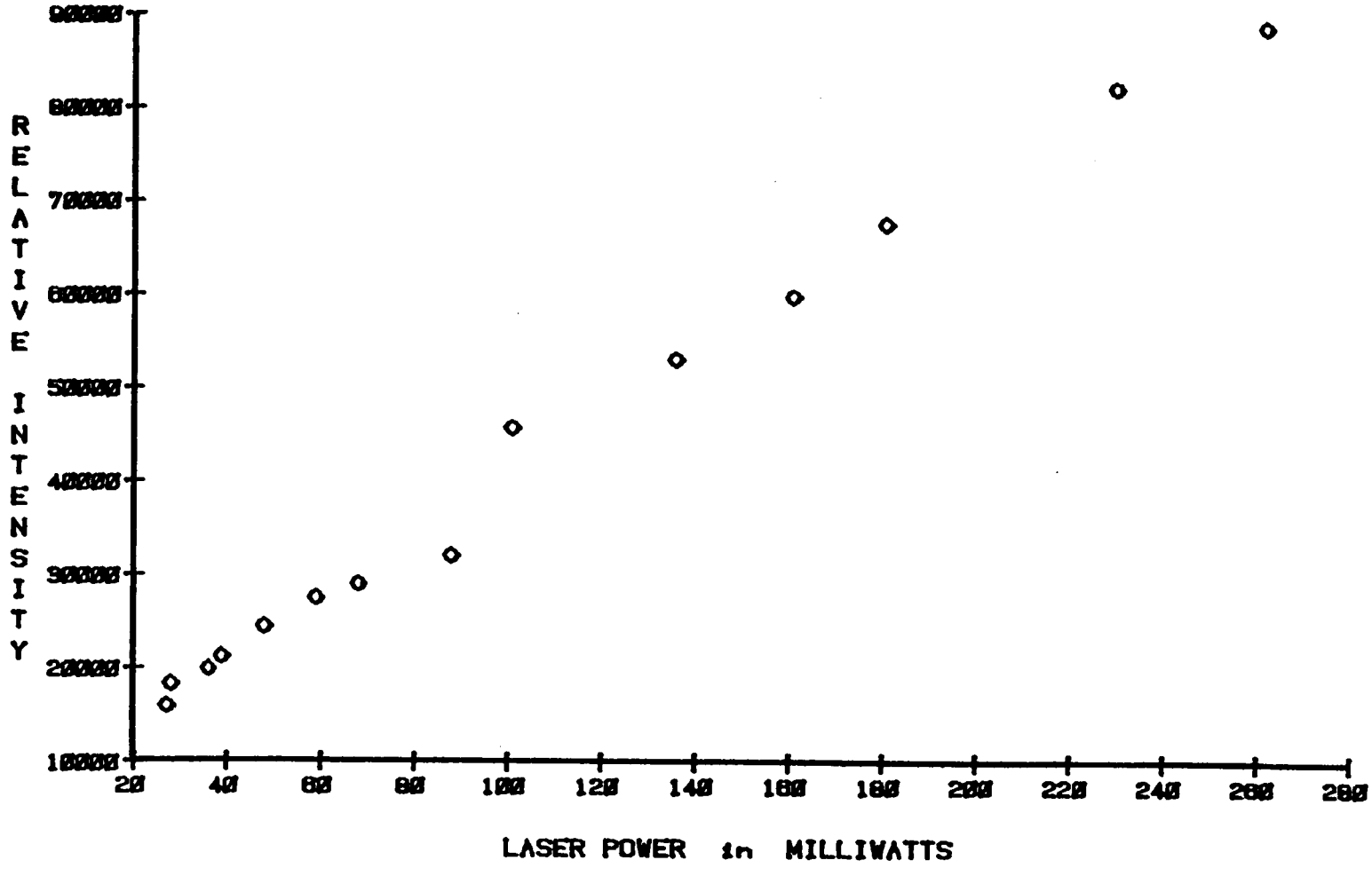

Figure 89. Laser Saturation Experiment - Barium - 50% Argon in Nitrogen Support Gas

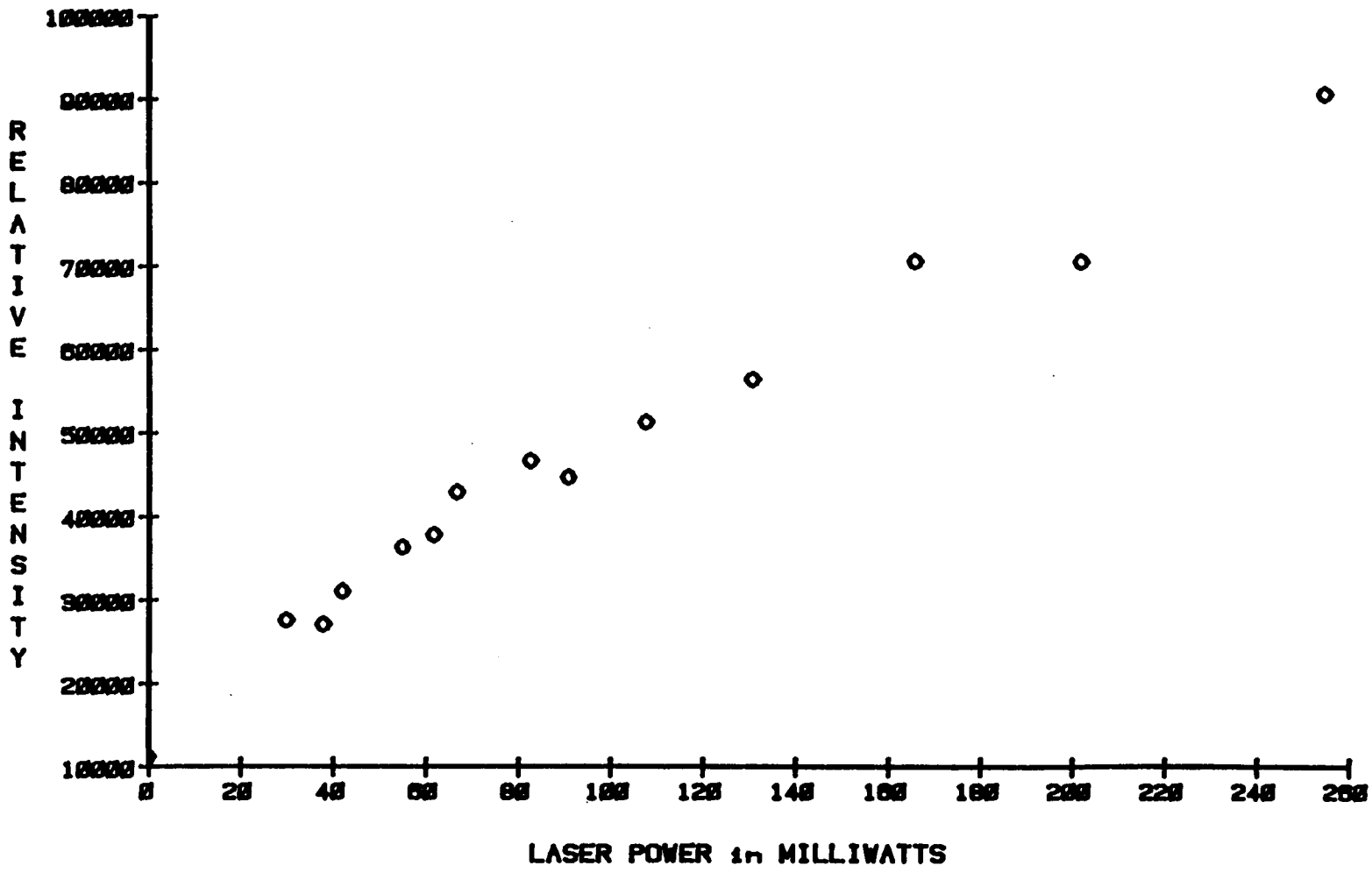

Figure 90. Laser Saturation Experiment - Barium - Pure Argon Support Gas

Noise Studies

In the low-power MIP background noise levels are very low and constant. Analyte flicker is the major contribution to background noise, adding to the electronic noise in the detection system (35). Because vaporization and atomization are fairly complete in the core of the MIP, the spatial distribution of noise due to analyte flicker is constant throughout the plasma tail-flame. Since background levels in the MIP tail-flame are so low compared to both the AES and LIF signals, the background noise levels measured for the limit-of-detection studies are sufficient to establish noise levels throughout the plasma studies. However, to better characterize system performance and to determine which variables most affect noise levels, some further experiments were performed.

In laser-induced resonance fluorescence the major source of noise is laser scatter. The measured DC background level due to emission was 2 to 3 orders of magnitude lower than the laser scatter signal level. The measured electronic noise due to the detection system was typically 3 orders of magnitude less than the noise due to analyte emission.

The results demonstrate that noise is fairly constant over the full span of the observation height, as can be seen from an examination of the graphs at the top of Figure 91 on page 234 and Figure 92 on page 235. Each signal data point is an average of 20 A/D samplings. Each noise data point is the standard deviation of 20 A/D samplings. The differences in the orders of magnitude of the y axis scales should be noted.

There is always some concern that noise might not be random, and might be correlated with increases in signal. The correlation plots shown at the bottom prove that this is not the case. Data for the correlation plots was taken from experiments run under typical operating conditions; i.e., Na LIF intensity versus observation height data for a 90 Watt pure nitrogen plasma using 1.8 L/min flow rate. Under the conditions typically used for experimentation,

(time constant = 300 msec or 1 second), all the high frequency noise is is averaged out. Only when a time constant of 30 msec is employed does the noise start to be positively correlated with increases in signal, (see Figure 93 on page 236). A 30 msec time constant was never used in other studies.

Results using different power levels, flow rates, and gas mixtures gave virtually similar results. The only variable that measurably affected the noise levels was the applied power. From Figure 94 on page 237, it can be seen that noise increases only slightly with an increase in applied microwave power. Sodium LIF was chosen because it represents a worst-case example, since signal goes down as applied microwave increases. Even at the highest applied power the signal-to-noise ratio is still 20. The system would never be operated under these power conditions since a greater signal intensity is achieveable at lower powers.

One problem that has to be avoided is laser scatter from the microwave torch. A typical scatter profile is shown in Figure 95 on page 238. For certain elements with an LIF maximum near the scatter signal this spike could be a problem. The exact position of the scatter maximum can be varied, and depends upon the exact displacement of the torch relative to the cavity. This knowledge can be used to advantage to remove the scatter maximum from coincidence with the analyte signal maximum. None of these studies had such a coincidence problem. In general this freedom from noise and scatter interference makes this a sensitive method for atomic analysis, as will be seen in the section on analytical feasibility studies.

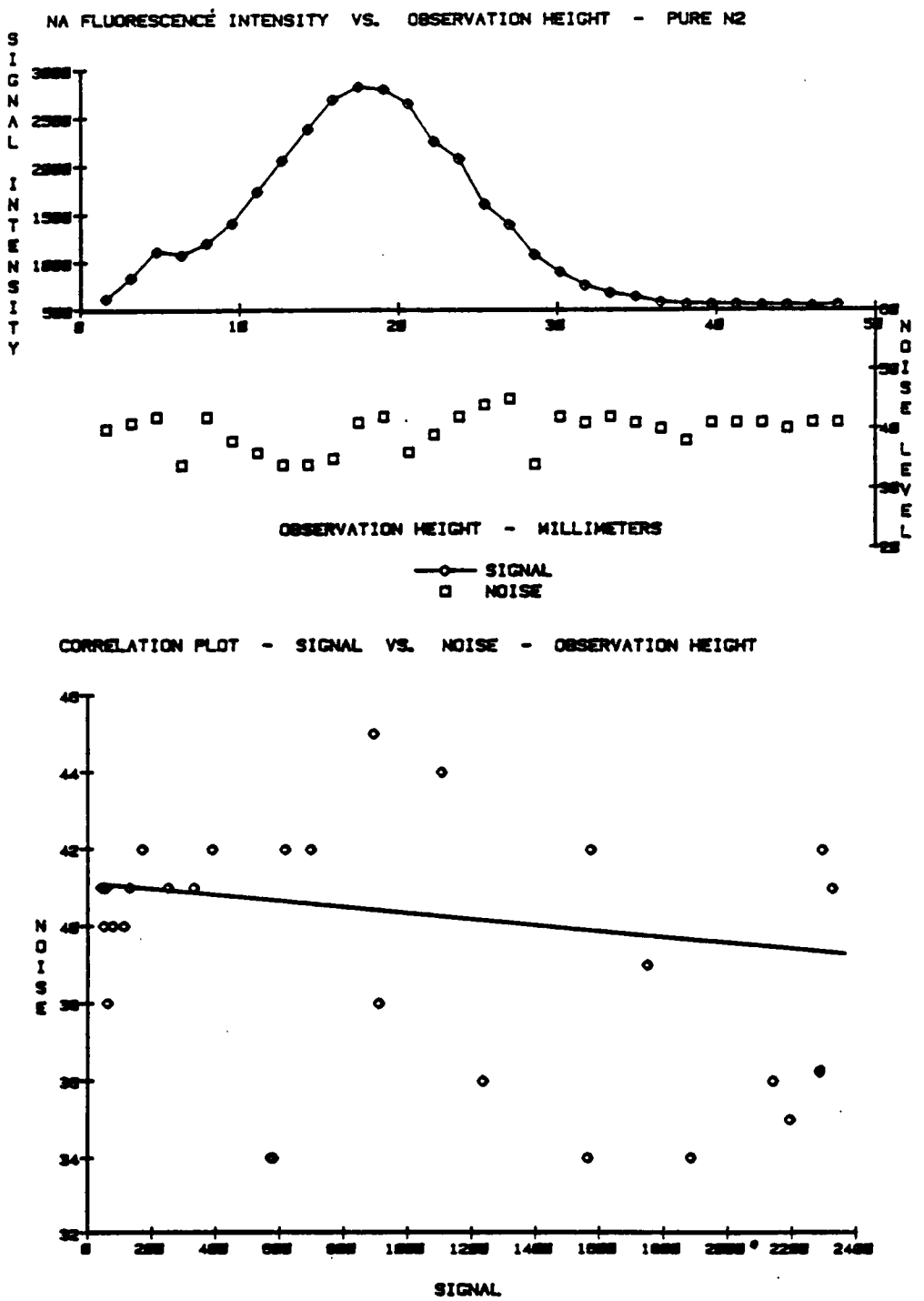

Figure 91. Noise Study as a Function of Signal Intensity - 53 Watts

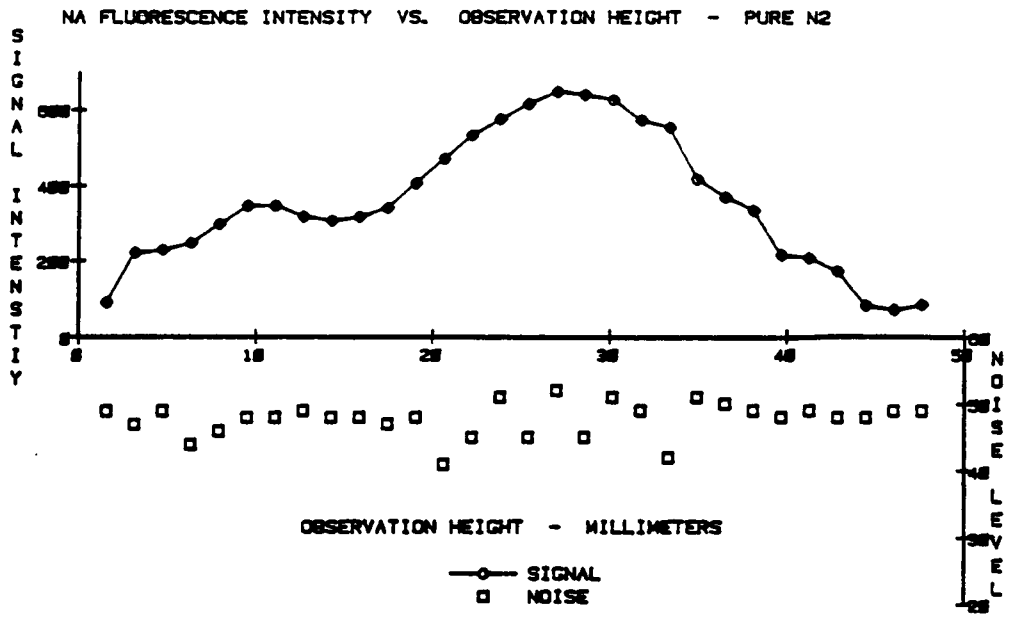

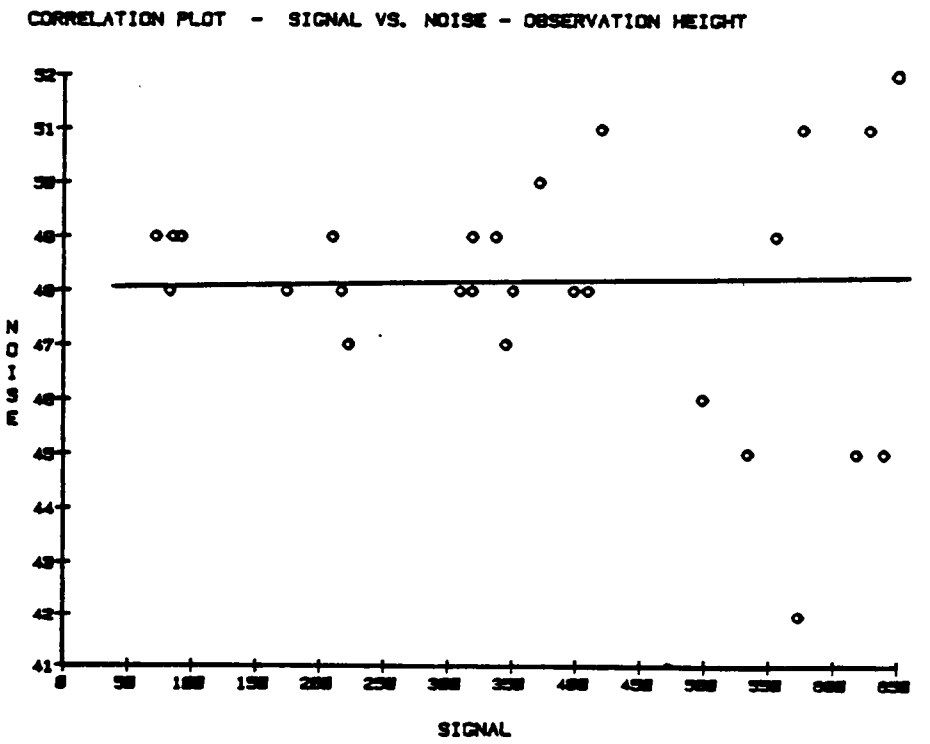

Figure 92. Noise Study as a Function of Signal Intensity - 145 Watts

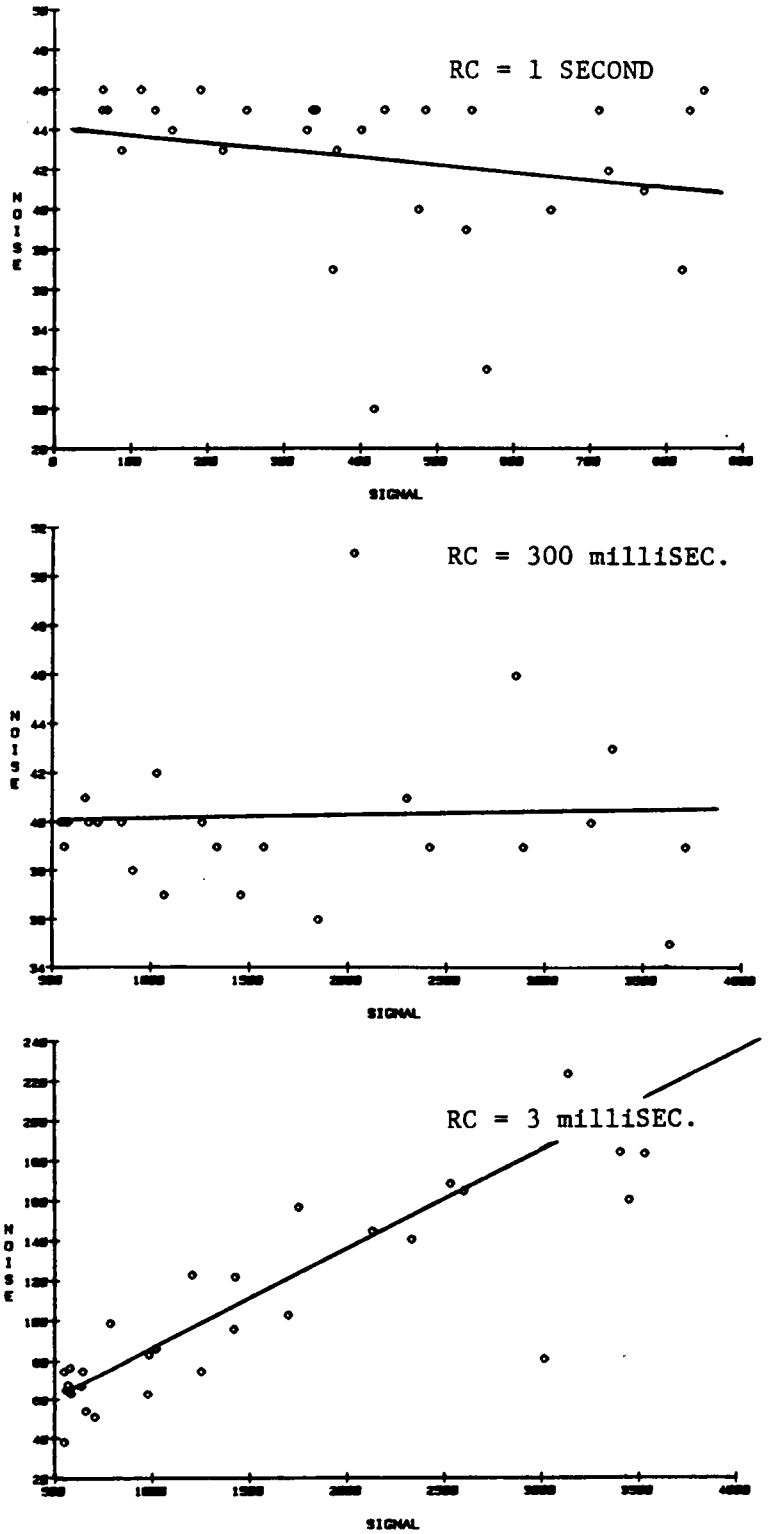

Figure 93. Correlation Plots of Signal vs. Noise - at Various RC Values

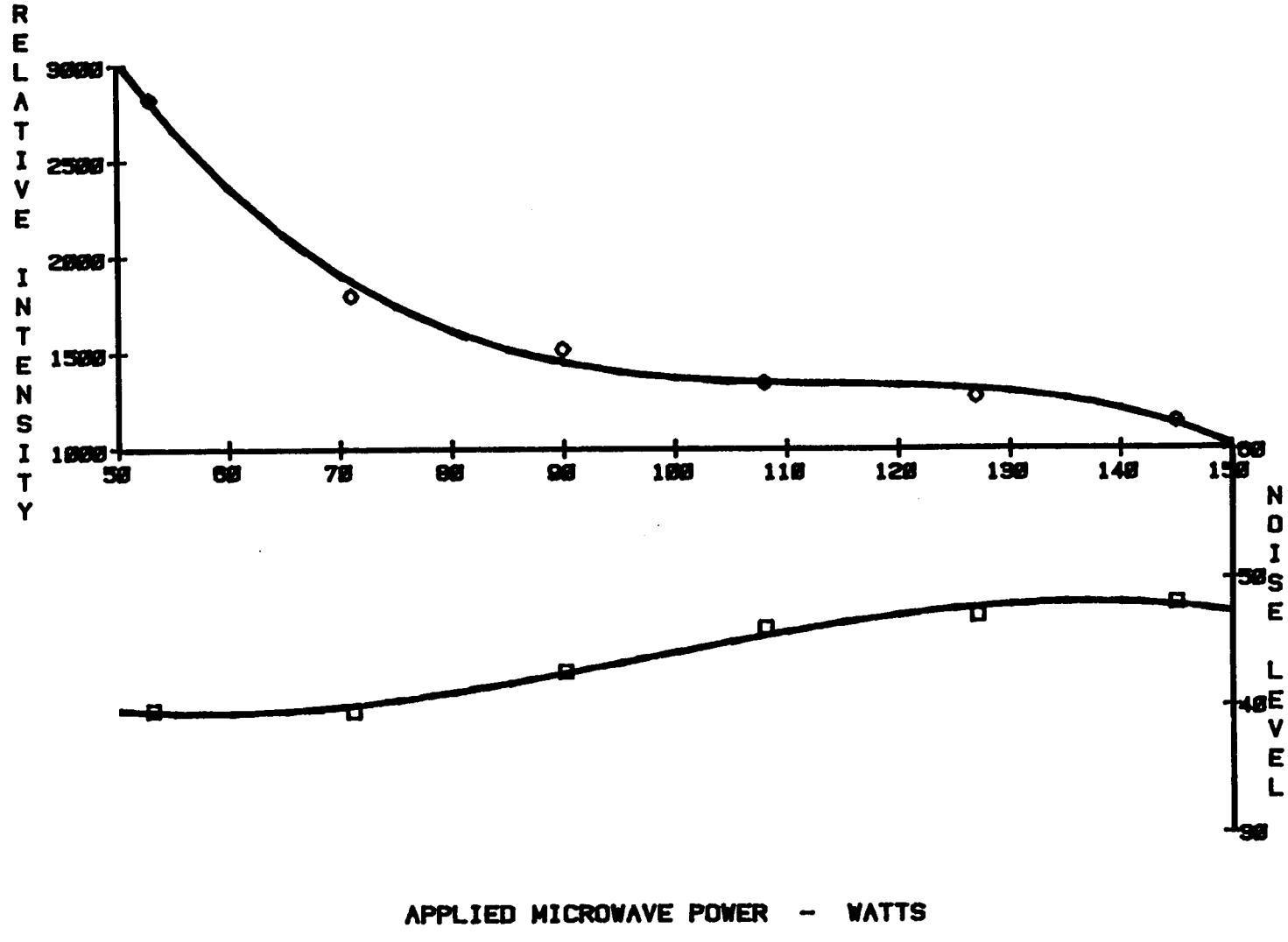

Figure 94. Signal and Noise Levels vs. Applied Microwave Power

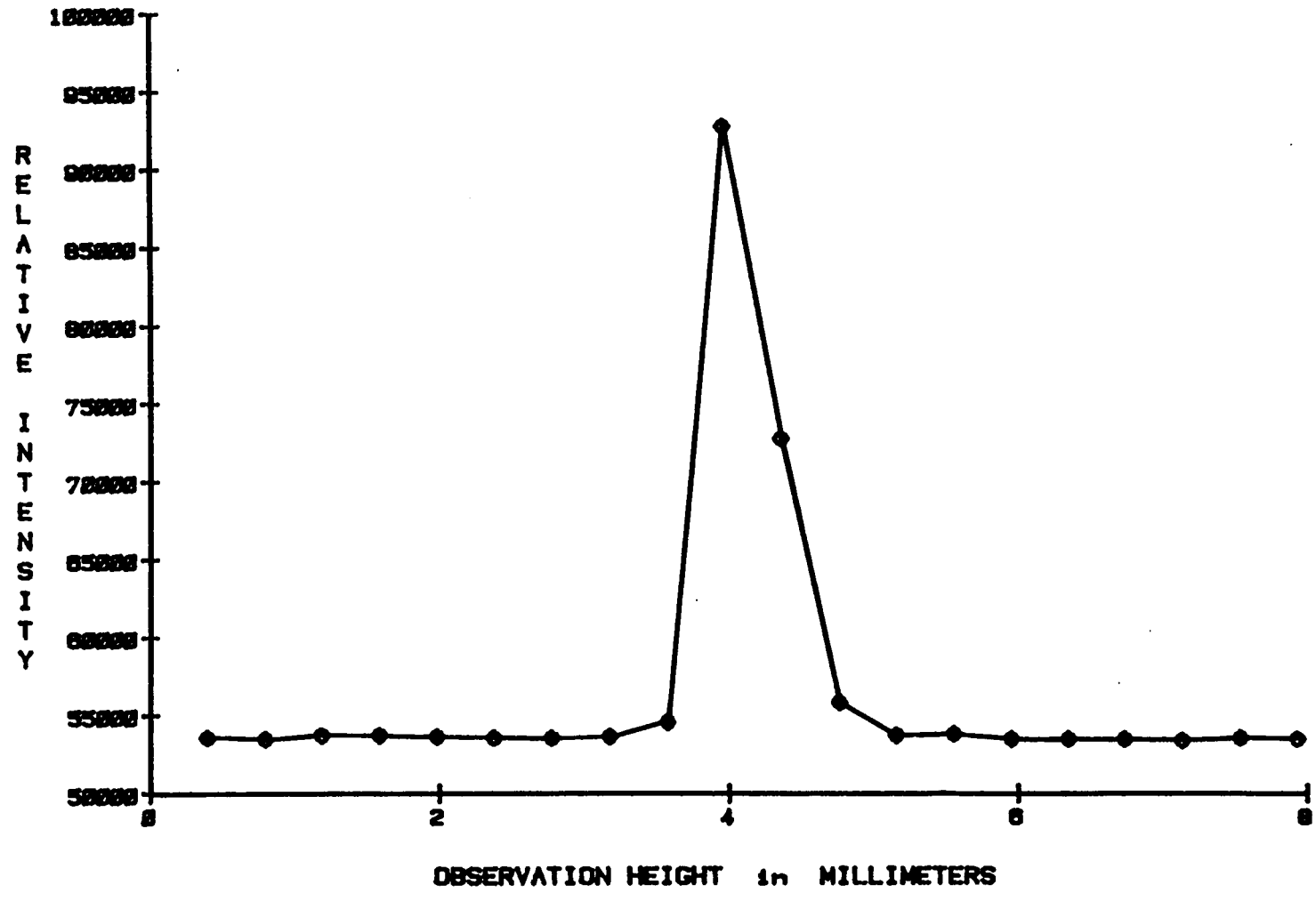

Figure 95. Laser Scatter from MIP Torch vs. Observation Height

Signal-to-Noise Studies

Experiments were conducted to study analyte behavior in the presence of spectral background. Monochrometer scans over the full wavelength range used for the LIF and AES studies are the easiest way to illustrate this. LIF in this low-noise plasma has only elemental atomic emission as the primary spectral background. For AES in the low-power MIP, plasma background is the primary spectral background. And this is only a problem under two circumstances: 1) the element of interest has a very high excitation potential, 2) a non-principal line (one which is not the most intense) is used because of spectral interference by another element. Neither of these problems were present for the elements selected to characterize this plasma spectrometer system.

Parts A and B of Figure 96 on page 241 compare the relative intensities of laser-induced fluorescence (A) with atomic emission (B). In part A, fluorescence was excited when the laser was centered on the 614.2 nanometer line of barium. The ionic fluorescence lines at 455.4, 493.4 nm, and 585.3 nm greatly decrease in intensity as the laser is moved off the excitation wavelength; this is shown in part B. The remaining spectral features are emission lines, with the very large off-wavelength laser scatter signal shown at near 614.2 nm. Part C shows the same experiment as part A, but with the detector sensitivity reduced so that the exciting laser intensity could be compared with the laser-induced fluorescence intensity. This set of spectral scans demonstrate the very large S/N ratios present when LIF is used, and the typical emission background that is always present.

A typical atomic emission background noise level is illustrated in Figure 97 on page 242. A solution having a concentration of 20 ppm each of Ca, Na, and Sr. was used. Background noise levels are low compared to signal levels. For the spectral region 510 nm up through 650 nm, the sensitivity had to be decreased because the sodium emission signal was off scale. Figure 98 on page 243 shows a spectral scan for a mixture of 20 ppm sodium

and 400 ppm of barium. This illustrates the sensitivities for these elements relative to one another, measured using atomic emission. More than a factor of 20X difference in concentration is required for their most intense spectral lines to exhibit equal intensities.

The signal-to-noise ratios of these experiments demonstrate that this plasma spectrometer system can easily discern elemental fluorescence and emission from the plasma background. The next section will show the analytical results available from such an instrument.

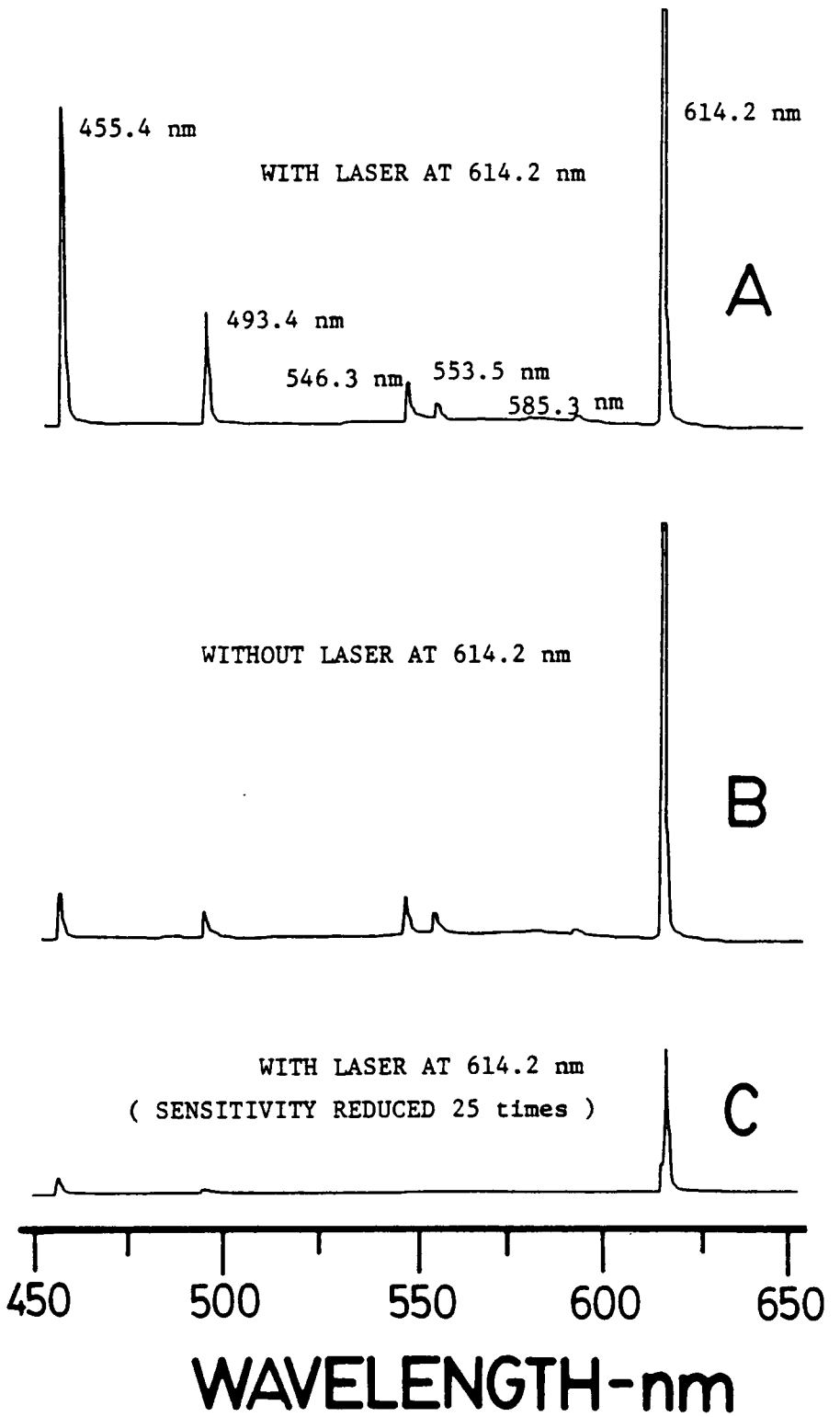

Figure 96. Spectral Scans of Signal and Noise Levels in LIF Methods: Barium Atomic & Ionic Transitions are Indicated.

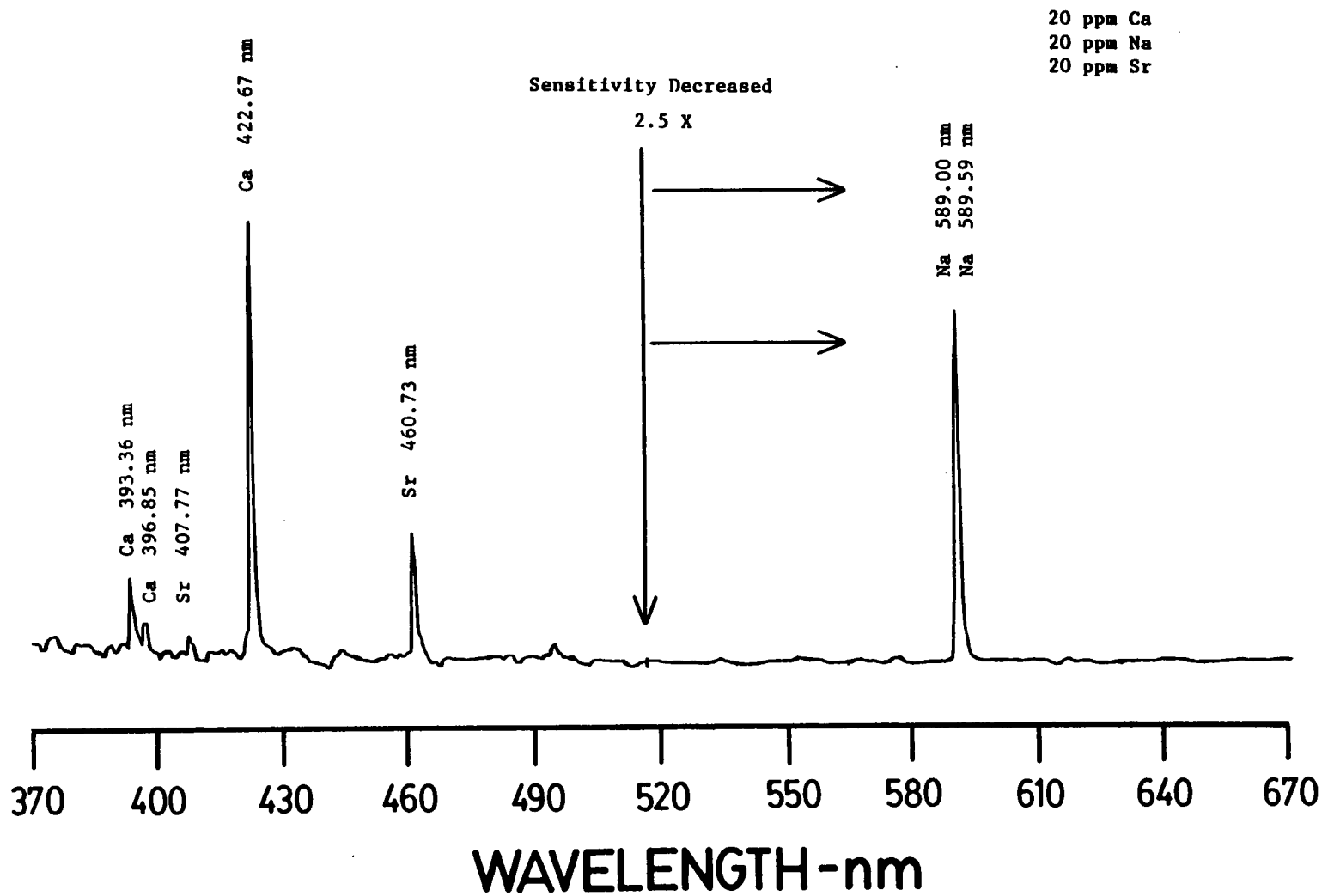

Figure 97. Spectral Scan for Atomic Emission of Na, Sr, and Ca

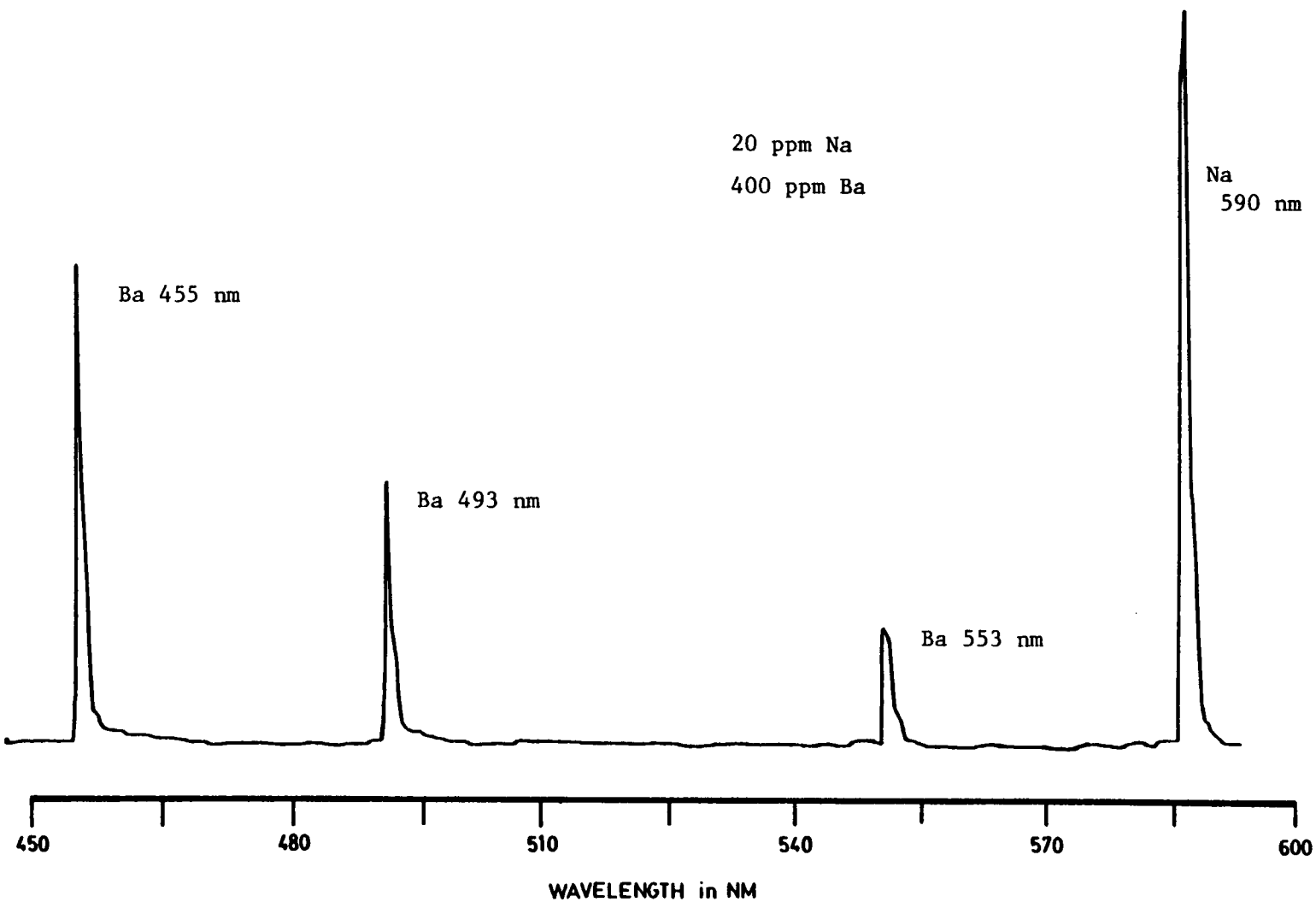

Figure 98. Spectral Scan for Atomic Emission of Sodium and Barium

Analytical Feasiblity Studies

The highly-efficient MIP cavity developed here offers a distinct practical advantage for analytical work. Solutions can be nebulized directly into the MIP, without an extra desolvation step. Earlier low-power MIP cavities could tolerate aerosol solutions best with a prior solvent removal step; that is no longer needed. Cavity tuning and matching conditions do not change appreciably as aerosol is introduced into the cavity.

Analytical feasibility studies included constructing analytical working curves. These illustrate the linearity, the linear dynamic range, and the slope sensitivity of the instrument. Analytical limits-of-detection were also calculated. These are the primary studies required to characterize a new type of instrument for analytical work. Experiments were conducted to measure the effects of plasma gas composition and microwave power on the working curves. Linear dynamic range, slope, and relative sensitivities can be affected by changing these variables.

Interelement interference studies would have been redundant and were not performed. Such studies for nitrogen and air MIP's have been done by other investigators (35 , 31). The results indicate that the vaporization interferences (aluminum and phosphate) depress analyte signals, as often observed in flames, and that the signal depression can be eliminated with the addition of 0.01 M EDTA. The phosphate interference was minimal, another indication that molecular decomposition is very efficient in molecular plasmas. Ionization interferences by easily ionizeable elements (sodium) caused both atom and ion line emission enhancements. This behavior is closer to that observed in an ICP or "wet" argon MIP than in a flame, which show both atom and ion line enhancements. This is to be expected since ionization is greater in MIP's and ICP's. A thermal mechanism was still proposed to be operative since the plasma with added sodium is wider, filling the discharge tube more, causing increased analyte/plasma interaction (35). The ionization interferences were eliminated by using a

cesium ionization suppressant. Interelement effects in atomic fluorescence generally reflect those observed in emission work and can be eliminated using the same techniques.

For all of the following studies, radial viewing of the plasma was used. A typical flow rate of 1.8 L/min was used. Microwave powers and observation heights were chosen to maximize signal intensity for the particular plasma being used and the particular element being observed. Analyte solutions ranged from 1 ppb to 1000 ppm. Solutions were made by serial dilution of 1000 ppm solutions of sodium chloride and barium chloride, made from crystalline powders (Fisher Scientific Co., Fair Lawn, N.J.). Solution water was deionized, distilled water.

Detection limits were measured as follows. At least 20 consecutive background readings were taken, separated by at least 5 RC time constants to insure independence of readings. The standard deviation of these readings was computed. The standard deviation was divided by the slope of the calibration curve (analytical working curve) in the vicinity of the limit of detection, and then multiplied by the noise factor k, to get the limit of detection (141 , 142).

$$c_L = \frac{(k \times s_B)}{m}$$

where k = 3 , if the IUPAC standard is used

s_B = standard deviation of background readings

m = slope of calibration curve

Generally, the LOD values reported in the literature are computed with k = 2. This defines the detection limit as the concentration of analyte that produces a signal that is 2 times the standard deviation of the background signal (97.7% confidence interval for a normal distribution). All of the experimental values reported here were therefore computed with k = 2 to allow direct comparisons with literature. To get IUPAC-consistent LOD's, the values in Table 13 on page 248 must be multiplied by 1.5. Values are reported here to 2 significant

figures for comparison purposes only, (eg., to discern an LOD of 260 ppb from an LOD of 300 ppb). The second significant figure in the following table is generally not statistically significant, i.e. the order of magnitude is most important. Unless there is a factor of 3 difference (one LOD is different from another by greater than 3 standard deviations) the differences are not significant.

The interpretation of these results is somewhat complex since fairly different plasmas are being compared. And it must be emphasized that the results within a class are so close to one another that statistically such comparisons may be unfounded. However, for mechanistic purposes some interpretation will be attempted.

In general, it can be said that the N_2 -based plasmas are thermally much hotter than the argon plasmas. And it has been postulated earlier that there is more analyte ionization occuring in the N_2-based plasmas. Thus one would expect poorer Na atom LOD's, and better Ba ion LOD's in the N_2-based plasmas. This is indeed the case for the fluorescence experiments.

For atomic and ionic emission, not all results follow a trend based on ionization mechanism alone. For the Ba atom and Ba ion, the ionization mechanism explains the observed trends. For Na atom emission the trend is reversed from what might be expected. But the differences are probably too small to be considered significant.

Working Curves for Fluorescence and Emission Experiments:

Working curves are shown in the sequence beginning with Figure 99 on page 249, through Figure 105 on page 255. Linear dynamic range is quite good, ranging from 4 to 5 orders of magnitude for fluorescence, and 4 to 6 orders of magnitude for emission. The linear dynamic range is limited at the lower end in the Ba emission experiments because of low signal intensities. For sodium emission, ample signals were present for all concentrations. Limits of detection are shown on the graphs, and were calculated using the methods outlined

in the previous section. Linearity is good, showing that instrumental drift is not a problem. These results show that these methods offer reliable and predictable signals for a large range of concentrations. Limits of detection are given in parts per billion (ppb), which is the equivalent of nanograms per millimeter (ng/mL) for aqueous solutions.

Table 13. Experimental Limits of Detection - This Work

Laser-Induced Fluorescence			
SODIUM ATOM	LOD(ppb)	***BARIUM ION***	LOD(ppb)
N_2 - 72W	2.6	N2 - 108W	8.6
50% N2 - 72W	2.5	50% N2 - 102W	10
Ar - 30W	0.26	Ar - 108W	18
Emission Spectroscopy			
SODIUM ATOM	LOD(ppb)	***BARIUM ATOM***	LOD(ppb)
N2 - 180W	4.0	N2 - 72W	2600
50% N2 - 171W	5.0	N2 - 126W	180
Ar - 48W	42	N2 - 182W	140
Ar - 108W	6.8	50% N2 - 72W	250
		50% N2 - 180W	140
		Ar - 138W	79
BARIUM ION			
N2 - 180W	91		
50% N2 - 180W	99		
Ar - 147W	85		

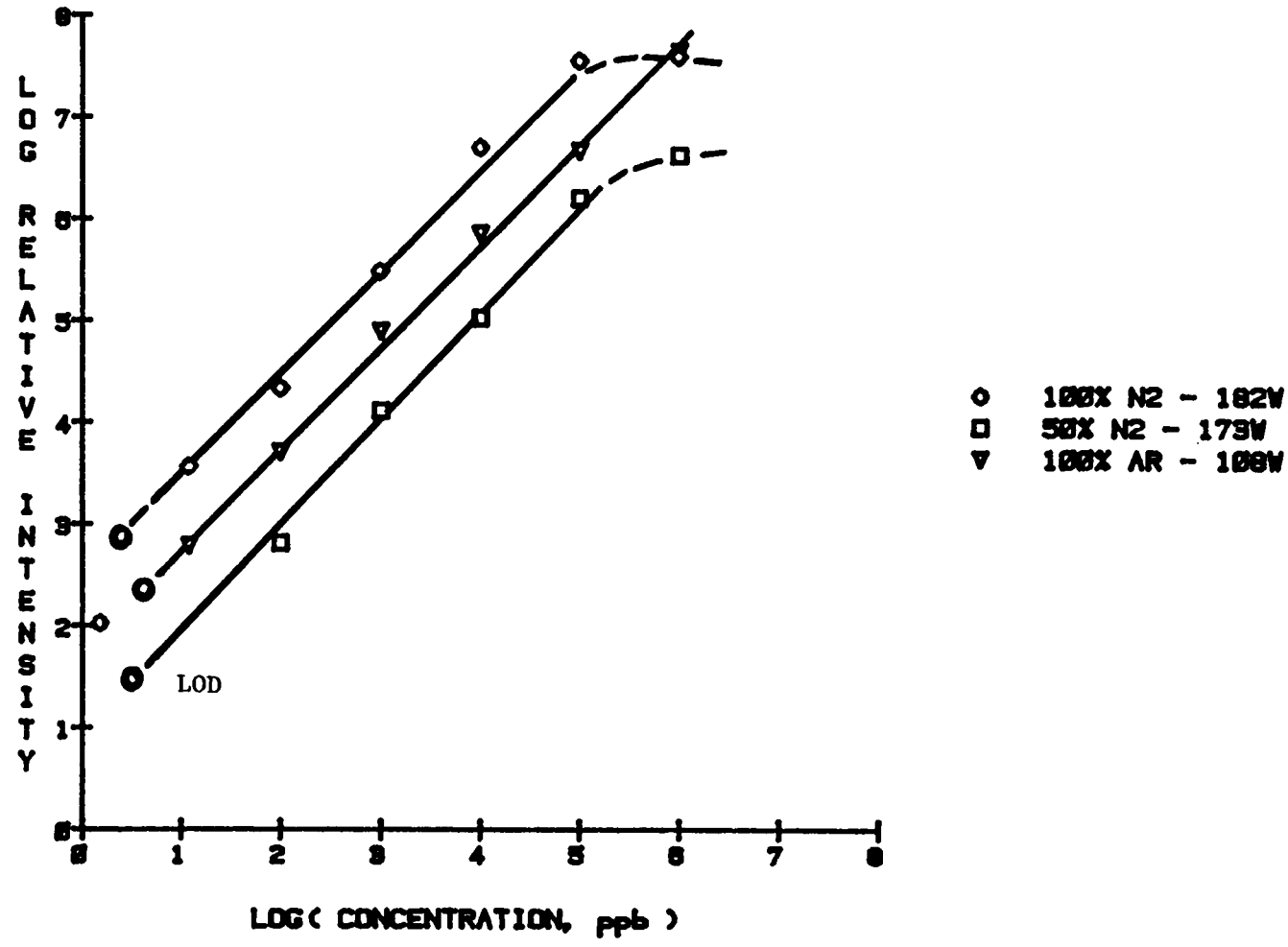

Figure 99. Sodium Atom Emission Working Curves - in Argon, Nitrogen, and Mixed Plasmas.

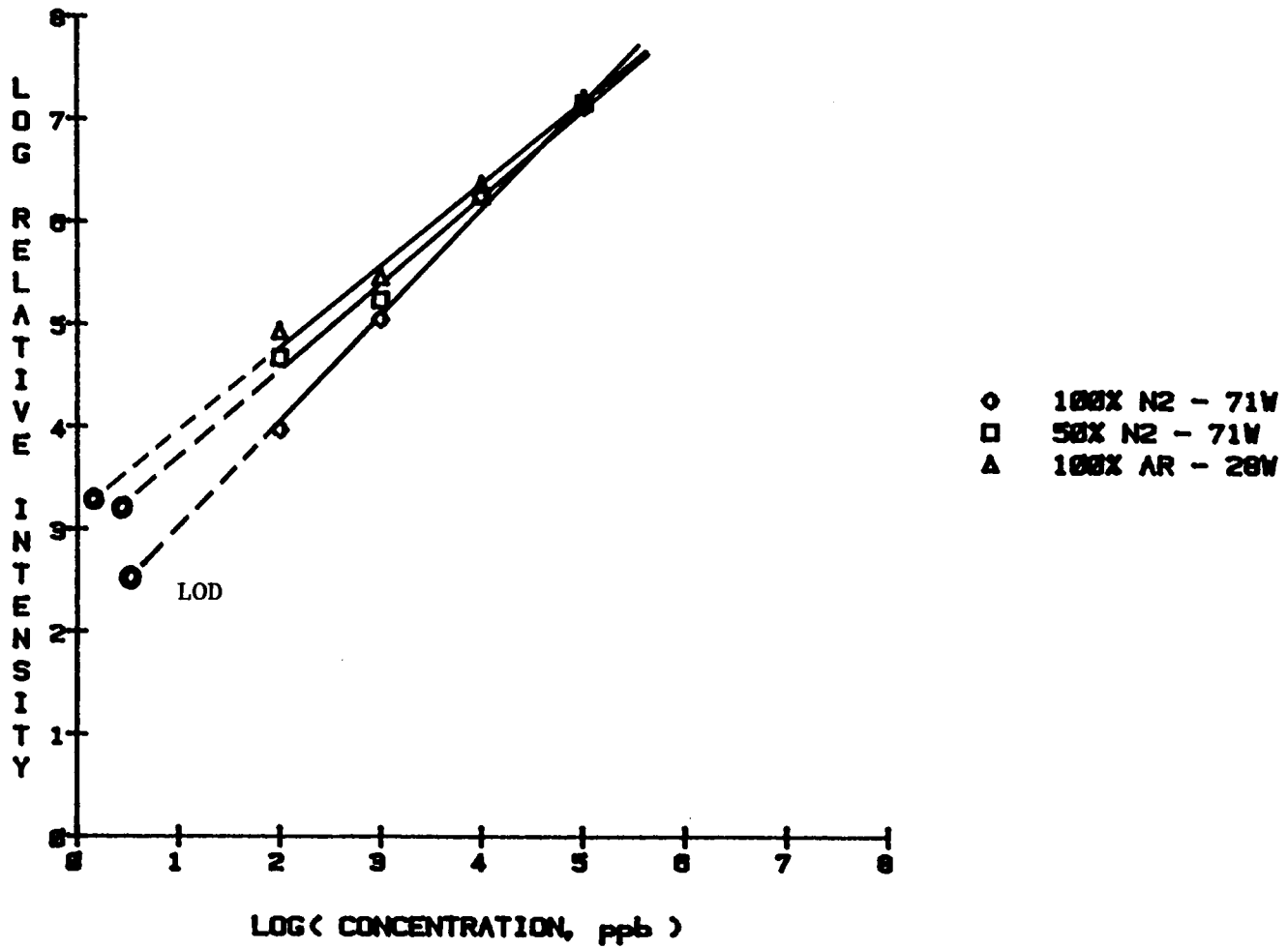

Figure 100. Sodium Atom Fluorescence Working Curves - in Argon, Nitrogen, and Mixed Plasmas.

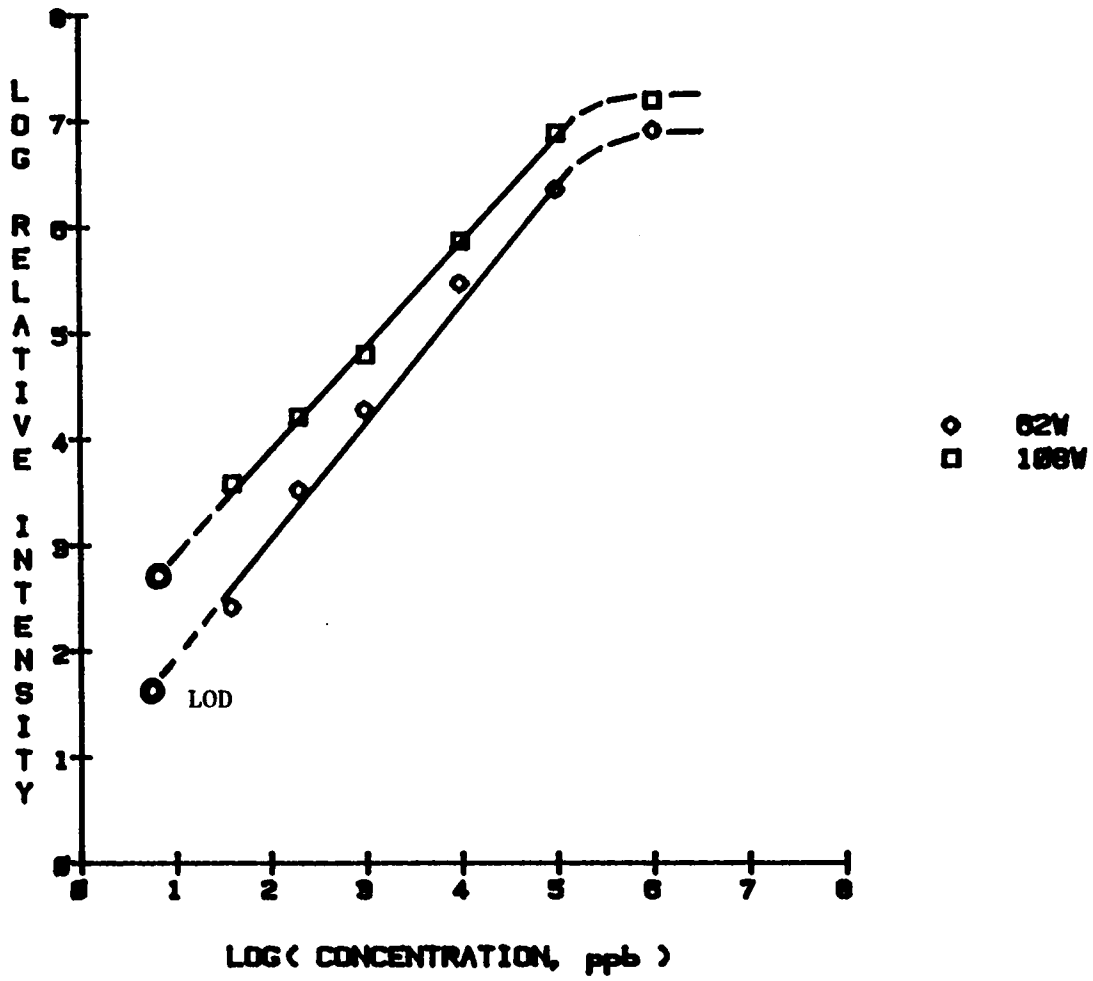

Figure 101. Barium Ion Fluorescence Working Curves - in Argon, at 2 Different Powers

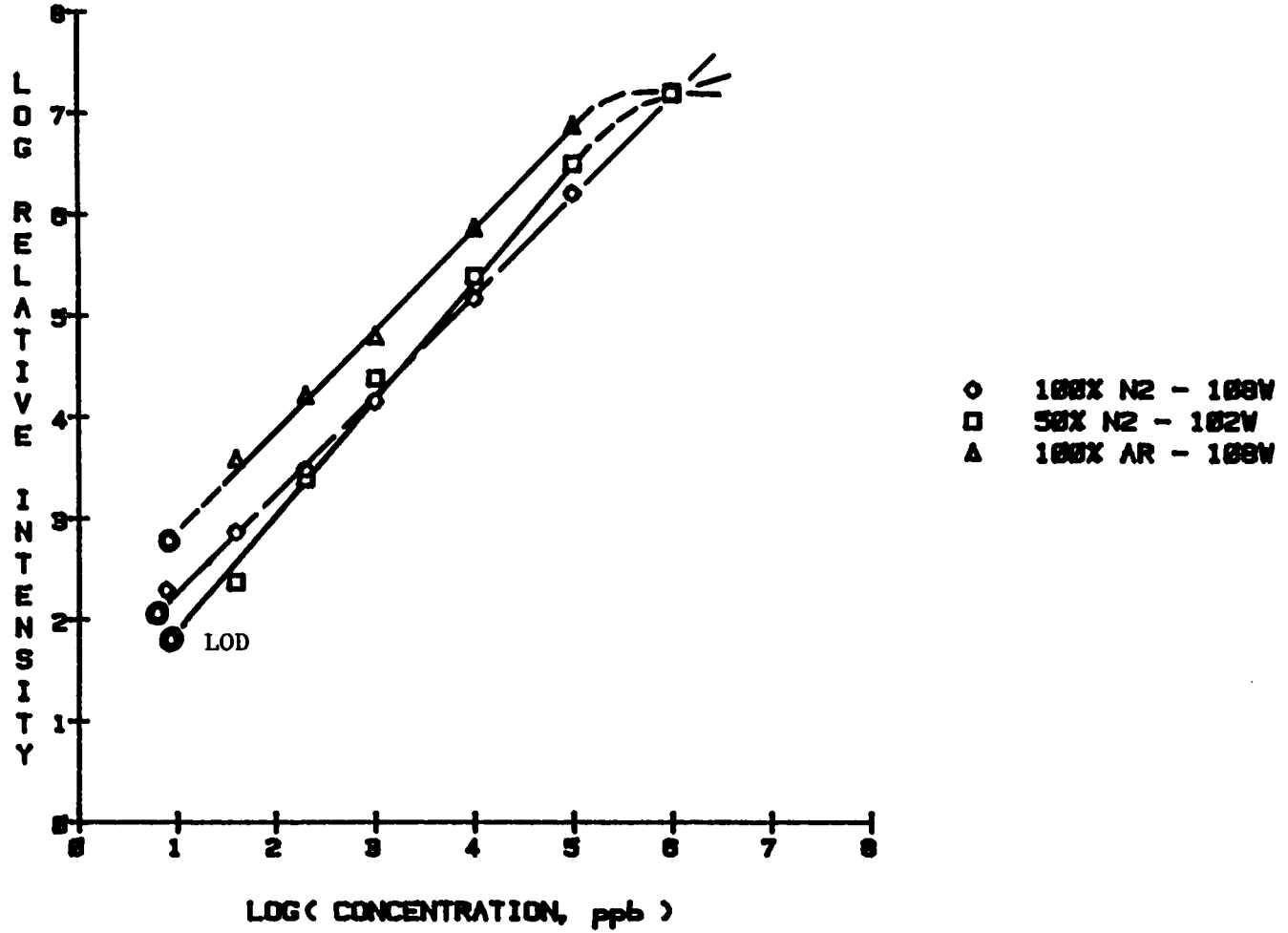

Figure 102. Barium Ion Fluorescence Working Curves - in Argon, Nitrogen, and Mixed Plasmas.

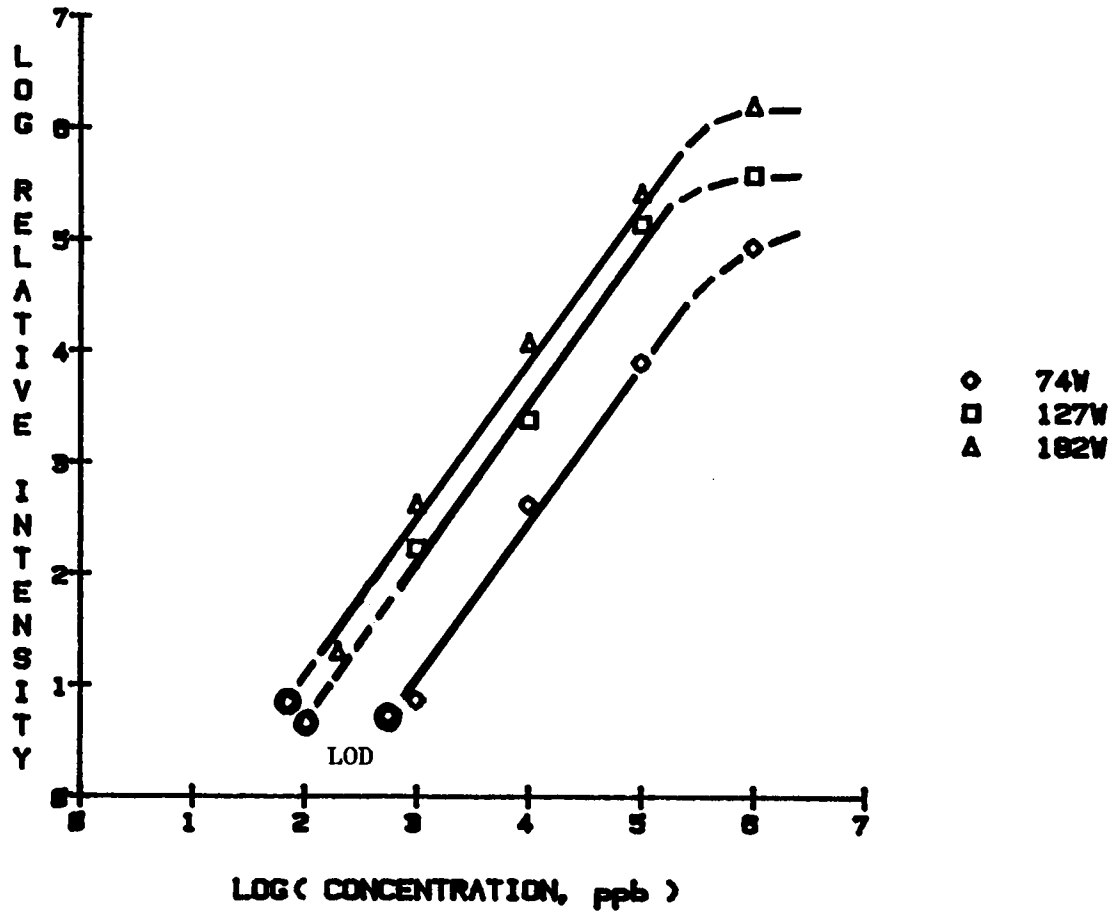

Figure 103. Barium Atom Emission Working Curves - in Nitrogen, at 3 Different Powers.

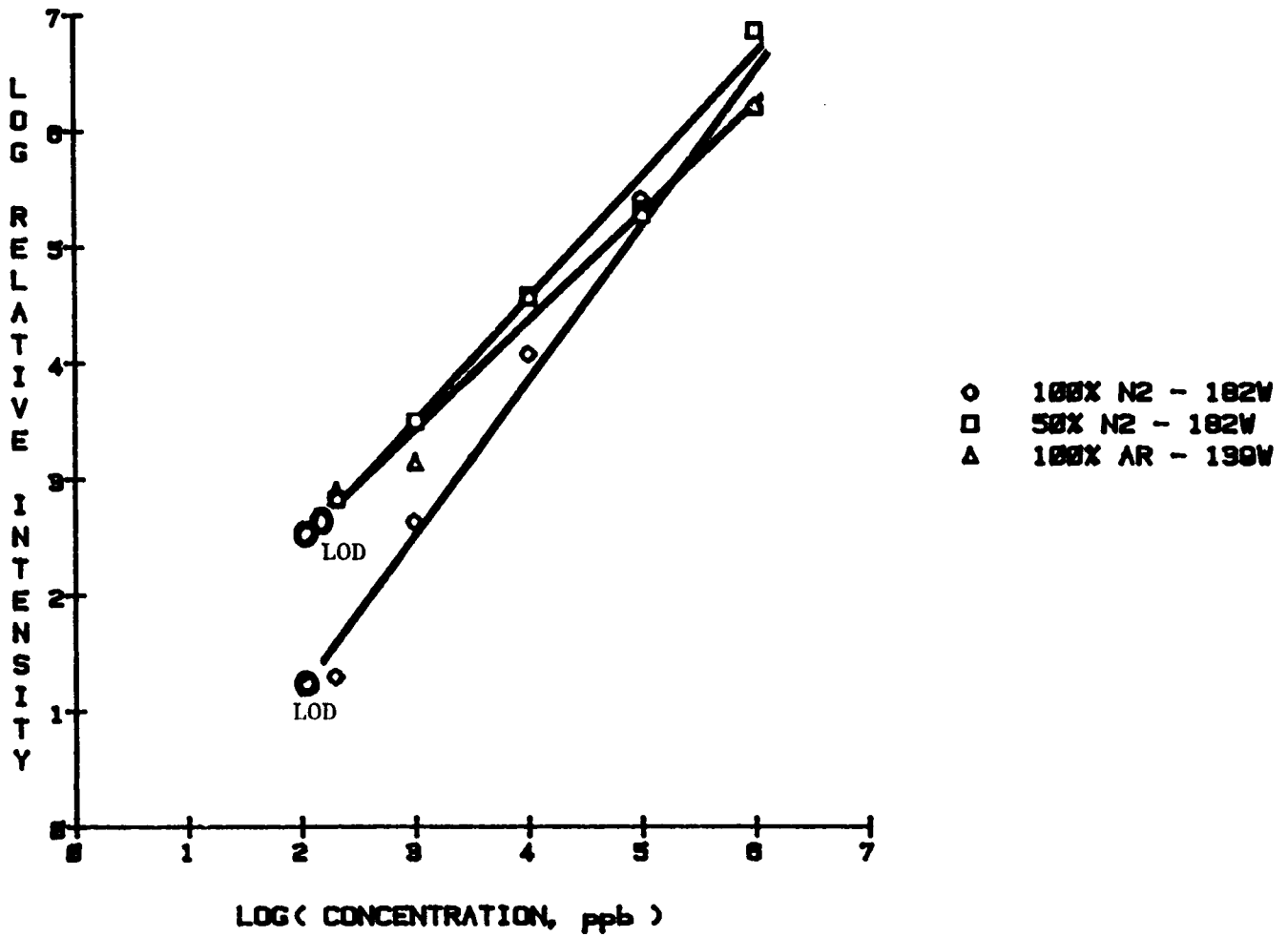

Figure 104. Barium Atom Emission Working Curves - in Argon, Nitrogen, and Mixed Plasmas.

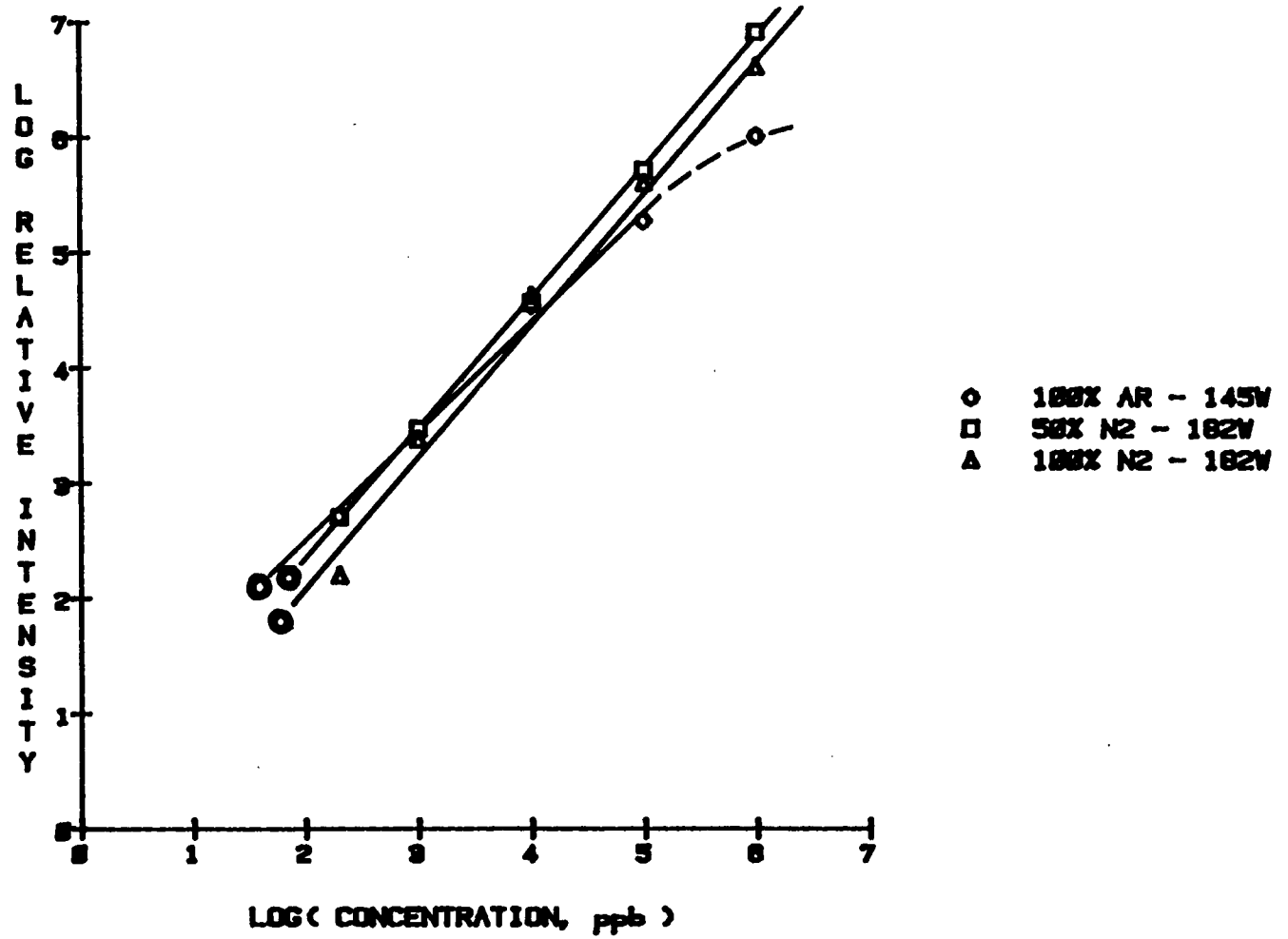

Figure 105. Barium Ion Emission Working Curves - in Argon, Nitrogen, and Mixed Plasmas.

Comparison of Experimental LODs with Literature Values:

These limit of detection studies show that the method gives results that are comparable to other more elaborate and expensive methods, such as ICP-AES, flame-AES, flame-AFS, and ICP fluorescence methods using both lasers and hollow-cathode lamps.

There are many problems associated with comparisons of LODs measured in different laboratories, on different designs of instrumentation, by different investigators. Different flame conditions, different wavelengths used for fluorescence excitation and observation, different flow rates, and different applied plasma powers are among some of the most obvious experimental variables that can vary from one laboratory to another. Such problems can be lessened through better specification of experimental conditions. investigators sometimes report or omit LOD's in such a way as to make their own appear better. The comparisons shown here represent a compilation of the most recent citations in Chemical Abstracts (On-line Search), and the current major analytical journals: Analytical Chemistry 1977-1986; Applied Spectroscopy 1979-1986; Spectrochimica Acta 1980-1986.

Sodium Detection Limits - Parts Per Billion

Table 14. Comparison of Best LODs with Current Literature LODs - Sodium

Method	Na detection limit (ng/mL)	reference
Conventional Spectroscopy		
Flame - AAS	0.2	(143)
Flame - AES	0.01	(143)
ICP - AES	0.1	(143)
MIP - AES	2	(144)
MIP - AES	4	This Work
Fluorescence Spectroscopy		
Flame - AFS - HCL excitation	500	(145)
ICP - AFS - HCL excitation	1	(145)
MIP - AFS - HCL excitation	10	(144)
Flame - AFS - laser excitation	0.3	(113)
ICP - AFS - laser excitation	0.1	(113)
MIP - AFS - laser excitation	0.3	This Work

Barium Detection Limits - Parts Per Billion

Table 15. Comparison of Best LODs with Current Literature LODs - Barium

Method	Ba detection limit (ng/mL)	ref.
Conventional Spectroscopy		
Flame - AAS	8	(143)
Flame - AES	1	(143)
ICP - AES	0.01	(143)
MIP - AES	18	(144.)
MIP - AES	79	This Work
Fluorescence Spectroscopy		
Flame - AFS - HCL excitation	220	(107)
ICP - AFS - HCL excitation	500	(145)
MIP - AFS - HCL excitation	18	(144)
Flame - AFS - laser excitation	0.7	(110)
ICP - AFS - laser excitation	6	(113)
MIP - AFS - laser excitation	9	This Work

IV - FINAL SUMMARY AND CONCLUSIONS

High-Efficiency Molecular Microwave Plasma Development:

The research described in this dissertation provides a foundation for further development and application of molecular microwave plasmas at one atmosphere for atomic analysis. The atom source developed provides a significant power-saving improvement on all previous microwave molecular plasma sources. It is easy to operate, consumes much less gas, and costs considerably less than it closest competitor, the ICP. The plasma's ability to desolvate aqueous solutions introduced directly into it, and to do this efficiently using low-power excitation conditions, gives it significant advantages over all previous molecular MIP's. Power transfer is such that the same excitation energies are attained as MIP's requiring 2-3 times more applied power.

Nitrogen plasmas in the Highly-Efficient Molecular Microwave Plasma "HEMMP" cavity have certainly more than enough energy available for atomization, and sufficient energy available for ionization and excitation of analytes. The frequency tuning and impedance matching properties of the cavity are relatively insensitive to alterations in support gas flow rate, applied microwave power, and introduction of aerosol. Nitrogen-containing gaseous plasmas are close to local thermodynamic equilibrium. Analyte excitation occurs by a predominantly thermal mechanism. However, there are also many "non-thermal" excitation processes caused by plasma species having much more than the average plasma thermal

energy. The principal excitation mechanisms operating in these plasmas are still not definitively known.

Analytical Applications of The HEMMP Cavity:

Analytical feasibility studies conducted in this work using laser-induced fluorescence, emission spectroscopy, and laser-enhanced ionization indicate that it is competitive with or equal to all commonly used techniques for atomic analysis. This work provides the physical and chemical background studies necessary to use atmospheric pressure MIP's for chemical analysis using LIF. The physical studies allow the initial selection of instrument operating conditions that produce the best analytical results.

One very important aspect of this work has been the direct comparison of LIF results with AES results, particularly analytical detection limits. A common difficulty when comparing detection limits for these two techniques measured in different laboratories is that optical system specifications are usually not identical. Variables such as optical collection efficiencies, geometries, detector sensitivities, gain, or spatial and electronic filtering are not always completely specified or possible to duplicate. Hence this direct comparison, using the exact same optical system for both methods, is timely.

The feeling of many analytical chemists is that these instrument and money-intensive projects are "curiosities", or novelty items designed to find yet another application for a laser. Others feel that these instrumental "tour de force" experiments will be replaced by simpler, cheaper, and less instrument-intensive physical and chemical sensor methods. However, atomic spectroscopic methods will not be replaced because of the great analytical flexibility they offer. The methods are tried and proven, and give good, reliable results,

As engineering improvements and cost decreases occur for lasers and light sources, ultrasensitive laser-based methods, will become more commonplace. Hollow-cathode lasers and atomic resonance-line lasers are particularly promising (147). They represent cheaper

sources of laser light perfectly suited for atomic spectroscopy. As element-specific line sources, they offer all the advantages of hollow-cathode lamps plus the advantages of a laser. These sources may one day allow laser-based fluorescence and ionization methods to become a routine ultra-high sensitivity technique.

The enormous differences between atomic and molecular plasmas make an exact comparison between the two types of plasmas very difficult, except in qualitative, phenomenological, practical, and functional ways. Initial phenomenological comparison of the two plasmas, with supporting theoretical interpretations, is one of the thrusts of this work. Future experimental investigations would assist in establishing the exact relationship of the argon MIP to the nitrogen-based MIPs. Further optimization of the cavities used for argon studies is the focus of work being carried out elsewhere (N.C. State, C. Boss et al.). This work's primary focus was on nitrogen plasma development and characterization.

More experiments and research need to be done in order to fully exploit the potential capability of MIP's as atom sources for laser induced fluorescence and atomic emission spectroscopy. With further optimization, detection limits can be improved, and linear dynamic ranges can be extended. Further improvements to MIP's, particularly to power transfer efficiency, will allow it to compete directly with inductively coupled plasma emission and atomic absorption spectroscopies as the methods of first choice in the analyst's arsenal.

V - APPENDICES

A) INSTRUMENT AUTOMATION

1) AUTOMATION OF SCANNING MONOCHROMETER

Hardware Interfaces - Descriptions and Schematics

This appendix describes a general-purpose digital stepping motor interface. The interface directly connects a DEC/DRV11 parallel board in a DEC LSI-11 microcomputer to an AIRPAX Model 82821-P2 stepping motor. It consists of two separate printed circuit boards. The first is a controller board that handles address decoding, clock pulse generation, motor start/stop signals, direction setting, step countdown, and electromechanical limit detection with automatic motor halt. The second printed circuit board is a stepper motor driver board. It contains a motor driver chip that provides the proper coil synchronization signals and currents to drive the motor. It also converts the controller board's TTL signals into the 12 volt signals needed by the motor. The circuitry was adapted from a design by James T. Currie (135). It was modified to include electromechanical limit detection, and to provide count-to-zero detection so the motor can be reloaded if necessary.

The software that drives the stepping motor interface was written by the author so as to be self-explanatory, containing many in-line comments. The software listings are given in the next section. A brief discussion of the interactions between the hardware and software is given in this section as the hardware description proceeds. The software scans the monochrometer over user-selectable wavelength ranges, while at the same time driving the X-axis of an XY-recorder, which plots the spectra from the monochrometer can be plotted. The software provides instructions to the operator about the sequence of operations of the system and the status of the moter (indicating whether or not it is operating or not). It signals the operator when the limits of the monochrometer have been reached. It also provides some error flagging for improper input by the operator.

Circuit Descriptions

Parallel Board Bit Assignments and Interface Control Codes The bit assignments of the output register (address = 167772) and status register (address = 167770) of the parallel interface are shown in Figure 106 on page 264The four possible interface control functions are also shown. These functions are: 1) halt the motor, 2) load the counter with the number of steps, 3) set motor direction = CW or CCW, 4) Start motor turning. These function codes, when loaded into the output register, operate the stepper motor.

Interface Address Detection and Device Select Circuitry:

The upper part of Figure 107 on page 266 shows the DIP switch-selectable address detection circuitry connected to bits 13 thru 15 of the DRV11 parallel board. It is possible to have up to 8 of these stepping motor interfaces connected to the same parallel board. IC-U6 requires logic "0" on all of its inputs in order to produce a logic "1" on its output, signaling a address "match" condition. Such a match condition occurs only when the logic levels of bits 13, 14, and 15 of the parallel board all match the logic levels of the switches SW1. After the address is sent through the parallel board, the NDR (New Data Ready) signal is sent out by

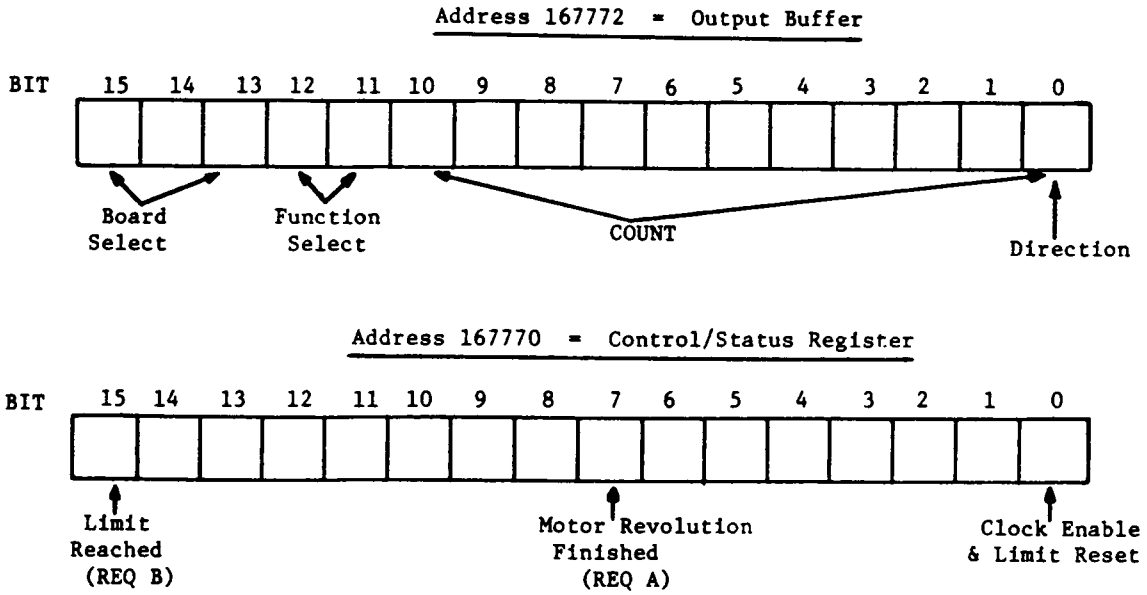

Control Sequence Codes For Address 167772

000000_8 - - - - - - - Halt Motor Movement

010000_8 + octal count - - Load Counters with Number of Steps

4000_8 or 4001_8 - - - - - Set Motor Direction = CCW or CW

140000_8 - - - - - - - Start Motor Turning

Figure 106. DEC-DRV11 Parallel Board Bit Assignments

the parallel board. These two signals are combined to produce a device select pulse for triggering the function select circuitry of controller board. Once this board is selected, bits 11 and 12 of the parallel board select one of the four possible control functions.

Some problems were encountered with the NDR pulse not being long enough to operate the 74155 function decoder (IC-U7 in Figure 108 on page 267) The settling time of the select lines is longer than the length of NDR. The 74121 monostable multivibrator stretches the NDR pulse so that it IS longer than the settling time.

There is a particular sequence the stepper motor driver chip (SAA1027) requires so the poles of the motor are set up properly. The stepper motor driver chip must be "SET" before movement starts, but **after** direction is selected. In this circuitry the "SET" pulse is sent to the SAA1027 drive board at the same time the counters receive their "LOAD" pulse. Thus the proper sequence of operations is accomplished by: 1) setting the direction, 2) loading the counters, and 3) starting the motor. Once this is done, the direction does not need to be set again until it is reversed. The counters can be reloaded immediately after counting down to zero. The 11-bit count register makes 2048 motor steps possible with one loading of the counters. One revolution of the motor occurs for every 480 steps. Thus approximately 5 revolutions are possible before reloading is necessary. Since the full count of 2048 steps is not an exact multiple of motor revolutions, a routine called ONETRN was written to turn the motor a single revolution at a time. After one revolution, a borrow pulse from the counters to the REQ A input flag (bit 7 of the parallel board) signals the computer to reload the counters. A flag check on REQ A signals the program whenever the counters count down to zero. The software keeps track of the number of revolutions by decrementing a variable called REVS. As long as this variable is nonzero at the end of a revolution, the counters are loaded another time.

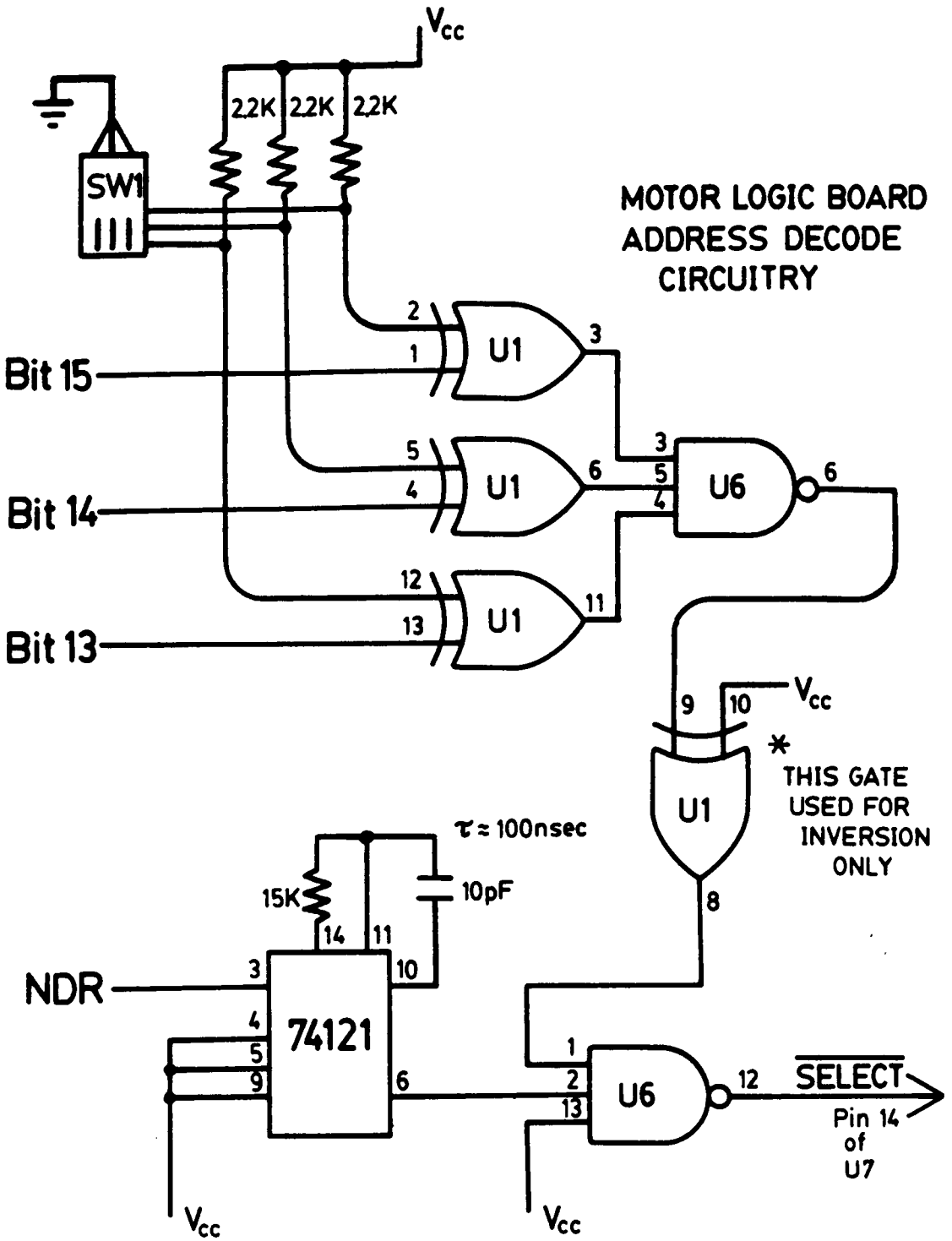

Figure 107. Stepping Motor Controller Device Select Circuitry

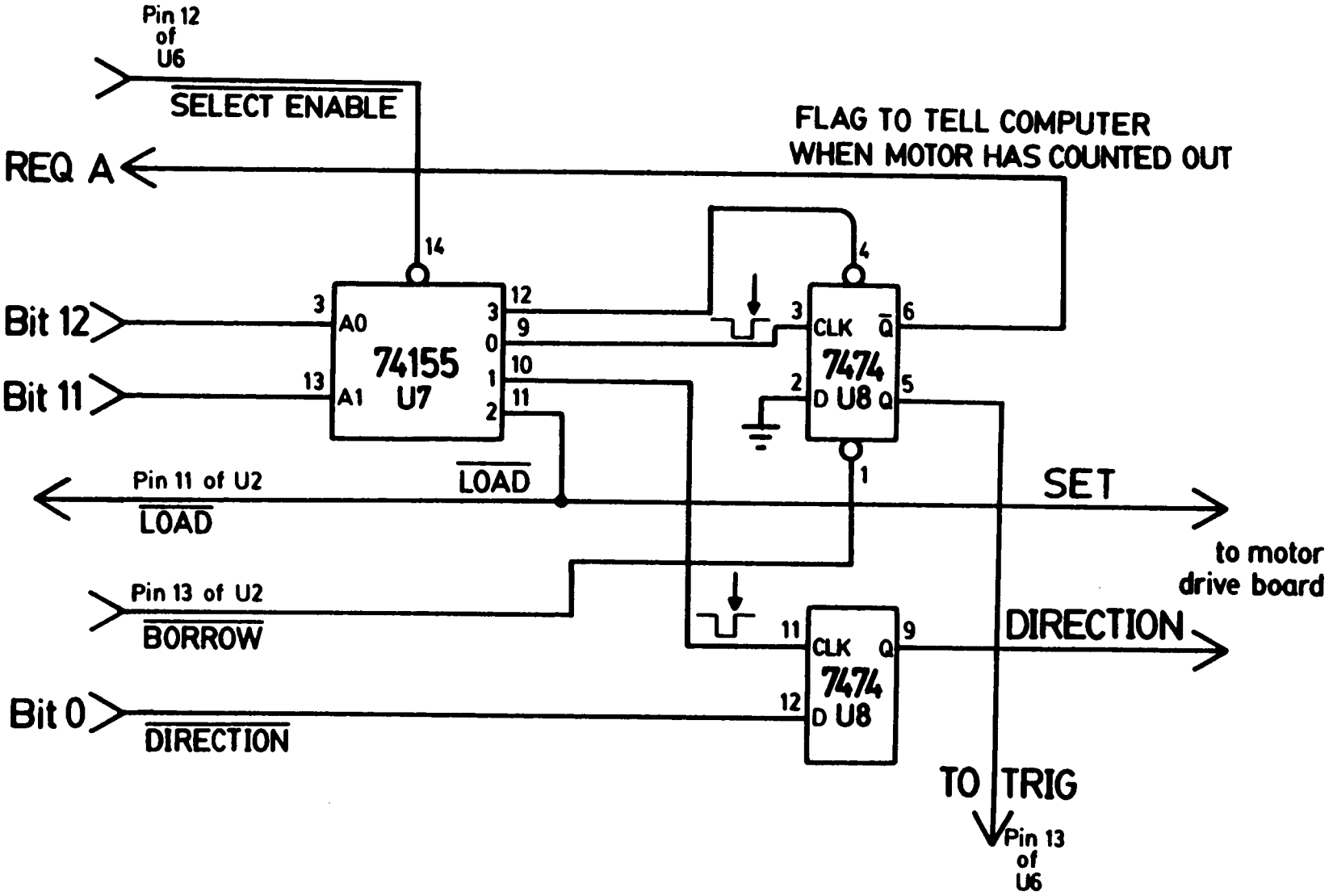

Figure 108. Stepping Motor Function Select Circuitry

After the desired number of revolutions are complete, the operator is prompted for one of three options: 1) repeat the same scan, with the same number of turns, after moving the motor to the beginning of that scan, 2) continue scanning in the same direction, with either the same number of turns, or a different number set by the operator at that time, or, 3) quit, and return the motor to its zero position at the directional limit.

Electromechanical Limit Switches and Clock Generator Circuitry:

If the motor reaches either one of the monochrometer drive's mechanical limits, it needs to be stopped instantaneously to prevent possible damage. Two microswitches were mounted with epoxy in the correct positions on the underside of the monochrometer. These switches halted the motor whenever a limit was reached. The circuitry shown in the bottom half of Figure 109 on page 269 is used to "debounce" the microswitches. The 555 monostable multivibrator generates a triggering edge when the switch closes, but no triggering pulse when the switch opens (as the monochrometer sinebar drive moves away from one of its limits). This is necessary because otherwise the trigger pulse from switch opening makes it appear as though another limit has just been hit, thus making impossible to ever move the sinebar drive away from the limits. The trigger edge sets the flip-flop (IC-U10) that monitors the limit switches. The output of this flip-flop is monitored as a flag check by REQ B; this is done after every time the motor reload flag is checked. The moment a limit is hit, the clock to the motor drive board is disabled. The clock must be re-enabled to move the motor away from the limit position. The CSR1 control signal (bit 1 of the control/status register CSRBUF, address = 167770) is used to generate a negative-going pulse that clears the limit switch flip-flop.

The clock is generated by a 555 monostable multivibrator operating in free-run mode. This is shown in Figure 109 on page 269. The clock is then fed into a NAND gate on IC-U6. This NAND gate passes the clock to the drive board and can be disabled by either the STOP signal from the 74155 function selector, or by the signal from the limit switch circuitry.

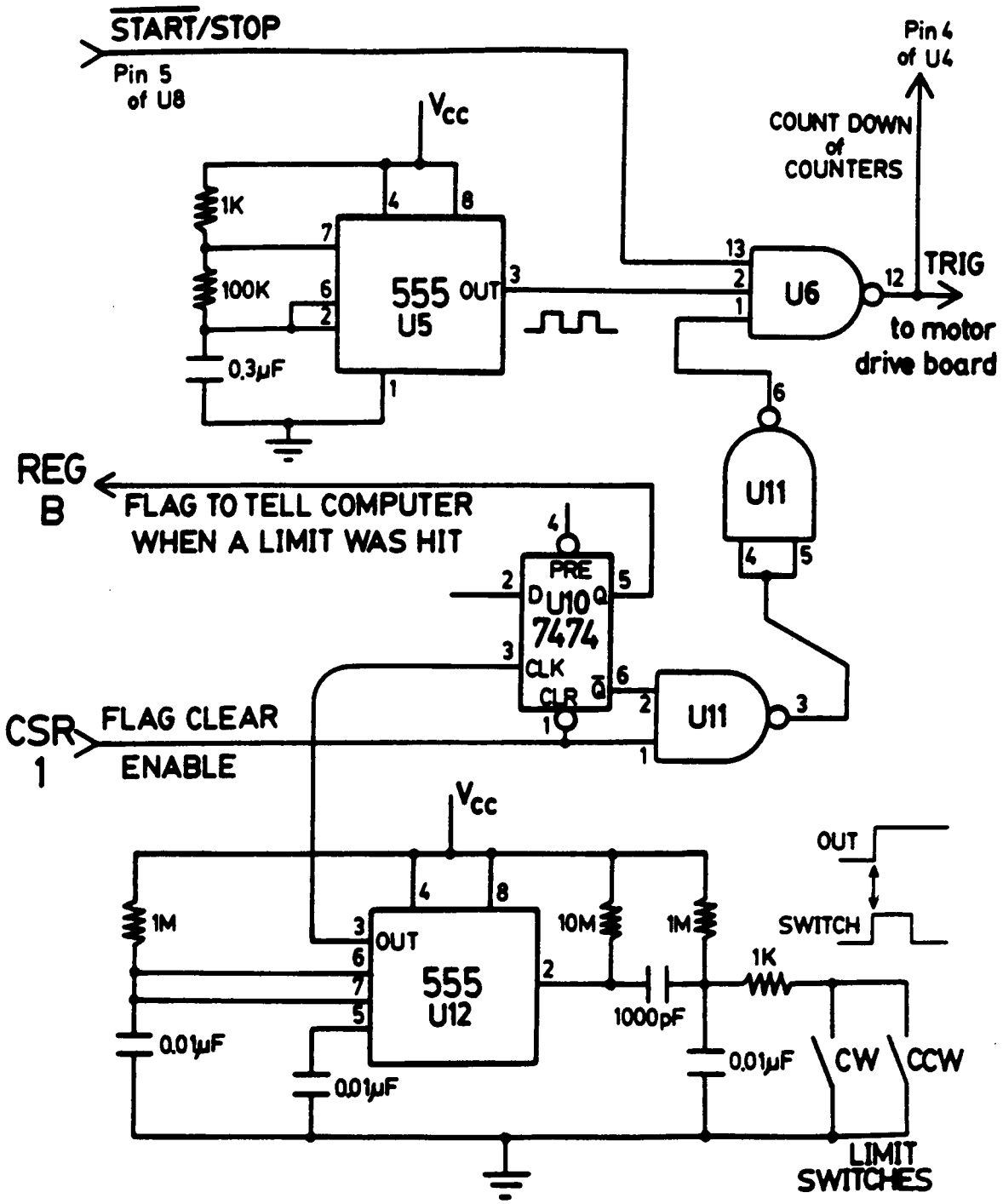

Figure 109. Stepping Motor Clock Circuitry and Limit Detect Circuitry

Counter Circuitry:

An 11-bit counter was made by cascading three 4-bit TTL binary (74193) counters. These counters keep track of how many steps the motor has turned. They are loaded using bits 0 thru 10 of the DRV11 parallel board. They can be cleared by loading them with a count of zero, or by an INIT pulse from the parallel board that occurs during power-up.

Stepper Motor Driver Board Circuitry:

This board translates the clock, direction, and load signals from the controller board into the TRIG, DIR, and SET signals needed by the SAA1027 stepper motor controller chip. It also converts the +5V TTL signals from the controller board into +12V signals the controller chip uses to drive the motor. This circuitry is shown in Figure 111 on page 272.

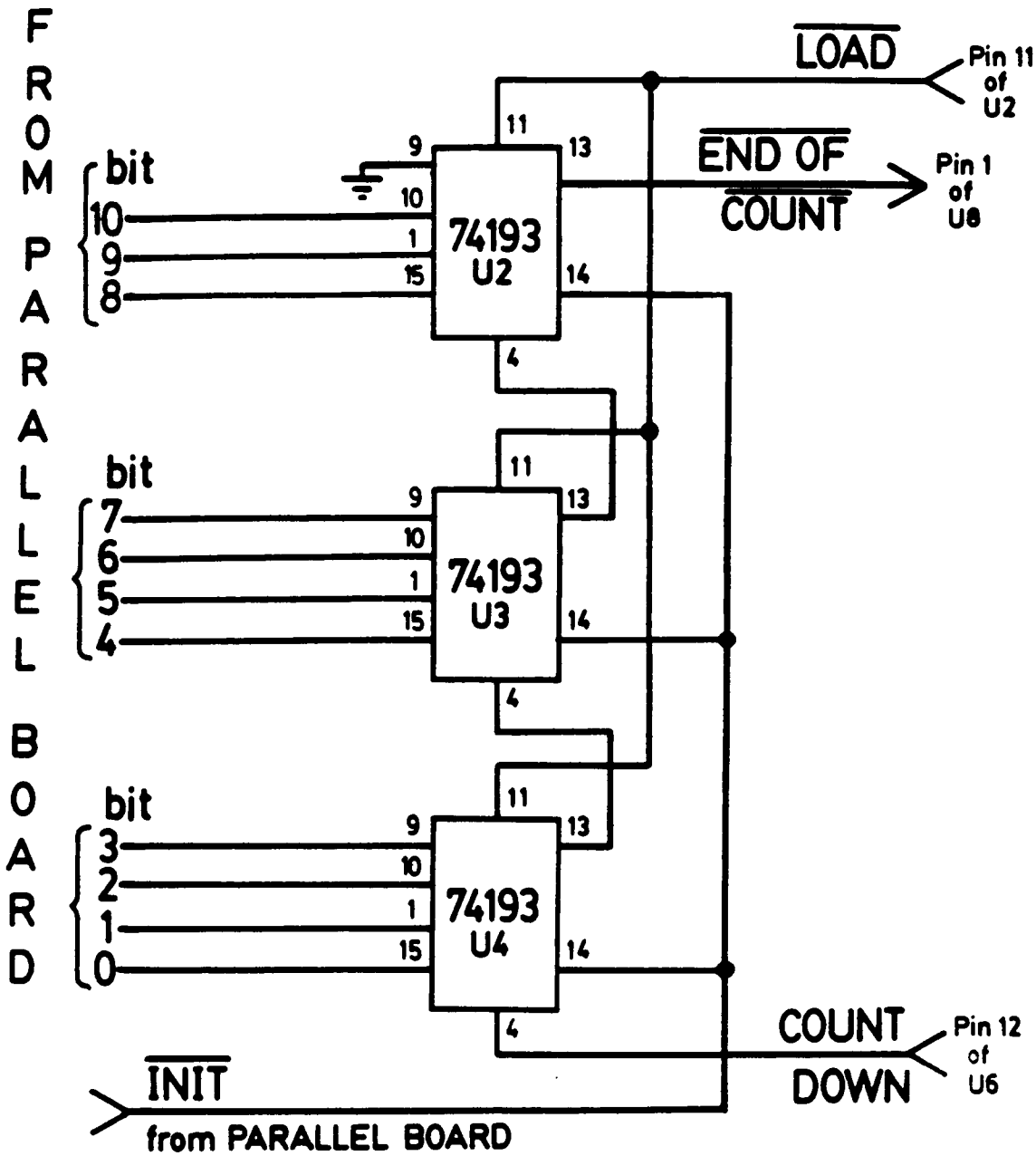

Figure 110. Stepping Motor Counter Circuitry

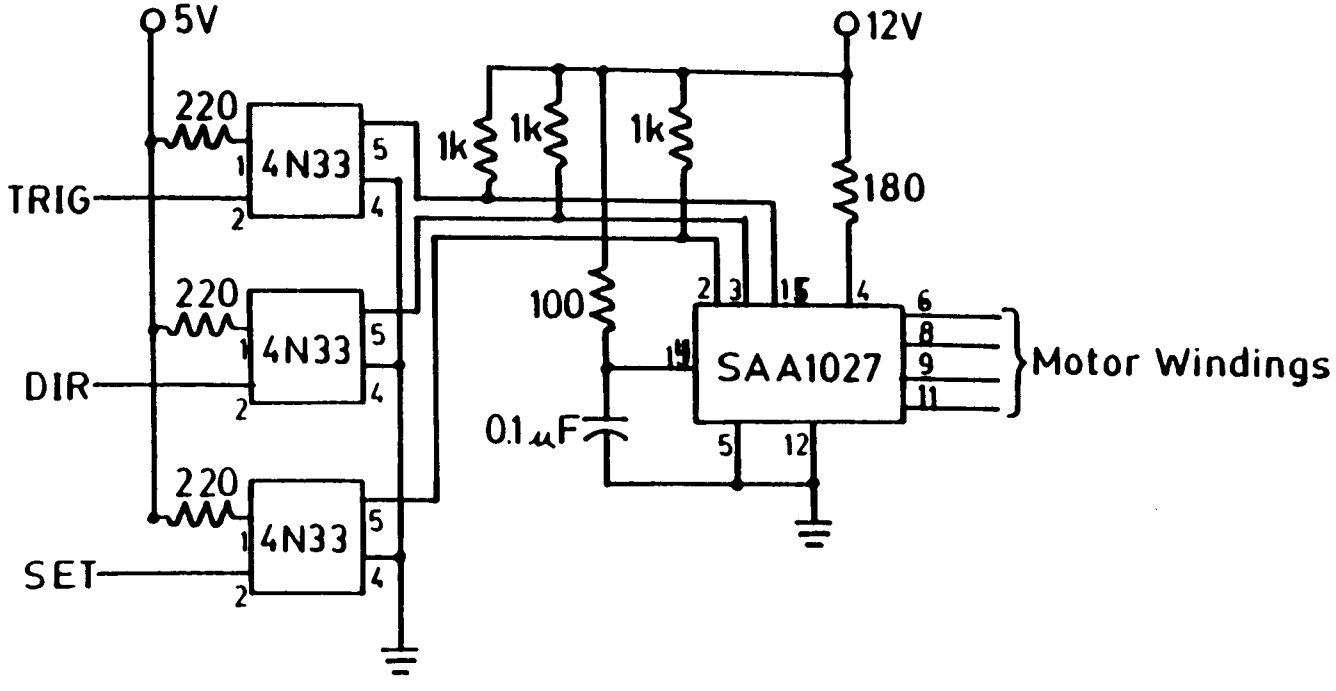

Figure 111. Stepping Motor Power Driver Board Circuitry

```
        .TITLE SPECTR.MAC

;***                                                          ***
;*** SPECTROMETER SCANNING PROGRAM - RICH LYSAKOWSKI - 2/23/84 ***
;***                                                          ***

;THIS PROGRAM SCANS A PERKIN-ELMER MODEL 980 UV/VIS MONOCHROMETER,
;AND CONTROLS THE X-AXIS OF AN X-Y RECORDER.

;THE OPERATOR CAN SELECT THE BEGINNING SCAN POSITION, THE SCAN
;   WIDTH IN 10 NONAOMETER INCREMENTS, AND SCAN DIRECTION.
;IT SCALES THE OUTPUT OF A D/A CONVERTOR TO MATCH THE SCAN WIDTH
;   SELECTED BY THE OPERATOR.
;REPEAT SCANS CAN BE DONE WITH THE SAME SCAN WIDTH, FURTHER SCANS
;   CAN BE DONE IN THE SAME DIRECTION WITH THE SAME OR A DIFFERENT
;   SCAN WIDTH, OR A NEW SCAN CAN BE DONE WITHOUT RESTARTING PROGRAM

;A STEPPING MOTOR INTERFACE DRIVEN BY A DRV11 PARALLEL INTERFACE
;   SCANS THE WAVELENGTH CONTROL OF THE MONOCHROMETER.

;CHANNEL 0 OF A DEC AAV11-A D/A CONVERTER INTERFACE DRIVES THE
;   X-AXIS OF AN XY CHART RECORDER.

;THE OUTPUT OF THE MONOCHROMETER DRIVES AN I/V CONVERTER, WHICH
;   DRIVES THE Y-AXIS OF THE XY RECORDER.

;FLAG CHECKS ARE USED TO MONITOR THE NUMBER OF STEPPER REVOLUTIONS.
;REQ A AT A LOGIC 1 SAYS THE PRESENT MOTOR REVOLUTION HAS FINISHED.
;REQ B AT A LOGIC 1 SAYS A PHYSICAL LIMIT HAS BEEN REACHED.
        .LIST ME
        .MCALL  .TTYIN,.TTYOUT,.EXIT,.PRINT,.INTEN
        .MACRO  .ONETRN
                BIS #4000,DIR   ;DIR COMMAND !
                MOV    DIR,@#OUTBUF
                MOV #ONEREV,@#OUTBUF
                MOV #MOVMOT,@#OUTBUF
        .ENDM
        .MACRO .STOPIT
                BIS #4000,DIR   ;DIR COMMAND FOR HARDWARE
                MOV DIR,@#167772
                MOV #HLTMOT,@#167772    ;MOVE ZERO TO COUNTER !
        .ENDM
        DAC0=170440             ;DEFINE CONSTANTS!
        CSRBUF=167770
        OUTBUF=CSRBUF+2
        AVECTR=340
        APSW=AVECTR+2
        BVECTR=344
        BPSW=BVECTR+2
        ONEREV=10740            ;740 OCTAL MOVES MOTOR 1 REV !
        MOVMOT=14000            ;THIS IS THE START COMMAND !
        HLTMOT=10000            ;THIS # CLRS COUNT WHEN USED W/DIR

   ; THE FIRST SEGMENT INITIALIZES AND ENABLES THE MOTOR INTERFACE.

 START: MOV #0,@#167770         ;INITIALIZE OUTBUF,DISABLE INTERRUPTS
                                ; CSR1 = 0, REQ B = 0
        .STOPIT                 ;MAKE SURE MOTOR COUNT IS ZERO !
        BIS #2,@#167770         ;ENABLE LIMIT SWITCHES
```

```
        .TTYOUT #12
        CALL CLRPEN             ;ZERO PEN POSITION !
        .TTYOUT #7
        .PRINT #FORMAT          ;TELL OPERATOR CHAR INPUT FORMAT !
        .TTYOUT #7

  ; THE NEXT SEGMENT ASKS OPERATOR FOR SCAN DIRECTION !

        .PRINT #ASKDR1          ;GET SCAN DIRECTION FROM OPERATOR
        .PRINT #ASKDR2
        .PRINT #ASKDR3          ;TELL OPERATOR WAVELENGTH DIRECTION.
        CALL GETCHR
        MOV R1,DIR
        .TTYOUT #7
        .TTYOUT #12
        .PRINT #QUERY1          ;SKIP OVER MOTOR INITIALIZATION ??
        CALL YESRNO             ;GET RESPONSE FROM OPERATOR
        CMP #116,R1             ;WAS RESPONSE = YES ??
        BEQ HOWIDE              ;YES, SKIP MOTOR POSITION INIT STUFF.
                                ;NO, INITIALIZE MOTOR POSITION.
        .TTYOUT #7
        .TTYOUT #12
        .PRINT #GETLIM          ;TELL OPERATOR MOTOR'S GOING TO LIMIT !
        CALL REVDIR             ;PREPARE TO MOVE TO LIMIT IN DIRECTION
                                ;OPPOSITE TO SCAN DIR !

  ; THE NEXT SEGMENT MOVES MOTOR TO PROPER LIMIT !

TOLIM:  .ONETRN                 ;GET TO LIMIT
        TST @#CSRBUF            ;IS REQ B = 1 ?
        BGE TOLIM               ;NO, WAIT.
        .STOPIT                 ;STOP MOTOR & CLEAR COUNT !
        CALL REVDIR             ;PREPARE TO MOVE IN SCAN DIRECTION !

  ; THE NEXT SEGMENT MOVES THE MOTOR OFF OF THE LIMIT !

        BIC #2,@#CSRBUF         ;START CLEAR PULSE FOR
                                ;ENABLING LIMIT SWITCHES.
        MOV #20,R5              ;DELAY 80 MICROSECS TO STRETCH OUT
1$:     DEC R5                  ;CLOCK ENABLE PULSE !
        BNE 1$
        BIS #2,@#CSRBUF         ;FINISH ENABLING LIMIT SWITCHES

  ; THE NEXT SEGMENT MOVES THE MOTOR TO THE BEGINNING SCAN POSITION !

        .TTYOUT #7
        .PRINT #SCANBG          ;STARTING WAVELENGTH = ?
        CALL GETCHR             ;IT MUST BE INPUT AS THE # REVS
                                ;AS THE # REVS FROM THE LIMIT !
        CMP R1,#0               ;START FROM THE LIMIT ?
        BEQ HOWIDE              ;YES, IGNORE NEXT 8 LINES !
        MOV R1,REVS             ;NO, START MOVING OFF THE LIMIT !
WAVBEG: .ONETRN
5$:     TSTB @#CSRBUF           ;TEST REQ A TO SEE IF 1 REV DONE !
        BGE 5$                  ;NO, WAIT !
        CMP #0,REVS             ;ALL REVS DONE ?
        BEQ HOWIDE              ;YES, PRINT SCAN WIDTH MESSAGE !
        CALL RELOAD             ;NO, START ANOTHER REV !
        BR 5$                   ;GO BACK, WAIT FOR NEW REV TO STOP !
```

```
        CALL CLRPEN             ;       THIS WILL STOP STARTUP PROBLEM
                                ;WITH THE CHART RECORDER !

 ;THE NEXT SEGMENT SETS UP FOR THE MONOCHROMETER SCAN !

HOWIDE: .PRINT #SCANWD          ;ASK FOR SCAN WIDTH !
        CALL GETCHR             ;REVS IS REASSIGNED WITH SCAN WIDTH!
        MOV R1,REVS             ;GET READY FOR SPECTRUM & CHART SCAN
        MOV R1,REPEAT           ;SAVE SCAN WIDTH FOR REPEAT SCANS !
        CALL LOOKUP             ;GET DAC DELAY THAT GOES WITH SCANWD !
        CMP DELAYS(R0),#-1      ;HAS WHOLE TABLE BEEN SEARCHED ?
        BEQ ERROR               ;YES, MATCH NOT FOUND, TELL OPERATOR !
        BR IGNORE               ;NO ERROR, IGNORE ERROR MESSAGE PRINT !
ERROR:  .PRINT #ERRMSG
        BR HOWIDE               ;GET CORRECT SCAN WIDTH !
IGNORE: MOV DELAYS(R0),DELAY    ;PUT DELAY TABLE VALUE INTO
                                ;THE VARIABLE "DELAY".
 ; ************** THIS IS THE MEAT OF THE PROGRAM ******************
        CLR R4
SCANST: CALL CLRPEN             ;ZERO PEN POSITION !
        .PRINT #PROCED          ;ASK OPERATOR TO PROCEED !
        CALL YESRNO             ;WAIT FOR OPERATOR ENTRY !
        .STOPIT                 ;CLEAR MOTOR COUNT !
        .ONETRN                 ;START MOTOR
NEXTPT: INC R4                  ;MOVE X AXIS TO NEXT POINT !
        MOV R4,@#170440         ;OUTPUT NEXT POINT !
        TSTB @#CSRBUF           ;SEE IF MOTOR NEEDS RELOAD !
        BGE 5$                  ;NO, GO TO NEXT POINT !
        CALL RELOAD             ;YES, RELOAD MOTOR !
5$:     MOV DELAY,R3            ;DELAY BEFORE NEXT X AXIS POINT
4$:     DEC R3                  ;IS OUTPUT !
        BNE 4$                  ;WAIT FOR DELAY TO FINISH !
        CMP #7777,@#170440      ;DON`T LET CHART RECORDER OVERRUN !
        BEQ OVRRUN              ;PRINT CHART OVERRUN MESSAGE !
        CMP #0,REVS             ;ALL REVS DONE ?
        BEQ STOP                ;YES, STOP !
        BR NEXTPT               ;NO, GO TO NEXT X AXIS POINT !
OVRRUN: .PRINT #CHRTMX
        BR QUIT                 ;NO USE CONTINUING ! ***********
STOP:   .TTYOUT #12
        .PRINT #FINISH          ;YES, OUTPUT SCAN DONE MESSAGE !
        .PRINT  #AGAIN          ;SCAN AGAIN WITH SAME PARAMETERS?
        .PRINT #NEWSCN          ;SCAN AGAIN WITH NEW PARAMETERS ?
        .PRINT #GOMORX          ;CONTINUE SCANNING FURTHER ?
        CALL YESRNO             ;INPUT Y OR N OR C !
        CMP R1,#131             ;IF "Y" RE-SETUP MONOCHROMETER !
        BEQ SAMERN
        CMP R1,#116             ;IF "N" , JUMP TO START AGAIN !
        BEQ RESCAN
        CMP R1,#103             ;IF "C",CALL GOMORE !
        BEQ 5$
        BR RESCAN               ;OTHERWISE, START ALL OVER !
5$:     CALL GOMORE             ;SETUP TO SCAN FURTHER !
        JMP SCANST              ;START CONTINUATION SCAN !
RESCAN: JMP START               ;START ALL OVER AGAIN !

 ; THIS SEGMENT RETURNS MONOCHROMETER TO DO SAME SCAN AGAIN !

SAMERN: CALL REVDIR             ;SETUP TO MOVE TO SCAN BEGINNING !
```

```
        MOV REPEAT,REVS
        DEC REVS                ;MAKES MOTOR RETURN TO BEGINNING OF
                                ;SCAN CORRECTLY  !
BAKTRN: .ONETRN                 ;START RETURN TO SCAN BEGINNING !
1$:     TSTB @#CSRBUF           ;TEST REQ A TO SEE IF 1 REV DONE !
        BGE 1$                  ;NO, WAIT !
        CMP #0,REVS             ;ALL REVS DONE ?
        BEQ 3$                  ;YES, AT SCAN BEGINNING AGAIN !
        CALL RELOAD             ;NO, KEEP STEPPING BACK !
        BR BAKTRN
3$:     MOV REPEAT,REVS         ;RELOAD REVS FOR RERUN !
        CALL REVDIR             ;GO IN PROPER DIRECTION AGAIN !
        JMP SCANST              ;START SCAN AGAIN !
QUIT:   .EXIT


 ; *************** SUBROUTINES START HERE ! *****************

 ; THIS SUBROUTINE ACCEPTS ASCII CHARACTERS 0 THRU 9 FOLLOWED BY
 ;   AN ASCII "D".  AN ASCII-TO-DECIMAL CONVERSION IS DONE FOR #S
 ;   UP TO 65535.  THE RESULT IS LEFT IN REGISTER #1.

GETCHR: CLR R0                  ;BEGINNING OF GETCHR SUBROUTINE !
        .TTYIN
        CMP R0,#15              ;IF CHAR = <CR>, GET NEXT CHAR
        BEQ GETCHR
        CMP R0,#12              ;IF CHAR = <LF>, GET NEXT CHAR
        BEQ GETCHR
        SUB #60,R0              ;DO ASCII TO NUMBER CONVERSION
        CMP #9.,R0              ;WAS ASCII CODE INPUT > 9 DECIMAL ?
        BLT STUPID              ;TRY AGAIN !
        CMP #0.,R0              ;WAS ASCII CODE INPUT < 0 DECIMAL ?
        BGT STUPID              ;TRY AGAIN !
        MOV R0,R1               ;PREPARE FOR MUL INSTRUCTION
NEXT1:  .TTYIN                  ;GET NEXT DIGIT
        CMP R0,#104             ;END IF ASCII LETTER "D" IS
        BEQ OUT                 ; ENTERED !
        MUL #10.,R1             ;MOVE DECIMAL POINT TO THE RIGHT
        SUB #60,R0              ;DO ASCII TO NUMBER CONVERSION
        ADD R0,R1               ;ADD NEXT DIGIT TO RUNNING SUM
        BR NEXT1                ;FINAL N DIGIT NUMBER (DECIMAL)
                                ;RESIDES IN R1
STUPID: .PRINT #NEWNTR
        BR GETCHR               ;START ALL OVER AGAIN !
NEWNTR: .ASCIZ / INPUT AGAIN STUPID, WITH NUMBERS ONLY !!/<12><15>
OUT:    RETURN                  ;RETURN TO MAIN PROGRAM !


 ; THIS SUBROUTINE ACCEPTS "Y" OR "N" OR "C" FOR PROGRAM CONTROL !

YESRNO: CLR R0                  ;CLEANUP INPUT REGISTER !
YNIN:   .TTYIN
        CMP R0,#12              ;STRIP OFF <CR> !
        BEQ YNIN
        CMP R0,#15              ;STRIP OFF <LF> !
        BEQ YNIN
        CMP #131,R0             ;WAS CHAR = "Y" ?
        BEQ SAVCHR              ;YES, SAVE IT !
        CMP #116,R0             ;WAS CHAR = "N" ?
```

```
        BEQ SAVCHR              ;YES, SAVE IT !
        CMP #103,R0             ;WAS CHAR = 'C' ?
        BEQ SAVCHR              ;YES, SAVE IT !
        .PRINT #BADCHR          ;NO, KEEP TRYING !
        BR YESRNO               ;START AGAIN !
SAVCHR: MOV R0,R1               ;FINAL ANSWER RESIDES IN R1 !
        BR QUITIT               ;JUMP TO END OF SUBROUTINE !
BADCHR: .ASCIZ / BAD ENTRY, ENTER 'Y' OR 'N' OR 'C' STUPID ! /
        .EVEN
QUITIT: RETURN                  ;RETURN THRU RT-11 !


 ;THIS SUBROUTINE ALLOWS ONE TO CONTINUE SCANNING FROM THE
 ;   END OF THE LAST SCAN !

GOMORE: .PRINT #MORREV
        CALL YESRNO             ;SAME SCAN WIDTH ?
        CMP R1,#116             ;NO, GET NEW SCAN WIDTH !
        BEQ 1$
        MOV REPEAT,REVS         ;YES, REINSTALL OLD # OF REVS !
        MOV REPEAT,R1           ;PREPARE TO REDO LOOKUP !
        BR GETOUT               ;BYPASS NEW SCAN WIDTH INPUT !
1$:     .PRINT #SCANWD          ;ASK FOR NEW SCAN WIDTH !
        CALL GETCHR
        MOV R1,REVS             ;INSTALL NEW SCAN WIDTH !
GETOUT: CALL LOOKUP             ;GET DELAY TO GO WITH # REVS !
        CMP DELAYS(R0),#-1.     ;HAS WHOLE TABLE BEEN SEARCHED ?
        BEQ ERRER               ;YES, MATCH NOT FOUND, TELL OPERATOR !
        BR NOERR                ;NO, IGNORE ERROR MESSAGE PRINT !
ERRER:  .PRINT #ERRMSG
        BR GOMORE               ;GET A CORRECT SCAN WIDTH !
NOERR:  MOV DELAYS(R0),DELAY    ;PUT DELAY TABLE VALUE INTO THE
                                ;VARIABLE 'DELAY' !
        RETURN                  ;RETURN THRU RT-11 !


 ;THIS SUBROUTINE RETURNS PEN TO ZERO POSITION SLOWLY !

CLRPEN: TST @#170440            ;IS PEN AT ZERO POSITION ?
        BEQ PENZRO              ;YES, BYPASS THIS SEGMENT !!
        DEC R4                  ;NO, DECREMENT PEN POINTER !
        MOV R4,@#170440         ;MOVE TO NEW PEN POSITION !
4$:     MOV #250.,R3            ;SET UP FOR DELAY !
1$:     DEC R3
        BNE 1$                  ;DELAY FINISHED?
        BR CLRPEN               ;YES, DECREMENT PEN POSITION !
PENZRO: RETURN                  ;RETURN THRU RT-11 !


  ; THIS SUBROUTINE TAKES CARE OF TABLE LOOKUPS FOR COORDINATING
  ;     THE MONOCHROMETER SCAN WIDTHS WITH DAC DELAYS !

LOOKUP:                 ;ASSUME R1 = SCANWD NUMBER TO MATCH !
                        ;R0 = OFFSET INTO TURNS TABLE AND
                        ;DELAY TABLE.
                        ;IF R0 = -1, ILLEGAL # TURNS SPECIFIED!
                        ;R2 = DATA ITEM COUNTER !
        MOV #15.,R2     ;SET UP COUNTER !
        CLR R0          ;POINT TO HEAD OF LIST !
```

```
1$:     CMP TURNS(R0),R1         ;MATCH ?
        BEQ 2$                   ;YES, FINISHED SEARCHING !
        TST (R0)+                ;NO, ADVANCE LIST POINTER !
        SOB R2,1$                ;TRY NEXT VALUE FOR A MATCH !
2$:     RETURN                   ;RETURN THRU RT-11 !


  ; THIS SUBROUTINE REVERSES MOTOR DIRECTION ONLY !

REVDIR: BIT #1,DIR               ;DIRECTION (0=CCW,1=CW)
        BEQ GO.CW                ;IF CCW, GO CW
GO.CCW: BIC #1,DIR               ;NOT CCW, GO CCW
        BR CMPDIR                ;
GO.CW:  BIS #1,DIR               ;
CMPDIR: NOP                      ;DIRECTION REVERSED !
        RETURN                   ;RETURN THRU RT-11 !
   ; REQ A MOTOR RELOAD SUBROUTINE STARTS HERE !
RELOAD: DEC REVS                 ;ONE REV HAS OCCURED ALREADY !
        BEQ DONE                 ;ALL REVS DONE ? IF YES, RETURN !
NEWREV: .ONETRN                  ;NO, START ANOTHER REV !
DONE:   RETURN                   ;RETURN THRU RT-11
        .EXIT


  ; ********* NOW START ALL PROGRAM MESSAGES AND PROMPTS !! **********

QUERY1: .ASCIZ / DO YOU NEED TO INITIALIZE MOTOR POSITION ? /<12><15>
FORMAT: .ASCIZ / INPUT ALL VALUES FOLLOWED BY A LETTER "D" ! /<12><15>
ASKDR1: .ASCIZ / WHICH DIRECTION DO YOU WANT TO SCAN ! /<12><15>
ASKDR2: .ASCIZ / TYPE 0 FOR CCW, 1 FOR CW ! /<12><15>
ASKDR3: .ASCIZ / CW SCAN GOES TO LONGER WAVELENGTHS /<12><15>
GETLIM: .ASCIZ / MOTOR SHOULD NOW BE MOVING TO THE LIMIT ! /<12><15>
SCANBG: .ASCIZ / SCAN START IN REVS (0 TO 30 ONLY) FROM LIMIT =  ? /
SCANWD: .ASCIZ / SCAN WIDTH (1 TO 15 ONLY) IN REVS = ? /
PROCED: .ASCIZ / HIT "Y" TO START SCAN ! /<12><15>
AGAIN:  .ASCIZ / HIT "Y" TO SCAN AGAIN WITH SAME PARAMETERS ! /<12><15>
NEWSCN: .ASCIZ / HIT "N" TO SCAN WITH NEW PARAMETERS ! /<12><15>
GOMORX: .ASCIZ / HIT "C" TO SCAN FURTHER IN SAME DIRECTION ! /<12><15>
MORREV: .ASCIZ / SAME SCAN WIDTH DESIRED, (Y OR N) ? /<12><15>
FINISH: .ASCIZ / <********** ! SCAN FINISHED ! **********> /<12><15>

 ; ********** ERROR MESSAGES HERE **********

ERRMSG: .ASCIZ / ILLEGAL SCAN WIDTH ENTERED ! /<12><15>
CHRTMX: .ASCIZ / CHART RECORDER OVERRAN, MAKE DELAYS LONGER ! /<12><15>
        .EVEN
DIR:    .WORD 0
DACVAL: .WORD 0
REVS:   .WORD 0
REPEAT: .WORD 0
DELAY:  .WORD 0
TURNS:  .WORD 15.
        .WORD 14.
        .WORD 13.
        .WORD 12.
        .WORD 11.
        .WORD 10.
        .WORD 9.
        .WORD 8.
```

```
        .WORD 7
        .WORD 6
        .WORD 5
        .WORD 4
        .WORD 3
        .WORD 2
        .WORD 1
        .WORD -1                    ;END OF TURNS TABLE !
 ; THESE ARE THE DELAYS FOR 100 MV/IN GAIN ON CHART RECORDER
  ; THE RC COMBINATION ON THE MOTOR CLOCK GIVES 25 HZ PULSES.
DELAYS: .WORD 3100.
        .WORD 2900.
        .WORD 2700.
        .WORD 2500.
        .WORD 2300.
        .WORD 2100.
        .WORD 1900.
        .WORD 1630.
        .WORD 1400.
        .WORD 1250.
        .WORD 1100.
        .WORD 850.
        .WORD 650.
        .WORD 425.
        .WORD 210.
        .WORD  -1                   ;END OF DELAY TABLE !
        .END    START
```

2) AUTOMATION OF FLUORESCENCE AND EMISSION MEASUREMENT SYSTEM

All data was collected using an DEC LSI-11/03 microcomputer with a DEC Model ADV-11 A/D convertor. The detection system components are described in Chapter IIIB in the body of the dissertation. The software for fluorescence and emission data measurement is written in FORTH. FORTH is an applications programming environment. This means it has the system functions of an operating system, and the programming capabilities of an conventional programming language. The basic FORTH system consists of a set of primitives for arithmetic, stack manipulation, bit manipulation, looping and conditional control functions, disk control, defining new operations, plus many other assorted functions, including a way to write complete assembly language routines. These assembly language routines run almost as fast as native machine-code routines, however, it is much easier to code routines quickly using the FORTH assembler. Learning to use FORTH takes longer than many other conventional computer languages, but once learned, programmer productivity is very high because of the rapidity with which routines can be modified and tested. The modification/testing iteration cycle time is greatly reduced because the code is modular and each module is compiled as soon as it is loaded.

From the FORTH kernel of primitives, the FORTH programmer writes increasingly higher-level definitions, building outward from the kernel like the shells of an onion, eventually being able to execute a single set of very high-level commands that operate an entire experiment, collect, process and report data. Because the scientist defines his own commands, the user software interface can have as much pertinent meaning as possible.

FORTH was used to create an applications-oriented language specifically for the operation of the instrument used to measure LIF and AES signals. James T. Currie wrote the kernel of the data acquisition, display and disk storage and retrieval definitions. His assistance on this task was invaluable. A general overview of the software system is given in the first few blocks of the FORTH listing. More specifics of the command language are given in-line in each of the blocks of code.

Software Interfaces - FORTH Code Listings

```
170 LIST

 0 ( DIRECTORY FOR INSTRUMENT SOFTWARE - BLK#0 )
 1                                                EXIT
 2  BLOCK #  -----------     CONTENTS     ------------------
 3
 4     170-171    DIRECTORY FOR INSTRUMENT SOFTWARE
 5     173-175    INSTRUCTIONS FOR DISK AND DISPLAY ROUTINES
 6     176-177    INSTRUCTIONS FOR DATA ACQUISITION ROUTINES
 7     178        EMPTY
 8     179        DEFINING BLOCK FOR INSTRUMENT SOFTWARE
 9     180        LOAD BLOCK FOR INSTRUMENT
10     181        FETCH-DATA-FROM-DISK ROUTINE
11     182        SAVE-DATA-ON-DISK INITIALIZATION ROUTINES
12     183        SAVE-DATA-ON-DISK ROUTINE
13     184        TTY AND SCOPE DISLAY CODE
14     185        DEFINITIONS USED IN ACQUISITION ROUTINES
15     186        DATA ACQUISITION ROUTINE
```

```
171 LIST

 0 ( DIRECTORY FOR RICH'S STUFF - BLK# 1 )
 1                                                    EXIT
 2  BLOCK#  ------------------ CONTENTS --------------------
 3
 4    187       FIND MIN/MAX AND RANGE IN DATA ARRAY
 5    188       ARRAY INTEGRATION ROUTINE
 6    189       POST-RUN DATA MASSAGE ROUTINES
 7    190       BACKGROUND NOISE DATA ACQUISITION ROUTINE
 8    191       MICROARC DATA ACQUISITION ROUTINE
 9    192       MICROARC SPECIAL ACQUISITION ROUTINE
10    193       STATISTICS CODE - DOUBLE PRECISION MEAN
11    194       STATISTICS CODE - DOUBLE PRECISION VARIANCE
12    195       CODE FOR AVERAGING FIVE RUNS
13    196       CODE TO DO N EXPTS OF 5 RUNS EACH
14    197       PRINTING ROUTINES FOR ALL JOBS
15    198       STEPPER MOTOR SCAN ROUTINES


172 LIST

 0 ( DIRECTORY FOR INSTRUMENT SOFTWARE - BLK# 2 )
 1                                                    EXIT
 2  BLOCK#  ------------------ CONTENTS --------------------
 3
 4    199        WAVELENGTH SEARCH ROUINTES
 5    200        LASER WAVELENGTH STABILITY TEST ROUTINE
 6    201        NEBULIZER FLOW STABILITY TEST ROUTINE
 7    202        ROUTINE TO SCAN LASER AND TAKE DATA
 8    203        CHART RECORDER X-Y PLOT ROUINTES
 9
10
11
12
13
14
15


173 LIST

 0 (  INSTRUCTIONS FOR INSTRUMENT SOFTWARE - RSL -  /4/85 )
 1                                              EXIT
 2 1) BOOT SYSTEM - INSTRUMENT SOFTWARE LOAD BLOCK 180 AND PRINT
 3      ROUTINES ARE LOADED FROM BLOCK 9 AT BOOTUP TIME.
 4 2) TYPE 'INITIALIZE'.
 5         THIS SHOULD BE DONE ANY TIME THE DISKS ARE TO BE USED.
 6         THIS INITIALIZES THE INSTRUMENT DISKING SOFTWARE.
 7         IT READS WORD # 1 OF BLOCK # 250 FROM THE DISK AND PUTS
 8         IT INTO THE VARIABLE 'BLOCK#'. THIS VARIABLE TAKES
 9         CARE OF ALL EXPERIMENTAL DATA DISK STORAGE & RETRIEVAL.
10         DATA IS ACQUIRED EITHER FROM DISK OR FROM THE EXPT INTO
11         THE AREA 'BUF' WHICH IS PAD + 100.
12
13 3) TYPE 'n ACQUIRE' WHERE n IS THE # OF POINTS TO BE ACQUIRED.
14
15
```

```
174 LIST

 0 (  INSTRUCTIONS FOR DISK AND DISPLAY SOFTWARE - 9/4/85 )
 1                                                  EXIT
 2
 3 4) TYPE "SAVE-DATA" TO HAVE THE DATA STORED ON DISK. THE DATA
 4         WILL BE WRITTEN TO DISK BLOCKS, STARTING AT BLK # GIVEN
 5         BY THE VARIABLE BLOCK# WHICH IS STORED AT BLOCK # 250
 6         WORD # 1. BLOCK # 250 IS NOT USED FOR ANYTHING ELSE !!
 7         IT ONLY KEEPS TRACK OF THE LAST BLOCK TO WHICH DATA WAS
 8         WRITTEN !!  THE ROUTINE "SAVE-DATA" FIGURES OUT HOW MANY
 9         BLOCKS ARE NEEDED FOR THE #POINTS SPECIFIED BY "n" IN
10         THE ROUTINE "ACQUIRE". "SAVE-DATA" TAKES CARE OF ALL
11         BLOCK# RECORDKEEPING AND UPDATING.
12
13 5) TYPE "TTY SEEDATA" OR "SCOPE SEEDATA" TO HAVE DATA APPEAR
14         ON THE TERMINAL IN NUMERIC FORM OR ON THE OSCOPE IN
15         REAL TIME.


175 LIST

 0 (  INSTRUCTIONS FOR DISK AND DISPLAY SOFTWARE - 9/4/85 )
 1         EXIT
 2
 3 6) TYPE "block#  #points  FETCH" WHERE block# IS THE STARTING
 4         BLOCK WHERE DATA WILL BE FETCHED FROM, #points IS HOW
 5         MANY DATA POINTS THERE ARE IN THE SPECTRUM TO BE VIEWED
 6         USING THE NEXT STEP. THE ROUTINE "FETCH" TAKES CARE
 7         OF FETCHING SPECTRA MORE THAN ONE BLOCK LONG (512 PTS.)
 8
 9 7) TYPE "TTY SEEDATA" OR "SCOPE SEEDATA" TO HAVE DATA APPEAR
10         ON THE TERMINAL IN NUMERIC FORM OR ON THE OSCOPE IN
11         REAL TIME.
12
13 8) GO TO STEP 3 AND TAKE MORE DATA, OR GO HOME !!!
14
15


176 LIST

 0 ( INSTRUCTIONS FOR DATA ACQUISITION SOFTWARE - RSL - 9/26/86 )
 1                                                      EXIT
 2  THERE ARE TWO WAYS TO USE THE ACQUIRE SOFTWARE:
 3
 4    1) UP TO 2000 DATA POINTS CAN BE ACQUIRED INTO MEMORY WITH
 5         A DELAY ("ACQ-DELAY") BETWEEN EACH DATA POINT.
 6         THE DATA IN MEMORY CAN THEN BE VIEWED AND/OR WRITTEN
 7         TO DISK AS EXPLAINED ABOVE.
 8         POST-RUN COMPUTATION OF DATA MIN/MAX AND RANGE, SCALING
 9         ZEROING, AND INTEGRATION CAN THEN BE DONE.
10
11    2) N POINTS ("#POINTS") CAN THEN BE TAKEN; N RUNS ("#RUNS")
12         OF N POINTS (("#POINTS") CAN BE DONE AND AN AVERAGE AND
13         VARIANCE WILL BE CALCULATED.
14         THIS CAN BE DONE FOR N EXPTS TOTAL ("#EXPTS").
15
```

```
177 LIST

 0 ( INSTRUCTIONS FOR LOADING SOFTWARE - RSL - 9/26/86 )
 1                                                    EXIT
 2
 3    ONLY THOSE TOOLS NEEDED FOR A GIVEN APPLICATION ARE LOADED
 4     INTO MEMORY. THIS IS DONE TO CONSERVE MEMORY SINCE 2 KBYTES
 5     ARE ALWAYS FOR DATA ACQUISITION, DISK AND DISPLAY SPACE.
 6     DATA IS NEVER LOST WHEN A USER DICTIONARY 'EMPTY' IS DONE.
 7
 8  TO LOAD ROUTINES FOR ACQUIRING, PROCESSING, AND PRINTING DATA,
 9         TYPE  'SYSLOAD'.
10
11  TO LOAD DISKING AND DISPLAY ROUTINES, TYPE  'DISK-LOAD' AND
12         THEN  'SHOW-LOAD'.
13
14  TO LOAD OTHER COMBINATIONS, TYPE THE INDIVIDUAL NAMES FOR THE
15         TOOL PACKAGES FOUND IN LOAD BLOCK 180.


178 LIST

 0 ( EMPTY )
 1
 2
 3
 4
 5
 6
 7
 8
 9
10
11
12
13
14
15


179 LIST

 0 (  DEFINING BLOCK FOR INSTRUMENT SOFTWARE - 9/2/85 )
 1 OCTAL 170400 CONSTANT ADCSR 0 ADCSR !  170402 CONSTANT A2DBUFF
 2    167770 CONSTANT PARCSR  0 PARCSR !  167772 CONSTANT PAROUT
 3    167774 CONSTANT PARIN        170440 CONSTANT DAC  DECIMAL
 4 VARIABLE 'DISPLAY                    VARIABLE MIN(Y)
 5 VARIABLE BLOCK#                      VARIABLE MAX(Y)
 6 VARIABLE #POINTS    25 #POINTS !     VARIABLE A-RANGE
 7 VARIABLE DELAY  90 DELAY !  ( 90 GIVES 100 HZ ACQUISITION RATE )
 8 VARIABLE BUF 4000 ALLOT  BUF 4000 ERASE
 9 VARIABLE #EXPTS   30 #EXPTS !
10 VARIABLE #RUNS   5 #RUNS !
11 VARIABLE N-POINTS 400 ALLOT  N-POINTS 400 ERASE
12 VARIABLE SIGNAL 400 ALLOT  SIGNAL 400 ERASE
13 VARIABLE 20AVGS 200 ALLOT  20AVGS 200 ERASE
14 VARIABLE 20VARS 200 ALLOT  20VARS 200 ERASE
15 VARIABLE 5SUM  0 5SUM !
```

```
180 LIST

 0 (  LOAD BLOCK FOR INSTRUMENT SOFTWARE - RSL - 1/11/85 )
 1 ( THE DEFINING BLOCK FOR THE INSTRUMENT SOFTWARE WAS LOADED )
 2 (  WITH THE FORTH SYSTEM SOFTWARE IN BLOCK 9 )
 3 : DISK-LOAD  181 LOAD 182 LOAD 183 LOAD ;
 4 : SHOW-LOAD  184 LOAD ;
 5 : ACQ-LOAD 185 LOAD 186 LOAD ;
 6 : PROCES-LOAD  187 LOAD 188 LOAD 189 LOAD ;
 7 : NOISE-LOAD    190 LOAD ;
 8 : SPECIAL-LOAD  191 LOAD 192 LOAD ;
 9 : STAT-LOAD 193 LOAD 194 LOAD 195 LOAD 196 LOAD ;
10 : MOTR-LOAD 198 LOAD ;
11
12 : SYSLOAD  ACQ-LOAD PROCES-LOAD STAT-LOAD MOTR-LOAD  ;
13
14
15


181 LIST

 0 (  FETCH DATA FROM DISK CODE - RSL - 9/2/85 )
 1 (  FETCH DATA FROM DISK TO MEMORY, GET IT READY TO DISPLAY.  )
 2 ( THIS BLOCK FIGURES OUT MANY BLOCKS WILL BE NEEDED FOR      )
 3 ( THE # OF POINTS SPECIFIED.   IT FETCHES THAT MANY BLOCKS,  )
 4 ( BEGINNING WITH BLOCK#, INTO THE BUF BUFFER, WHOSE LENGTH   )
 5 ( IS SPECIFIED BY #POINTS.                                   )
 6
 7 : FETCH   (  BLOCK# , #POINTS , ---)
 8     DUP  #POINTS !
 9     512 /MOD SWAP IF 1+ THEN ( FIGURE OUT # BLOCKS FOR #POINTS )
10     0 DO I OVER + BLOCK      ( FETCH THAT # BLOCKS INTO MEMORY )
11     BUF I 1024 * +           ( ALLOCATE 1024 BYTES STARTING AT )
12     1024 MOVE LOOP DROP ;    ( BUF, FOR EACH BLOCK READ IN FROM)
13                              ( DISK.  CLEAN UP STACK WHEN DONE.)
14
15


182 LIST

 0 (  SAVE-DATA INITIALIZATION ROUTINES - RSL - 9/2/85 )
 1 (  ======= MANAGES WRITE DATA TO DISK SOFTWARE ======== )
 2
 3 (  DRIVE 1 SHOULD CONTAIN THE DATA DISK. THE FIRST WORD OF    )
 4 (  BLOCK 250 CONTAINS THE BLOCK # OF THE LAST BLOCK TO WHICH  )
 5 (  EXPERIMENTAL DATA WAS WRITTEN.   BLOCKS 251 - 265 ARE USED )
 6 (  FOR AN EXPERIMENTAL DATA DISK DIRECTORY.                   )
 7
 8 : INIT-PROMPT CR 7 EMIT ." CHECK DATA STORAGE BLK POINTER ! " ;
 9                                  INIT-PROMPT
10 : WRITE-DB#  250 BLOCK !  UPDATE FLUSH ;
11 : NEW-DISK  264 WRITE-DB# ;     ( POINT TO START OF DATA AREA.)
12
13 : WHERE  ." LAST BLOCK USED IS "  BLOCK# ? ;
14 : INITIALIZE  250 BLOCK @  BLOCK# ! WHERE ; ( RESET BLOCK# TO )
15    CR CR INITIALIZE     CR CR               ( VALUE ON DISK  )
```

```
183 LIST

 0 (  SAVE-DATA ON DISK ROUTINES  - RSL - 9/2/85 - BLOCK 5 )
 1 (  =========== WRITE DATA TO DISK ROUTINES ============ )
 2
 3 ( THIS BLOCK WRITES DATA TO THE BLOCKS ON DISK STARTING WITH )
 4 ( 1+ THE LAST DATA DATA BLOCK WRITTEN TO ON DISK, GIVEN BY   )
 5 ( THE CONTENTS OF THE FIRST WORD OF BLOCK 250.               )
 6
 7 : SAVE-DATA       ( THIS TAKES NO ARGUMENTS. )
 8     #POINTS @ CR .* Blocks Used: *   ( FIGURE OUT # BLOCKS FOR )
 9     512 /MOD SWAP IF 1+ THEN         ( #POINTS SO LOOP COUNTER )
10     DUP  0 DO  BUF I 1024 * +        ( IS CORRECT. FIGURE OUT  )
11     BLOCK# @ 1+ I + DUP .            ( SRC & DEST ADDRESS FOR  )
12      BLOCK 1024 MOVE                 ( MOVE INSTRUCTION. MOVE  )
13          UPDATE  FLUSH  LOOP         ( BLOCKS TO DISK, PRINTING)
14                                      ( THOSE BLOCKS USED.      )
15    BLOCK# +!  BLOCK# @ WRITE-DB# ;   ( UPDATE SAVE DATA POINTER)


184 LIST

 0 (  TTY & SCOPE DISPLAY CODE - RSL - 9/2/85 )
 1 (  ================ DATA DISPLAY CODE ================ )
 2 : (TTY)  BUF #POINTS @ 2* DUMP ; ( DUMP WHOLE BUF AREA )
 3         ( BUF IS FULL OF THE SPECTRUM CALLED IN BY GET-DATA    )
 4
 5  CODE  (SCOPE)
 6         0  S )+  MOV                ( PUT BUF ADDRESS INTO R0  )
 7         1  #POINTS  MOV                ( PUT #POINTS INTO R1  )
 8     BEGIN  DAC 0 )+ MOV 1 SOB  NEXT    ( DISPLAY UNTIL DONE   )
 9
10 : (SCOPE)  BEGIN BUF (SCOPE) ESCAPE 0 END ;
11                ( TYPE "TTY SEEDATA" TO CHANGE DISPLAY MODE TO )
12 : TTY  ['] (TTY)  'DISPLAY ! ;     ( VIEW RAW DATA ON TTY TUBE )
13 : SCOPE ['] (SCOPE)  'DISPLAY ! ;  ( TYPE "SCOPE SEEDATA" TO  )
14 : SEEDATA 'DISPLAY @ EXECUTE ;     ( VIEW IT ON OSCILLOSCOPE. )
15  SCOPE  ( SET DEFAULT TO DISPLAY ON SCOPE )


185 LIST

 0 (  DEFN'S USED IN ACQUIRE CODE - RSL - 9/2/85 - BLOCK 6 )
 1 (  ============ DATA ACQUISITION ROUTINES ============== )
 2   CODE  START-CONVERT  ADCSR 1 # MOV  NEXT
 3   CODE  DONE??  BEGIN  ADCSR TST B  0< END  NEXT
 4   CODE  GET-BUFFER  S -) A2DBUFF  MOV  NEXT
 5                                ( PUTS DATA ONTO TOP OF STACK  )
 6 : GET-POINT  START-CONVERT DONE?? GET-BUFFER ;  ( GET 1 POINT )
 7
 8   CODE  RELAX  0 65535 # MOV BEGIN 0 SOB  NEXT
 9                    ( DELAY LOOP TO GET RID OF SAMPLER NOISE )
10 : 30-SEC  75 0 DO  RELAX  LOOP ; : 20-SEC 50 0 DO RELAX LOOP ;
11 : PRE-WAIT  3 0 DO RELAX LOOP ;
12                    ( DELAY LOOP TO LET SAMPLE GET TO PLASMA )
13   CODE  FIRE  OCTAL 167770 1 # MOV  NEXT        ( SAMPLER ON  )
14   CODE  EXTINGUISH OCTAL 167770 0 # MOV  NEXT   ( SAMPLER OFF )
15
```

```
186 LIST

 0 (   DATA  ACQUISITION ROUTINES - RSL - 9/2/85 )
 1                DECIMAL
 2 ( ROUTINE FOR ACQUIRING N DATA POINTS WITH A DELAY IN BETWEEN )
 3 ( EACH DATA POINT. DATA IS STORED IN MEMORY AREA CALLED BUF.  )
 4
 5 : ACQ-DELAY DELAY @ 0 DO  PARIN @ DROP  LOOP ;
 6
 7 : ACQUIRE   ( #POINTS , --- )
 8    DUP #POINTS !                        ( SAVE #POINTS FOR LATER )
 9       FIRE                                      ( FIRE SAMPLER )
10    2* BUF +  BUF DO  GET.POINT I !     ( FILL UP BUF WITH DATA )
11       ACQ-DELAY  2 +LOOP                ( PAUSE BETWEEN POINTS )
12         EXTINGUISH       ;                  ( TURN OFF SAMPLER )
13                                  DECIMAL
14
15


187 LIST

 0 (  FIND MIN & MAX , RANGE IN DATA ARRAY - RSL - 9/14/85 )
 1
 2 : A-PRESET  7777 MIN(Y) !  0 MAX(Y) !  0 A-RANGE ! ;
 3                          ( DEFINE SEEDS , ZERO RANGE )
 4
 5 : ARRAY-MIN/MAX  ( -- MIN MAX )  ( FIND MIN & MAX IN BUF ARRAY )
 6       MIN(Y) @  MAX(Y) @       ( PUT SEED VALUES ONTO P-STACK )
 7       BUF  #POINTS @                  ( SET UP DO LOOP VALUES )
 8       2* OVER + SWAP               ( DO FROM BUF TO BUF+2*#PTS )
 9       DO I @ ROT OVER             ( SET UP FOR MIN/MAX COMPARE )
10       MIN ROT ROT MAX 2 +LOOP        ( LEAVE MIN MAX ON STACK )
11       MAX(Y) !  MIN(Y) ! ;        ( MAKE MIN MAX READY TO USE )
12
13 : ARRAY-RANGE  MAX(Y) @  MIN(Y) @  -   A-RANGE ! ;
14 : PRINT-ARRAY-PARAMETERS CR MAX(Y) @ ." MAX(Y) IS " . CR MIN(Y)
15    @ ." MIN(Y) IS " . CR  A-RANGE @ ." ARRAY RANGE IS " . CR ;


188 LIST

 0 (  POST-RUN INTEGRATION ROUTINE - RSL - 9/23/85 )
 1                  0,0  2VARIABLE  DP.RESULT
 2                     0,0  DP.RESULT  2!
 3 : GGGG     #POINTS @ 0 DO  I BUF I 2* + !  LOOP ; ( MAKE & SHOW)
 4 : SHOWBUF  #POINTS @ 0 DO  BUF I 2* + @ .  LOOP ; ( TEST DATA )
 5
 6 : SUM-DP-ARRAY  0  0  #POINTS @  0 DO    ( GET STACK RDY FOR D )
 7       BUF I 2* + @                          ( FETCH DATA ONTO PS )
 8       0 D+              ( CONVERT SINGLE TO DOUBLE PRECISION )
 9       LOOP  DP.RESULT 2! ;       ( ADD SINGLE PRECISION DATA )
10                                 ( GET DOUBLE PRECISION RESULT )
11                                   ( STORE ANSWER IN DP.RESULT )
12 : PRINT-SUM-RESULT DP.RESULT 2@ ." INTEGRATION RESULT = "  D. ;
13 : PRINT-RESULTS  PRINT-ARRAY-PARAMETERS  PRINT-SUM-RESULT ;
14
15
```

```
189 LIST

 0 (  POST-RUN DATA MASSAGE ROUTINES - RSL - 9/20/85 )
 1
 2 ( ZERO-A/D-OFFSET SHIFTS BIPOLAR DEC DAC DATA TO UNIPOLAR DATA )
 3                          ( IT HELPS TO SCALE THE DATA !! )
 4 : ZERO-A/D-OFFSET
 5         MIN(Y) @ MINUS
 6         BUF  #POINTS @ 2* OVER + SWAP        ( SET UP DO LOOP )
 7       DO  DUP I +! 2 +LOOP DROP ;                    ( DO IT ! )
 8
 9 : POST-RUN  A-PRESET  ARRAY-MIN/MAX  ARRAY-RANGE  SUM-DP-ARRAY ;
10
11 : POST-RUN-0  A-PRESET  ARRAY-MIN/MAX  ZERO-A/D-OFFSET
12                                                  POST-RUN  ;
13
14
15


190 LIST

 0 ( MICROARC DATA ACQUISITION ROUTINES - RSL - 12/4/85 )
 1 : ?RUNS  CR ." #RUNS = " #RUNS 1 EXPECT #RUNS @ 48 -  #RUNS ! ;
 2 : SBELL 40 0 DO  7 EMIT  LOOP ;  : LBELL 20 0 DO  SBELL  LOOP ;
 3 : GO-4-IT  CR ." HIT <CR> TO START EXPTS "  S0 @ 1 EXPECT CR ;
 4 : LOAD-FILAMENT!  CR ." PUT SAMPLE ONTO FILAMENT ! "  SBELL
 5       S0 @ 1 EXPECT CR  ;
 6 : 0-SIGNAL  SIGNAL 160 ERASE ;
 7 : CLEAN-BURN  FIRE  12 0 DO RELAX LOOP EXTINGUISH ;
 8 : 1SAMPLE  #POINTS @ ACQUIRE POST-RUN-0  ( ACQ. & PROCESS DATA )
 9   (   20-SEC  CLEAN-BURN  20-SEC ;  COOL, CLEAN, COOL SAMPLER )
10
11 : RUNS  CR ?RUNS  GO-4-IT  ( DOES MANY RUNS OF A SINGLE [] )
12   #RUNS @ 0 DO  LOAD-FILAMENT!  DP-RESULT 2@ I 4 * SIGNAL + 2!
13    SIGNAL-PRINT  ESCAPE LOOP ;
14
15 : 1RUN 1SAMPLE PRINT-RESULTS ;


191 LIST

 0 ( BACKGROUND NOISE DATA ACQUISITION ROUTINE - RSL - 12/5/85 )
 1
 2 : ACQUIRE-NOISE   ( USED TO DO 20 BKGND RUNS FOR LOD STUDIES )
 3 (    CR  CLEAN-BURN  30-SEC     )       ( CLEAN OFF SAMPLER )
 4      #EXPTS @ N-POINTS + N-POINTS DO  ( SET UP ARRAY POINTERS )
 5      #POINTS @ ACQUIRE POST-RUN       ( ACQ. DATA, POSTRUN IT )
 6      DP.RESULT 2@  I 2!      ( STORE RESULT IN N-BKGNDS ARRAY )
 7      PRINT-RESULTS                  ( SHOW RESULTS TO OPERATOR )
 8 (  20-SEC                             COOL SAMPLER )
 9      4 +LOOP ;                                ( GET NEXT DATUM )
10
11
12 ( REMOVE PARENTHESES WITHIN ABOVE DEFINITION WHEN USING MICRO )
13 ( ARC SAMPLER )
14
15
```

```
192 LIST

 0 (  MICROARC SPECIAL DATA ACQUISITION ROUTINE - RSL - 9/2/85 )
 1        DECIMAL
 2  ( THIS ROUTINE TAKES SOME POINTS WITH THE SAMPLER ON  )
 3  ( THEN TURNS THE SAMPLER OFF AND TAKES A FEW MORE POINTS  )
 4  ( SO THAT THE FLUORESCENCE DECAY PROFILE CAN BE SEEN.  )
 5   VARIABLE ONPOINTS   VARIABLE OFFPOINTS
 6
 7 : 2ACQUIRE   ( #POINTS , -- )
 8    #POINTS  !   300 OFFPOINTS !
 9    #POINTS @  OFFPOINTS @  -   ONPOINTS !
10    FIRE
11    ONPOINTS @ 2* BUF + BUF DO GET.POINT I ! ACQ-DELAY  2 +LOOP
12    EXTINGUISH    7 EMIT
13    ONPOINTS @ 2*  OFFPOINTS @ 2* + BUF +   ONPOINTS @ 2* BUF +
14    DO    GET.POINT I ! ACQ-DELAY       2 +LOOP ;
15 : RUNIT 2000 2ACQUIRE POST-RUN-0 SEEDATA ;


193 LIST

 0 (  STATISTICS CODE - MEAN ABS DEVIATION - RSL - 1/27/86)
 1
 2         2VARIABLE  RUN-SUM      2VARIABLE  AVG
 3
 4 : AVG-RUNS      0.  RUN-SUM  2!          ( CLEAR RUNNING SUM )
 5                 0.    AVG    2!          ( AND FINAL AVERAGE )
 6    #RUNS @ 4 * N-POINTS +  N-POINTS  DO
 7      RUN-SUM 2@  I 2@  D+  RUN-SUM 2!    ( FETCH DATA & SUM IT )
 8    4 +LOOP
 9      RUN-SUM 2@ 1 #RUNS @ M*/              ( DIVIDE BY #EXPTS )
10      2DUP AVG 2! CR ." AVG. = " D. ;     ( STORE, PRINT RESULT )
11
12
13
14
15


194 LIST

 0 ( DOUBLE PRECISION VARIANCE ROUTINE - RSL - 1/27/86 )
 1  ( THIS ROUTINE CALCULATES THE AVERAGE OF THE DEVIATIONS FROM )
 2  ( THE MEAN FOR A DOUBLE PRECISION ARRAY N-POINTS )
 3         2VARIABLE  VAR         2VARIABLE  SUM-DEV
 4
 5 : VARIANCE      0.   SUM-DEV  2!  ( ZERO THESE VARIABLES EACH )
 6                 0.   VAR      2!    ( TIME ROUTINE IS CALLED )
 7     #RUNS @ 4 * N-POINTS +  N-POINTS  DO
 8           I 2@  AVG 2@  D-              ( CALCULATE DEVIATION )
 9           DABS                      ( GET SQUARE OF DEVIATION )
10        SUM-DEV 2@  D+              ( SUM DEVIATIONS UNTIL DONE )
11     SUM-DEV 2!  4 +LOOP              ( STORE SUM OF DEVIATIONS )
12     SUM-DEV 2@  1 #RUNS @ 1 -  M*/  2DUP    ( DIVIDE BY #EXPTS )
13     CR ." VARIANCE = "  D. VAR 2! CR ;     ( PRINT OUT RESULT )
14
15
```

```
195 LIST

 0 ( ROUTINE FOR AVERAGING 5 RUNS - RSL - 12/5/85 )
 1
 2 ( DO N RUNS FOR #POINTS EACH, AVERAGE RESULTS, COMPUTE MEAN )
 3 ( DEVIATIONS. SHOW ALL REULTS TO OPERATOR. )
 4              2VARIABLE  DC.LEVEL   0. DC.LEVEL 2!
 5 : NRUN  CR
 6    #RUNS @ 4 * N-POINTS + N-POINTS DO  ( SETUP ARRAY POINTERS )
 7      #POINTS @ ACQUIRE     POST-RUN   ( ACQ. DATA, POSTRUN IT )
 8      DP.RESULT 2@    ( DC.LEVEL 2@  D-  SUBTRACT DC OFFSET !  )
 9         I 2!                  ( STORE RESULT IN N-POINTS ARRAY )
10      PRINT-SUM-RESULT  CR   ( SHOW OPERATOR INTEGRATED RESULT )
11    ESCAPE   4 +LOOP                          ( GET ALL 5 POINTS )
12      AVG-RUNS                          ( AVG RESULTS OF 5 RUNS )
13      VARIANCE ;                                ( MEASURE NOISE )
14
15


196 LIST

 0 ( ROUTINE TO DO 20 EXPERIMENTS OF 5 RUNS EACH - RSL - 2/1/86 )
 1
 2 ( DO N RUNS, GET AVG Y VAR, PUT RESULTS IN RESPECTIVE ARRAYS )
 3
 4
 5 : N-EXPTS             N-POINTS 400 ERASE    ( START FRESH NOW )
 6         SIGNAL 200 ERASE  20AVGS 200 ERASE  20VARS 200 ERASE
 7     #EXPTS @ 0 DO
 8       ." EXPT# = " I 1 + .  NRUN       ( DO NRUN, SHOW RESULTS )
 9         AVG 2@ 20AVGS I 4 * + 2!  ( STORE AVG IN ARRAY 20AVGS )
10         VAR 2@ 20VARS I 4 * + 2!  ( STORE VAR IN ARRAY 20VARS )
11         ." HIT ANY KEY AFTER MAKING ADJUSTMENTS !"
12         SO @ 1 EXPECT 13 EMIT 10 EMIT    (   WAIT FOR OPERATOR )
13     ESCAPE  LOOP ;       ( TO CHANGE EXPERIMENTAL PARAMETERS ! )
14
15


197 LIST

 0 ( PRINTING ROUTINES FOR ALL JOBS - RSL - 2/3/86 )
 1
 2 : SIGNAL-PRINT
 3     CR CR ." SAMPLE    ------ SIGNAL ------       " CR #RUNS @
 4   0 DO  3 SPACES I . 10 SPACES SIGNAL I 4 * + 2@ D. CR LOOP ;
 5
 6 : NOISE-PRINT  CR ." ------- NOISE ------- " CR CR
 7  #EXPTS @ N-POINTS + N-POINTS DO CR  7 SPACES I 2@ D. 4 +LOOP ;
 8
 9 : ASDF    ( ANOTHER NAME FOR N-EXPTS-PRINT )
10  CR CR  ." EXPT# --- AVG. SIGNAL ---- SIG. VARIANCE ---- " CR
11     9 0 DO  2 SPACES I 1 + .  7 SPACES   20AVGS I 4 * + 2@ D.
12    11 SPACES  20VARS I 4 * + 2@ D.  CR  LOOP
13  #EXPTS @ 9 DO 2 SPACES I 1 + . 6 SPACES 20AVGS I 4 * + 2@ D.
14    11 SPACES  20VARS I 4 * + 2@ D.  CR  LOOP CR CR CR ;
15
```

```
198 LIST

 0 ( STEPPER MOTOR TEST ROUTINES - RSL - 2/6/86 )
 1   CODE  DISABLCLK  OCTAL 167770 0 # MOV NEXT
 2   CODE  ENBLCLK  OCTAL 167770 2 # MOV  NEXT
 3   CODE  CW-SET  OCTAL 167772 4001 # MOV  NEXT
 4   CODE  CCW-SET OCTAL 167772 4000 # MOV  NEXT
 5   CODE  REV-DIR OCTAL 167772 1 # BIT  0= IF 167772  4001 # MOV
 6           ELSE  167772 4000 # MOV  THEN  NEXT
 7   CODE  1STEP  OCTAL 167772 10001 # MOV 167772 14000 # MOV NEXT
 8 : 1STEP  DISABLCLK ENBLCLK  1STEP ;
 9
10   CODE  DELAY  0 200 # MOV  BEGIN 0 SOB  NEXT
11     (   CW TURNS TOWARD THE RED  !!!  )
12 : CW  DISABLCLK ENBLCLK  BEGIN S0 @ 1 EXPECT  CW-SET 1STEP
13                 DELAY  ESCAPE 0 END  DECIMAL ;
14 : CCW DISABLCLK ENBLCLK  BEGIN S0 @ 1 EXPECT  CCW-SET 1STEP
15                 DELAY  ESCAPE 0 END  DECIMAL ;  DECIMAL


199 LIST

 0 ( WAVELENGTH SEARCH ROUTINE - RSL - 2/6/86 )
 1 (         ACQ-LOAD PROCES-LOAD 193 LOAD )    198 LOAD
 2 : LAMBDA
 3    BEGIN                                        ( FOR REV-DIR LOOP )
 4        BEGIN                                ( FOR SCAN & MEASURE LOOP )
 5          1STEP  S0 @ 1 EXPECT                ( MOVE MOTOR 1 STEP )
 6        ESCAPE 0 END                           ( LET ME GET OUT ! )
 7      REV-DIR                                ( IF CHAR = R REV-DIR )
 8    ESCAPE 0 END ;                             ( LET ME GET OUT ! )
 9
10 : FIND-MAX
11         BEGIN   CW  REV-DIR  CCW   ESCAPE 0 END ;
12
13
14
15


200 LIST

 0 ( LASER WAVELENGTH STABILITY TEST - RSL - 2/15/86 )
 1
 2 : LASER-TEST                          ( GET A POINT, WAIT 30 SEC )
 3         500 0 DO                           ( LOOP FOR 100 EXPTS )
 4            CR GET.POINT . 20-SEC
 5         ESCAPE  LOOP ;
 6
 7
 8
 9
10
11
12
13
14
15
```

```
201 LIST

 0 ( ROUTINE FOR TESTING NEBULIZER - RSL - 2/18/86 )
 1
 2 ( COLLECT A/D POINTS FOR #RUNS, AVERAGE RESULTS, COMPUTE MEAN )
 3 ( DEVIATIONS. SHOW RESULTS TO OPERATOR. )
 4
 5 : ?DRIFT   CR
 6    #RUNS @ 4 * N-POINTS + N-POINTS DO  ( SETUP ARRAY POINTERS )
 7      GET.POINT 0 I 2!   ( ACQ. DATA, DP IT, STORE IT IN ARRAY )
 8      I 2@ D.   RELAX                  ( SHOW OPERATOR A/D POINT )
 9    ESCAPE   4 +LOOP                        ( GET ALL N POINTS )
10      AVG-NOISE                        ( AVG RESULTS OF N RUNS )
11      VARIANCE ;                               ( MEASURE NOISE )
12
13 : N-?DRIFT  #EXPTS @ 0 DO I . CR ?DRIFT  ESCAPE LOOP ;
14
15


202 LIST

 0 ( ROUTINE TO SCAN LASER AND TAKE DATA POINTS AT EACH STEP )
 1
 2
 3 : 5ACQAVG       ( TAKE 5 POINTS AT EACH WAVELENGTH & AVERAGE )
 4           0 5SUM !   ( START FRESH EACH CALL OF THIS ROUTINE )
 5      5 0 DO  GET-POINT  +  LOOP    ( ADD EACH POINT TO STACK )
 6           5SUM !   ;               ( PUT PS RESULT INTO 5SUM )
 7
 8 : SCAN  ( #POINTS , ---)
 9     DUP #POINTS !
10      2* BUF + BUF DO 1STEP   5ACQAVG  5SUM @  I !
11                  ACQ-DELAY  2 +LOOP ;
12
13
14
15


203 LIST

 0 (  XY-PLOT CODE DEFINITION - RSL - 9/28/85 )
 1 ( DATA MUST BE MADE UNIPOLAR BEFORE USING XY-PLOT ROUTINE !!! )
 2  OCTAL  170440 CONSTANT XDAC   170442 CONSTANT YDAC   DECIMAL
 3         0 XDAC !              0 YDAC !
 4  CODE  0-PEN  BEGIN  2 200 # MOV  BEGIN 2 SOB  XDAC DEC
 5     S )  XDAC MOV   0= END  NEXT
 6
 7  CODE  CHART  0 BUF # MOV          ( PUT BUF ADDRESS INTO R0 )
 8          1 ' #POINTS   MOV            ( PUT #POINTS INTO R1 )
 9    BEGIN  YDAC  0 )+ MOV  XDAC INC    ( OUTPUT X & Y VALUES )
10          2 2000 # MOV BEGIN 2 SOB     ( WAIT BETWEEN POINTS )
11           1 SOB NEXT                  ( GO AGAIN UNTIL DONE )
12 : XY-PLOT
13   CR  POST-RUN-0 0-PEN  CR ." PUT PEN DOWN & HIT CR" CR
14     SO @ 1 EXPECT  CHART CR ." LIFT PEN" 1000 0 DO 7 EMIT LOOP
15          ."  & HIT CR" SO @ 1 EXPECT CR   0-PEN  ;
```

B) TUNING OF SPECTRA PHYSICS MODEL 375 DYE LASER

The purpose of this appendix is to clarify information about the complete realignment procedure given in the Spectra Physics Model 375 Dye Laser Operations Manual. It is meant as a supplement to that manual, not as a replacement to it. To derive full benefit, one must read this appendix after completely reading and understanding what is written there.

The full alignment procedure should be done only if it is impossible to get satisfactory laser intensity and stability using the horizontal and vertical thumbwheels, and the output mirror controls. The complete alignment procedure is VERY tedious and time-consuming and should be done only as a last resort. Check everything else before attempting this procedure, including the thumbwheels, the output mirror controls, the dye quality and pressure, the dye jet angle, and the pump laser output intensity and alignment.

1) Descriptions of Problems

The Spectra Physics Model 375 dye laser has problems with short-term wavelength and intensity fluctuations when used for atomic spectroscopy. Conversations with service engineers at Spectra Physics revealed that this type of dye laser was not designed to hold steady on the exact center of an atomic line profile. The stability could, however, be greatly improved with the use of an expensive (about $1,400) birefringent filter assembly. The problems were eventually solved through four successive realignments of the optical system comprised of the dye resonator cavity and its tuning components.

The best performance that can be expected from the dye laser system is about 1.5 watts at the 590 nanometer sodium D line. This is when the full argon pump laser power is used (about 5 to 6 watts with the all-lines mirror). This is without the tuning etalon in place. The tuning wedge stabilizes the output intensity and wavelength greatly but it cuts down the maximum possible intensity to about 1.2 watts. These performance figures are applicable only under the following conditions: Freshly-made Rhodamine 6G laser dye must be used. All mirrors must be free from contamination. The Brewster angle must be properly set (experimentally) to maximize dye laser output. The dye laser resonator cavity internal optics must be optimally aligned. The dye circulator pressure should be around 90 psi. The Spectra Physics Model 165 Argon Ion pump laser must be suitably aligned with the dye laser in the horizontal and vertical directions. The all-lines mirror must be used for the pump laser. The pump laser output intensity must be peaked. This is done by monitoring the output with a power meter and simultaneously "walking" the output mirror in the vertical and horizontal directions until the optimum location on the output mirror is found. "Walking" of the output mirror is described in the Operations Manual for the argon pump laser.

3) Alignment Procedure

The final goal of the tuning procedure is to have the reflections of the input mirror, the end mirror and the collimating mirror simultaneously focussed tightly on the same spot on the dye jet. This requires rather precise positioning of the input mirror, the dye jet stream envelope, and the collimating mirror. The end mirror is more or less fixed. The other mirrors and the jet stream can be focussed relative to it. For a clear picture of the dye laser optical system, see Figure 112 on page 295.

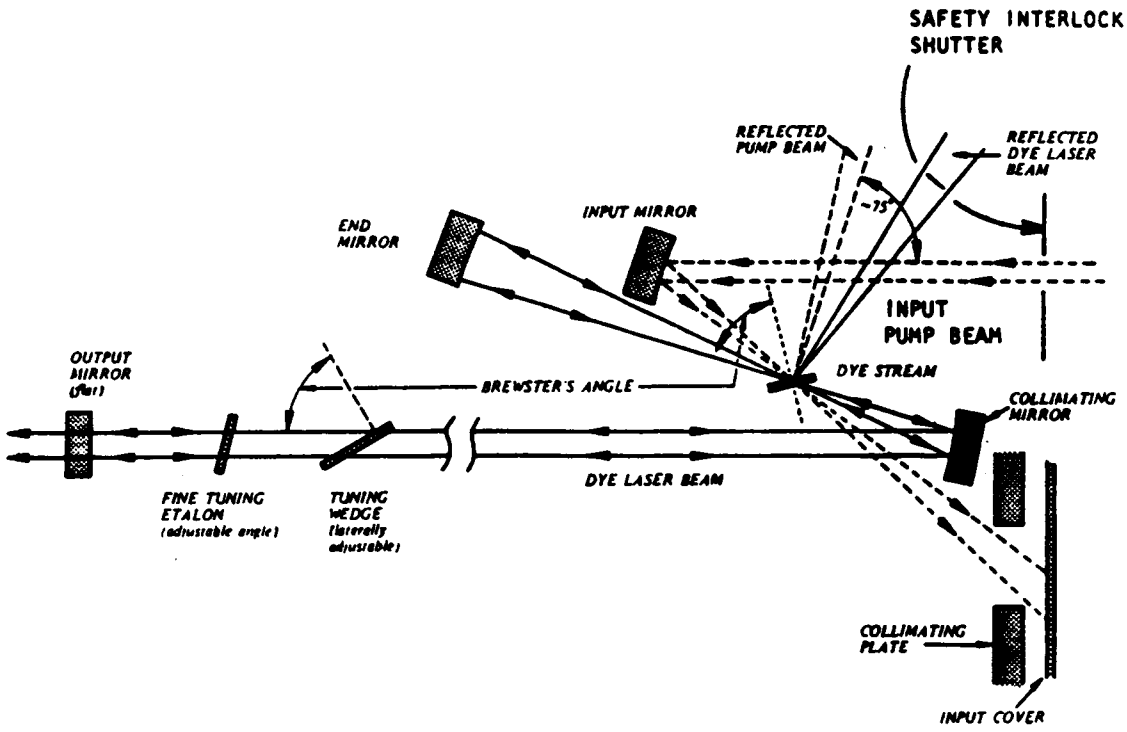

Figure 112. Model 375 Dye Laser Optical System: Reprinted from the Model 375 Dye Laser Operations Manual.

The order of operations in the alignment procedure is:

1. Input Mirror
2. Dovetail Gap (only if it has moved)
3. Collimating Mirror
4. End Mirror
5. Output Mirror

Begin with the dye circulator turned off. At the beginning of the alignment procedure, the output mirror, end mirror, and collimating mirror plates should be near the midway points of their travel. The input mirror plate is slightly different. The threads on the thumbwheel screws and the input mirror plate pivot screw should barely protrude out of the rear side of the plate. Only the bearing surface plus 1 or 2 threads should be showing. A picture of this is given in part A of Figure 113 on page 297.

Now one is ready to begin the alignment of the pump beam. The argon ion laser pumping beam should be centered approximately above the center of the input mirror and reflect off the mirror slightly below center. See part B of Figure 113 on page 297 for clarification.

Setting the Position of the Dye Jet Stream

There is a set screw which positions the dye nozzle block assembly relative to the dovetail clamp. (See part D of Figure 113 on page 297.) This set screw establishes what is called the "dovetail gap" between the nozzle block assembly and the rear part of the dovetail clamp. This sets the proper longitudinal position of the dye nozzle assembly along the laser beam axis so that a simultaneous focus of the input, end, and collimating mirrors is possible. Normally, the dovetail gap is set at the factory. However, one may have trouble with the dye nozzle assembly being tilted at an angle in the dovetail clamp. The dovetail set screw is a single point on which the dye nozzle block assembly can possibly pivot. The dye nozzle block

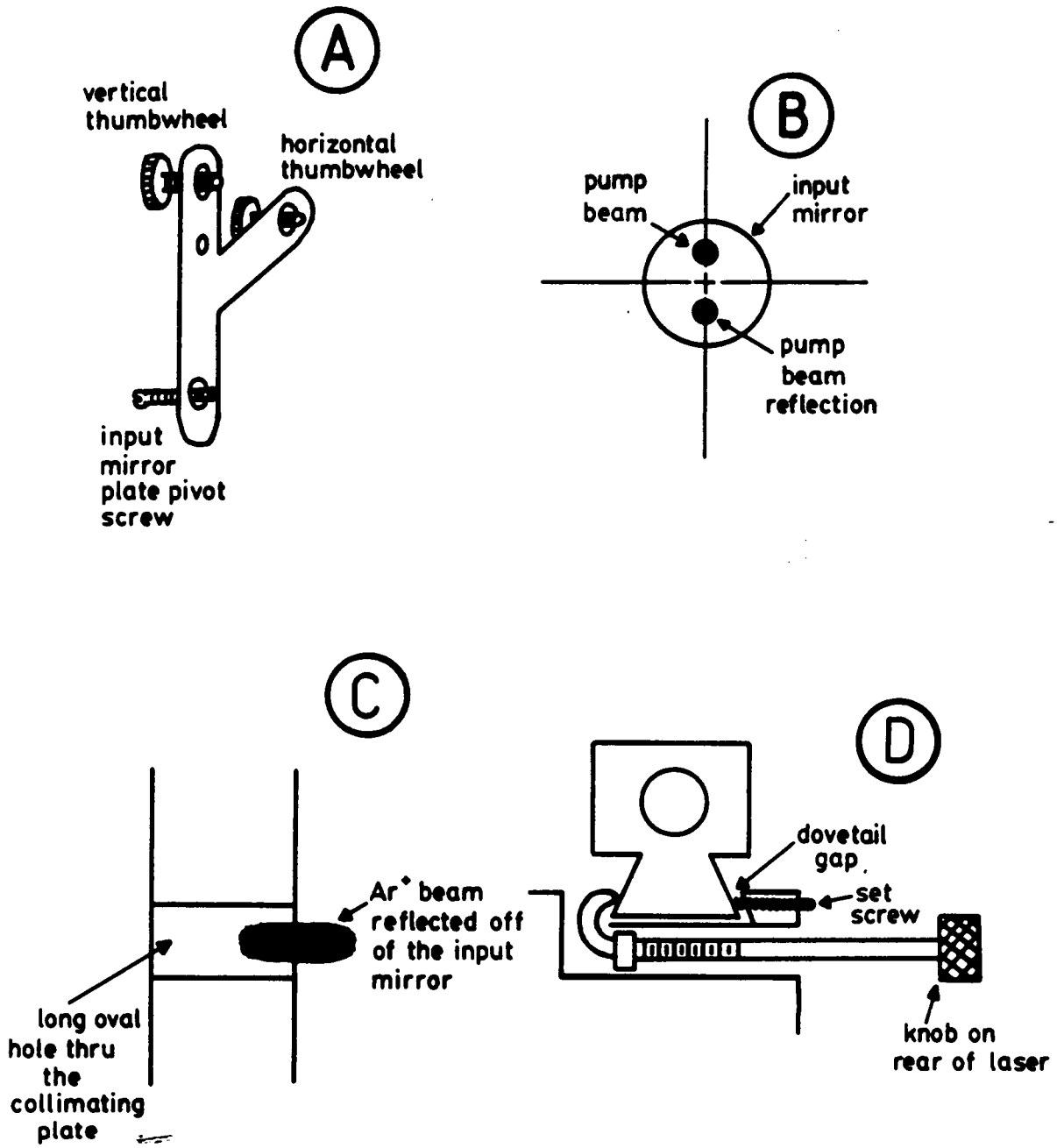

Figure 113. Pictures to Clarify the Tuning Procedure

assembly needs to be exactly parallel to the rear edge of the dovetail clamp, i.e., the width of the dovetail gap should be constant along the whole length of the dovetail gap. This is important to insure proper operation of the dye laser later. The gap should be set at 0.060 inches (1.5 mm) and then left alone. It can be set using two 0.062 inch welding rods inserted into the dovetail gap on both sides of the dovetail set screw. Such spacers allow one to easily position the dye nozzle block assembly so that it is parallel to the dovetail block. The spacers can be left on the dovetail block for later use since the dovetail block assembly is removed (albeit very infrequently) when cleaning the dye nozzle.

The position of the input mirror needs to be set before the position of tip of the dye jet stream can be set. The dye circulator should be turned off for the first part of this procedure. The argon ion laser pump beam should reflect off the input mirror and pass through the vertical oval hole in the collimating plate. It should reflect off the lower rearside surface of the hole. This is shown in part C of Figure 113 on page 297.

When the dye circulator is turned on, the pump beam reflection from the input mirror should be in approximately the middle of the dye stream (along the longitudinal axis of the dye laser). It should be as close as possible to the tip of the nozzle. The most stable part of the jet stream is about 1 mm away from the tip of the nozzle; as one moves the focal spot away from the tip of the nozzle, one sees greater frequency and intensity instabilities in the laser output.

The dye jet stream can be positioned slightly using the Allen head screws in the nozzle mounting plate. If one cannot get a good tight focus at 60 cm, one can move the nozzle plate slightly vertically and diagonally with these screws. This is preferably done with the dye circulator off. However, when the dye laser is very poorly aligned, moving the nozzle mounting plate can greatly change the foci of all reflections, greatly facilitating alignment (it can also really mess them up!). Should this be necessary (only as a last resort), one must be very careful not to move the jet stream out of the dye drain hose aperture. If it does, dye

will splatter all over the inside of the dye laser, including the focusing mirrors, necessitating a thorough cleaning.

Focusing the Output of the Dye Laser:

One of the the most difficult parts of aligning the laser from scratch is deciding which spots to use. There is a broad and diffuse yellow background which floods the whole laser cavity. This is due to dye broadband fluorescence. There is a rather diffuse orange spot that will focus down to 2 to 3 mm at best. This is NOT the spot of interest !! The spot of interest is the yellow bright spot that focuses tightly.

Block the end mirror with a piece of paper and set up a target at a distance of 60 cm from the front end of the laser. One should get a yellow spot coming through the output plate aperature. Using a combination of the input mirror thumbwheels, the collimating mirror set screws, and the nozzle mounting plate movement, get a yellow spot focused tightly at 60 mm to a diameter of 1 mm or less. It should look like a candle's image on the target. This is shown in the following picture.

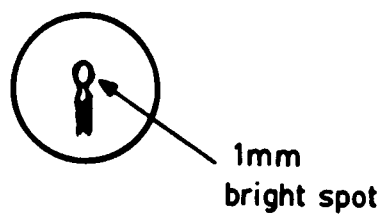

Do not confuse the yellow spot with the orange spot, which will NOT focus tightly to a 1 mm bright spot, no matter what is done. The yellow spot will focus tightly with proper positioning of the jet stream, the collimating and input mirrors.

More Information Useful for the Alignment Procedure.:

The yellow spot should be as round as possible before exiting the the laser cavity. There is a tendency for the output beam to get clipped before going out of the cavity. This should

be minimized since it distorts the beam shape and cuts down on ultimate power levels attainable. This is a persistent problem and there is no easy way to solve it. It seems to be an inherent problem with such a folded-beam cavity design. The clipping problem is something to remain aware of while going through the tuning procedure.

With the protective cover of the dye laser removed, there will be blue and green spots on the ceiling. These are reflections off of the front and back surfaces of the dye jet stream. They should be approximately oval, and they should move in unison when the vertical thumbwheel is moved (over a small one-eighth turn of the thumbwheel). There should be two orange spots at about the 2:00 or 2:15 o'clock position. They should be adjacent to each other, straddling the axis of the laser beam.

The setting of the Brewster's angle of the dye jet is critical to laser operation. It can be set using the blue and green reflections on the ceiling. Standing in line with the dye drain hose and looking up at the ceiling, the blue and green spots should be at about the 1:30 to 2:00 o'clock position. The blue and green spots should be approximately lined up with one another, i.e., superimposed, although this is not always the case. If there is a set of fringes running through the reflections on the ceiling (parallel lines perpendicular to the laser beam axis), then the quality of the dye jet is very good. The blue and green spots do not really focus but when the dye laser is working well the spots will be slightly smaller than when the dye laser is working poorly. Under good operating conditions the blue green spots will be about 6 inches in diameter on a 10 foot high ceiling.

Tuning the Laser to An Atom Line:

With the following procedure the dye laser can be tuned so that it is "stable" (about 5 minutes) on an atomic linewidth.

1. With the etalon completely pulled out - move the tuning wedge until the atomic line is found.
2. Put the etalon into its mount in the output wall of the laser.

3. Retune the etalon to the atom line.
4. Adjust the tuning wedge until recentered on the atomic line.

It should be relatively stable using this procedure. The tuning wedge and etalon are interacting to form an interference filter pair.

Severe Tuning or Alignment Problems:

The Spectra Physics service personnel are very willing to answer questions. They have a number of full-time servicemen, some on each coast. It is most helpful if the questions are VERY specific. The best individuals for servicing the Model 375 dye laser are, in order of experience and expertise with the Model 375 dye laser: Niradge Bhott in N.J. (1-800-631-5693, x26) ; Ron Humphrey in California (1-800-227-8054) ; Joe Mastermarino in California.

C) LÁSER-ENHANCED IONIZATION

Introduction and Historical Section

This research was originally motivated by a desire to find an alternative way of doing resonance ionization spectroscopy (RIS). RIS uses 1, 2 or more high-powered pulsed lasers, and is costly and complicated. RIS is the technique which makes single-atom detection (SAD) possible. It is a very exciting area of research because of the analytical possibilities it offers. The discovery of a way to bypass the complication and cost of conventional RIS would make it more accessible to analytical scientists.

While the idea of single atom counting is perhaps an esoteric novelty to most scientists, analytical chemistry has been increasingly asked to push limits of detection and minimum detectable quantities to ever smaller values. RIS methods offer analysts a general approach. Their characteristics of very low detection limits, coupled with high selectivity, demand a full investigation of the area.

Excellent theoretical treatments and reviews for both RIS and SAD have been published (148 , 149). A full historical and bibliographic treatment of the optogalvanic effect (OGE), which is the most popular RIS-related technique, has appeared (150). A succinct review giving the most salient theoretical points of these methods, as they relate to laser-enhanced ionization in microwave plasmas, is included here to clarify further discussions. The history of this project as it developed to a successful working stage will then be outlined. And finally the results of a working instrument will be presented and discussed.

Theoretical Section

Methods related to RIS, which are all special cases of RIS, are: multi-photon ionization (MPI), two-photon ionization (TPI), and laser-enhanced ionization (LEI), which is also known as the optogalvanic effect (OGE). These methods are illustrated in Figure 114 on page 304. RIS, TPI and MPI use two or more laser photons to promote an atom to successively higher energy excited states, until finally the ionization continuum is reached. The optogalvanic effect (OGE) first uses thermal energy to promote an atom to an intermediate excited state, then a laser photon to reach a a higher excited state, and finally, more thermal energy to promote the atom up to the ionization continuum where the ion can be detected.

The particular strength of ionization detectors is that every ion or electron produced can be collected with unit efficiency when strong electric fields are used. This accounts for the extremely high sensitivity that is possible with ionization detectors. This is not true of any type of photon spectroscopy since photons are usually emitted from a reaction center in all directions and cannot all be collected.

Lasers possess excellent monochromaticity and very narrow linewidths that allow selection of one particular transition of an element. In the case where two different elements have coincident excitation wavelengths, the element of interest can be furthered selected using a second laser photon to excite it to an excited state which only it possesses. If there is still a problem with selecting one particular element out of all the others, the probability of any remaining overlap can be virtually eliminated by using a third laser photon. And if the laser beams are intense enough, every atom with the correct energy states within the laser excitation volume can be excited and ionized.

It is because of the unit collection efficiency of ion detection methods, combined with the selectivity and the ability to excite every selected analyte atom (unit excitation efficiency)

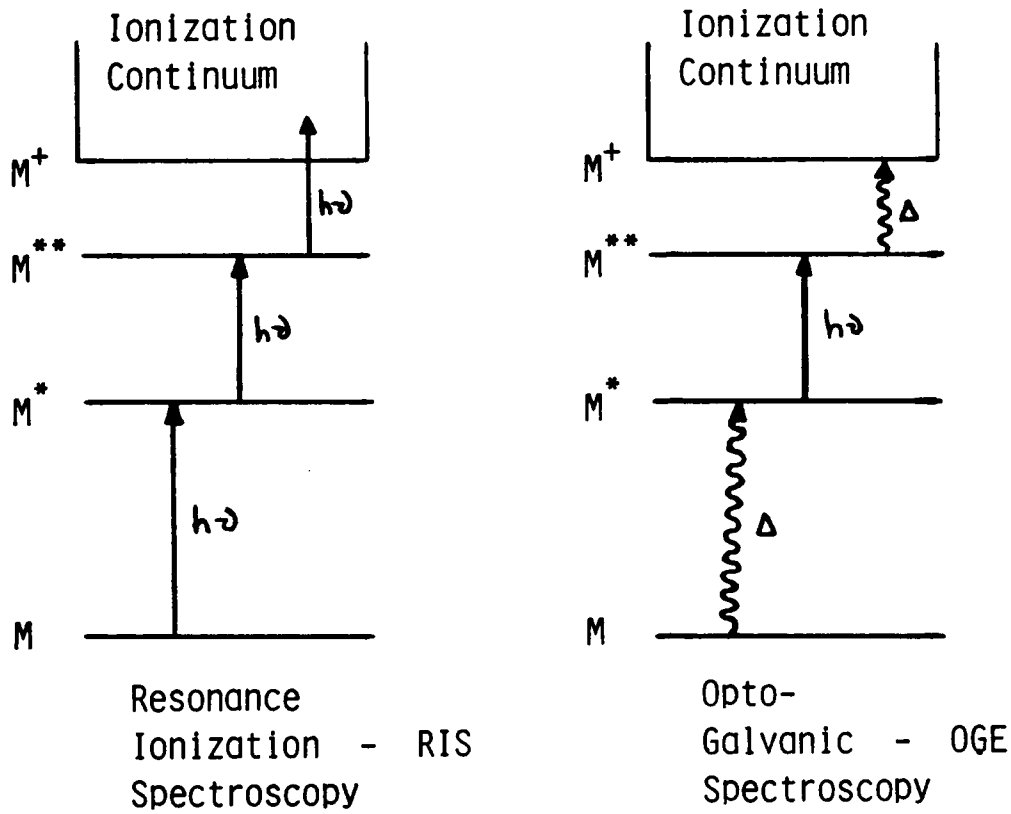

Figure 114. Ultrasensitive Laser Ionization Methods

offered by lasers, that RIS methods are the most powerful available for atomic analysis. The biggest problem with the application of these techniques to everyday problems has been the expense and complications involved with using 2 or 3 high-powered pulsed lasers.

History of This Project

The original intent was to use the energy of the metastable nitrogen molecule to replace the energy that would normally come from a laser in a conventional RIS scheme. This scheme is illustrated in Figure 115 on page 306. Early attempts to detect metastable energy transfer assisted RIS (METARIS) were carried out by James Berkquist in our laboratory (36). Even after heroic efforts, no measureable signals were found. It is believed that either there was a sensitivity problem, i.e., there was an order of magnitude fewer ions being produced at steady state than the detector could measure; or, not enough active nitrogen was present. Since very sensitive amplifiers were used, it was believed that the concentration of active nitrogen was too low.

The literature pointed to high pressures as the simplest means to increase the concentration of active nitrogen metastables (55). Therefore the high-efficiency N_2-MIP cavity operating at 1 atmosphere was developed. Spectroscopic characterization of the discharge revealed that a detectable amount of $N_2(A)$ metastables was not being produced. The METARIS experiments were attempted anyway. And, as often happens in science, though the originally sought-after result did not materialize as planned, an observed side-effect led to a very fruitful end result. Though the METARIS signals were virtually buried in noise, ***VERY*** strong laser-induced fluorescence (LIF) signals were observed. Characterization of this LIF in the N_2-MIP provided the basis for the bulk of this dissertation.

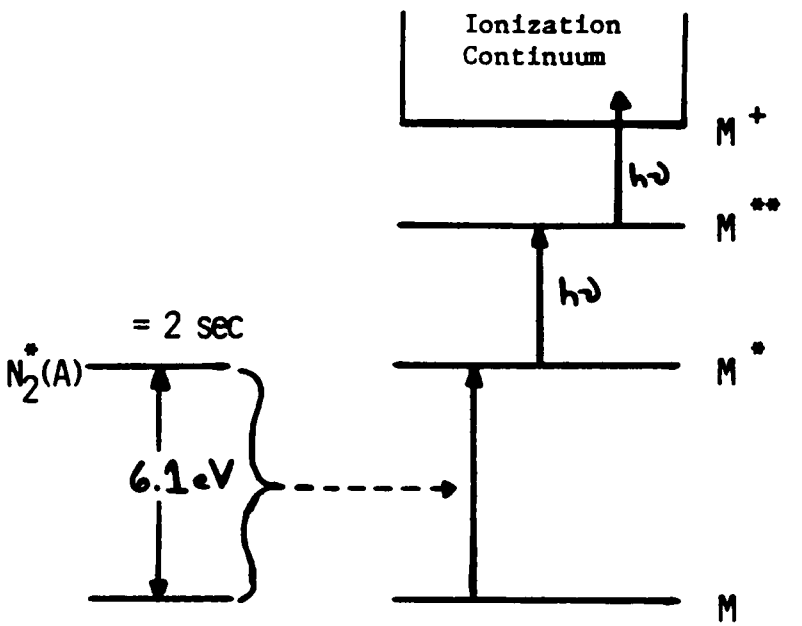

METASTABLE ENERGY TRANSFER ASSISTED

RESONANCE IONIZATION SPECTROSCOPY

(METARIS)

Figure 115. Metastable-Energy-Transfer-Assisted Resonance Ionization Spectroscopy

Toward the end of the LIF and AES characterizations of the N_2 -MIP, it was noticed that whenever the laser was turned away from the center of the plasma, it always took a noticeable amount of time (2-3 seconds) for the background emission intensity to return back to "ambient" level. This was observed both visually and electronically. This indicated the laser was perturbing it from its normal steady-state and that significant plasma heating was probably occurring. Plasma heating alone can cause significant changes in the ionization rates in the plasma. It seemed important to try the METARIS experiments once again after the LIF experiments were complete. The S/N ratio problems in the early initial METARIS experiments had, to a large extent, been caused by noise generated by the microarc sampler and both frequency and intensity instability in the laser. These problems were eliminated during the course of optimizing the LIF instrument response.

Laser-Enhanced Ionization - Background Information

It was hoped that even if the METARIS process was not efficient enough to allow detection, another RIS-type process, laser-enhanced ionization (LEI), would be observable. LEI is the name applied to the optogalvanic effect when it is done on analytes in flames. The optogalvanic effect has two components, one being wavelength-specific and the other being non-wavelength-specific. The non-wavelength-specific component is a global heating effect due to electrons being accelerated by the intense electric field of the laser. The wavelength-specific effect is much more pronounced and is due to energy absorbers such as atoms and molecules. These atoms and molecules can be the plasma support gas, or they can be analytes "seeded" into the plasma. Atoms and molecules typically absorb ultraviolet or visible photons from the the laser field. Once absorbed, they cause much more plasma heating and ionization than the global heating effect. The photon energy can be converted to heat by radiationless processes. The increase in the ionization rates caused by plasma heating is easily detected as a current by using high-voltage electrodes in the plasma.

The literature reports that laser-enhanced ionization has been done in thermal flames (150 , 151 , 152 , 153 , 154), glow discharges (155 , 156), hollow cathode plasmas (157 , 158 , 159), heat pipes and atom ovens (160 , 161 , 162), thermionic diode discharges (163 , 164 , 165), RF discharges (166 , 167 , 168), in an ICP (169), and in a microwave plasma (170). Most of these studies were for plasma diagnostics. Small molecules or inert gases acting as the discharge support gas were photo-excited and the excited state spectra were measured opto-galvanically (155 -159 , 163 -165 , 166 -168 , 170). A perusal of the citations contained in reference (154) show that the vast majority of all OGE studies have been physical diagnostic studies of various gases supporting the plasma discharge. This includes heat pipes and atom ovens, in which physical studies of atomic excited states were done. These excitation sources have provided exceptional minimum detectable quantities, typically in the ***femtogram*** range. The low temperatures, hence low-noise backgrounds, of these sources account for these exceptional results. However, the low temperatures also limit the atomization capabilities, and the practicality of these sources for routine analysis. A minority of the OGE studies have addressed analytes introduced into a plasma (151 -154 , 169)

The literature points to the potential success of the LEI experiment in a MIP. The atomization and excitation properties of the N_2-MIP suggest that it is a nearly-thermal atom source. LEI works very well in a flame. LEI has been observed in the ICP, even though the limits of detection were very poor because of excessive background ionization inherent in the ICP (169). Roughly speakly, the MIP is intermediate in its ability to atomize, excite, and ionize; i.e., it lies between the ICP and chemical flames. For these reasons, it was felt that LEI in the MIP would be successful, and would be expected to fall somewhere near chemical flames in utility. Indeed, the work performed in this laboratory by the author has established this to be true.

Initial Laser Enhanced Ionization Experiments - History & Results

A few different attempts and approaches were used in this study to search for LEI signals in the MIP. These are reported here in brief outline for three reasons: 1) to record the results of the different approaches in an accessible place; 2) to allow others to ascend the experimental learning curve more quickly; 3) to eliminate repetition by others of the less successful approaches.

Vacuum Flow System with Microprobe Ionization Detector:

The earliest approach to detecting LEI in the MIP is shown in Figure 116 on page 311. It was thought that this flow system would provide the capability to do both LEI and LIF in the MIP afterglow. However, no LEI analyte signals or global heating LEI signals could be observed in the afterglow region. The system involved a tubular quartz system with quartz windows vacuum-epoxyed onto various positions on the flow system that were convenient for viewing emission and fluorescence from three different positions. One viewing position was immediately after the MIP cavity, another farther along in the afterglow, and finally one opposite the MIP cavity.

Originally the ion detection system was offset from the main axis of the MIP cavity with the intent of protecting the electrodes from photoelectric emission caused by UV light emitted from the plasma. The entire system was vacuum-tight and allowed the MIP to be studied at reduced pressures. It was used for studying the N_2 plasma discharge emissions at low and high pressure. Emissions were viewed from the window opposite the MIP cavity using a long focal-length lens.

The afterglow did not extend to the opposite end of the flow system and around the bend as was expected, even at reduced pressures. The METARIS process had no chance of

working until the detection electrodes were moved into a very energy-rich region of the afterglow.

A new vacuum flow system made of 1 inch square quartz tubing was constructed. It was 6 inches long, straight, with no bend, and had a connection to a vacuum on-off valve that could be used for regulating the flow, and hence pressure, of the gases coming from the cylinders. The square tubing with parallel walls provided the advantage that signals could be searched for by moving the laser and detection electrodes along the MIP axis continuously.

A new type of detector was used with the new flow system. It is shown in Figure 117 on page 315. It comes from an original design by Terrill Cool (171). It was constructed entirely of platinum wire and ceramic insulators. The ball on the end of the tip of the probe was formed by heating 18-gauge Pt wire with an oxy-acetylene torch. The surface tension of the molten Pt pulled up enough metal to form a spherically-shaped ball on the end of a piece of wire hung upside-down.

This probe offers many advantages over parallel plate detection electrodes. A very intense electric field exists around the very small tip, with up to 1000 volts applied relative to the cathode. This very strong positive electric field causes electrons to be pulled to the tip as soon as they are created by the ionizing laser radiation. Electrons are detected so quickly, that ions do not even have time to make it to the cathode. Electrons move very fast compared to ions because of their much smaller size. The resultant current pulse is shown in Figure 117.

This probe promises to greatly improve detection of laser-produced ions. It provides very good temporal filtering of electrons from ions. Space-charge effects are eliminated because of the very small time scale on which the probe operates. Virtually all electrons are collected by the probe tip before space-charge effects have time to occur. The small size of the probe makes it ideal for a miniaturized LEI detection system.

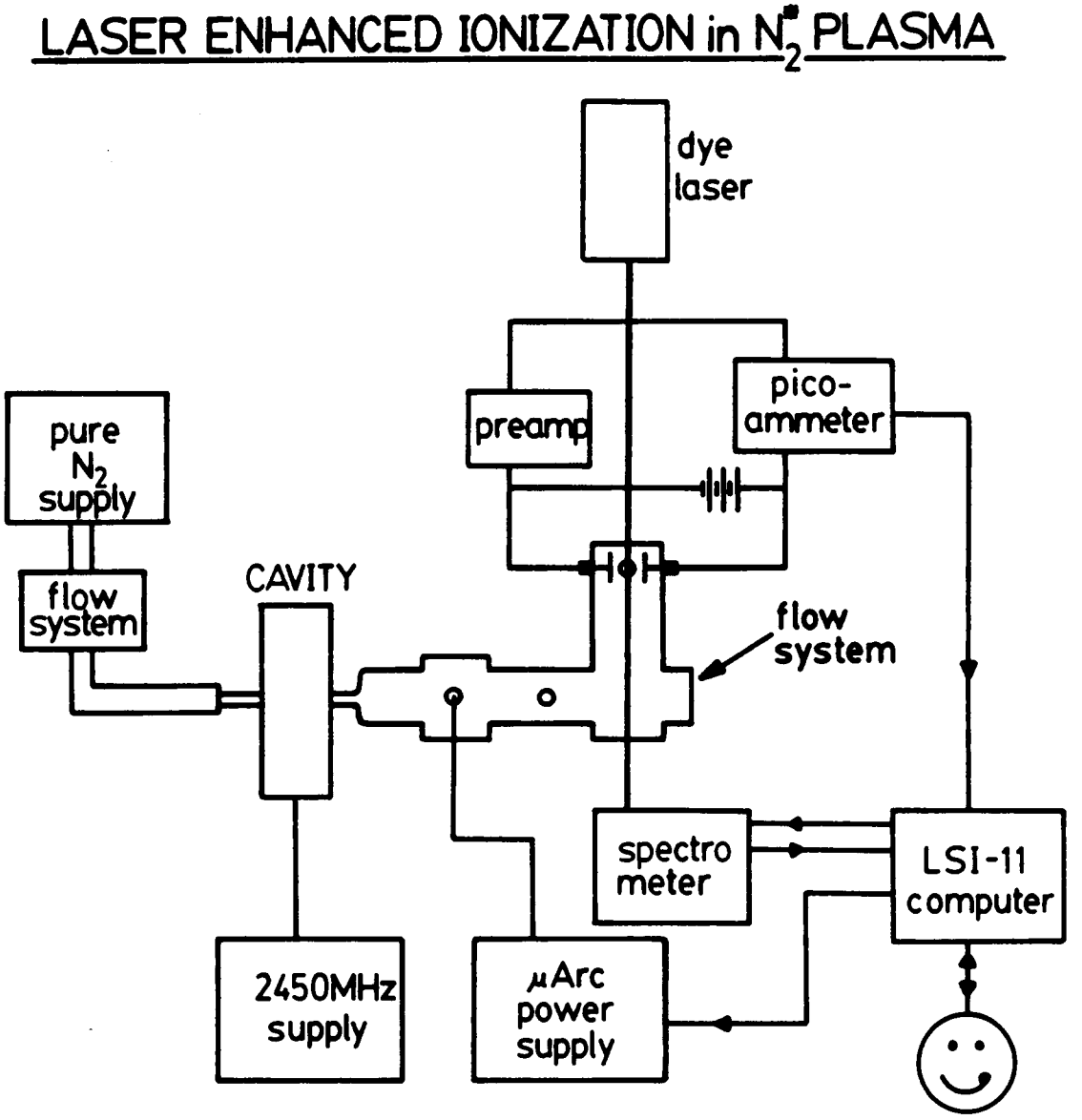

Figure 116. Early Flow System & Detection System Used for Experimentation

The probe detector was mounted in a miniature pyrex glass holder. The holder was positioned inside the square quartz flow system. The probe holder could be easily repositioned. The probe leads were long enough to be adjusted by bending before they exited the vacuum flow system thru a set of electrical feed-throughs. The experimental design shown in Figure 118 on page 316

Initial Results Using The New Flow System and Microprobe Detector:

Initial attempts to measure LEI of analytes failed. At first, direct LEI of the analytes was attempted, and then a search for the global heating effect was made. No signals were detected above the background as the laser wavelength was scanned. It was realized that if signals were present, they were too fast to be detected with a lockin amplifier. The detection system must detect the electron pulse before the recombination of the ions and electrons produced by the laser occurs. At 1 atmosphere the atom-ion recombination times are on the order of 100 microseconds. A synchronous motor chopped the laser beam at a frequency of 1440 Hz. This gave laser pulses that were 694 microseconds long. Laser pulses **much** shorter than 100 microseconds should be used with the microprobe detector, in order to resolve the ionization processes occurring. Much faster chopping of the laser light was needed, and a gated detection system was needed.

One design with potential involved a photoelastic modulator on the output of the CW laser. This could modulate the laser beam faster than the recombination time of the ions and electrons. These devices can provide 50% duty cycle modulation at video frequencies, i.e., faster than 1 MHz. A Biomation transient recorder would solve the problem of a gated detector on the output of the amplifier. In the process of installing these devices, with the ancillary gating circuitry, another approach was found in the literature which greatly simplified the whole experiment (170).

Direct Approach - Electrodes Near Discharge Region at 1 Atmosphere:

This new approach put detection electrodes directly in the tail-flame of the MIP. This is shown in Figure 119 on page 317. Suzuki et al. used this to perform OGE on the Ar and He support gases in a reduced pressure MIP (170).

Initially, high voltage electrodes very near the discharge region were avoided because of concerns that arcing from the electrodes to the cavity and microwave circuitry would interfere with or damage either the microwave cavity or the magnetron. Earlier studies done for this dissertation demonstrated problems with arcing through the ceramic insulator separating the electrodes of the microprobe detector when it was placed in the afterglow region with 900 to 1000 volts applied to it. However, when two tungsten welding rods were bent and clipped into an extended discharge torch, arcing between the tungsten electrodes did not occur until an applied voltage of 1500 to 1800 volts was used. A much larger gap (1.5 mm) existed between the W electrodes than for the electrodes of the microprobe detector (about 1 mm). There was an even larger gap between the detection electrodes and the microwave cavity, thus avoiding the arcing problem.

Unfortunately, the expected signals were not seen, (see Figure 119 on page 317). The background noise level was quite high because of erratic operation of the microarc sampler. Large intensity fluctuations were visually observed in laser-induced fluorescence. These fluctuations in LIF signals seen were attributed to fluctuations in Na mass flow through the system.

Laser Enhanced Ionization with Background Correction Using LIF:

The LIF signal fluctuations were used to correct for the mass flow fluctuations of the sampler. One lockin detection system was used to monitor the Na mass flow variations measured by the LIF signals. A second lockin detection system was used to monitor the LEI signals. Using a ratioing option built into the second lockin amplifier, a ratio was taken which

corrected for the portion of the LEI signal due to mass flow variations alone. The full detection scheme is shown in Figure 120 on page 318.

The output of the ratioing option on the second lockin amplifier was fed to a level shifter constructed from a 318 operational amplifier. The level shifter circuit was needed to bring the signals from the ratioing unit into the range of -1 to +1 volt needed for the HP 3990A integrator. The integrator was used to sum signals over a period from 10 seconds to 1 minute. Longer integration times provided better signal-to-noise ratios.

LEI signals were obtained despite the excessive noise. This noise was due to microarc sampler noise, laser intensity and frequency instabilities, and inherent electrical noise in the MIP electrical discharge. However, the best results were very poor, having a signal-to-noise ratio of 6 or 7 divided by 1E+6. These results precluded the use of the instrumental design for analytical studies.

At that point the LEI experiments were temporarily abandoned in favor of the LIF experiments. The emphasis of the research shifted to the physical characterization of LIF in the MIP (LIF/MIP). A short time later the microarc sampler was abandoned because it was too noisy and irreproducible. The glass frit nebulizer discussed in the chapter on LIF apparatus was developed for the MIP. It provided continuous, stable, low-noise and low-drift operation for all experiments. The laser instabilities were corrected with 3 total realignments of the internal optical train. The overall performance of the system was optimized and the physical and analytical characterization reported in the body of this dissertation was completed.

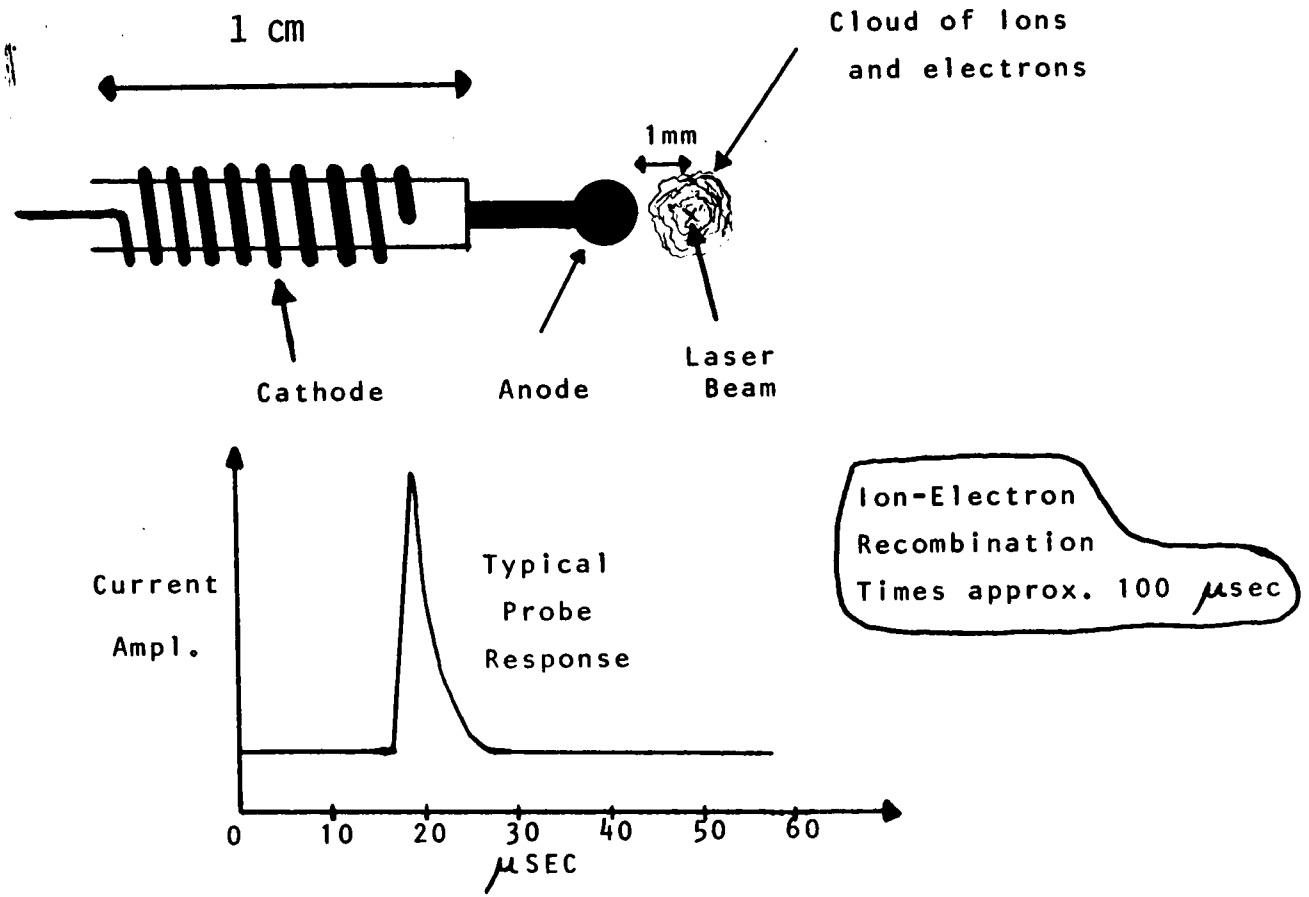

Figure 117. Microprobe Ionization Detector.

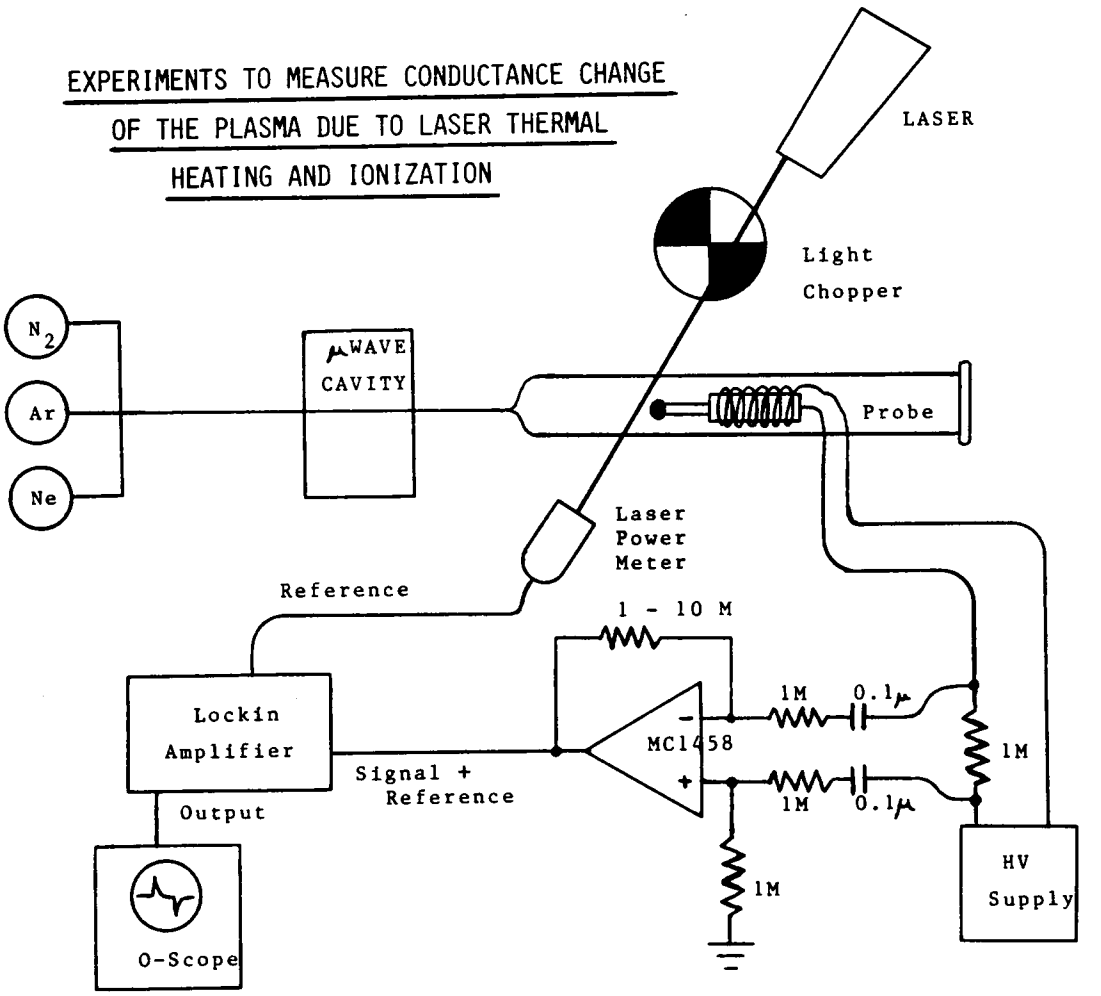

Figure 118. Experimental Configuration Used for Initial LEI Experiments

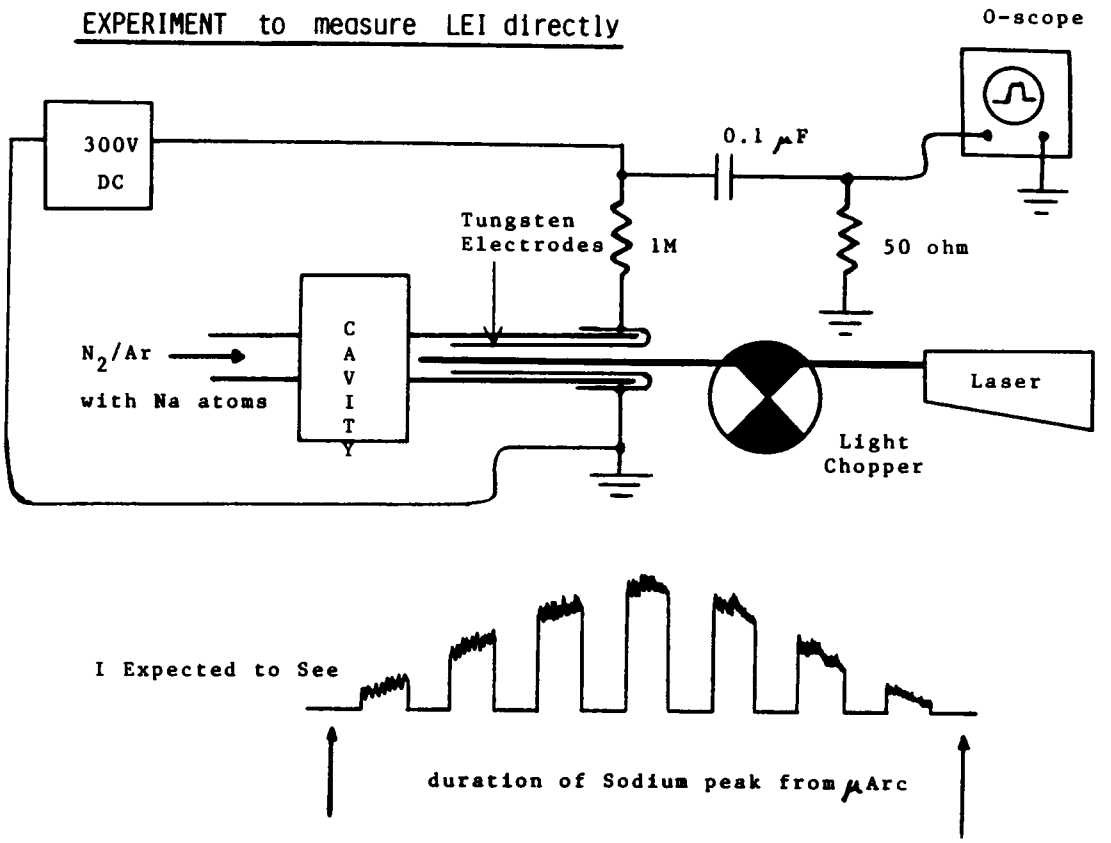

Figure 119. Direct Approach for Ionization Detection.

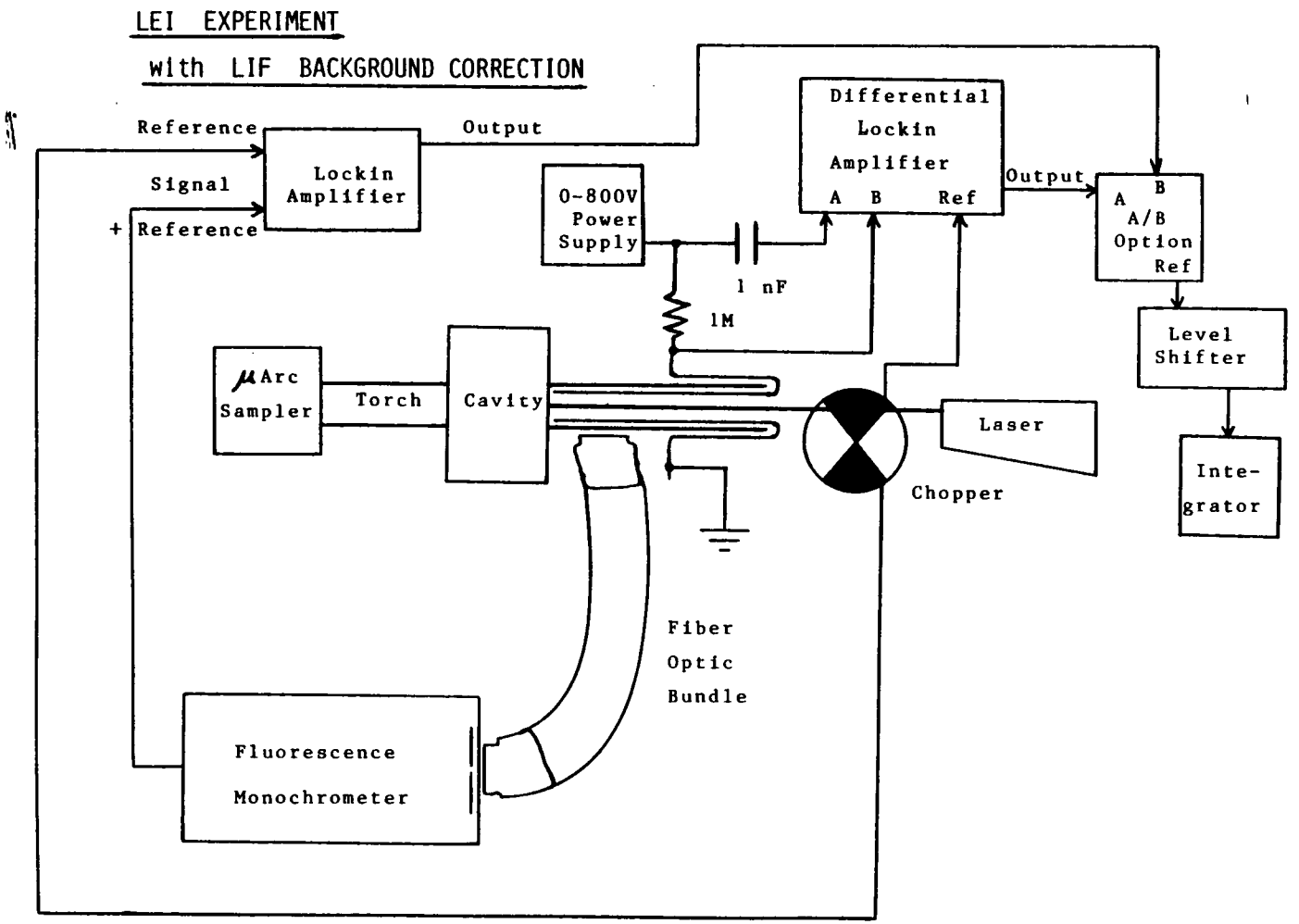

Figure 120. Combined LEI/LIF Approach for Ionization Detection

Final Laser Enhanced Ionization Experiments - Apparatus & Results

Apparatus

After the LIF/MIP research was completed, the LEI/MIP experiment was attempted again before dismantling the entire apparatus. The final LEI instrument configuration used is shown in Figure 120 on page 318. At first, tungsten welding rods bent into clips which looked like bobby-pins were placed in the extended tangential flow torch. The distance from the electrode tips to the discharge could be adjusted by sliding the clips toward or away from the cavity wall. This may be better understood by looking at Figure 119 on page 317.

Strong Na LEI signals were obtained! The largest LEI signals were obtained when the electrodes were immediately outside the cavity wall. However, in this position there was a problem with electrode heating. They actually fused into the walls of the tangential flow torch after about 3 hours. To eliminate this problem, the extended torch was cut off at the exit wall of the cavity, and an electrode support structure was constructed as shown in Figure 122 on page 321. The electrode spacing was adjusted by loosening the locking set screws, setting the desired gap, and then relocking the set screws. The distance of the electrodes from the cavity wall was adjusted by moving the entire assembly toward or away from the cavity wall. In this way, the LEI signals were profiled as a function of electrode distance above the cavity.

Two different types of electrodes were used. They are shown in Figure 122 on page 321. The 1 mm tungsten welding rods were bent using an oxy-acetylene torch and then put into the holder. Each of the 18 MM diameter circular stainless steel (SS) plate electrodes, and the small rods for mounting and making electrical connections, were machined from a single piece of 1-inch diameter 316-type stainless steel.

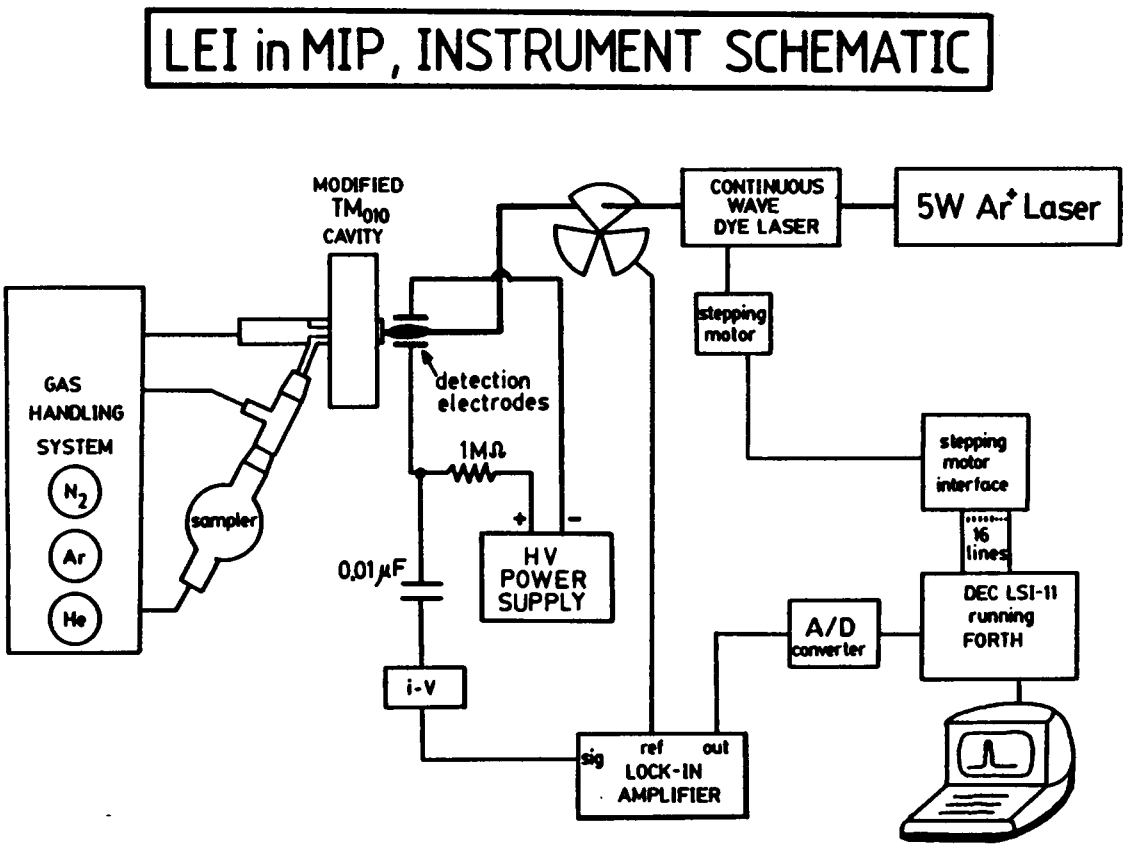

Figure 121. Final Laser Enhanced Ionization Instrument Schematic

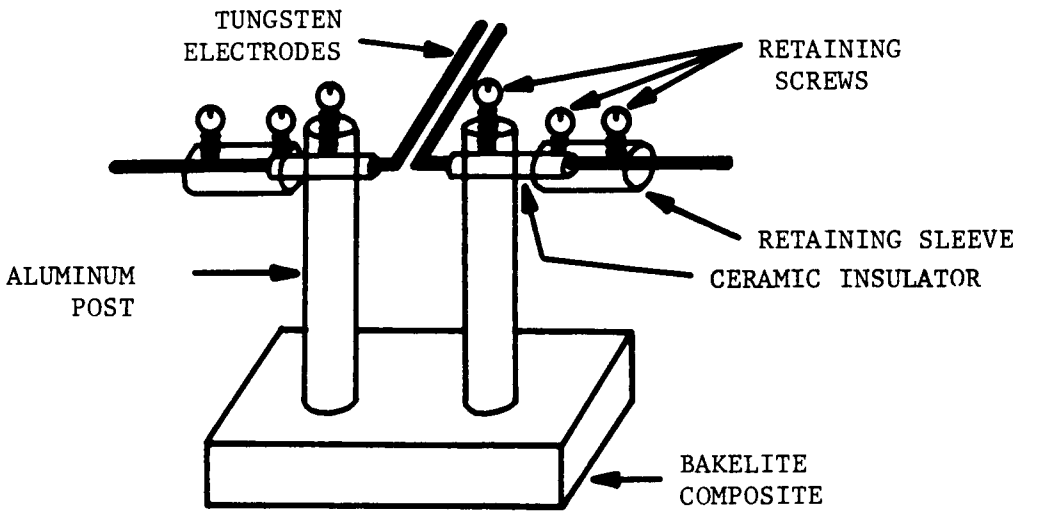

ELECTRODE
MOUNT

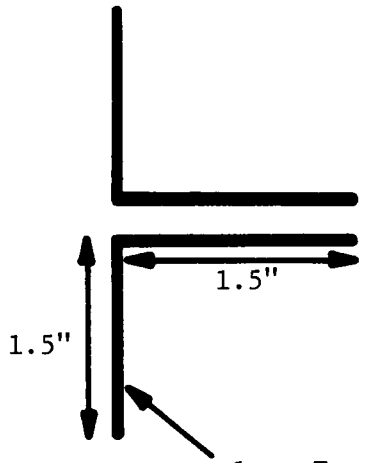

TUNGSTEN WELDING
ROD ELECTRODES

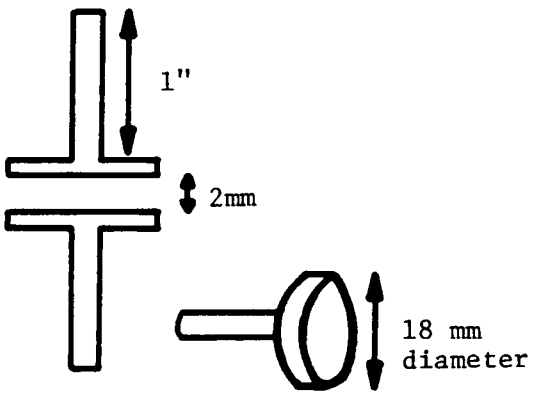

STAINLESS STEEL
CIRCULAR PLATE
ELECTRODES

Figure 122. LEI Detection Electrode Mount with Electrode Geometries Shown

Results

LEI signals were detected for Na, Ba, and Li. Na was chosen as a diagnostic probe for the LEI studies because the laser had the greatest intensity and stability at the sodium D line (589 nm). The experimental variables that most significantly affect LEI signal intensity are : 1) electrode geometry, spacing, voltage, and distance above the cavity, 2) applied microwave power, 3) gas composition in a N_2/Ar mixture, and 4) laser intensity. Experiments were performed to measure Na LEI signals as a function of each one of these variables. An analytical working curve was constructed for Na, and a limit of detection was calculated. Results for each type of experiment are presented sequentially in the following sections.

Electrode Geometry and Voltage Effects on LEI Signals:

Detection electrode geometry significantly influence LEI signal intensity. Electrode spacing and voltage are interrelated. There is a sheathing effect due to a very strong spatial polarization of ions and electrons in the plasma, called the "space-charge" effect. Because electrons move much faster than ions, they are depleted in the vicinity of the electrodes, leaving behind a positively-charged sheath of ions around the cathode. At increased voltages and current densities, the sheath gets very dense and the electrons no longer feel the full effect of the applied electric field. In severe cases it reduces to zero the net electric field felt by the electrons. The voltage must then be increased, to the point where the edge of the sheath extends beyond the anode. When the sheath extends beyond the anode, the electric field is everywhere non-zero. This voltage is called the saturation voltage since every electron-ion pair is detected. It is desireable to operate the detection electrodes in saturation mode, with the applied voltage as large as possible without arcing. However, sometimes arcing occurs too close to the signal saturation point.

A voltage and geometry must be experimentally determined which allow efficient signal collection without arcing. Achievement of the saturation condition depends greatly on

electrode shape, and extent of plasma ionization (which depends on signal detection height in the MIP). Experiments were conducted to determine the effects of electrode shape, voltage, spacing, and detection height in the MIP.

One-millimeter diameter tungsten welding rods were used first. Electrode spacings of 1.0, 1.5, and 2.0 MM were tried. An electrode spacing of 1.5 millimeters gave the strongest signals for all voltages up to the arcing thresholds, and at all distances away from the cavity. From the increasing slope of Figure 123 on page 325, it is obvious that detector signal increases as the electrode voltage increases. This occurs up to the value of 700 volts, where electrode arcing begins to occur. The ion-collection saturation point is beginning to be reached, where every ion-electron pair created by the laser is detected. This is indicated by the "bending over" of the curve in Figure 123 as higher voltages are used.

These small diameter electrodes have very high electric fields around their tightly-curved surfaces, and they collect electrons very efficiently. However, electrons moving in the vicinity of the electrodes experience a very anisotropic electric field, which can cause non-linear and unpredictable effects. For the 1 mm tungsten electrodes, arcing occured too close to signal saturation. The anisotropic electric field caused problems with signal non-linearity in the analytical working curves. This will be seen in the section on analytical feasibility studies at the end of this appendix.

The 18 mm diameter SS plate electrodes have a very different voltage/current characteristic. This is shown in Figure 125 on page 327. Above 2100 volts arcing invariably occurred. The arcing threshold voltage for the circular plate electrodes is considerably higher than for the tungsten rods. The SS plates do not have the highly-curved surfaces of the 1mm diameter W electrodes. Also, the circular plate electrode spacing was 2 mm instead of the 1.5 mm spacing used for the tungsten rods.

Electrode distance was varied to find the best position along the plasma axis for measuring LEI signals. Results are shown in Figure 124 on page 326. Identical results were obtained for both types of electrodes. In both cases the signal maximum occurred when the tips of the electrodes were 5 mm away from the cavity wall. The signal maximum decreased rapidly as the electrodes were moved away from this position. The electrodes were positioned at 5 mm for all studies.

It appeared as though signal detection was not occurring over the full length of the either type of electrode. Signals were approximately the same magnitude for either set of electrodes. What mattered most was the position of the electrode tips, not the length of the electrodes in the tail-flame. This was also evident because when arcing occurred, it always started at the very tips of the electrodes closest to the cavity wall. This was anticipated since the MIP plasma ionization plume is spatially very nonisotropic, and arcing will initiate in the the region of highest conductance.

Microwave Power Study Results:

The applied microwave power affects plasma and analyte ionization, and particularly the "thermal" energy in molecular plasmas. Signal generation in LEI and OGE relies on thermal energy for the analyte ionization. Thus signals can be expected to increase exponentially with a linear increase in plasma energy, as predicted by a Boltzmann distribution. In LEI in flames, collisional ionization probabilities increase by 2 orders of magnitude for each eV of energy that moves an atom closer to its ionization limit (172). A similar increase is expected in the MIP. Experiments were conducted to measure the influence of MIP power on LEI signal intensity.

Both types of electrodes gave the same type of response when the applied microwave power was varied. The LEI signal increases very rapidly when the applied microwave power is increased, until arcing across the electrodes occurs. This rapid rise in signal intensity is

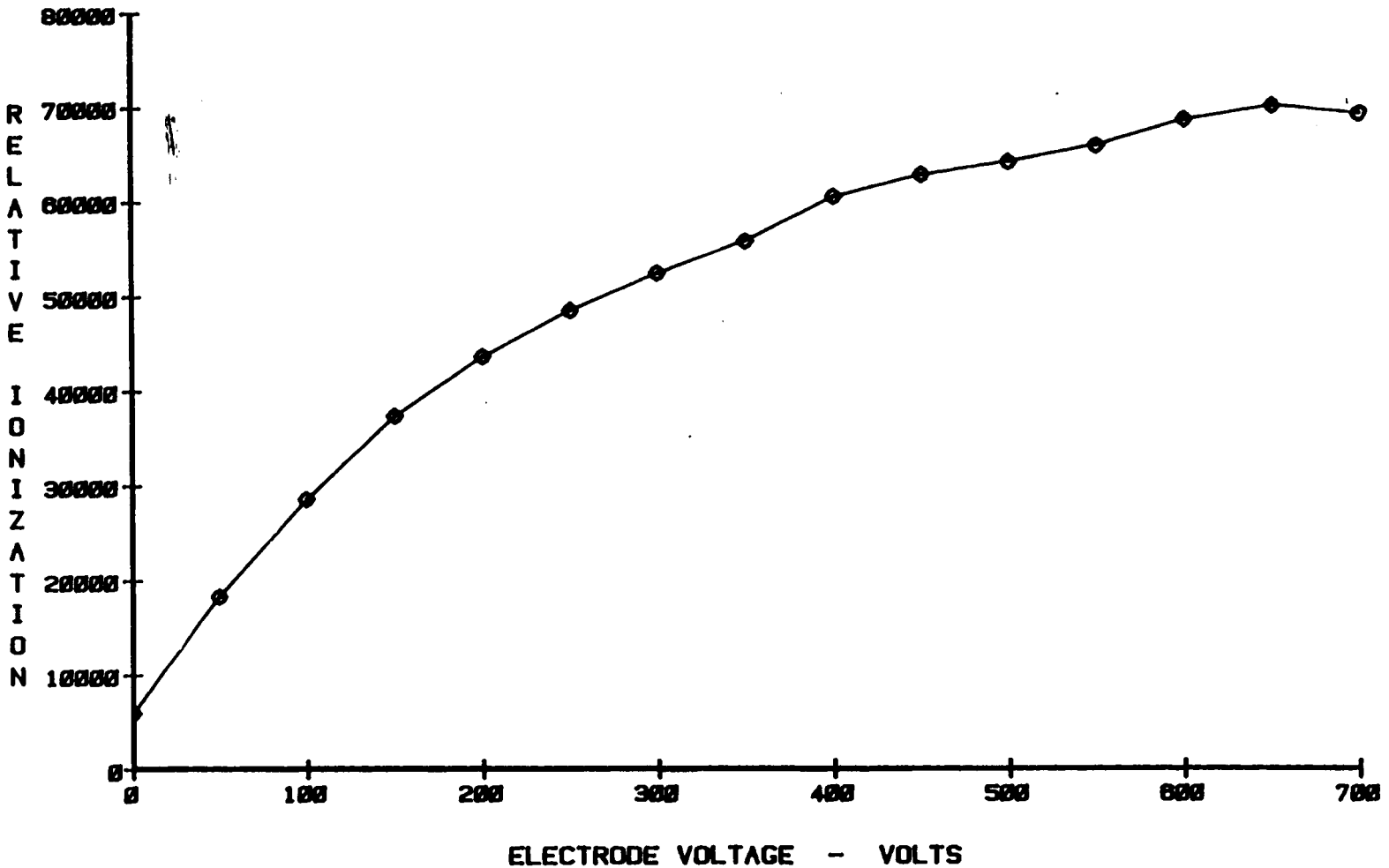

Figure 123. Na LEI Signal Intensity vs. Electrode Voltage - Tungsten Rod Electrodes

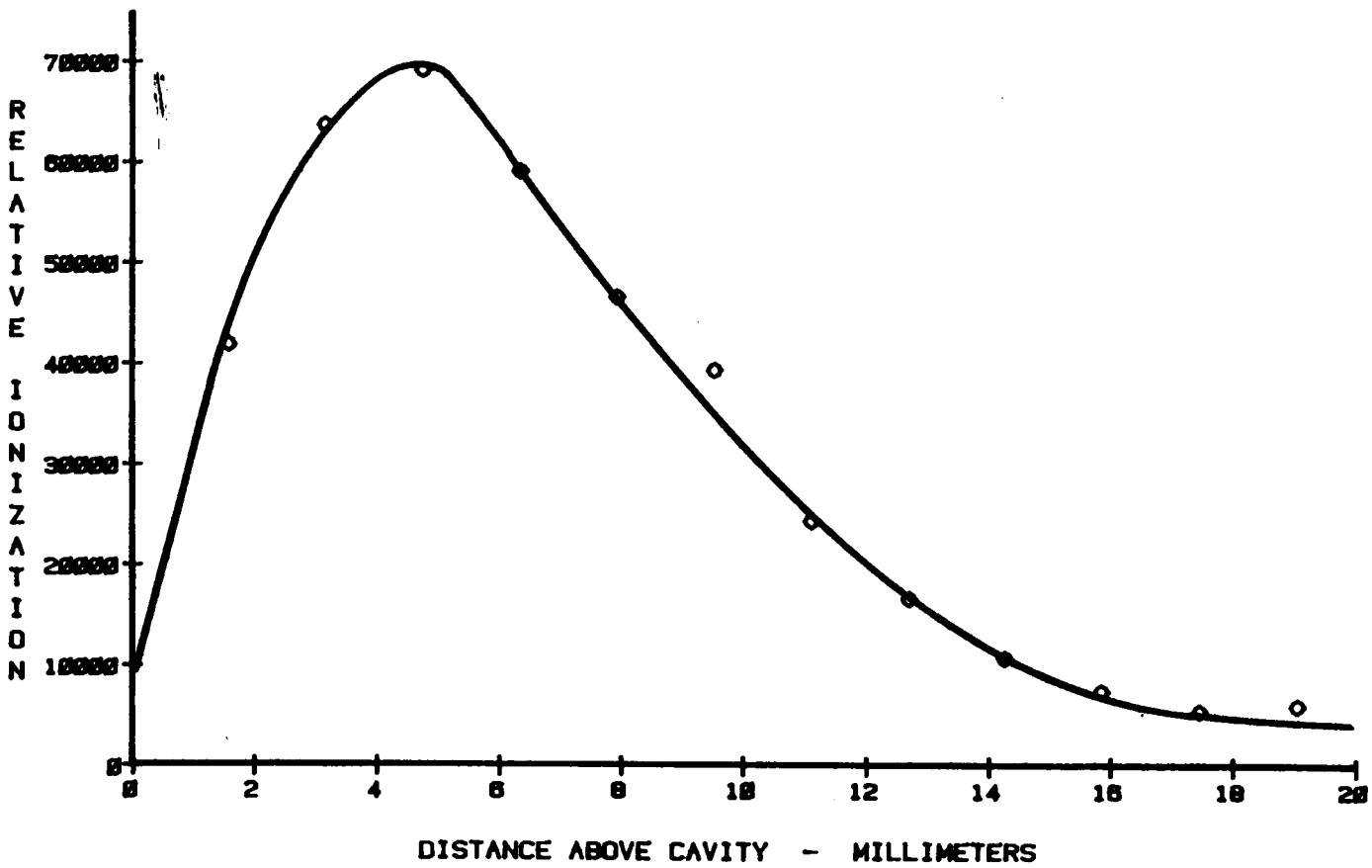

Figure 124. Na LEI Signal Intensity vs. Electrode Distance - Tungsten Rod Electrodes

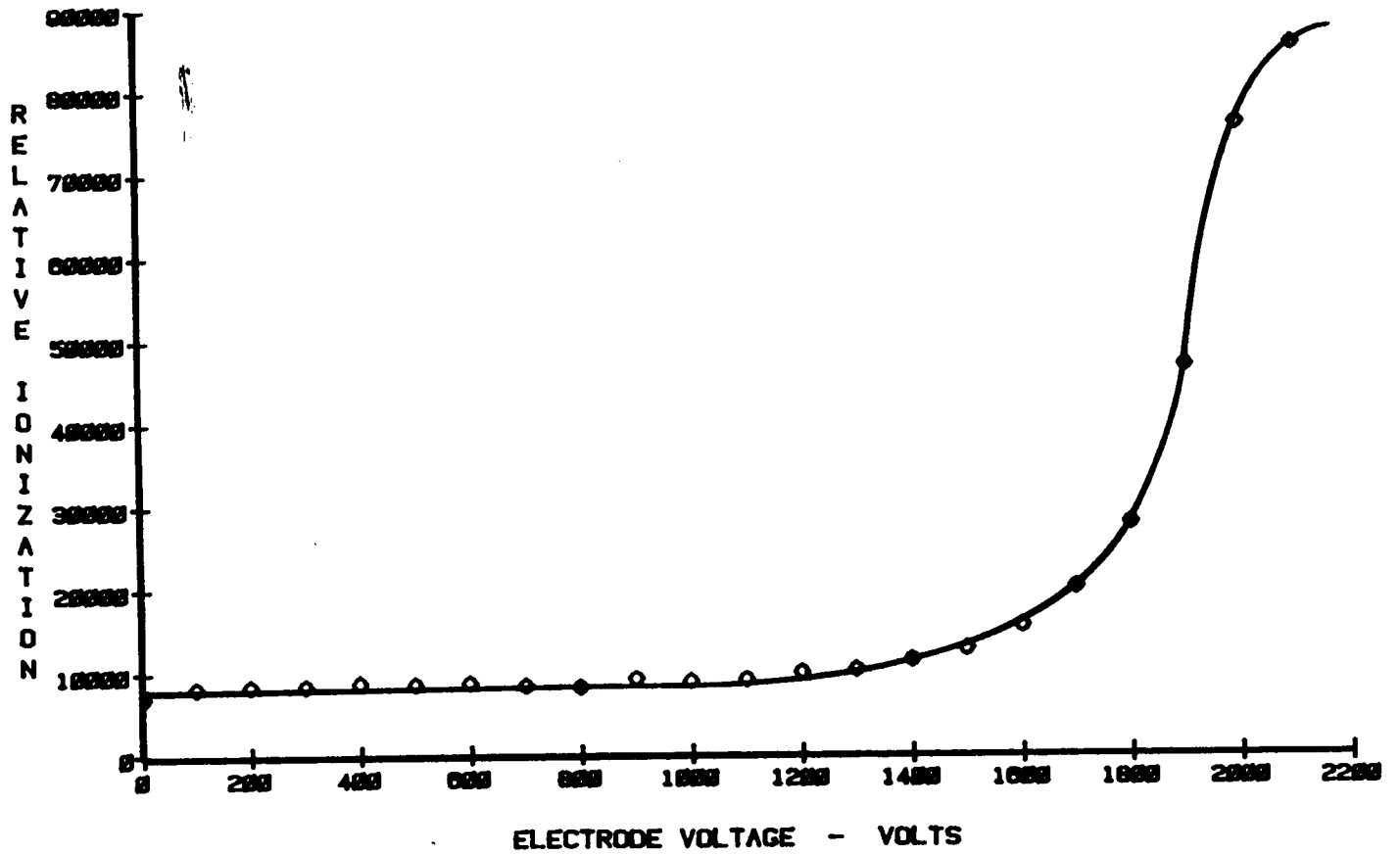

Figure 125. Na LEI Signal Intensity vs. Electrode Distance - Stainless Steel Disc Electrodes

consistent with that predicted by a Boltzmann distribution. This increase is illustrated in Figure 126 on page 329.

The threshold for arcing was highly dependent upon the electrode voltage used. Generally the electrode voltage and the microwave power were set as high as possible, without being too close to the arcing threshold. The voltages and MIP power used were: 700 volts for the W electrodes, 1900 volts for the SS electrodes, and 60-70 watts MIP power. These settings were safest for the instrumentation and gave the largest LEI signals.

Gas Composition Study Results:

Gas composition in mixed inert/molecular plasmas greatly influences plasma conductivity because of the large differences in neutral gas electrophilicity. Thus, gas composition greatly affects LEI signals in the MIP. Experiments were performed to measure these effects.

The Na LEI signal nearly doubles as 10-20% nitrogen is added to a pure argon plasma. For 20 to 100% nitrogen gas composition, the LEI signal linearly decreases, almost to its value in pure argon. This is shown in Figure 127 on page 330. This appears to be caused by the same phenomena that caused similar looking peaks in the Na atom emission, Ba ion LIF, Ba atom emission, and Ba ion emission results.

It is unknown exactly what causes these peaks. It does not occur in Na atom LIF. Na atom LIF is the only process studied that does not require excitation energy from the plasma. Na LEI requires approximately 3 eV to reach the ionization continuum after the laser excites the Na atom from the ground state to the 2.10 eV excited state. It is unlikely that 3 eV of energy are absorbed from the high-energy electrons in the plasma since this would require electron temperatures over 20,000 degrees Kelvin. Metastable energy states of the support gas possess enough energy for excitation and are more likely the cause of analyte excitation.

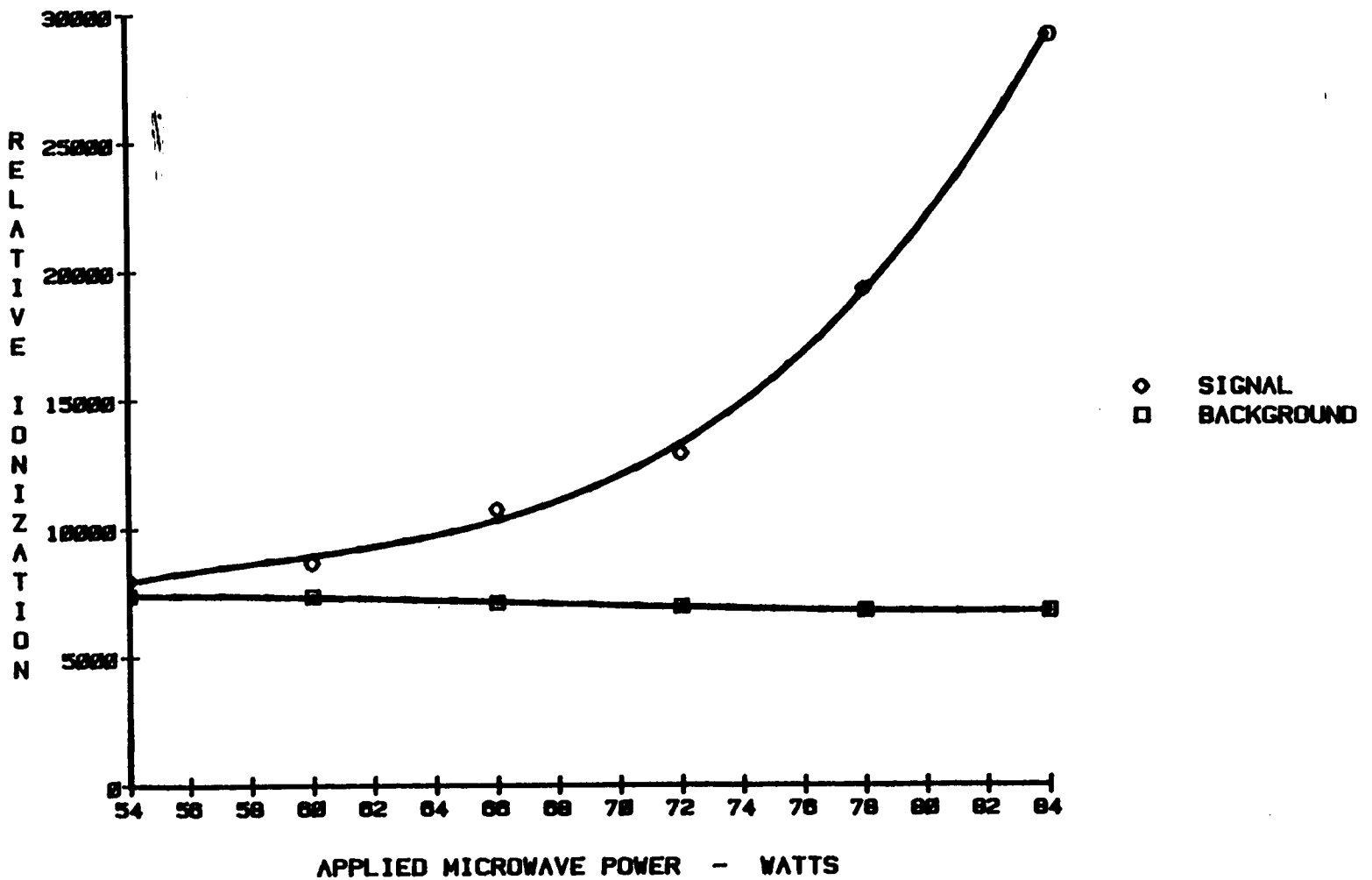

Figure 126. Na LEI Signal Intensity vs. Applied Microwave Power

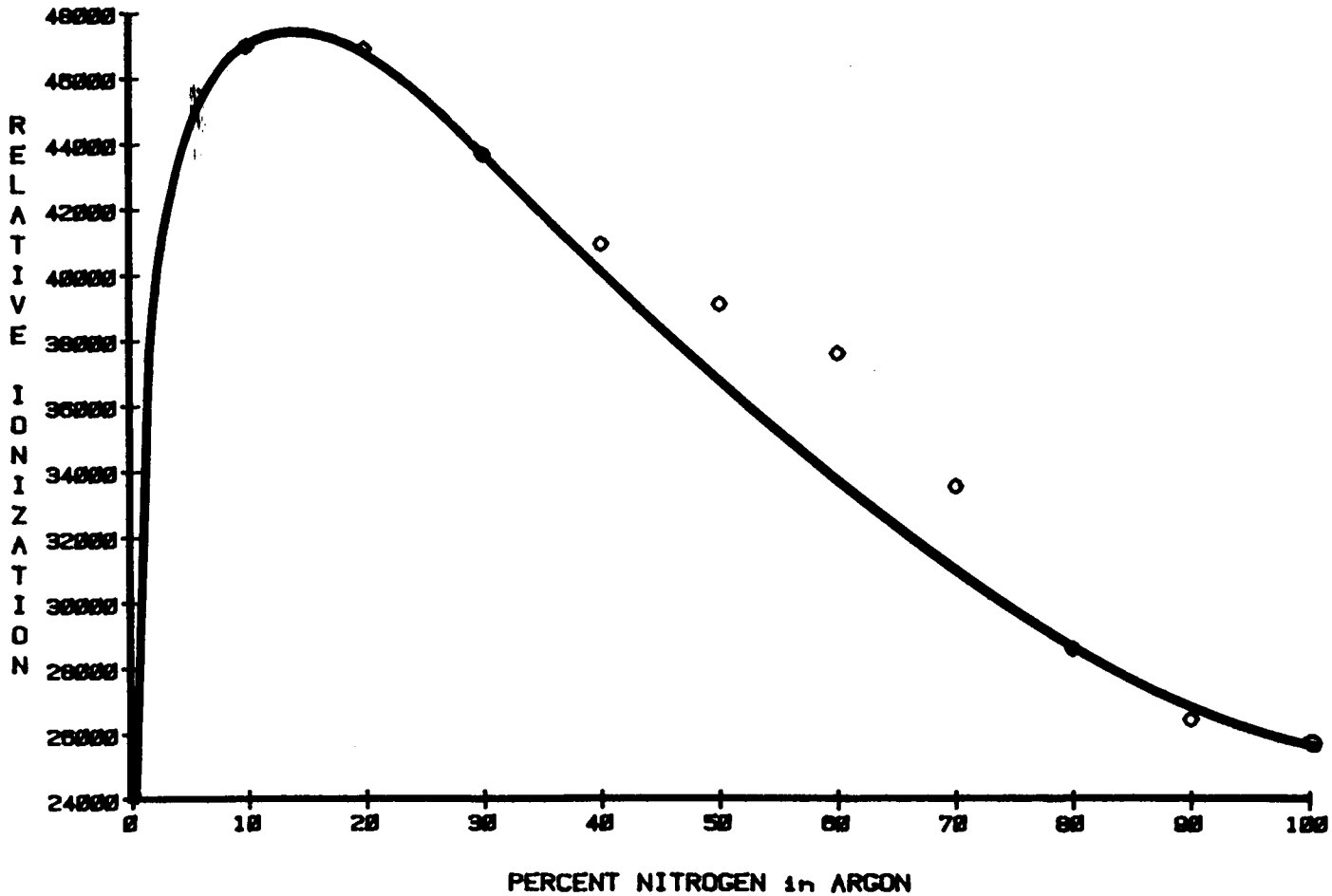

Figure 127. Na LEI Signal Intensity vs. Gas Composition

Na LEI Signals as a Function of Laser Intensity:

LEI signal intensity increases steadily as the laser power increases, (see Figure 128 on page 332). Signal saturation is not as easy to achieve with LEI as it is with LIF (173). With very high photon fluxes nonlinear, multiphoton ionization begins to occur, and is seen as a large increase in the ionization signal. No large increase in ionization rate is observed. Signal saturation is not occurring. The signals could be increased with greater laser photon fluxes. This would greatly improve the ultimate sensitivities and LOD's attainable.

Analytical Feasibility Studies:

The analytical working curve studies yielded very different results for the different types of electrodes. The analytical studies using the 1 mm tungsten electrodes produced a very nonlinear working curve. This is shown in Figure 129 on page 333. An order of magnitude increase in signal is normally expected for every order of magnitude increase in analyte concentration. The non-linearity is attributed to the anisotropic electric field.

Replacing the small diameter detection electrodes with 18 mm diameter flat SS electrodes eliminated the highly non-linear response of the instrument. The improved analytical working curve shown in Figure 130 on page 334. Identical instrumental settings were employed for both working curves, except that 2000 volts was used with the plate electrodes, which required this increased voltage for proper operation.

A linearity of 3 orders of magnitude was obtained with the flat plate electrodes. A detection ~~limit~~ of 10 ppb for Na was obtained. This compares quite favorably with the LIF results, for which the best case was 0.4 ppb for Na. This LOD was performed using analytical calibration solutions of Na in pure deionized water. Ionization buffering of the solutions with 100 ppm Li did not affect the LOD calculated for Na. Nor did it improve the nonlinearity for the 1 mm tungsten electrodes.

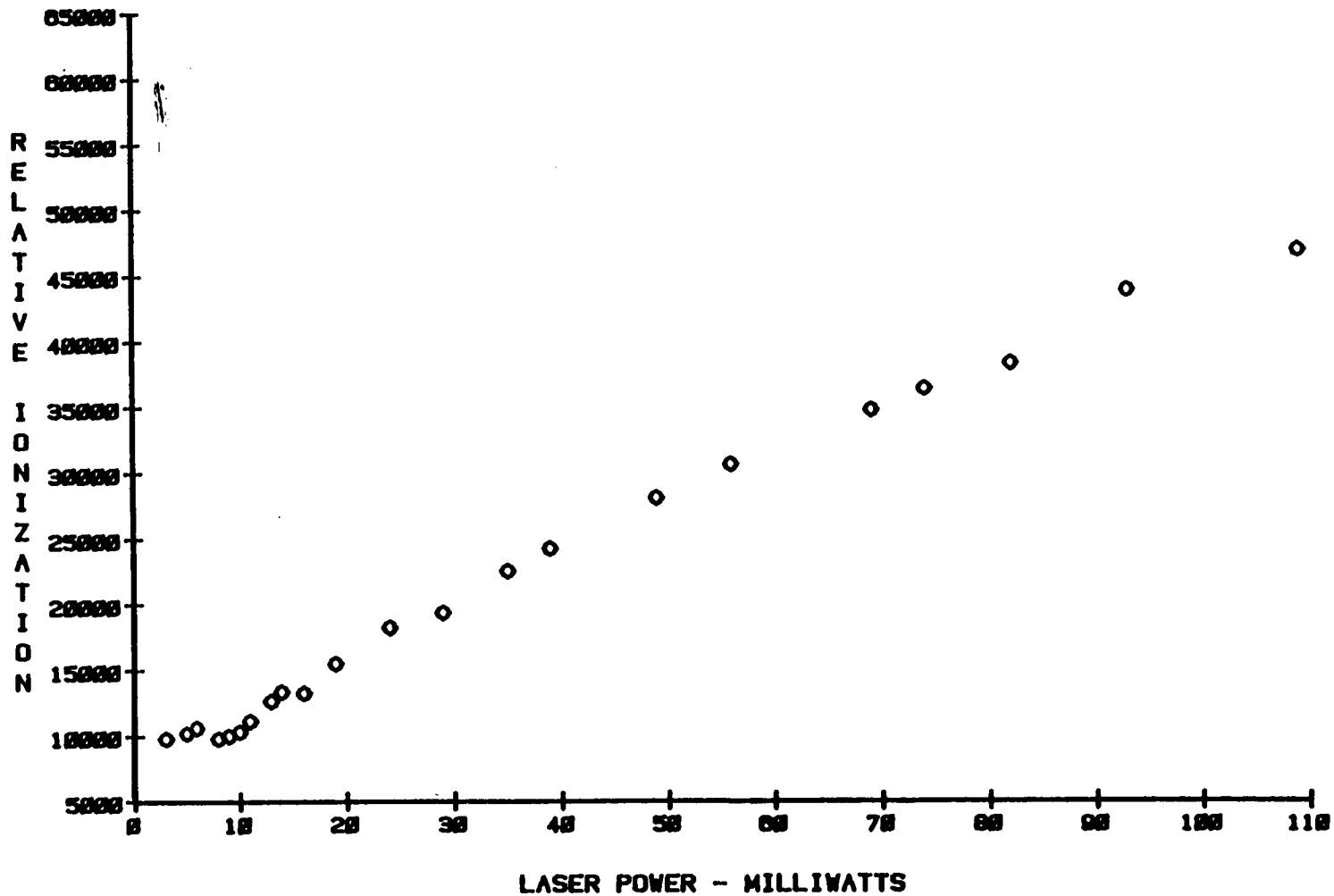

Figure 128. Na LEI Signal Intensity vs. Laser Power - Detector Saturation Study

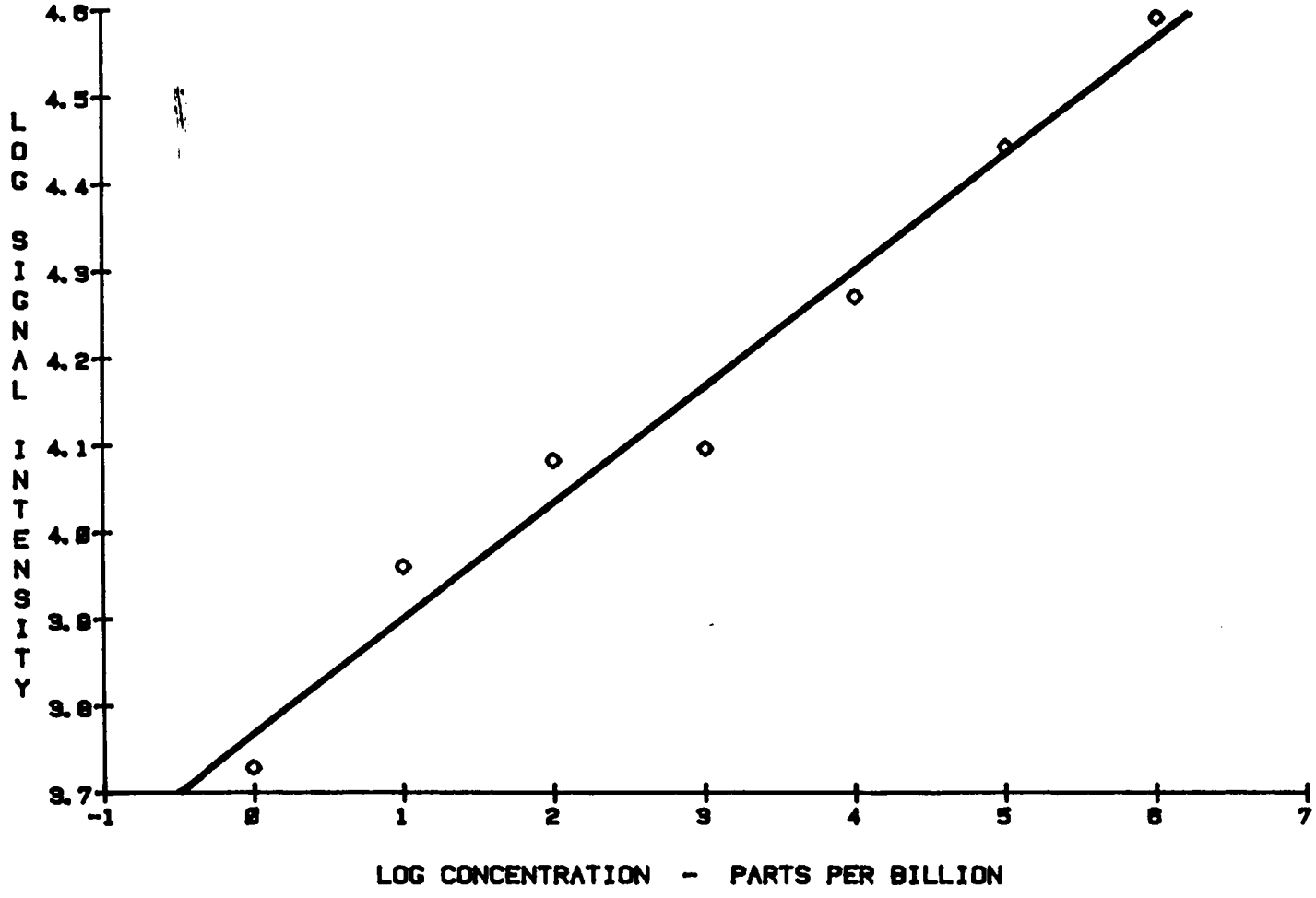

Figure 129. Na Laser Enhanced Ionization Working Curve - W Electrodes

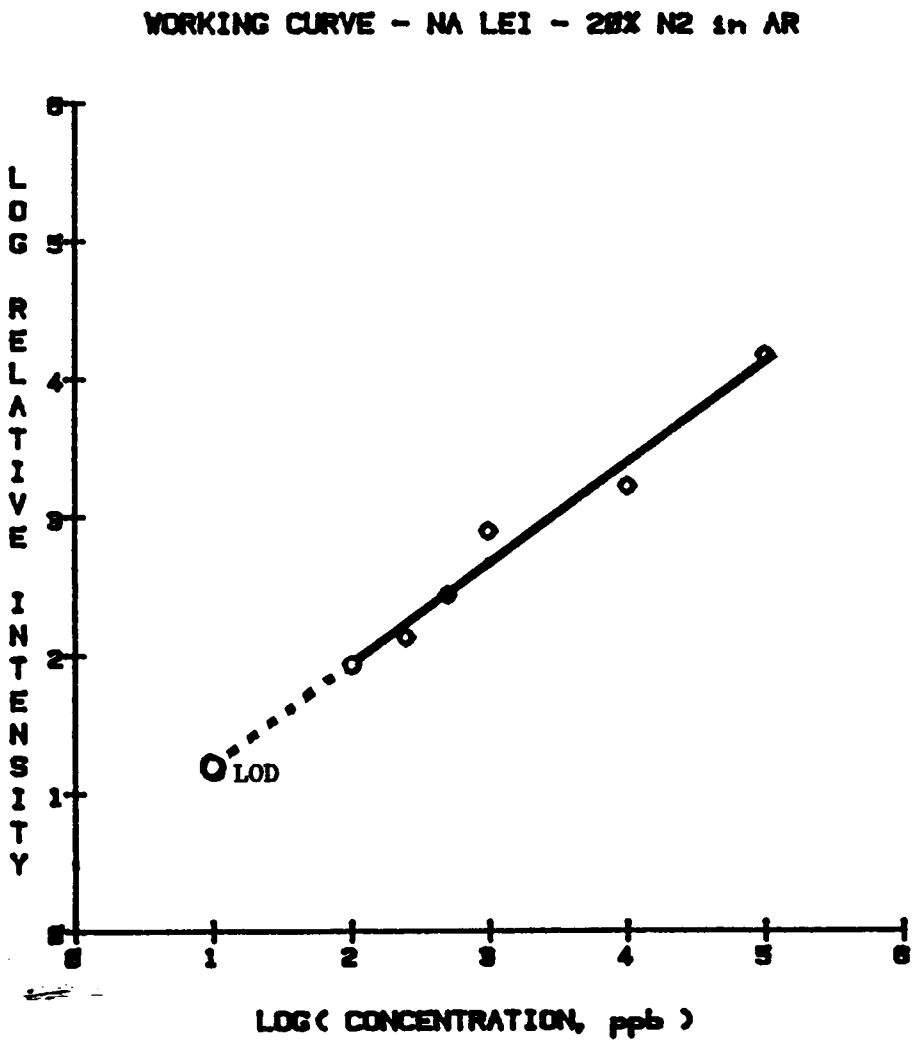

Figure 130. Na Laser Enhanced Ionization Working Curve - SS Electrodes

Other Observations:

Na LEI signals were observed to increase with a decrease in flow rate. Decreasing the support gas flow increases its residence time in the discharge region. This also increases the plasma/analyte contact time, hence the plasma energy transferred to the analyte. Excited Na atoms can then be more efficiently ionized, thereby increasing signal intensities.

Lithium LEI signals were detected at 610.3 nanometers using a 100 ppm solution. This optogalvanic effect was used to tune the dye laser to exactly 610.3 nanometers. Then LIF signals were found almost inside the MIP cavity. An observation height profile of the Li LIF signal revealed that Li LIF did not extend more than 0.5 MM beyond the cavity wall. No further characterization of Li LIF or Li LEI were done. Ba LEI signals were detected at 614.3 nanometers. No further characterization was done since feasibility for this technique has been demonstrated with the Na test probe.

Final Conclusions

LEI of analytes introduced into the MIP is a viable analytical technique. Signals can be measured with a simple lockin detection system and a CW dye laser for excitation. MIP plasma operation is not perturbed by the presence of high-voltage detection electrodes nearby. Microwave induced noise in the detection system is not a problem. Neither is the background ionization noise of the plasma. Analyte signals increase greatly with increases in MIP power and detection electrode voltage. Detection electrode geometry is very critical to obtain analyte working curves that are linear.

LEI of analytes in the MIP is at least as sensitive as LIF for detecting Na. It provides complementary information to the other spectroscopic methods. It will provide further insight into MIP plasma diagnostics and analyte excitation dynamics. With further research the linear dynamic range for analytes can be extended, and detection limits can be lowered.

D) PROGRAM TO CALCULATE SPECTROSCOPIC EXCITATION TEMPERATURE

```
10 PRINT : PRINT "PLASMA TEMPERATURE CALCULATION PROGRAM"
20 PRINT : INPUT : TITLE OF DATA SET = ";T$
30 REM  PROGRAM FINDS SLOPE OF PLOT OF Eq VS. Ln(gAv/I)
40 REM  PLASMA EXCITATION TEMPERATURE = (1/.695*SLOPE)
50 REM  THIS IS FOR THE FOLLOWING IRON LINES : 371.994, 373.713,
60 REM    374.556, 382.043, 385.991 NANOMETERS.
70 REM  TO USE OTHER EMISSION LINES CHANGE PROGEAM LINES 25 THRU 34.
80 REM  STATISTICAL WEIGHTS, STATE ENERGY DATA AND TRANSITION
90 REM  PROBABILITY VALUES ARE TAKEN FROM 2 SOURCES :
100 REM  I. REIF, V.A. FASSEL ET AL., SPECTROCHIM. ACTA, 33B,807(1978)
110 REM  NBS WAVELENGTH TABLES, 1980
112 REM  THE LINEAR REGRESSION ROUTINE WAS TAKEN FROM A PROGRAM
114 REM    BY DR. GARY L. LONG.
116 REM  IT IS WRITTEN IN APPLESOFT BASIC FOR THE APPLE IIe.
120 LET N = 5
130 DIM A(5),C(5),D(5),E(5),X(50),Y(50),XX(50),XY(50),YY(50)
140 PRINT : PRINT "INPUT PEAK HEIGHT DATA"
150 FOR I = 1 TO 5
160 INPUT "PK DATA = ";A(I)
170 NEXT I
180 REM  LINES 250-290 USE FASSEL'S TRANSITION PROBABILITIES
190 REM  LINES 300-340 USE THE NBS TRANSITION PROBABILITIES
200 LET E(1) = 26875
210 LET E(2) = 27167
220 LET E(3) = 27395
230 LET E(4) = 33096
240 LET E(5) = 25900
250 LET C(1) = (11 * .163E8 * (2.998E8 / 3719.94E-10)/A(1))
260 LET C(2) = (9 * .143E8 * (2.998E8 / 3737.13E-10)/A(2))
270 LET C(3) = (7 * .115E8 * (2.998E8 / 3745.56E-10)/A(3))
280 LET C(4) = (7 * .638E8 * (2.998E8 / 3820.43E-10)/A(4))
290 LET C(5) = (9 * .095E8 * (2.998E8 / 3859.91E-10)/A(5))
300 LET D(1) = C(1)
310 LET D(2) = (9 * .142E8 * (2.998E8 / 3737.13E-10)/A(2))
320 LET D(3) = C(3)
330 LET D(4) = (9 * .668E8 * (2.998E8 / 3820.43E-10)/A(4))
340 LET D(5) = (9 * .097E8 * (2.998E8 / 3859.91E-10)/A(5))
360 PRINT "FIRST FASSEL'S DATA WILL BE USED !"
380 FOR I = 1 TO 5
400 LET Y(I) = LOG(C(I))
410 LET X(I) = E(I)
420 NEXT I
430 GO TO 480
440 FOR I = 1 TO 5
450 LET Y(I) = LOG(D(I)
460 LET X(I) = E(I)
```

```
470 NEXT I
480 PRINT : INPUT "CHECK THE DATA ? (Y/N) ";A$: IF A$ = "N" THEN 540
490 PRINT : PRINT : PRINT "PT#     ENERGY     Ln(gAv/I)"
500 PRINT "-------------------------"
510 FOR I = 1 TO N : PRINT I;SPC(7);X(I);SPC(5);Y(I)
520 NEXT I
530 PRINT : PRINT "IF DATA'S INCORRECT THE PROGRAM CAN START OVER !!"
540 PRINT : INPUT "START OVER ?? (Y/N) ";C$: IF C$ = "Y" THEN 150
550 REM  SUM OF VARIABLES
560 X=0:Y=0:XX=0:XY=0:YY=0
570 FOR I = 1 TO N
580 X = X + X(I)
590 Y = Y + Y(I)
600 XX = XX + (X(I) * X(I))
610 YY = YY + (Y(I) * Y(I))
620 XY = XY + (X(I) * Y(I))
630 NEXT I
640 REM  CALCULATION OF SLOPE
650 M = (((N * XY) - (X * Y)) / ((N * XX) - (X * X)))
660 REM  CALCULATION OF INTERCEPT
670 B = (Y / N) - (M * (X / N))
680 X0 = -1 * (B / M)
690 REM  CALCULATION OF SUM OF ERRORS
700 SX = XX - ((X * X) / N)
710 SY = YY - ((Y * Y) / N)
720 SZ = XY - ((X * Y) / N)
730 ER = SY - (M * SZ)
740 REM  CALCULATION OF ERROR
750 S = SQR ((SY - (M * SZ)) / (N-2))
760 REM  CALCULATION OF SLOPE ERROR
770 SM = S / (SQR(SX))
780 REM  CALCULATION OF INTERCEPT ERROR
790 SB = (S * (SQR(XX) / (SQR(N * SX))))
800 REM  CALCULATION OF COEFFICIENT OF CORRELATION
810 R = SZ / (SQR(SX * SY))
820 REM  CALCULATION OF TEMPERATURE FROM SLOPE
830 PT = 1 / (.695 * M)
840 REM  DATA OUTPUT
850 PR#1  : REM  SET OUTPUT TO GO TO PRINTER
860 PRINT : PRINT : PRINT T$;"DATA SET"
870 PRINT : PRINT "PT# --- ENERGY(cm-1) --- Ln(gAv/I) --- INTENSITY"
880 PRINT "-------------------------------------"
890 FOR I = 1 TO 5
900 PRINT I;SPC(7);E(I);SPC(5);Y(I);SPC(5);A(I)
910 NEXT I
920 PRINT : PRINT
930 PRINT : PRINT "LINEAR REGRESSION RESULTS"
940 PRINT "-------------------------------------"
950 PRINT : PRINT "SLOPE   = "M"   Y-INT = "B"
960 REM  DON'T PRINT ALL THE ERROR STATISTICS
970 GOTO 1090
980 PRINT "X0 = ";X0
990 PRINT : PRINT "SM = "SM
1000 PRINT : PRINT "PLASMA TEMPERATURE = ";PT
1010 GOTO 1110
1020 REM  DON'T PRINT ALL THE ERROR STATISTICS
```

```
1030 GOTO 1110
1040 PRINT : PRINT "SSE = ";ER
1050 PRINT : PRINT "SXX = ";SX
1060 PRINT "SXY = "SZ
1070 PRINT "SYY = "SX
1080 PRINT "S   = "S
1090 PRINT : PRINT "CORRELATION COEFFICIENT = ";R
1100 PRINT : PRINT "PLASMA TEMPERATURE = ";PT
1110 PRINT : PRINT "-----------------------------------------------"
1120 PR#0 : REM  SET PRINTER PORT BACK TO CONSOLE
1130 PRINT : INPUT "RECALCULATE WITH NBS DATA ?? (Y/N) ";C$: IF C$ =
"Y" THEN 440
1140 HOME : VTAB(12) : HTAB(15) : PRINT "GOODBYE !" : VTAB(22) : END
```

E) FUTURE WORK

Cavity Improvements:

Power transfer characteristics of the cavity could be further improved by adding 1 or two more quartz tuning rods. Tuning and matching capability should be greatly increased, possibly giving perfect tuning and matching ability at any input power. In the cavity used for the studies in this dissertation, there was reflected power at the higher applied power levels, above 120 watts. All reflected power can probably be eliminated with extra quartz tuning rods. This will probably increase plasma temperatures and result in a more nearly thermal plasma. This may require further optimization studies being done on the N_2 plasma coupling probe.

More systematic studies of power transfer vs. probe position (penetration depth and radial position) are needed. Probe geometry and probe position are the most critical factors for efficient power transfer. The process of dismantling the cavity in order to change penetration depth does not promote rapid optimization. Nor does it allow optimization to be done while the plasma is in operation. The present impedance matching networks require that the cavity usually be removed from the vicinity of the spectrometer system. Then the penetration depth is set using a series of shims. This does not easily allow continuous variation of the penetration depth. The cavity is then reassembled, repositioned in the optical system, and the optical system is realigned. This whole process is very tedious and will be greatly simplified with a z-direction translator incorporated into the radial-direction translator.

A microwave cavity should be constructed which has a 2-dimensional translation stage to move the microwave antenna probe. Such a design is shown in Figure 131 on page 341. This will allow continuous variation of probe position in both the radial direction and in probe depth. This new design will allow researchers to quickly find the optimum probe position under any set of conditions of gas composition, applied power, and flow rate. They will allow

the cavity to be further improved to transfer more power into the plasma. It is believed that the 6 MM O.D. torch studies were plagued with overheating because of poor impedance matching due to probe geometry and positioning problems. The 2-dimensional probe translator (shown in Figure 131 on page 341) will facilitate the incorporation of smaller diameter tangential flow torches.

Instrumentation Improvements:

Other improvements that will increase power transfer into the plasma are the use of low-loss cables and connectors. The flexible RG-214/U has a rather large attenuation factor. At 3 GHz it is 0.62 dB/m. This represents a 20% power loss for a 1 meter cable at 3 GHz. For this reason all cable lengths should be as short as possible. The power handling capability of flexible RG-214/U cable is 95 watts at 40 degrees Centigrade at 3 GHz. It is felt that this may be the reason for the upper limit on power transfer into the cavity. A semi-rigid coaxial cable with a solid Teflon dielectric has an attenuation factor of 0.34 dB/m, and a power handling capability of 830 watts at 40 degrees Centigrade. The semi-rigid cable is available from STORM Co., Hinsdale, Illinois. The connectors that should be used are military specifications MIL-C-39012 because of their low insertion loss and VSWR ratio is 1.06 + (0.007 * f), where f is in GHz, (54). With these precautions and further improvements to the power transfer characteristics of the cavity the energy content of microwave plasmas would improve to the point where it may rival that of the ICP.

New cavity designs should make the support gas exit wall of the cavity as thin as possible. It can be made quite thin, only as thick as required for structural support (perhaps 0.100" thick). A different mount design will be needed which does not rely on the exit wall for mounting support. Electrically, only the inner 1.5 microns is needed for current conduction (this is why the cavity interior must be free from dirt and oxidation). This will allow the plasma discharge to extend as far outside of the cavity as possible, hence elements with high excitation potentials can be studied without cutting a hole in the radial wall of the cavity.

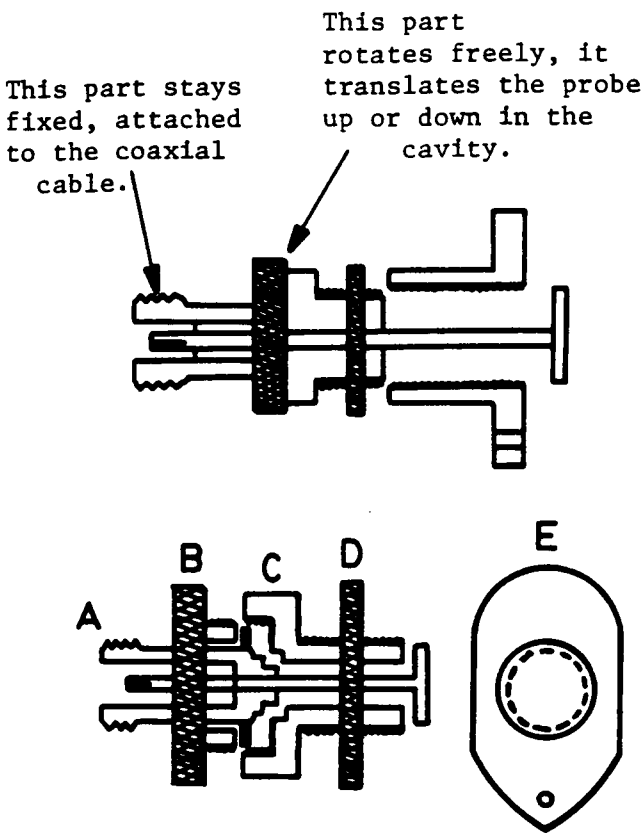

The Locking and Retaining collars maintain good electrical contact between the Type N connector and the cavity lid.

There are 5 main parts:

A. Type N Connector (modified)

B. Retaining Collar for locking the modified Type N connector into the threaded collar (C.)

C. Threaded Collar for up/down movement

D. Locking Collar for the threaded collar (C.)

E. Threaded Mount to mount onto the radial translator

If an extra long Type N connector is available, parts A,B and C can be combined by turning down the Type N connector and then threading it.

Figure 131. Two-Dimensional Probe Translation Mechanism

Annular Plasma:

The curious annular plasma seen when the flow pattern becomes uncentered and begins to circulate could be of special use. The signal intensity is seen to increase approximately 5 times !! If this were further investigated and developed it could pave the way for a stable "doughnut" plasma, as used in ICPs. It already resembles a donut as it is circulating. The most intriguing thing about it is the great increase in signal intensity. It has not been systematically explored as an alternative to the tangential flow torch with a centered plasma bolus. The primary difficulties with this bolus configuration are the torch overheating problem and the signal noise problem. Signals from the annular plasma are modulated by the circulation of the bolus. This may be easily eliminated electronically. Or it may require a new torch geometry, i.e., a different ratio of the inner tube O.D. to the outer tube I.D. Also, the present ratio of the center-tube flow rate to tangential "side-arm" flow is about 1:100, (10-20 mL/min center-tube flow rate, 1.5 L/min side-arm flow rate). Drastically altering this flow rate ratio may cure the overheating problem and produce a spatially stable "donut" plasma. Preliminary experiments indicate that a donut plasma could be generated by having an approximate flow rate ratio of 1:1. A combination of torch geometry and flow ratio changes may also be necessary.

Microarc Sampler:

The microarc was eventually stabilized using a thicker cathode (0.040 inch instead of 0.015 inch), and a larger syringe needle (18 gauge instead of 20 gauge). The body of the sampler was made larger and the material was changed from pyrex to quartz to reduce overheating problems and the concomitant high levels of Na outgassing. The resulting sampler is more rugged, tolerates longer firing times, and has better cooling characteristics. The microarc should be investigated as an atom source in its own right. It is a cathodic sputtering source that is very efficient and could offer some very promising results as an atom source for atomic fluorescence.

Sampling System Improvements:

The nebulizer and flow torch could be better matched to each other to achieve better overall performance. In the present system, the nebulizer optimal flow rate is approximately 0.75 L/min, and the tangential flow torch's optimal flow rate is approximately 1.5 L/min. The extra flow required to make up the total volume flow rate had to be introduced as the "auxiliary flow". This caused sample dilution. This problem can be eliminated in a couple of different ways. The nebulizer dimensions could be enlarged further to obtain a nebulizer whose optimal flow rate coincides with the optimal flow of the MIP torch. Or the MIP torch could be redesigned to work well at a lower flow rate.

Experiments to determine the sample transport efficiency through the newly-designed glass frit nebulizer would be helpful. Studying sample transport efficiency as a function of nebulizer size would help determine the optimum size for the sampler. This is important since the sampling system is usually the weakest part of an atomic analysis system.

It is not clear which approach will give the best results in terms of system performance AND economics. It is imperative that the best atomization system be employed, yet it is also desireable to get the considerable economic benefits that are possible by cutting flow rates in half. It will probably be true that a tradeoff will not be necessary. The 20 mm diameter frit appeared to be near the size limit for this type of nebulizer since a single droplet from the underside sample-to-frit dispensing tube barely wetted the full area of the frit. However, this may be solved with larger droplets from a larger diameter sample-to-frit dispensing tube. Clearly more work is needed to find the best sampling system for this MIP source.

Optical System Optimization:

Rotating the MIP cavity so that the plasma plume is parallel to the monochrometer slits may increase the limits of detection by as much as 2 orders of magnitude. Signals will then be integrated over the full length of the slits. A cylindrical mirror placed opposite the slits,

on the other side of the plume, will allow twice as much light to be focussed on the slits. The detections limit may be improved by a factor of two.

Extended Torch Experiments:

An MIP torch which extends 2-3 inches beyond the cavity wall should be studied. It will provide greater freedom from air entrainment in the plasma gases, which may be causing significant fluorescence quenching. This may cause increased torch scatter to reach the monochrometer, however, with proper optimization of geometry and scatter shields detection limits may be improved.

Other Studies:

Studies of analyte emission intensity should be done as a function of gas composition and elemental excitation energy. These will provide more insight into the processes responsible for analyte excitation in N_2/Ar mixed plasmas. A linear increase to higher % N_2 concentrations with increases in elemental excitation energy would provide further support for a thermal mechanism.

A more complete study of active nitrogen emissions as a function of % nitrogen-in-argon would help elucidate the excitation mechanism in these plasmas. These studies should include monitoring the First and Second Positive emission bands to ascertain what role the N_2(B) and N_2 (C) states are playing in excitation. Studying them as a function of MIP power over their entire spectral range as the gas composition is varied from 0% to 100% will allow one to predict at what compositions and powers their effect on excitation is a maximum.

Electron density measurements using the double probe method, though much more difficult than the spectroscopic methods, would yield useful mechanistic information, including electron temperatures. Electron density measurements done from 0 to 100% N_2 in Ar would confirm whether the peaks seen at 10% N_2/Ar are because of changes in electron density. Exact measurements of the electron temperatures in the atmospheric pressure N_2-MIP would

allow further comments to be made about excitation by high-energy electrons in the plasma, the proximity of the plasma to thermal equilibrium, and other mechanistic information.

LIST OF REFERENCES

1. G.A. Capelle, and D.A. Sutton, Rev. Sci. Instrum. **49**,1125(1978).
2. K.M. Aldous, R.M. Dagnall, B.L. Sharp, and T. S. West, Anal. Chim. Acta, **54**, 233 (1971).
3. R.H. Wendt, and V.A. Fassell, Anal. Chem. **37**, 920 (1965).
4. C. Veillon, and M. Margoshes, Spectrochim. Acta, **23B**, 503 (1968).
5. P.J. Slevin and W.W. Harrison, Appl. Spectrosc. Rev., **10(2)**, 201 (1975).
6. J. Kishman, E. Barish, and R. Allen, Appl. Spectrosc. **37**, 545 (1983)..
7. B. Chambers, Ph.D. Dissertation, University of South Carolina, 1984.
8. N. Omenetto and J.D. Winefordner, Prog. Analyt. Atom. Spectrsc., **2**, 1 (1979).
9. C.I.M. Beenakker, Spectrochim. Acta **31B**, 483 (1976).
10. C.I.M. Beenakker, Spectrochim. Acta, **32B**, 172 (1977).
11. C.I.M. Beenakker, B. Bosman, and P.W.J.M. Boumans, Spectrochim. Acta, **33B** 373 (1978).
12. J.P. Matousek, B.J. Orr, and M. Selby, Prog. Analyt. Atom. Spectrosc. **7**, 275 (1984).
13. J. Bergquist, Ph.D. Dissertation, Virginia Tech, 1983.
14. A.T. Zander, and G.M. Heiftje, Appl. Spectrosc., Vol. **35**, 357 (1981).
15. L.R. Layman and G.M. Heiftje, Anal. Chem. **47**, 194 (1975).
16. L.R. Layman and F.E. Lichte, Anal. Chem. **54**, 638 (1982).
17. L. Matus and C. Boss, Rev. Sci. Instr. **54** (12) 1667, (1983).
18. J.P.J. van Dalen, P.A. de Lezenne Coulander, and L. de Galan, Spectrochim. Acta **33B**, 545 (1978).
19. C.I.M. Beenakker, and P.J.W.M. Boumans, Spectrochim. Acta, **33B**, 53 (1978).
20. A. Bollo-Kamara, and E.G. Codding, Spectrochim. Acta, **36B**, 973 (1981).
21. N. Rait, D.W. Golightly, C.J. Massoni, Spectrochim. Acta, **39B**, 931 (1984).
22. L. Matus, Ph.D. Dissertation, North Carolina State University, 1983.
23. C. Boss, Private Communication.
24. W.B. Dodge and R.O. Allen, Anal. Chem. **53**, 1279 (1981).

25. C.F. Bauer and R.K. Skogerboe, Spectrochim. Acta, **38B**, 1125 (1983).

26. J.P. Matousek, B.J. Orr, and M. Selby, Appl. Spectrosc. **38**, 231 (1984).

27. I.J.M.M. Raaymakers, P.W.J.M. Boumans, B. van der Sijde, and D.C. Schram, Spectrochim. Acta **38B**, 697 (1983).

28. L. de Galan, Spectrochim. Acta **39B**, 537 (1984).

29. C.Th.J. Alkemade and R. Herrmann, "Fundamentals of Analytical Spectroscopy", John Wiley and Sons, New York, 1979.

30. R.D. Deutsch and G.M. Heiftje, Appl. Spectrosc. **39**, 214 (1985).

31. J.J. Urh, and J.W. Carnahan, Appl. Spectrosc. **40**, 877 (1986).

32. Y.K. Zhang, S. Hanamura, and J.D. Winefordner, Appl. Spectrosc. **39**, 226 (1984).

33. P.W.J.M. Boumans and F.J. DeBoer, Spectrochim. Acta **32B**, 365 (1977).

34. I. Reif, V.A. Fassel, R.N. Kniseley, D.J. Kalnicky, Spectrochimica Acta, **33B**, 807 (1978).

35. R.D. Deutsch, Ph.D. Dissertation, Indiana University, 1983.

36. R. M. Barnes and S. Nikdel, Appl. Spectrosc., **30**, 310 (1970).

37. M. Capitelli, F. Cramarossa, L. Triolo, and E. Molinari, J. Combust. Flame, **15**, 23 (1970).

38. S. Greenfield and P.B. Smith, Anal. Chim. Acta, **57**, 341 (1972).

39. A. Montaser and J. Mortazavi, Anal. Chem., **52**, 255 (1980).

40. R. M. Barnes and G.A. Meyer, Anal. Chem., **52**, 1523 (1980).

41. H. U. Eckert, F. L. Kelly, and H. N. Olsen, J. Appl. Phys., **39**, 1846 (1968).

42. J. D. Cobine and D. A. Wilbur, J. Appl. Phys., **22**

43. W.B. Dodge, Ph.D. Dissertation, University of Virginia, 1981.

44. G.A. Capelle, and D.G. Sutton, Appl. Phys. Lett., **30**, 407 (1977).

45. A.N. Wright, and C.A. Winkler, "Active Nitrogen", Academic Press, N.Y., 1968.

46. M.M.C. Dupret, B. Vidal, and B. Goudmand, Rev. de Phys. Appl. **5**, 337 (1970).

47. M. Locqueneu Lefevre, and A. Ricard, Rev. de Phys. Appl. **12**, 1213 (1977).

48. S. Hanamura, B.W. Smith, and J.D. Winefordner, Can J. Spectrosc. **29**, 13 (1984).

49. B. Kirsch, S. Hanamura, and J.D. Winefordner, Spectrochim. Acta **39B**, 955 (1984).

50. R.D. Deutsch, Private Communication.

51. S. Chilukuri, and W.L. Lichten, Rev. Sci. Instr. **50**, 256 (1979).

52. D.L. Haas, J.W. Carnahan, and J.A. Caruso, Appl. Spectrosc., **37**, 82 (1983).

53. P.G. Brown, J.M. Workman, D.L. Haas, P.A. Fleitz, D.C. Miller, C.J. Seliskar, and J.A. Caruso, Appl. Spectrosc., **40**, 477 (1986).

54. J. Hubert, M. Moisan, and Z. Zakrzewski, Spectrochim. Acta **41B**, 205 (1986).

55. M. Outred, Spectrochim. Acta **35B**, 447 (1980).

56. J. Caruso, Private Communication.

57. C. Boss, Private Communication.

58. Brad Burns, North Carolina State Univ., Ph.D. Dissertation, 1987.

59. F. Llewellyn-Jones "The Glow Discharge", Wiley, New York, 1966.

60. S.R. Goode, and D.C. Otto, Spectrochim. Acta **35B**, 569 (1980).

61. Brad Burns, Private Communication.

62. S.R. Goode, N.P. Buddin, B. Chambers, K.W. Baughman, and J.P. Deavor, Spectrochim. Acta **40B**, 317 (1985).

63. K. Fallgatter, V.Svoboda, and J.D. Winefordner, Appl. Spectrosc. **25**, 347 (1971).

64. A.T. Zander, and G.M. Heiftje, Anal. Chem. **50**, 1257 (1978).

65. A.T. Zander, R.K. Williams, and G.M. Heiftje, Anal. Chem. **50**,1257 (1978).

66. J.M. Workman, P.G. Brown, D.C. Miller, C.J. Seliskar, and J.A. Caruso, Appl. Spectrosc., **40**, 857 (1986).

67. G.R. Kornblum, and L. deGalan, Spectrochim. Acta, **32B**,71 (1977).

68. M.H. Abdullah, and J.M. Mermet, Spectrochim. Acta, **37B**391 (1982).

69. R.A. Young, Can. J. Chem. **44**, 1171 (1966).

70. J.F. Noxon, J. Chem Phys. **36**, 926 (1962).

71. W.B. Dodge, Ph.D. Dissertation, University of Virginia, Charlottesville, Va., 1980.

72. G.G. Mannella, Chem. Reviews, **63**, 1 (1963).

73. V. Sychra, I.V. Svoboda, and I. Rubeska, "Atomic Fluorescence Spectroscopy", Van Nostrand Reinhold Co., London, 1975.

74. R.F. Browner, Analyst **99**, 617 (1974).

75. T.S. West, Analyst, **99**, 886 (1974).

76. J.D. Winefordner, J. Chem. Ed. **55**, 72 (1978).

77. S.J. Weeks and J.D. Winefordner, In "Lasers in Chemical Analysis"; G.M. Hieftje, J.C. Travis, F.E. Lytle, Eds. Humana Press, 1981; pp. 159-83.

78. N. Omenetto, Anal. Chem. **48**, 75A (1976).

79. J.C. Van Loon, Anal. Cehm. **53**, 333 (1981).

80. A.L. Boers, C.T.J. Alkemade, and J.A. Smit, Physica **22**, 358 (1956).

81. H.V. Malmstadt, C.G. Enke, and G. Horlick, "Electronic Measurements For Scientists", W.A. Benjamin, Inc., Menlo Park, CA. 1974.

82. J.D. Winefordner and T.J. Vickers, Anal. Chem. **36**, 161 (1964).

83. W.R. Ware, "Transient Luminescence Measurements" in "Creation and Detection of the Excited State", A.A. Lamola, Ed., Vol. 1, Part A, Marcel Dekker, New York, 1971.

84. M.L. Elder, G. Zizak, D. Bolton, J.J. Horvath, and J.D. Winefordner, Appl. Spectrosc. **38**, 113 (1994).

85. H. Haraguchi, S. Weeks, and J.D. Winefordner, Can. J. Spectrosc. **22**, 61 (1977).

86. T.B. Stewart and H.S. Judeikis, Rev. Sci. Instr. **45**, 1542 (1974).

87. J.W. Daily, Appl. Opt. **16**, 568 (1977).

88. S.J. Pearce, L. de Galan, and J.D. Winefordner, Spectrochim. Acta **23B**, 793 (1968).

89. N. Omenetto, "Analytical and Diagnostic Applications of Laser Induced Fluorescence in Flames and Plasmas", Chap. 7 in "Analytical Laser Spectroscopy", Ed. by S. Martellucci and A.N. Chester, Plenum Press, New York, 1985.

90. J.D. Bradshaw, N. Omenetto, G. Zizak, J.N. Bower, and J.D. Winefordner, Appl. Opt. **19**, 2709 (1980).

91. W. Demtroeder, Chem. Anal. (N.Y.), **50**, 219 (1979).

92. W.M. Fairbanks, Jr., T.W. Hansch, and A.L. Schawlow, J. Opt. Soc. Am., **65**, 199 (1975).

93. G.S. Hurst, M. N. Nayfeh, and J.P. Young, Appl. Phys. Lett., **30**, 229 (1977).

94. R.F. Browner and A.W. Boorn, Anal. Chem. **56**, 786 (1984).

95. C.T.J. Alkemade, "Proceedings of the 10th Colloquium Spectroscopicum Internationale, p. 143, Spartan Books, Washington D.C., 1963.

96. C.A. van Dijk, N. Omenetto, and J.D. Winefordner, Appl. Spectrosc. **35**, 389 (1981).

97. D.R. Olivares and G.M. Hieftje, Spectrochim. Acta **33B**, 79 (1978).

98. D.R. Olivares and G.M. Hieftje, Spectrochim. Acta **36B**, 1059 (1981).

99. E.H. Peipmeier, Spectrochim. Acta **27B**, 431 (1972).

100. "Atomic Absorption Spectroscopy" Ed. by A Pinta; Adam Hilger Co., London 1975.

101. R. Mavrodineanu and H. Boiteaux, "Flame Spectroscopy", Wiley and Sons, New York, 1965.

102. N. Omenetto and J.D. Winefordner, CRC Critical Reviews in Analytical Chemistry **13**, pg.62 (1981).

103. R.B. Green, J.C. Travis, and R.A. Keller, Anal. Chem. **48**, 1954 (1976).

104. J.D. Winefordner and T.J. Vickers, Anal. Chem. **42**, 206R (1970).

105. J.D. Winefordner and R.C. Elser, Anal. Chem. **43**, 24A, (1871).

106. L.M. Fraser and J.D. Winefordner, Anal. Chem. **43**, 1693 (1971).

107. B. W. Smith, M. B. Blackburn, and J. D. Winefordner, Can. J. Spectrosc. **22**, 57 (1977).

108. S.J. Weeks, H. Haraguchi, and J.D. Winefordner, Anal. Chem. **50**, 360 (1978).

109. S.V. Kachin, B.W. Smith, and J.D. Winefordner, Anal. Chem. **39**, 587 (1985).

110. F.E. Hovis and J.A. Gelbwachs, Anal. Chem. **56**, 1392 (1984).

111. D.R. Demers and C.D. Allemand, Anal. Chem. **53**, 1915 (1981).

112. D.R. Demers, D.A. Busch, and C.D. Allemand, Am. Laboratory, March 1982.

113. B.D. Pollard, M.B. Blackburn, S. Nikdel, A. Massoumi, and J.D. Winefordner, Appl. Spectrosc. **33**, 5 (1979).

114. M.S. Epstein, S. Nikdel, J.D. Bradshaw, M.A. Kosinski, J.N. Bower, and J.D. Winefordner, Analytica Chimica Acta **113**, 221 (1980).

115. H. Uchida, M.A. Kosinski, and J.D. Winefordner, Spectrochim. Acta **38B**, 5 (1983).

116. N. Omenetto, S. Nikdel, R.D. Reeves, J.B. Bradshaw, J.N. Bradshaw, and J.D. Winefordner, Spectrochim. Acta **35B**, 507 (1980).

117. X. Huang, K.S. Yeah, and J.D. Winefordner, Spectrochim. Acta **40B**, 1379 (1985).

118. M.A. Kosinski, H. Uchida, and J.D. Winefordner, Anal. Chem. **55**, 688 (1983).

119. N. Omenetto and H.G.C. Human, Spectrochim. Acta **39B**, 1333 (1984).

120. N. Omenetto and H.G.C. Human, Spectrochim. Acta **39B**, 1345 (1984).

121. A. Montaser and V.A. Fassel, Anal. Chem. **48**, 1490 (1976).

122. M.A. Kosinski, H. Uchida, and J.D. Winefordner, Talanta **30**, 339 (1983).

123. G.L. Long and J.D. Winefordner, Appl. Spectrosc. **38**, 563 (1984).

124. S. Neumann and M. Kreise, Spectrochim. Acta **29B**, 127 (1974).

125. V.I. Balykin, V.S. Letokhov, V.I. Mishin, and V.A. Senchishen, JETP Lett. **26**, 357 (1977).

126. M.A. Bolshov, A. V. Zybin, and I.I. Smirenkina, Spectrochim. Acta **36B**, 1143 (1981).

127. P. Wittman and J.D. Winefordner, Can. J. Chem. **29(3)**, 75 (1984).

128. M.S. Hendrick, M.D. Seltzer, and R.G. Michel, Spectrochim. Acta **41B**, 335 (1986).

129. M.M. Miller, D. Eastwood, and M.S. Hendrick, Spectrochim. Acta **38B**, 13 (1984).

130. M.S. Hendrick, M.D. Seltzer, and R.G. Michel, Spectrosc. Lett. **19(2)**, 141 (1986).

131. B.W. Smith, N. Omenetto, and J.D. Winefordner, Spectrochim. Acta **39B**, 1389 (1984).

132. C. van Dijk, B.W. Smith, and J.D. Winefordner, Spectrochim. Acta **37B**, 759 (1982).

133. L.D. Perkins, Master's Thesis, Virginia Tech, 1987.

134. L.R. Layman and F. E. Lichte, Anal. Chem., **54**, 638 (1982).

135. J.T. Currie, Ph.D. Dissertation, Virginia Tech, 1984.

136. L. Brodie, "Starting FORTH", Prentice-Hall, 1981.

137. M.W. Blades, Spectrochim. Acta **37B**, 869 (1982).

138. A.T. Zander, and G.M. Heiftje, Appl. Spectrosc. **35**, 357 (1981).

139. H.R. Griem, Spectral Line Broadening by Plasmas, Academic Press, New York, 1974.

140. "Principles of Laser Plasmas" Ed. by George Bekefi, Wiley-Interscience N.Y., 1976.

141. G.L. Long, and J.D. Winefordner, Anal. Chem. **55**, 712A (1983).

142. M.J. Youden and E.H. Steiner, "Statistical Manual of the Official Analytical Chemists", AOAC, Washington, D.C., 1975.

143. M.L. Parsons, S. Major, and A.R. Forster, Appl. Spectrosc. **37**, 411 (1983).

144. L.D. Perkins, and G.L. Long, FACCS Meeting 1986, Federation of Analytical and Spectroscopy Societies, 13th Annual Meeting, Sept. 28 - Oct 3, 1986, St. Louis, MO.

145. D.R. Demers, Spectrochim. Acta, **40B**, 93 (1985).

146. M.S. Hendrick, M.D. Seltzer, and R.G. Michel, Spectrosc. Lett. **19**, 141 (1986).

147. D. Erlich, R.M. Osgood, G.C. Turk, J.C. Travis, Anal. Chem., **52**, 1354 (1980).

148. G.S. Hurst, M.G. Payne, S.D. Kramer, and J.P. Young, Rev. Mod. Phys., **51**,767 (1979).

149. C.T.J. Alkemade, Appl. Spectrosc. **35**, 1 (1981).

150. G.C. Turk, J.C. Travis, J.R. DeVoe, T.C. O'Haver, Anal. Chem. **50**, 817 (1978).

151. R.B. Green, R.A. Keller, G.G. Luther, P.K. Schenk, and J.C. Travis, Appl. Phys. Lett., **29**, 727 (1976); J.A.C.S., **98**, 8517 (1976).

152. P.K. Schenck, J.C. Travis, G.C. Turk, T.C. O'Haver, J. Phys. Chem., **85**, 2547 (1981).

153. C.A. van Dijk, C.Th. Alkemade, J. Combus. Flame. **38**, 37 (1980).

154. P. Camus, "Optogalvanic Spectroscopy and Its Applications" Proceedings from International Colloquium, Aussois, France, 1983, published in J. de Physique, C7, Tome **44**, (1983).

155. N.S. Kopeika, J. Rosenbaum, IEEE Trans. Plasma Sci. PS **4**, 51 (1976).

156. D. Feldmann, Opt. Comm. **29**, 67 (1979).

157. R.A. Keller, E.F. Zalewski, Appl. Optics **19**, 3301 (1980).

158. E.F. Zalewski, R.A. Keller, R. Englemann, J. Chem. Phys., **70**, 1015 (1979); J. Opt. Soc. Am. **69**, 738 (1979).

159. J. Pfaff, M. H. Begeman, R.J. Saykally, Proc. Intl. Conf. on Lasers, Dec. 13-17, 1982.

160. R. Beigang, K. Lucke, A. Timmermann, P.J. West, D. Frolich, Opt. Comm. **42**, 19 (1982).

161. U. Brinkmann, W. Hartig, H. Telle, H. Walther, Appl. Phys. **5**, 109 (1974).

162. P. Camus, M. Dieulin, C. Morrilon, J. de Phys. **40**, L-513 (1979).

163. I. Popescu, C. Ghita, N. Niculescu, Phys. Lett., **24**, A, 276 (1966).

164. D. Popescu, I. Popescu, C.B. Collins, B.W. Johnson, G. Musa, M.L. Pascu, Phys. Rev. **16**, 63 (1965).

165. E. Badareu, I. Popescu, C. Ghita, G. Musa, Rev. Roum. Phys. **10**, 785 (1965).

166. C. Stanciulescu, R. Bobulescu, A. Surmeian, D. Popescu, I. Popescu, C.B. Collins, Appl. Phys. Lett., **37**, 888 (1980); Rev. Roum. Phys. **25**, 783, 915 (1980).

167. T. Suzuki, Opt. Comm. **38**, 364 (1981).

168. P. Labastie, F. Biraben, E. Giacobino, J. Phys. B. At. Mol. Phys. **15**, 2595 (1982); J. Phys. B. At. Mol. Phys. **15**, 2605 (1982).

169. G.C. Turk, and R.L. Watters Jr., Anal. Chem. **57**, 1979 (1983).

170. T. Suzuki, H. Sekiguchi, and T. Kasuya, J. de Phys. C7, **44**, 419 (1983).

171. T. Cool, Appl. Optics, **23**, 1559 (1984). **30**, 229 (1977).

172. J.C. Travis, G.C. Turk, and R.B. Green, Anal. Chem. **54**, 1006 (1982).

173. J.C. Travis, J.R.DeVoe, In "Lasers in Chemical Analysis"; G.M. Hieftje, J.C. Travis, F.E. Lytle, Eds. Humana Press, 1981; pp. 92-124.

174. T.H. Risby and Y. Talmi, CRC Crit. Rev. Anal. Chem., **14**, 231 (1983). Comparison of LEI, LIF, AES.

The vita has been removed from the scanned document